COMBINATION THERAPY STUDIES WITH THE VASCULAR DISRUPTIVE AGENT COMBRETASTATIN-A4-PHOSPHATE (CA4P)

Dr Andrew Mark Gaya

Thesis submitted for the degree of

Doctor of Medicine (MD)

University College London
Faculty of Oncology

2009

Department of Medical Oncology, Mount Vernon Hospital

Department of Medical Oncology, The Royal Free Hospital

Paul Strickland Scanner Centre, Mount Vernon Hospital

The Gray Cancer Institute, Northwood, Middlesex

Declaration of Authenticity

I certify that the following work presented in this thesis is my own. Where other individuals work is presented or quoted, this is stated clearly in the text.

Dr Andrew Gaya
University College London
March 2009

Abstract

CA4P leads to rapid vascular shutdown of tumour core, with minimal effects at the well perfused periphery. CA4P showed minimal anti-tumour activity in single agent phase I studies. This thesis examined the feasibility of CA4P combination therapy, examining the hypothesis that two agents may be additive or synergistic, eliminating separate tumour cell subpopulations and thus increasing the effectiveness of both drugs. Chemotherapy using paclitaxel & carboplatin (UKCTC-207) or ^{131}Iodine anti-CEA radioimmunotherapy (A5B7) was studied. CA4P toxicity was mild and similar to single agent studies - fatigue, tumour pain, flushing, pruritis, headache and hypertension. The DLT was ataxia. A5B7 combination therapy led to dose limiting myelosuppression with minimal efficacy at a ^{131}I-A5B7 dose 66% of single agent antibody MTD. In UKCTC-207, 70% of patients either responded or had disease stability with symptomatic improvement.

We also investigated whether CA4P effect is mediated via decreases in cardiac output (CO) and also evaluated heterogeneity of blood flow related dynamic contrast enhanced MRI (DCE-MRI) parameters between different patients and in lesions within patients on the A5B7 study. Increases in CO (mean +14%, p=0.026) occurred after CA4P whilst falls in tumour K^{trans} values were seen (mean -25.1%; p=0.011). There was no evidence for CO fall as a cause for reduced K^{trans}. Metastatic lesions within-patients were more similar compared to between-patients in DCE-MRI kinetic parameters, both at baseline and in their response to CA4P. A separate perfusion CT analysis revealed no late alterations (over weeks) in tumour blood flow parameters.

Correlating DCE-MRI kinetic variable changes following CA4P with tumour immunohistochemical angiogenic markers using standard immunohistochemical techniques, we studied whether the angiogenic profile can explain differential sensitivity of human tumours to CA4P. We found no strong relationships between DCE-MRI variable change following CA4P and the angiogenic markers.

Table of Contents

List of Abbreviations

5HT	5-Hydroxy Tryptamine (Serotonin)
A5B7	131-Iodine Labelled anti-CEA monoclonal antibody
ADEPT	Antibody Dependent Enzyme Prodrug Therapy
AE	Adverse event
AIF	Arterial Input Factor
ALP	Alkaline Phosphatase or Arterial Liver Perfusion
ALT	Alanine Amino-transferase
Ang-1 , Ang-2	Angiopoietins
ANOVA	Analysis of Variance
APPT	Activated Partial Thromboplastin Time
AST	Aspartate Amino-Transferase
AUC	Area Under the Curve
AVOT	Atrio-Ventricular Outflow Tract
BOLD	Blood Oxygen Level Dependent
BP	Blood pressure
BSA	Body surface area
BSO	Bilateral Salpingo-Oophorectomy
CA1(P)	Combretastatin A1 (Phosphate) (OXi4503)
CA4G	Combretastatin A4 Glucuronide
CA4(P)	Combretastatin A-4 (Phosphate)
CEA	Carcino-embryonic antigen
CK	Creatinine kinase
CNS	Central Nervous System
CR	Complete response
CRF	Case report form
CR-UK	Cancer research UK
CT	Computerised tomography
CTC	Common toxicity criteria
CWRU	Case Western Reserve University Hospital, Detroit, Michigan
DAB	Diaminobenzidine
DCE-MRI	Dynamic Contrast Enhanced Magnetic Resonance Imaging
DLT	Dose limiting toxicity
DMXAA	Vascular Disrupting Agent
EBRT	External Beam Radiotherapy
EC	Endothelial Cell
ECG	Electro-Cardiogram
EDTA	Ethylene diamine tetra-acetic acid
EES	Extravascular Extracellular Space
FAA	Flavone Acetic Acid
FDG-PET	Fluorodeoxyglucose positron emission tomography
Gd-DTPA	Gadolinium-based MRI Contrast Agent
GGT	Gamma glutamyl transpeptidase
GTP	Guanine Triphosphate
HAMA	Human anti-mouse antibody
Hb	Haemoglobin
HHT	Hereditary Haemorrhagic Telangiectasia
HIF-1	Hypoxia Inducible Factor 1
HPI	Hepatic Perfusion Index
HPLC	High performance liquid chromatography
HR	Heart rate
HRP	Horse Radish Peroxidase
HU	Hounsfield Unit
^{131}I	Iodine-131
IAUGC	Initial Area Under The Gadolinium Concentration-Time Curve

INR	International normalised ratio
IV	Intravenous
k_{ep}	Rate Constant Between EES & Plasma. $K_{ep} = K^{trans}/V_e$
K^{trans}	Volume Transfer Constant Between Plasma & EES
LFT	Liver Function Tests
LREC	Local research ethics committee
LVEF	Left Ventricular Ejection Fraction
MDCT	Multidetector Computerised Tomography
MHRA	Medicines & Healthcare Regulatory Agency
MIP	Maximum Intensity Projection
MRI	Magnetic resonance imaging
MRT	Mean Residence Time
MTD	Maximum Tolerated Dose
MVD	Micro Vessel Density
NAC	N-Acetyl Colchinol
NC	No change
NCI	National Cancer Institute
NSCLC	Non Small Cell Lung Cancer
PCI	Pericyte Coverage Index
PD	Progressive disease
PDGF	Platelet Derived Growth Factor
PET	Positron emission tomography
PIS	Patient information sheet
PK	Pharmacokinetics
Plt	Platelets
PR	Partial response
PT	Prothrombin time
PVP	Portal Venous Perfusion
QTc	ECG corrected QT Interval
rBF	Relative Blood Flow
rBV	Relative Blood Volume
RECIST	Response Evaluation Criteria In Solid Tumours
RFA	Radiofrequency Ablation
RIT	Radioimmunotherapy
ROI	Region Of Interest
RP2D	Recommended Phase 2 Dose
SAE	Serious adverse event
SD	Stable disease
SMA	Smooth Muscle Actin
SPECT	Single photon emission computerised tomography
SUSAR	Severe Unexpected Serious Adverse Reaction
TAH	Total Abdominal Hysterectomy
TDS	Three times daily
TE	Transverse Echo Time
TGF	Transforming Growth Factor
TNF	Tumour Necrosis Factor
TR	Transverse Relaxation Time
ULN	Upper Limit Of Normal
UPENN	University of Pennsylvania
U/S	Ultra-sound
UTI	Urinary Tract Infection
VDA	Vascular Disruptive Agent
v_e	Volume of EES per unit volume of tissue = K^{trans}/k_{ep}
VEGF	Vascular Endothelial Growth Factor
VMI	Vascular Maturation Index
VSMC	Vascular Smooth Muscle Cell
WBC	White blood cells
wCV	Within Patient Coefficient Of Variation
WHO	World Health Organisation
wSD	Within Patient Standard Deviation
ZD6126	Vascular Disruptive Agent

List of Tables

Chapter 1 – Introduction

Chapter 2 - A Phase Ib Trial of Radioimmunotherapy with ^{131}Iodine-Labelled A5B7 Anti-CEA Antibody in Combination with Combretastatin-A4-Phosphate In Advanced Gastrointestinal Carcinomas.

Chapter 3 - Interpatient & Intrapatient Variability of DCE-MRI Response Following Infusion of CA4P

Chapter 4 - A5B7 Study Liver Perfusion CT Analysis

Chapter 5 – MRI Cardiac Output Analysis Following CA4P

Chapter 6 - A Phase Ib trial of CA4P in Combination with Carboplatin and/or Paclitaxel Chemotherapy in Patients with Advanced Cancer

Chapter 7 - Relationship Between Human Tumour Angiogenic Profile And Combretastatin-Induced Vascular Shutdown – An Exploratory Study

Chapter 8 - Appendices

List of Figures

Chapter 1 – Introduction

Chapter 2 - A Phase Ib Trial of Radioimmunotherapy with ^{131}Iodine-Labelled A5B7 Anti-CEA Antibody in Combination with Combretastatin-A4-Phosphate In Advanced Gastrointestinal Carcinomas.

Chapter 3 - Interpatient & Intrapatient Variability of DCE-MRI Response Following Infusion of CA4P

Chapter 4 - A5B7 Study Liver Perfusion CT Analysis

Chapter 5 – MRI Cardiac Output Analysis Following CA4P

Chapter 6 - A Phase Ib trial of CA4P in Combination with Carboplatin and/or Paclitaxel Chemotherapy in Patients with Advanced Cancer

Chapter 7 - Relationship Between Human Tumour Angiogenic Profile And Combretastatin-Induced Vascular Shutdown – An Exploratory Study

Chapter 8 - Appendices

Chapter 1 - Background Information

Introduction

Targeted drug therapies fall into two categories; agents which act against cell surface receptors and second messenger signalling systems, or against tumour vasculature - Vascular Disrupting Agents (VDAs) or antiangiogenic agents (Chaplin et al., 2006; Cooney et al., 2006; Gaya & Rustin, 2005; Lippert, 2007) (Rhee & Hoff, 2005). VDAs act against pre-existing vasculature, whilst antiangiogenic agents prevent new vessel formation. These agents compliment conventional cytotoxic agents and radiation, and are currently being integrated into clinical practice.

Angiogenesis & VDAs

In 1971 Judah Folkman first proposed that tumour growth required the formation of new vasculature, and that blockage of this process could provide novel anti-cancer therapies (Folkman, 1971).

Tumour angiogenesis is under dynamic regulation by stimulatory and inhibitory factors released by tumour and host cells. Tumours can grow to about 1mm without neoangiogenesis by obtaining oxygen and nutrients through diffusion from surrounding tissues (Hanahan & Folkman, 1996). For further growth they must acquire an angiogenic phenotype. Angiogenesis involves several processes including proliferation of endothelial cells, proteolytic degradation of the extracellular matrix and migration of endothelial cells, leading to the formation of a functioning vessel with a lumen (Risau, 1997). VDAs selectively block or destroy the pre-existing blood vessels of tumours, leading to rapid vascular shutdown, and thereby killing tumour cells by depriving them of oxygen and nutrients. VDAs exploit the known differences between the vascular endothelium and basement membranes of tumours and normal tissues (Morikawa et al., 2002) (**Table 1.1**).

Table 1.1 - Differences Between Tumour And Normal Vasculature (Kakolyris et al., 2000)

Vessel tortuosity
Thin walled and fragile
Increased Interstitial Pressure within tumour
Immunohistochemical immaturity
Increased permeability
Variable flow rates & vascular density
Poor vascular smooth muscle & pericyte coverage
Poor lymphatic drainage
Constant vascular remodelling
Abnormalities of endothelial cell and pericyte structure and function

Two classes of VDA are being developed: Biological or ligand-directed VDAs, which use antibodies or peptides to target toxins or pro-coagulants to the tumour endothelium; and the small molecule VDAs (**Figure 1.1 & Table 1.2**). Both types produce a characteristic pattern of central necrosis, leaving a peripheral rim of viable tumour cells (Blakey et al., 2002; Ching et al., 1999; Huang et al., 1997; Thorpe et al., 2003; Tozer et al., 2002) (**Figure 1.2**) .

Biological VDAs	
Antibody – TF	Induces coagulation
Anti – VCAM1 – TF	Induces coagulation
L19 scFv – TF	Targets fibronectin
VEGF – Gelonin	Plant toxin
Anti – Endoglin – Ricin A	Antibody – Toxin
Anti – TES-23 – Neocarzinostatin	Antibody – Cytotoxic
L19 scFv – IL12	Antibody – Cytokine
L19 scFv – TNFα	Antibody – Cytokine
Anti – PS	Antibody
Targeted ATPᵘ - *Raf* gene	Blocks signalling
Flk – 1 fused to Fas	Induces apoptosis
Small Molecule VDAs	
CA4P (Combretastatin A4 Phosphate)	Prodrug of CA4
ZD6126	Prodrug of N-acetylcolchinol
AC7700 (AVE8062A)	Combretastatin analogue
Oxi4503 (Combretastatin A1 Phosphate)	Prodrug of CA1
TZT-1027	Synthetic derivative of dolastatin 10
DMXAA	Flavonoid

Table 1.2 - Current Vascular Disrupting Agents in Development (Thorpe et al., 2003)

Figure 1.1 - Chemical Structure of Selected Small Molecule VDAs

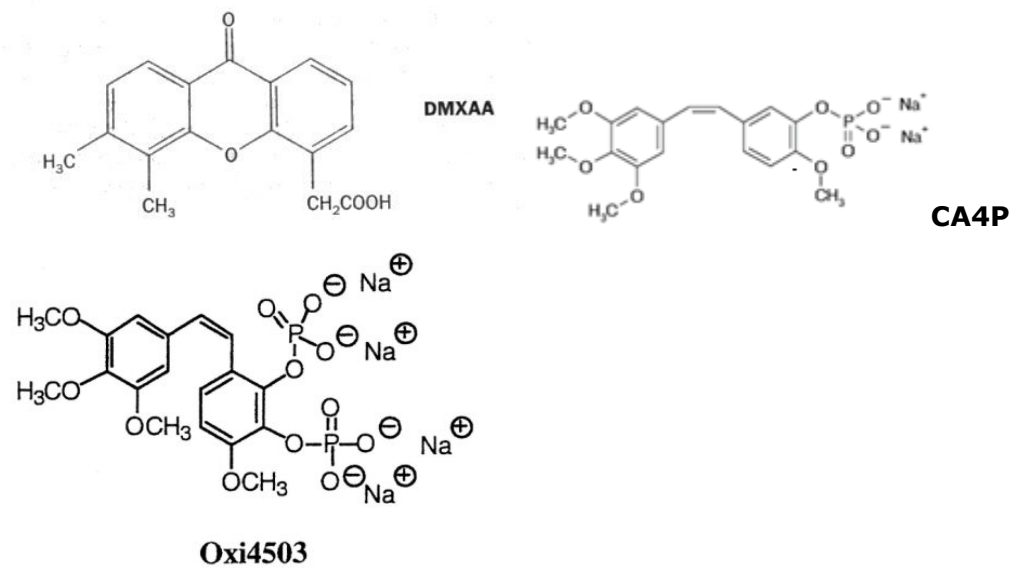

Figure 1.2 - VDA Tumour Effect (N=central necrosis, V=viable tumour cells at periphery) Courtesy of Dr Gill Tozer

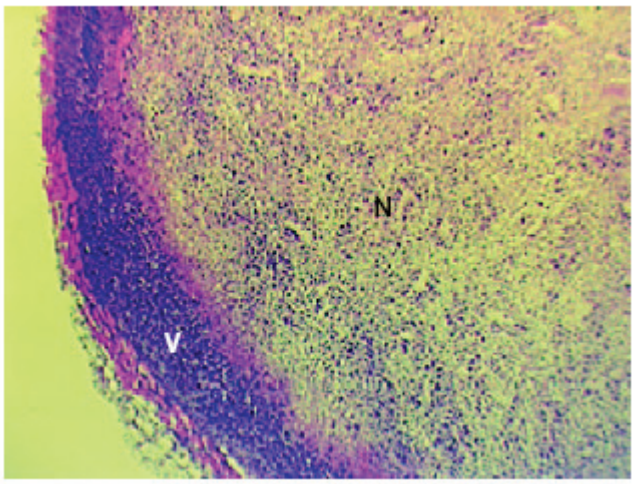

Advantages of VDAs

There are a number of potential advantages of VDAs over other classes of anticancer drug. There can be a significant bystander effect to vascular shutdown as one single vessel may provide oxygen and nutrients for thousands of downstream tumour cells. The endothelial cell itself does not need to be killed by the VDA – a change of structure or local initiation of the coagulation cascade may be all that is needed. As the endothelium comprises normal untransformed cells, it is unlikely to become drug resistant by genetic alteration (Boehm et al., 1997). The endothelium has a very slow turnover, with 99.9% of endothelial cells being quiescent at any one time. However, it has already been shown that some tumours can form luminal blood vessels lined with tumour cells and devoid of endothelium entirely

(Folberg et al., 2000; Griggs et al., 2001a; Maniotis et al., 1999; McDonald et al., 2000). VDAs do not need to exert their effects for long. One study suggested that greater than 99% of tumour cells *in vivo* can be eradicated within a 2 hour period of ischaemia (Chaplin & Horsman, 1994), although other studies suggest longer periods of ischaemia are required.

Ligand-Directed VDAs

Vascular endothelial cells in different tissues express unique surface markers, and so the development of drugs to selectively target tumour endothelium is gathering pace (Thorpe, 2004). The result may be thrombosis within tumour vasculature caused by direct injury or apoptosis, initiation of an immune attack on the tumour vasculature, or a change of conformation of the tumour endothelium, which leads to occlusion of tumour vessels.

Small Molecule VDAs

Flavonoids

Flavone acetic acid (FAA) was originally synthesised as a non-steroidal anti-inflammatory agent, but was found to have widespread anti-cancer effects in pre-clinical studies (Smith et al., 1987), inducing haemorrhagic necrosis within animal tumours (Corbett et al., 1986). Unfortunately, it was inactive in human clinical trials (Kerr & Kaye, 1989). DMXAA(5,6 – dimethylxanthenone-4-acetic acid) was developed as a more active analogue(**figure 1.1**), and is twelve times more potent (Rewcastle et al., 1991).

DMXAA

DMXAA induces vascular shutdown in murine tumours within 30 minutes of administration (Lash et al., 1998) and apoptosis in tumour endothelial cells (Ching et al., 2002). There is a dose dependent increase in plasma 5HT, released by platelets in response to the vascular damage (Baguley et al., 1997). DMXAA induces synthesis of TNF and nitric oxide(NO) in plasma and tumour tissue (Ching et al., 1999; Thomsen et al., 1991). FAA, unlike DMXAA, cannot induce synthesis of TNF in cultured human cells in vitro, and this may explain why FAA was inactive in human phase I trials (Philpott et al., 2001).

DMXAA damages tumour vascular endothelium, causing DNA strand breaks and the induction of apoptosis (Ching et al., 2002). The exact molecular target is unknown, but its action involves pathways leading to upregulation of the nuclear transcription factor NFκB (Ching et al., 2002) which leads to production of TNF and other cytokines. There is a rapid reduction in tumour blood flow and an increase in 5HT which is a marker for vascular

damage (Lash et al., 1998; Zwi et al., 1994). 5HT is probably released from platelets, and is a likely factor required for the vascular effect of DMXAA as the serotonin inhibitor cyproheptadine reduces the degree of induced haemorrhagic necrosis. Following this, TNF production is induced which mediates the anti tumour effects of DMXAA and probably its toxicity. Antibodies to TNF can prevent the reduction in blood flow caused by these agents (Mahadevan et al., 1990), and tumour growth delay is shorter in mice with an inactivated TNF gene.

NO induces vascular smooth muscle relaxation, which actually improves blood flow to the tumour. It also increases vascular permeability, which increases the effect of TNF and 5HT (Moilanen et al., 1998). The balance of these two opposing forces depends on where NO is released. Local increase within tumour tissue increases the vascular permeability and anti vascular effect in contrast to systemic release which leads to vasodilatation. It is still unclear whether DMXAA induces nitric oxide production in human tumour tissue.

Clinical Trials of DMXAA

Phase I trials in patients with advanced cancer were conducted in parallel by Cancer Research UK in New Zealand and the UK (Jameson et al., 2003; McKeage et al., 2006; Rustin et al., 2003a). In the UK study 46 patients received 247 twenty-minute weekly infusions of DMXAA over 15 dose levels ranging from 6 – 4900mg/m^2. In New Zealand, 63 patients received DMXAA every 3 weeks also as a twenty-minute infusion. Reversible DLT at 4900mg/m^2 was neurological – tremor, anxiety, visual disturbance, urinary incontinence and expressive dysphasia. There was also an episode of left ventricular failure in one patient. The drug was otherwise well tolerated; the most frequent side effects were visual disturbance, tumour pain, nausea, vomiting, headache, hypertension and malaise. There was no significant haematological toxicity. MTD was 3700mg/m^2.

Brief partial responses were seen in a patient with metastatic melanoma at 1300mg/m^2, and a patient with metastatic cervical carcinoma at 1100mg/m^2. DMXAA was highly protein-bound to albumin(>99%) until saturation occurred at higher doses, leading to a rapid increase in the free fraction (up to 20%) and greater concentrations of DMXAA bound to non-albumin proteins. The main determinant of the non-linearity of the PK appeared to be sequential saturation of elimination mechanisms, including hydroxylation and glucuronidation (Jameson M 2000; Jameson et al., 2007; McKeage et al., 2006). Terminal elimination half-life was 8.1±4.3h. At doses of DMXAA ranging from 500 – 4900mg/m^2, evidence of reduction in tumour blood flow was seen with DCE-MRI (Galbraith et al.,

2002b; Zhao et al., 2005). There was also a dose-dependent increase in the plasma concentration of 5-hydoxy indole acetic acid(5-HIAA), which is the measurable metabolite of 5HT, at DMXAA dose levels of 650mg/m^2 and above, which correlated with the MRI findings. There were no consistent dose-dependent increases in plasma nitrate or TNFα, however the finding of elevated TNF in tumour biopsies suggests that DMXAA actions are predominantly local (M Jameson,personal communication,2003).

It is too early to know if there is sufficient local TNF induction after tolerable doses of DMXAA to induce tumour regression in humans when given alone. The way forward is to try combination therapy with DMXAA (Cliffe et al., 1994; Lash et al., 1998; Lippert, 2007; Pruijn et al., 1997; Wilson et al., 1998). Pedley et al (Pedley et al., 1996; Pedley et al., 1999) have demonstrated cure of human colorectal tumour xenografts in mice treated with a combination of DMXAA and radioimmunotherapy at a dose of DMXAA that produced no growth delay as a single agent.

The visual toxicities of DMXAA such as blurring, colour disturbance and photophobia are thought to be due to inhibition of phosphodiesterase type 6 (PDE6), which exists exclusively in the retina. DMXAA has been shown to inhibit this enzyme *in vitro* at therapeutic concentrations (Jameson et al., 2003). In the UK study, all patients receiving ≥1750mg/m^2 experienced some disturbance of colour vision(usually mild) following infusion.

DMXAA is currently in Phase II clinical trials for the treatment of prostate cancer (sponsored by Antisoma Research; AS1404). In this trial a DMXAA/docetaxel regimen is being compared with docetaxel alone. DMXAA is also undergoing three additional Phase II clinical trials in combination with carboplatin and paclitaxel for the treatment of lung, ovarian, and prostate cancer.

Tubulin Binding Agents

Spindle poisons such as colchicine and vinblastine disrupt tumour vasculature only at doses close to their MTD, which has prevented their use as VDAs. Newer agents have since been developed which have a much wider therapeutic window such as Dolastatins and Combretastatins (Chaplin et al., 1996). Vessels with low flow rates may be particularly sensitive to VDAs, as they will have longer to act and are more likely to induce thrombosis.

The increased proliferative activity of tumour endothelium renders it more susceptible to the anti vascular effects of these agents (Galbraith et al., 2001; Griggs et al., 2001c).

VDAs act near the colchicine binding site on the β-subunit of endothelial cell tubulin, resulting in depolymerisation of microtubules and disorganisation of actin and tubulin. Endothelial cells are particularly reliant on the cellular cytoskeleton to maintain their elongated shape. A rapid change in endothelial cell shape (Galbraith et al., 2001) causes micro vessel blockage and loss of flow; it also disrupts the endothelial cell layer, exposing the basement membrane and increasing tumour vascular permeability. This leads to high interstitial pressures, vessel congestion and further loss of flow (**Figure 1.3**). Exposure of the basement membrane may also lead to induction of the coagulation cascade and local thrombus formation. Newly formed endothelial cells in tumour vessels are more sensitive to anti tubulin drugs because mature cells have a highly developed actin cytoskeleton which maintains cell shape despite depolymerisation of the tubulin cytoskeleton (Chaplin & Dougherty, 1999).

Figure 1.3 - Mechanism of Vascular Shutdown (Tozer et al., 2005)

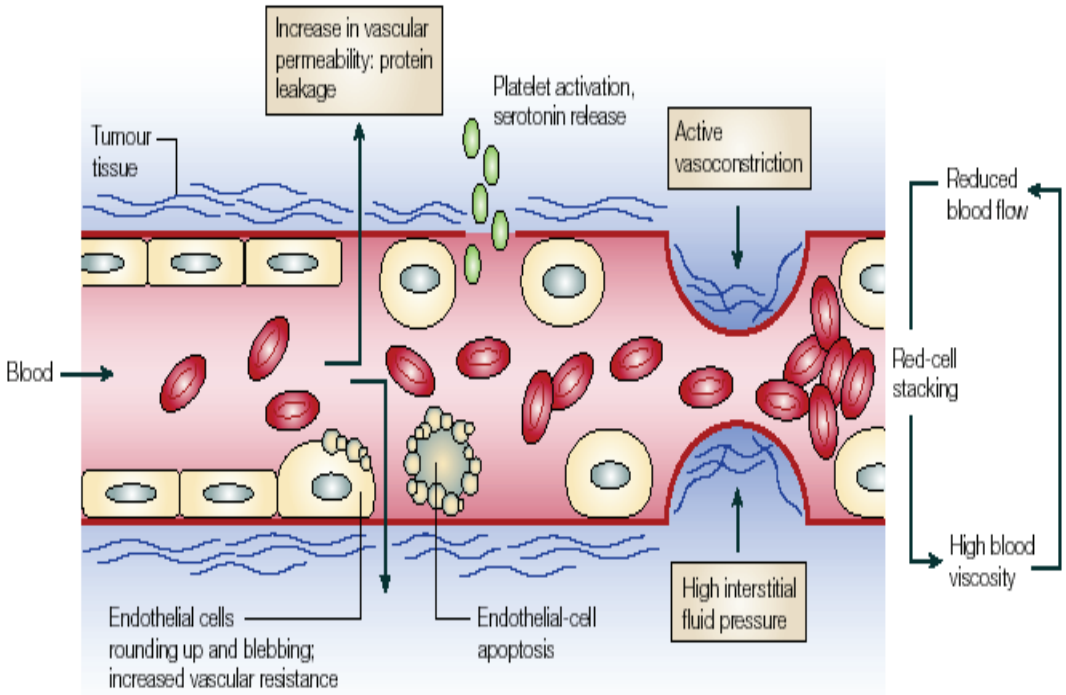

Combretastatin A4 Phosphate

Combretastatin-A4(CA4) [*cis*-1-(3,4,5,-trimethoxyphenyl)-2-(4'-methoxyphenyl) ethene-3'-0-phosphate, disodium salt] was originally isolated from the bark of the African Bush Willow *Combretum Caffrum* and binds much more avidly than colchicine to tubulin (Lin et al., 1989;

Pettit et al., 1989; Pettit et al., 1995). CA4P is the synthetic water-soluble prodrug of CA4. Light promotes isomerisation to the less active *trans*-CA4 form of the drug, so it is stored and administered protected from light. The exact mechanism of action of CA4 is unknown, but it induces apoptosis rather than necrosis indicating that intracellular signalling pathways are involved (Iyer et al., 1998). The morphological changes induced by CA4, including cell retraction and membrane blebbing, involve reorganisation of the actin cytoskeleton, leading to the formation of actin stress fibres and focal adhesions. Specific cell signalling pathways linking the actin and tubulin cytoskeleton entail activation of the GTP binding protein RHO (Dachs et al., 2006; Kanthou & Tozer, 2002)(**Figure 1.4**).

Figure 1.4 - Proposed Molecular Mechanism of CA4P Action (Tozer et al., 2005)

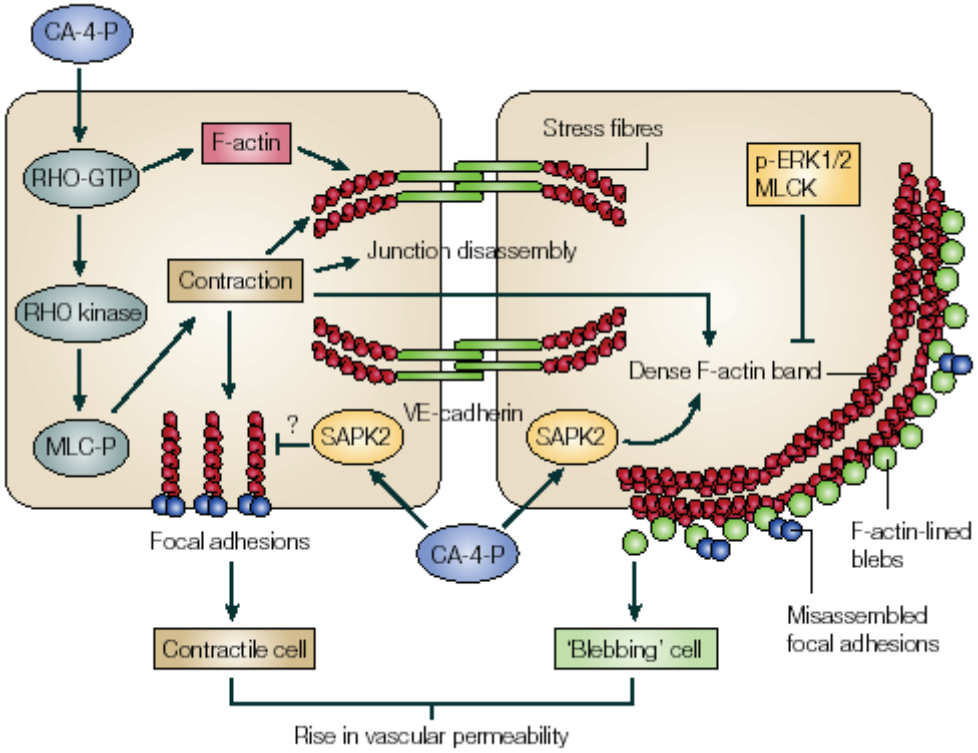

The endothelial cell shape changes induced by CA4 can be reversed on drug removal *in vitro* (Galbraith et al., 2001). The irreversibility of the effects of colchicine and vinblastine on tubulin is one explanation of why these drugs primarily have effects on long-term processes like cell division, which takes place over many hours. At doses that cause vascular effects in the tumour, colchicine and vinblastine induce a profound inhibition of rapidly proliferating stem cell populations in critical normal tissues. The reduced toxicity of CA4P can be attributed to its reversible effects on tubulin as well as its rapid clearance from the plasma and tissues(Hill et al., 2002b).

CA4P Preclinical Studies

Studies in mice have shown that a single administration of CA4P does not significantly affect tumour growth (Chaplin et al., 1999; Grosios et al., 1999; Grosios et al., 2000), however repeated doses can result in substantial growth delays (Griggs et al., 2001b). In all studies the effect of CA4P was seen as haemorrhagic necrosis. Further studies (Dark et al., 1997; Horsman et al., 1998) support the hypothesis that CA4P causes rapid vascular collapse and shutdown leading to haemorrhagic necrosis. Acute anti vascular effects are seen at about 10% of the MTD (Dark et al., 1997). Tumour blood flow reduction is rapid and can drop to 1% of the starting value as soon as one hour after administration, accompanied by increased vascular permeability (Tozer et al., 2001). Animal DLT was gastrointestinal haemorrhage or ulceration. In rats, 360 mg/m^2 caused severe toxicity or death in 10%

Histological studies as well as DCE-MRI show that the anti vascular effects of CA4P are restricted to the core of the tumour, leaving viable tumour cells at the periphery which rapidly regrows (Beauregard et al., 1998). The drug caused a 100 fold decrease in blood flow to p22 carcinosarcomas, with a much smaller reduction in blood flow to spleen, skeletal muscle and brain. No significant reduction was observed in heart, kidney and intestine (Tozer et al., 1999).

The change in tumour blood flow after administration of CA4P is much greater than that seen with drugs affecting systemic haemodynamics. Limited changes in tumour blood flow in rats have been seen with hypertensive agents such as angiotensin II (Tozer & Shaffi, 1993), but only at doses that caused much larger changes in systemic blood pressure and heart rate than CA4P. Also, larger reductions were seen in normal tissue blood flow. Reduced tumour blood flow has also been observed after treatment with high doses of the vasodilator hydralazine (Horsman et al., 1992), which reduced systemic blood pressure by 50%. This evidence indicates that changes seen after CA4P are due to a direct effect on local tumour vasculature rather than systemic effects such as change in cardiac output(CO). There may be tissue specific differences in CA4P vascular response. The haemodynamic changes seen after CA4P probably reflect a response to increased peripheral vascular resistance in a range of tissues. The lack of effect on stroke volume indicates that CA4P has no direct effect on the heart (Anderson et al., 2003). Microtubule depolymerisation is known to affect vasomotor tone and peripheral resistance – the changes in heart rate and BP possibly reflect this as well. The effect of CA4P on CO is studied in **Chapter 5**.

CA4P Phase I Studies

Three Phase I trials of CA4P in humans investigated three different dose schedules based on toxicity data from animals (Dowlati et al., 2002): 1) Case Western Reserve University, Cleveland, OH(CWRU), 2) University of Pennsylvania, Philadelphia, PA(UPENN), and 3) London, United Kingdom at Mount Vernon and Hammersmith Hospitals . A small unpublished study was also performed by Bristol Myers Squibb (**Table 1.3**).

Table 1.3 - Phase I Trials of CA4P

	UK CRC PH1/066(Rustin et al., 2003b)	UPENN CA4P-102(Stevenson et al., 2003)	CWRU CA4P-101(Dowlati et al., 2002)	BMS CA178 - 002
Schedule	Weekly x 3 every 28 days	Daily x 5 every 21 days	Single dose every 21 days	Initially a single dose every 21 days then changed to weekly x 3 every 28 days
Infusion Time	10 mins	10 mins	10 mins 60 mins in 7 pts at 54 mg/m^2	10 mins
Number Pts	34	37	25	18
CA4P Dose Range	5 – 114 mg/m^2	6 – 75 mg/m^2	18 – 90 mg/m^2	30 – 70 mg/m^2
DCE-MRI	Yes	Yes	Yes	No
PET	Yes	No	No	Yes
MTD (per dose)	68 mg/m^2	75 mg/m^2	60 mg/m^2	70 mg/m^2
DLT	Ataxia Motor neuropathy Syncope Diplopia Tumour pain Dyspnoea	Tumour pain Sensorimotor neuropathy Syncope Dyspnoea	Cardiac ischaemia Dyspnoea	Tumour pain Cardiac ischaemia
Recommended Ph. 2 Dose	52 – 68 mg/m^2	52 mg/m^2	≤60 mg/m^2	-
No. Doses of CA4P given	167	700	104	-
Terminal half life CA4P (hr)	0.489	0.36	0.47	-
Terminal half life CA4 (hr)	2.23	3.3	4.26	-

The UK trial (Anderson et al., 2003; Galbraith et al., 2003; Rustin et al., 2003b) used a 10 minute weekly infusion of CA4P for 3 weeks every 28 days, starting at 5 mg/m^2, with intra patient dose escalation and accelerated titration (Simon et al., 1997). Doses were doubled until CTC grade 2 toxicity was seen after which subsequent dose escalation was by a factor of 1.3. Thirty-four patients with advanced solid tumours received 167 infusions. The MTD was 68mg/m^2 and the recommended Phase II dose was 52 - 68mg/m^2.

Significant reductions in tumour blood flow were seen at these doses by PET and DCE-MRI (Anderson et al., 2003; Galbraith et al., 2003). Increases in neutrophil counts of mean 80% were seen 4 hours following CA4P at doses ≥55mg/m^2, corresponding with a rise in the patients' core temperature – This would be consistent with an inflammatory/cytokine response to endothelial attack by CA4P.

The UPENN trial (Stevenson et al., 2003), the most dose intense of the Phase I trials, used a 10min infusion daily for 5 days every 3 weeks. Thirty-seven patients with advanced solid tumours received 133 cycles at doses ranging from 6 – 75mg/m^2. All patients were assessable for toxicity. The MTD was 65mg/m^2 and recommended Phase II dose was 52mg/m^2.

The CWRU trial (Dowlati et al., 2002) used a single dose schedule of CA4P every 21 days using doses up to 90mg/m^2 in advanced solid tumours. Both ten-minute and sixty-minute infusion schedules were investigated. Twenty-five patients received 107 cycles of treatment (dose ranges 18 – 90mg/m^2). The MTD was 60mg/m^2.

The unpublished BMS study used single doses of CA4P 30 – 70mg/m^2 every 21 days, in 18 patients. The primary purpose of this study was to evaluate myocardial blood flow and tumour blood flow changes with PET, not CA4P pharmacokinetics and safety. Tumour blood flow decreased for all five patients by up to 78%

CA4P Pharmacokinetics (PK)

In humans CA4P is rapidly converted by endogenous phosphatases to CA4, which has a half-life of 2-10min, and an elimination half-life of 1-2h.

Pharmacokinetics of CA4P was assessed from plasma and urine for all patients in the three Phase I trials.

PK data from all three trials was in agreement that plasma AUC and plasma C_{max} of CA4P and CA4 have dose proportional linear kinetics. There was rapid dephosphorylation of CA4P to CA4 and rapid glucuronidation of CA4. There was no evidence of accumulation of CA4P over time with repeated doses.

Linear kinetics was seen in the terminal half-life and systemic clearance of CA4P across all dose levels in all studies. 58% - 67% of the dose was excreted as CA4G in the first 24 hours of urine collection. The mean plasma half-life($t_{1/2}$) across the three trials for CA4P, CA4 and CA4G were 0.4, 3.8 and 4.5 hours respectively. Volume of distribution ranged from 3.8 to 7.5 litres, and clearance ranged from 24.5 to 28.2 l/hr. C_{max}(μM) of CA4P ranged from 4.9 at 6mg/m^2 to 48.7 at 114mg/m^2. Corresponding AUC (μM/hr) for CA4P

were 1.31 and 11.6 respectively. CA4 C_{max} ranged from 0.31 at 6mg/m^2 to 4.2 at 114mg/m^2 with corresponding AUC of 0.24 and 2.49 respectively.

CA4P Toxicity (Non Dose Limiting)

Across all three studies, adverse events were generally mild and manageable, and very different from the usual cytotoxic effects of alopecia, myelosuppression, nausea and mucositis. No significant haematological toxicity was seen in any of the studies. Cardiotoxicity was reported in one study.

In the UK study the only drug related toxicity seen up to 40mg/m^2 was grade 1 tumour pain in 35% of infusions. It is not clear whether this pain relates to tumour ischaemia or to acute swelling of the tumour caused by alteration in endothelial cell permeability after CA4P. The most common site of pain was in the abdomen, which was the most frequent site of tumours. It was not possible to exclude mesenteric angina as a possible cause of pain in some patients. Median time to onset of tumour pain was 40min from the start of the CA4P infusion (range 2min to 10h, duration 1 – 180min). Other side effects were mainly cardiovascular – tachycardia (53%), hypertension (35%), hypotension (30%), bradycardia (24%), fatigue (23%), nausea (21%), visual disturbance (9%) and dyspnoea (6%). Mean increase in blood pressure at doses ≥52 mg/m^2 was 8–10% over the first hour followed by a mean decrease in blood pressure of 6-7%, most obvious at four hours.

Toxicity in the UPENN and CWRU studies was very similar to the UK experience. Tumour pain did not appear to correlate with either clinical response or DCE-MRI parameters, and appeared more common following the 60-minute infusion schedule. Gastrointestinal side effects were considered to be the DLT in animals. Whilst GI side effects were common in the human phase I trials, they were usually mild.

A wide range of neurological effects were seen mainly at the higher doses. Effects such as perineal and perirectal paraesthesia, peripheral neuropathy, visual blurring, diplopia, ataxia and leg weakness were seen; they were transient, mild and self-limiting at lower doses.

CA4P DLT

In the UK study, four DLTs were reported. The first was a grade 3 vasovagal episode that occurred on the patient's second dose (88mg/m^2). This began 4½ hours following CA4P

and lasted three minutes. The patient recovered fully with supportive treatment. It is possible that an early swelling of this patient's neck mass might have contributed to the vasovagal episode by compressing the carotid body. There were two cases of transient and reversible grade 2 ataxia at 114mg/m^2. Upon reducing the dose back to 88mg/m^2 there was an episode of reversible grade 4 ataxia, grade 3 diplopia and grade 3 leg weakness in one of the patients who experienced ataxia at the higher dose level. The final DLT in this study was an episode of grade 4 small bowel ischaemia at 52mg/m^2, which led to the patient's death. Autopsy revealed small bowel ischaemia was confined to a previously treated radical radiation field, which contained evidence of late radiation fibrosis and small vessel damage. The patient's tumour also involved the mesentery of the affected bowel segment. Concern that normal tissue vasculature might be compromised by previous radical radiotherapy has led to patients who have received radical radiotherapy being excluded from future CA4P trials.

In the CWRU study, four DLTs were also reported: Dyspnoea at 90mg/m^2 in a patient with ovarian cancer and pleural involvement, and stridor and apnoea at 60mg/m^2 in a patient with advanced thyroid cancer. The third and fourth DLTs were cardiac, and will be discussed below.

In the UPENN study, there were also four DLTs. Two episodes of grade 3 tumour pain at 75 mg/m^2, transient and reversible grade 3 hypoxia, and grade 4 dyspnoea. This patient had poor lung function at baseline and had been requiring home oxygen therapy. Lastly, there was an episode of syncope, secondary to dehydration-induced grade 2 hypotension and grade 3 hypoxia also at 75 mg/m^2.

CA4P Cardiotoxicity

Significant cardiotoxicity was only reported in the CWRU Phase I trial (the least dose intense regimen). This was probably related to chance or patient selection. Cardiovascular effects such as transient hypertension, hypotension, tachycardia or bradycardia were seen in all three studies.

In the CWRU trial, two cases of cardiotoxicity were reported at 60mg/m^2 and one at 90mg/m^2. The first patient (60 mg/m^2) was a diabetic with known ischaemic heart disease, although this was not initially disclosed. The patient's screening ECG revealed a QTc interval in excess of 450ms. Shortly after CA4P he experienced shoulder and neck pain,

followed by bradycardia and hypoxia. He was treated with opiate analgesia and oxygen. Approximately 90min later he developed stridor, lethargy, sinus tachycardia, ventricular arrhythmia and dizziness, and after 3h, apnoea. Naloxone was given successfully to reverse the effects of opiate toxicity. The following day the patient's QTc interval peaked at 533ms, most likely due to hypomagnesaemia, hyperglycaemia and myocardial ischaemia (T-wave changes on ECG). Cardiac enzymes remained within normal limits. Post mortem examination several weeks later revealed metastatic carcinoma within the heart in addition to the known ischaemic disease.

The second cardiac event occurred in a male with a long history of hypertension, on triple antihypertensive therapy. The patient was hypomagnesaemic and bradycardic at baseline, so their β-blocker was stopped. The following morning the patient's BP rose as high as 210/88, and following CA4P 229/95. Approximately 90min post CA4P, ECG revealed ST segment depression, and an hour later there was evidence of myocardial infarction associated with raised serum troponin. It was subsequently shown that the patient's ejection fraction had declined prior to the study from 60% (eight months before) to 42% (post CA4P) and ischaemic heart disease was also diagnosed. Abrupt cessation of β-blockers has been previously documented to cause MI (Astra Zeneca Pharmaceuticals (Macclesfield).

The third cardiac event occurred at 90mg/m^2, one hour following the second infusion of CA4P. The patient had ischaemic ECG changes and underwent immediate cardiac angiography, which revealed minimal occlusion of the distal left anterior descending coronary artery. There was no rise in cardiac enzymes, and the ECG normalised within a few hours. His only cardiac risk factor was smoking.

CA4P ECG Repolarisation (QTc) Effects

In vitro ion channel studies have demonstrated that CA4P and CA4 are weak inhibitors of the HERG potassium channel, and CA4P is also a weak inhibitor of the L-type calcium channel. CA4 decreased the action potential duration (APD) and CA4G increased the APD by less than 20% in rabbit Purkinje fibres at a concentration of 30μM. The human PK data indicates that plasma concentrations of CA4P, CA4 and CA4G are well below these levels and should not have any significant clinical safety effects (Young & Chaplin, 2004). In all three Phase I studies, ECGs were performed hourly for 6h and at 24h following CA4P.

ECGs were analysed centrally, and both Bazett's(QTcB) and Fridericia's(QTcF) formulae were used (Bazett, 1920; Fridericia, 1920).

There was inconsistency of QTc results between the three studies. In the CWRU study, there were significant increases in QTc interval at the 3h (27.2ms, $p<0.0001$) and 4h (30.8ms, $p<0.0001$) time points (Cooney et al., 2004). Three of 25 patients had prolonged QTc intervals at baseline, whereas 15 (60%) of 25 and 18(75%) of 24 patients had prolonged QTc interval at 3 and 4 hours. The slope of HR and QTc increasing as a function of time during the first 4 hours was correlated to dose of CA4P ($p=0.005$, $r=0.55$ for QTc) and also to CA4 AUC ($p=0.02$, $r=0.44$ for QTc). No patients had a QTc >500ms, and no patients' QTc increased more than 25% over baseline (Cooney et al., 2004).

In the UK study, two patients had a mean QTc prolongation of ≥30ms, but less than 60ms. This study used doses as high as 114mg/m^2 CA4P. The UPENN study, the most dose intensive Phase I trial, showed mean increases in QTcB of >20ms at Day 1 hours 3-4 at 56mg/m^2, and Day 1 hour 4 at 75mg/m^2.

In conclusion, there may be a dose dependent prolongation of QTc interval at doses ≥56mg/m^2, but the data should be interpreted with caution due to the variable time points of the data collection, large standard deviations, small sample sizes and lack of control groups.

CA4P Anti-tumour Activity

Significant clinical benefit from single agent CA4P was not anticipated. In the UK study, one patient with metastatic adrenocortical carcinoma had an unmaintained partial response of their liver metastases to therapy. The tumour shrank by 51% however this effect was not sustained for long enough to be classified a partial response.

In the UPENN study, one patient with lung metastases from a fibrosarcoma had a partial response at 56mg/m^2, and 14 patients showed stable disease over 3–29 cycles of CA4P. One patient with metastatic medullary thyroid carcinoma received 29 cycles of CA4P with stable disease and no cumulative toxicity.

In the CWRU study, one pathological and radiological complete response was observed in a patient with metastatic anaplastic thyroid cancer (60mg/m^2) who received eight cycles of therapy, with the patient disease free 48 months later. Two further patients, one with metastatic colorectal cancer (24 cycles over 19 months at 60mg/m^2) and another with advanced medullary thyroid cancer (15 cycles over 12 months at 50mg/m^2) both had prolonged responses to therapy of >12 months. One patient with metastatic kidney cancer had stable disease for 6 months on 18mg/m^2.

CA4P Recommendations

Since these studies completed, it has been recommended that patients with a history of ischaemic heart disease, myocardial infarction, uncontrolled hypertension, arrhythmias, clotting disorders, or patients who have previously received radical doses of radiation therapy should not receive CA4P.

Rat data shows that CA4P induced hypertension can be effectively controlled with prophylactic antihypertensive therapy, and that these agents do not alter the effects of CA4P on tumour blood flow (Tozer, 2003). In the combination phase I/II studies, patients experiencing a rise in blood pressure above 160/100 following the first dose of CA4P are given sublingual GTN, and subsequently treated with prophylactic doses of dexamethasone and amlodipine. In addition to controlling blood pressure the steroid also appears to reduce the incidence of neurological toxicity (Gordon Rustin, personal communication, 2007). It is hoped that these measures will improve the safety profile of this otherwise well tolerated drug. To date, no further significant cardiotoxicity has been reported.

CA4P DCE-MRI Assessment

In the UK trial, changes in kinetic DCE-MRI parameters K^{trans}, v_e, k_{ep} and $IAUGC_{60}$ over 24 hours after treatment with CA4P were measured in 18 patients, and compared with those obtained in the rat p22 carcinosarcoma model (Galbraith et al., 2003). A similar pattern and time course of change in tumour and normal tissue parameters was seen in rats and humans. After treatment there was a marked reduction in K^{trans} values, particularly in the centre of the tumour, with some sparing of the peripheral rim. Significant reductions were seen in tumour K^{trans} in 6 of 16 patients treated at ≥52 mg/m^2 (up to 77%), with a significant group mean reduction of 37% and 29% at 4 and 24 hours respectively after treatment. The reduction in K^{trans} showed evidence of a dose effect, with the magnitude of

reduction correlating with an increase in CA4 AUC. No change was seen in muscle or kidney parameters.

In the CWRU study, seven patients underwent DCE-MRI at 60mg/m^2. A significant decrease in the gradient peak signal intensity, consistent with a decrease in tumour blood flow, was seen in six out of the seven patients 4 – 6h post CA4P. In the UPENN study, 8 of 10 evaluable patients had decreases in K^{trans} values. Three patients demonstrated a marked loss of perfusion following CA4P. There was a more consistent pattern of alteration in tumour leakage space (v_e) after CA4P, with 7 of 10 patients demonstrating a decrease in assessable volume fraction of ≥10%.

The MRI data should be interpreted with caution due to the small numbers of patients, the wide variety of tumour types, and the fact that the imaging techniques were being altered and fine tuned during the course of the studies. Current ongoing CA4P studies are also using these techniques and will increase the volume of data available on the use of DCE-MRI in assessing tumour perfusion.

ZD6126

ZD6126 (Astra Zeneca, Macclesfield,UK) is rapidly converted by serum phosphatases to N-acetylcolchinol(NAC), a tubulin binding agent that inhibits tubulin polymerisation and causes microtubule destabilisation. ZD6126 disrupts endothelial cell morphology in a similar manner to CA4P. ZD6126 has significant anti tumour activity against a broad range of human xenografts in rodent models (Blakey et al., 2002; Davis et al., 2002). The vascular targeting activity of ZD6126 was seen at doses 1/8 to 1/16 of the MTD, and was selective for tumour blood vessels (Blakey et al., 2002; Davis et al., 2002).

In Phase I clinical trials (Beerepoot et al., 2006; DelProposto Z 2002; Gadgeel SM 2002; LoRusso S, 2001; Radema SA 2002; SC, 2002; Thorpe et al., 2003), illustrated in **Table 1.4**, stable disease lasting 4 or more cycles was seen in three patients, and one patient had a minor response lasting 19 cycles. Radema et al reported vascular damage in 4 of 5 patients 4 – 6h post infusion of ZD6126, indicated by a doubling of circulating endothelial cells, which were viewed as a surrogate marker for vascular damage (Radema SA 2002). Adverse events seen include hypokalaemia, anorexia, constipation, dyspnoea, fatigue, headache, nausea, pain and vomiting. One patient had asymptomatic, reversible, grade 2 ischaemic changes on ECG and grade 3 elevation of Troponin I, with subsequent demonstration of

coronary artery disease (Gadgeel SM 2002). Two other patients developed transient reversible declines in left ventricular ejection fraction(LVEF). Two patients with undiagnosed brain metastases developed symptoms of raised intracranial pressure shortly after treatment (Radema SA 2002).

In the largest study (Beerepoot et al., 2006), one patient treated at 10mg/m^2 with a history of ischaemic heart disease experienced acute myocardial infarction two weeks after drug discontinuation. Four others had asymptomatic creatine phosphokinase elevation. DLT's at 28mg/m^2 were hypoxia from a pulmonary embolism and an asymptomatic decrease in LVEF. No antitumour responses were observed.

	(LoRusso S, 2001)	(Gadgeel SM 2002)	(Radema SA 2002)	(DelProposto Z 2002)	(Beerepoot et al., 2006)
Schedule	Single dose, q21d	Single dose, q21d	Weekly infusion	Single dose, q21d	Weekly infusion
Infusion Time	10min	10min	10min	-	10min
Number Pts	19	27	12	6	32
ZD6126 Dose Range	5 – 40mg/m^2	5 – 112mg/m^2	5 – 7mg/m^2	56 – 112mg/m^2	5 – 28mg/m^2
Elimination T1/2	2 – 3h	2 – 3h	2 – 3h	-	1 – 3h
DLT	Anaemia Cardiac Ischaemia	Anorexia, Constipation Dyspnoea, Fatigue Headache, Pain Nausea	Hypokalaemia Reduced LVEF Increase ICP with brain mets	-	Myocardial Infarction Pulm Embolism Reduced LVEF CPK-MB Increase Hypokalaemia

Table 1.4 - Phase I Trials of ZD6126

ZD6126 was in Phase II clinical trials in the United States for the treatment of metastatic renal cell carcinoma, and an additional separate trial incorporating combination therapy with oxaliplatin, 5-fluorouracil and leucovorin in metastatic colorectal cancer. Cardiac events have halted these studies.

AVE8062A (AC7700)

AVE8062A (Aventis Pharmaceuticals) is a synthetic water soluble Combretastatin analogue, which has more potent effects on tumour blood flow stasis and anti tumour effects when compared to CA4P (Hori & Saito, 2003). AVE8062A has undergone single agent Phase I trials in humans (Tolcher AW 2003), and synergism has been seen in animal models when the drug is given in combination with conventional cytotoxic agents (Vrignaud, 2004).

Nine reported patients with advanced cancer received 48 infusions of AVE8062 (4.5–30mg/m^2) weekly for 3 weeks every 28 days over 30min (Tolcher AW 2003). Asymptomatic hypotension without any other cardiac toxicity was dose limiting at 30mg/m^2. Preliminary evidence of decreased vascular flow by DCE-MRI was observed at 15.5mg/m^2. AVE8062A was rapidly eliminated with a $t_{½}$ of 15min and a clearance of 50 L/h/m^2, leading to an active metabolite, RPR258063, with a t½ of 7h.

OXi4503

OXi4503 (Oxigene Inc, Boston,MA) is the diphosphate pro-drug of Combretastatin A1(CA1). OXi4503 shows comparable effects to CA4 *in vitro*, however head to head comparisons indicate that OXi4503 is at least 10 times more potent *in vivo* when tumour vascular shutdown is used as the endpoint (Hill et al., 2002a). Over 50% of tumour blood vessels are no longer perfused 24 hours after a dose as small as 1mg/kg of OXi4503. Single dose studies indicate that the MTD in mice is similar to CA4P therefore OXi4503 has a much larger therapeutic window. Pre-clinical studies have demonstrated prolonged tumour growth retardation, regressions and even prolonged complete responses in some tumour models (Hill et al., 2002a; Malcontenti-Wilson et al., 2007; Salmon et al., 2006; Salmon & Siemann, 2006). Additional activity may be due to the rate of dephosphorylation, or the production of a quinone metabolite with cytotoxic activity (Hill et al., 2002a).

Oxi4503 commenced human Phase I trial in July 2005 (Patterson & Rustin, 2007). It was administered by 3 weekly iv infusions to a maximum of 6 cycles. Starting dose was 0.06mg/m^2. 100% dose escalation in single patient cohorts proceeded to 3.84mg/m^2, when cohorts were expanded to three patients and 30% dose escalation due to emergence of grade 2 thrombocytopaenia. Several pharmacodynamic asessments were performed prior to and after the first infusion of OXi4503 including functional MRI or PET imaging with [^{18}F]-FDG and ^{15}O-labelled water. By March 2007, 16 patients had received OXi4503 (median age 53 years). Common adverse events included pyrexia, lethargy and hypertension. Pharmacokinetic profiles show a dose-dependent linear increase in peak plasma concentrations and AUC of both OXi4503 and CA1. CA1 concentrations at 6.5mg/m^2 are close to that seen at the MTD in animals. DCE-MRI showed significant reduction in K^{trans} in one patient. Changes in standard uptake values were observed in all four patients studied with FDG-PET. H_2O-PET showed that the distribution volume of water was reduced in 3 out of the 5 metastases in one of the three patients studied. Of the

14 patients fully assessed, 3 have stable disease and 11 disease progression (Daniel Patterson, personal communication, 2007).

Combination VDA Therapy

Combined approaches can be used to target viable tumour cells remaining at the well-oxygenated peripheral rim after VDA treatment. Cells in this viable rim of tumour tissue are likely to be in a state of rapid proliferation and excellent nutrition and more susceptible to killing by conventional therapies. Additional response and delays in tumour regrowth have been seen in animal studies when CA4P is combined with 5-Fluorouracil (Grosios et al., 2000) , cisplatin, Irinotecan (Wildiers et al., 2004), Paclitaxel (Chaplin & Dougherty, 1999; Rustin GJ 2005), doxorubicin (Nelkin & Ball, 2001), radiation (Chaplin et al., 1999; Li et al., 1998; Ng et al., 2007), or radioimmunotherapy (Pedley et al., 2002; Pedley et al., 2001). Tumour cell kill by cisplatin or cyclophosphamide was enhanced 10 – 500 times by post treatment administration of CA4P and with no additional bone marrow toxicity (Siemann et al., 2002). Other groups have also reported enhancement of response or cures by combining various anticancer therapies with antiangiogenic agents or VDAs (Burrows & Thorpe, 1993; Lode et al., 1999; Mauceri et al., 1998).

Combining a VDA with radiation would allow the two treatments to act in a complementary and synergistic manner in tumours. Sequencing is vital as giving the VDA before radiotherapy could increase the hypoxic radio-resistant cell population. Giving VDAs after radiotherapy is the obvious approach at a time when vessels may be more permeable, and when prevention of radiation damage repair is most important. This approach has proven effective when combining DMXAA, CA4P and ZD6126 with radiation (Horsman & Murata, 2002; Landuyt et al., 2001; Li et al., 1998; Murata et al., 2001; Ng et al., 2007; Siemann & Rojiani, 2002; Siemann & Rojiani, 2005; Siemann & Shi, 2003; Wilson et al., 1998). The radiosensitising effects of CA4P do not appear to enhance either acute or late toxicity of radiotherapy (Murata et al., 2001).

Cures were obtained when CA4P was combined with radioimmunotherapy (Pedley et al., 2001). Single agent CA4P was initially given to nude mice implanted with SW1222 colorectal xenografts. CA4P rapidly reduced tumour blood flow by 62% at 1h and 32 – 36% from 6 – 24h after administration. This induced central haemorrhagic necrosis, however the peripheral rim continued to grow and survival was unaffected. In further studies, 7.4MBq ^{131}I-labelled anti-CEA antibody plus a single 200mg/kg dose of

intraperitoneal CA4P given 48 hours later produced cures in 5 out of 6 mice. The success of this novel approach is probably synergism between the two agents.

A phase I trial of CA4P in combination with radiotherapy in patients with advanced lung & prostate cancer is also currently recruiting patients in the UK. To date, 12 patients with NSCLC and 10 patients with prostate cancer have received 50mg/m^2 CA4P either as a single dose, or as a weekly infusion, in combination with their radiotherapy treatment, with no grade 3 or 4 drug related toxicity. The CA4P dose is due to be escalated to 63mg/m^2 (Quan Ng, personal communication, 2006 (Ng QS, 2005; Ng et al., 2007)).

Other active studies include a phase II trial of single agent CA4P in advanced anaplastic thyroid carcinoma, a phase I/II trial of CA4P in combination with doxorubicin and cisplatin in newly diagnosed anaplastic thyroid carcinoma, a phase I trial of CA4P + cisplatin in advanced or recurrent cervical cancer, a phase I/II study of CA4P in patients with age related macular degeneration, and a phase I study of CA4P with the VEGF inhibitor Bevacizumab in advanced cancer.

DMXAA when combined with Antibody Dependent Enzyme Pro-drug Therapy (ADEPT) or radioimmunotherapy in colorectal xenografts also gave significantly enhanced therapy, with no increase in systemic toxicity (Pedley et al., 1996; Pedley et al., 1999).The combination of DMXAA with Paclitaxel has been very successful, with some cures seen in animal models (Siim, 2004)..

Combining VDAs with antiangiogenic approaches is also likely to achieve a complementary tumour effect. Encouraging pre-clinical data has been seen with the combination of ZD6126 and ZD6474(antiangiogenic) (Siemann, 2004; Varghese HJ, 2004), and ZD6126 with ZD1839(Iressa) (Raben et al., 2004).

Tumour Vascular Maturity

Tumours contain a high proportion of immature blood vessels due to continuous angiogenesis and the production of high levels of pro-angiogenic growth factors by the tumour, and the surrounding stromal tissues. Neoangiogenesis is essentially a change in the balance of proangiogenic to antiangiogenic factors.

Neovascularization is tightly regulated during embryogenesis and during a variety of biological processes in adults. In response to angiogenic factors, pre-existing vessels

become dilated and supporting cells such as smooth muscle cells and pericytes detach from the vessel wall. Endothelial cells then migrate into the perivascular space by degrading basement membrane and extracellular matrix, multiply and form new vascular sprouts. Under normal circumstances, this transient proliferation phase is followed by the establishment of a stable, hierarchical vascular network. Pericytes are again recruited to the vasculature in response to growth factors such as platelet derived growth factor B (PDGF-B); these pericytes reduce endothelial cell proliferation and stabilize the newly formed vasculature (Ganss, 2006; Jain, 2003).

There is increasing evidence that pericytes, characterized as αSMA , desmin, NG2 proteoglycan or PDGFRβ positive cells, play an important role during tumour growth (Abramsson et al., 2003). Tumour pericytes are loosely associated with the endothelium, having cell processes that extend away from the vessel wall, and in contrast to their normal tissue counterparts, are sensitive to PDGF signalling (Benjamin et al., 1998; Morikawa et al., 2002). Pan-endothelial cell markers (e.g. CD31, CD34) are used to identify all vessels present in a histological section. A pericyte coverage index (PCI), can be defined as the percentage of blood vessels staining positive for αSMA or desmin.

$$PCI\,(\%) = \left(\frac{\alpha\text{SMA (or desmin) Positive Vessels}}{\text{Total Number Of Vessels}} \right) \times 100$$

PCI for most normal tissues is usually in the range 85 – 95%, however there are exceptions in angiogenic tissues such as the *corpus rubrum* of the ovary, where the PCI is ≈ 60% (Goede et al., 1998). Human tumours have an enormous range of PCI, as illustrated in **figure 1.5** (Eberhard et al., 2000). The PCI would be inaccurate if a proportion failed to stain positively for αSMA or desmin, or if partial coverage was missed in very thin, non co-planar histological sections (Morikawa et al., 2002).

Figure 1.5 - PCI For Various Human Tumour Types (Eberhard et al., 2000)

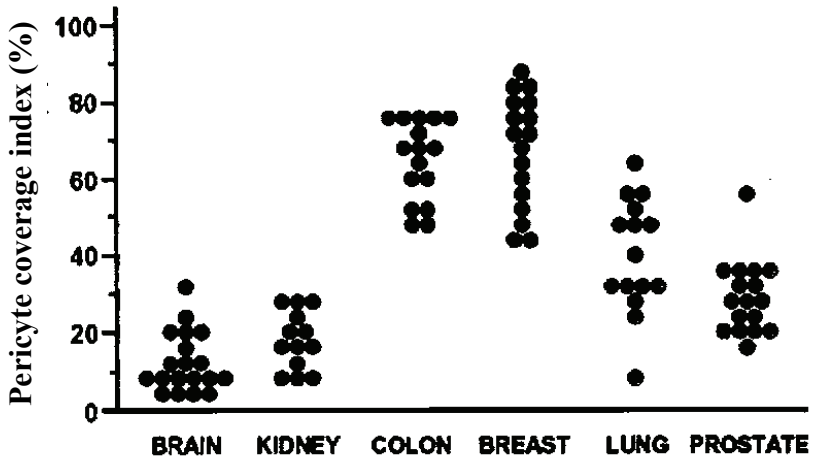

Among the pathways involved in pericyte recruitment during embryonic development, the contribution of PDGF-B and sphingosine 1-phosphate is confirmed in tumour angiogenesis. The effect of angiopoietin 1 depends on the tumour model. Transforming growth factor-β1 enhances tumour vascularization and microvessel maturation. The number of proliferating endothelial cells is reduced by half when tumour vessels are covered by pericytes (Gee et al., 2003).

Pericyte plasticity is demonstrated by their capacity to transdifferentiate into other mesenchymal cell types such as smooth muscle cells, fibroblasts, osteoblasts and adipocytes (Farrington-Rock et al., 2004). The most reliable criterion for the identification of pericytes is that they are surrounded by a basement membrane shared with EC, as demonstrated by electron microscopy (Gerhardt & Betsholtz, 2003). Pericytes are in contact with EC through discontinuities in the shared basement membrane.

In physiological angiogenesis, pericytes have multiple functions that seem to be relevant in the development and the maintenance of tumour microvasculature (**Fig. 1.6**).

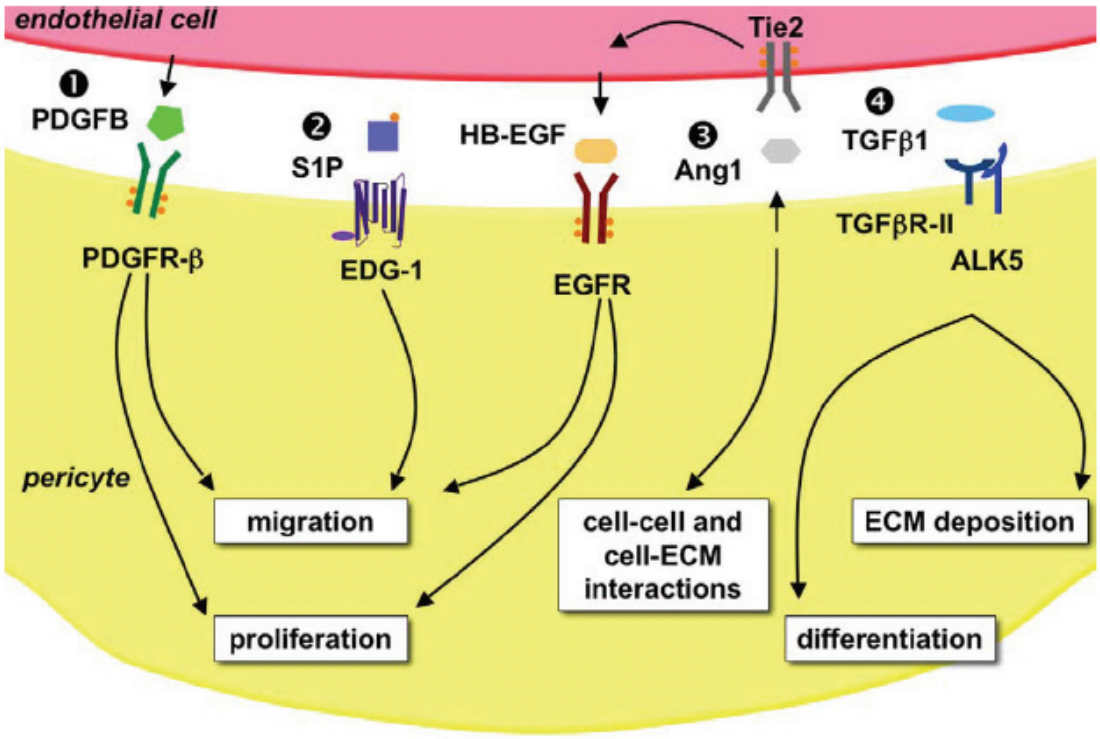

Fig. 1.6 - Regulation of pericyte recruitment by four major pathways: (1) PDGF-B released by endothelial cells binds to PDGFRβ on pericytes and stimulates their migration and proliferation; (2) sphingosine 1-phosphate (S1P) binding to endothelial differentiation gene-1 (EDG-1) promotes cell migration; (3) angiopoietin 1 (Ang1)/receptor tyrosine kinase with immunoglobulin and epidermal growth factor homology domains-2 (Tie2) enhances cell–cell and cell–extracellular matrix (ECM) interactions and activates the expression and release of heparin-binding epidermal growth factor like growth factor (HB-EGF), that also promotes cell migration and proliferation; and (4) transforming growth factor-β1 (TGF-β1) binding to receptor II (TGFβR-II) leading to activin-like kinase-5 (ALK5), stimulates pericyte differentiation and ECM deposition. Figure taken from Chantrain (Chantrain et al., 2006).

In **Chapter 7**, I describe a study to assess the vascular maturity of a broad range of human tumours immunohistochemically, using a panel of vascular markers. It is thought that CA4P has a preferential effect on tumour vessels because they are relatively immature, lacking the smooth muscle coat and pericytes of mature vessels. Vessels lacking a smooth muscle coat would be more prone to a catastrophic effect once the endothelium has been damaged by CA4P. The current 'gold standard' surrogate marker of CA4P effect is DCE-MRI. What is not currently known is whether CA4P effect measured by DCE-MRI correlates with a more immature vasculature in human tumours.

VEGF

VEGF was initially identified in 1983 as a tumour-produced factor capable of increasing vascular permeability (Senger et al., 1983). VEGF is essential for normal development in the embryo, where it promotes the differentiation, proliferation and survival of endothelial cells, and growth of the vascular tree (Glade Bender et al., 2004).

VEGF signaling (**Fig.1.7**) elicits a rapid angiogenic response from endothelial cells in arteries, veins and lymphatics. Activation of the VEGF receptor VEGFR2(flk-1) appears to be the principle pathway supporting its proliferative functions (Ferrara, 2004).

VEGF is ubiquitously expressed in nearly all human tumours. Higher levels of expression have been associated with increased tumour vascularity, rapid growth, invasion, metastasis, and poor clinical prognosis in various tumours including breast (Linderholm et al., 2000), colon (Tokunaga et al., 1998), lung (Fontanini et al., 2002; O'Byrne et al., 2000), kidney cancer (Jacobsen et al., 2000), and head and neck cancer (Sauter et al., 1999).

CD105 (Endoglin)

CD105 is a proliferation-associated marker on endothelial cells that binds with high affinity to TGFβ1 and TGFβ3. The TGFβ family of cytokines regulates a wide range of cellular processes, including proliferation, differentiation, apoptosis and migration CD105 is strongly expressed in the vascular endothelium of tumour tissues, with weaker expression in normal vascular tissue (Burrows et al., 1995). CD105 MVD can vary widely (**Fig. 1.8**)(Akagi et al., 2002). Higher levels of CD105 have been associated with a worse prognosis in patients with prostate cancer (Joseffson et al., 2005).

Fig. 1.7 The VEGF Family & Receptors. The family consists of seven ligands (VEGF A,B,C,D,E, placenta growth factor (PIGF1, PIGF2). mRNA splicing leads to several isoforms of some ligands e.g. VEGF-A. VEGF family members have specific binding affinities to the various tyrosine kinase receptors. Neuropilin (NRP-1, NRP-2) are also co-receptors for certain VEGF isoforms. From(Hicklin & Ellis, 2005)

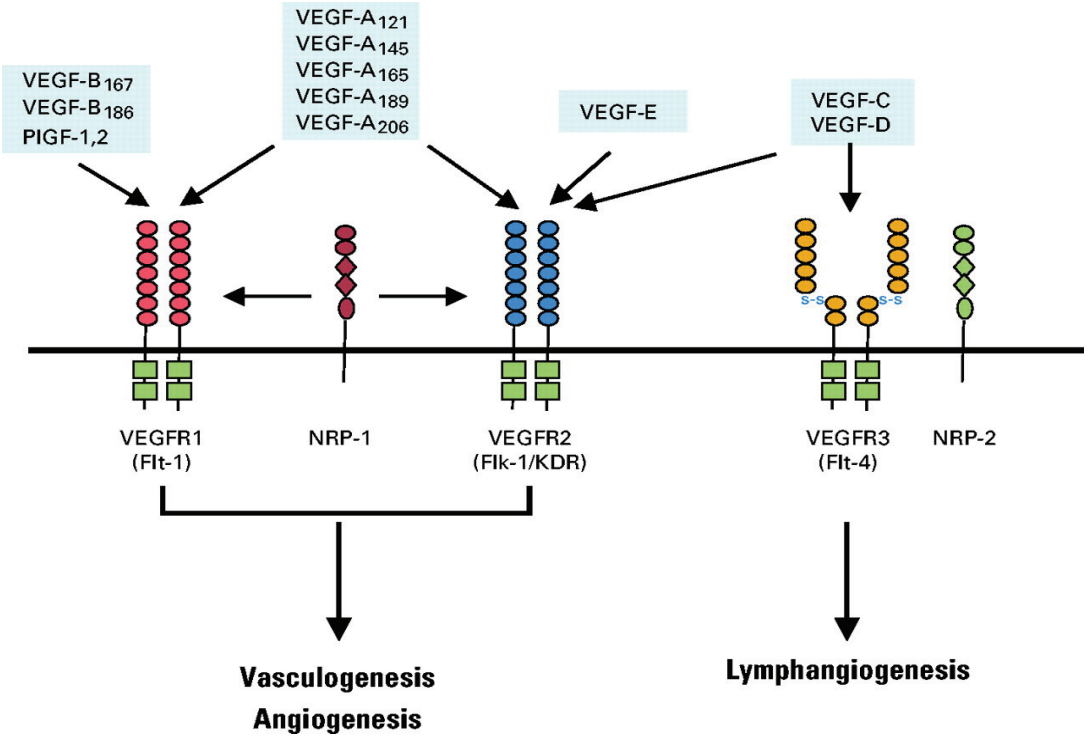

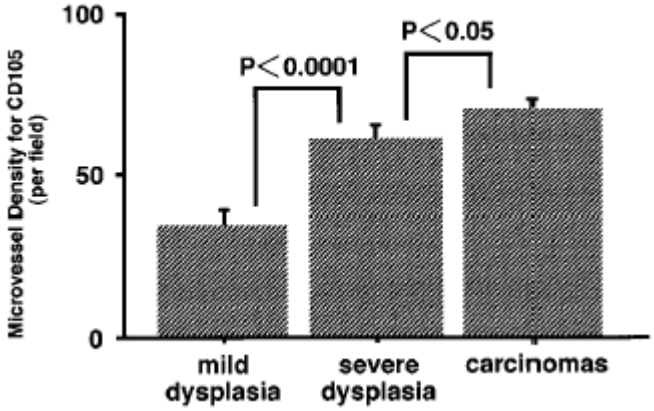

Fig. 1.8 – CD105 in Carcinoma Development

Alteration of CD105 MVD in the development of colorectal carcinoma. From Akagi (Akagi et al., 2002)

Glut-1

Tumour cells have an increased rate of glucose uptake and glycolysis. This up regulation helps maintain the increased energy requirements of rapidly proliferating cells. In tumours, increased glucose uptake is largely achieved through the up regulation of a family of proteins, known as "*facilitative glucose transporters*".

Glut-1 is a target gene of the HIF-1α transcription factor, and has been considered a candidate endogenous marker of tumour hypoxia (Mayer et al., 2005). Expression of Glut-1 may also serve as an indicator for the induction of the transcriptional response to hypoxia, which has been linked to enhanced proliferation, resistance to therapy, and metastatic potential of tumours (Sullivan & Graham, 2007). Over expression of Glut-1 has been shown to correlate with poor prognosis and clinical outcome in several human tumour types, including cervical cancer (Airley et al., 2001), lung cancer (Younes et al., 1997), bladder cancer (Younes et al., 2001), colorectal cancer (Cooper et al., 2003), and head and neck cancer (Oliver et al., 2004).

Ki-67

Ki-67 has an essential role in cell proliferation (Scholzen & Gerdes, 2000), although its exact biological function has not been fully determined. During cell cycle interphase, the antigen can be exclusively detected within the nucleus, whereas in mitosis the protein relocates to the chromosomes. The fact that the Ki-67 protein is present during all active phases of the cell cycle but is absent from resting cells (G_0), makes it an excellent marker for determining the growth fraction of a cell population (Scholzen & Gerdes, 2000).

The fraction of Ki-67 positive tumour cells (Ki-67 labelling index) is often correlated with clinical outcome, for example in soft tissue sarcoma (Heslin et al., 1998), astrocytomas (Kirla et al., 2000), prostate cancer (Borre et al., 1998; Pollack et al., 2004), and breast cancer (Haerslev et al., 1996).

Angiopoietins

The angiopoietins(ang-1,2,3,4) are critically involved in angiogenesis, and belong to a family of proteins that bind to the Tie-2 receptor (Tait & Jones, 2004). Ang-3 represents the murine orthologue of human ang-4.

The involvement of angiopoietins in the angiogenic switch has been suggested by Tanaka (Ahmad et al., 2001a; Tanaka et al., 2003). The angiogenic switch is a change in balance, in which a higher relative level of angiogenic inducers leads to angiogenesis and a higher relative level of inhibitors leads to inhibition of angiogenesis (**Fig. 1.9**). The angiopoietins are known for their antagonistic roles on Tie-2 receptors where ang-1 stabilises the vessels by maintaining pericyte endothelial cell coverage, and ang-2 permits the removal of these cells from the vessel, which in the presence of VEGF facilitates the angiogenic response and in the absence of VEGF induces vessel regression (Bach et al., 2007; Moon et al., 2006; Shim et al., 2007; Winter et al., 2007). VEGF expression is not modulated by overexpression of ang-1 or ang-2 (Hawighorst et al., 2002). However, depending on the tumour model, stabilization of blood vessels by ang-1 may either promote tumour angiogenesis or reduce tumour growth, possibly by rendering endothelium unresponsive to further angiogenic stimulation (Metheny-Barlow & Li, 2003). Ang-1 and ang-2 are expressed in the cytoplasm and sometimes membrane of tumours.

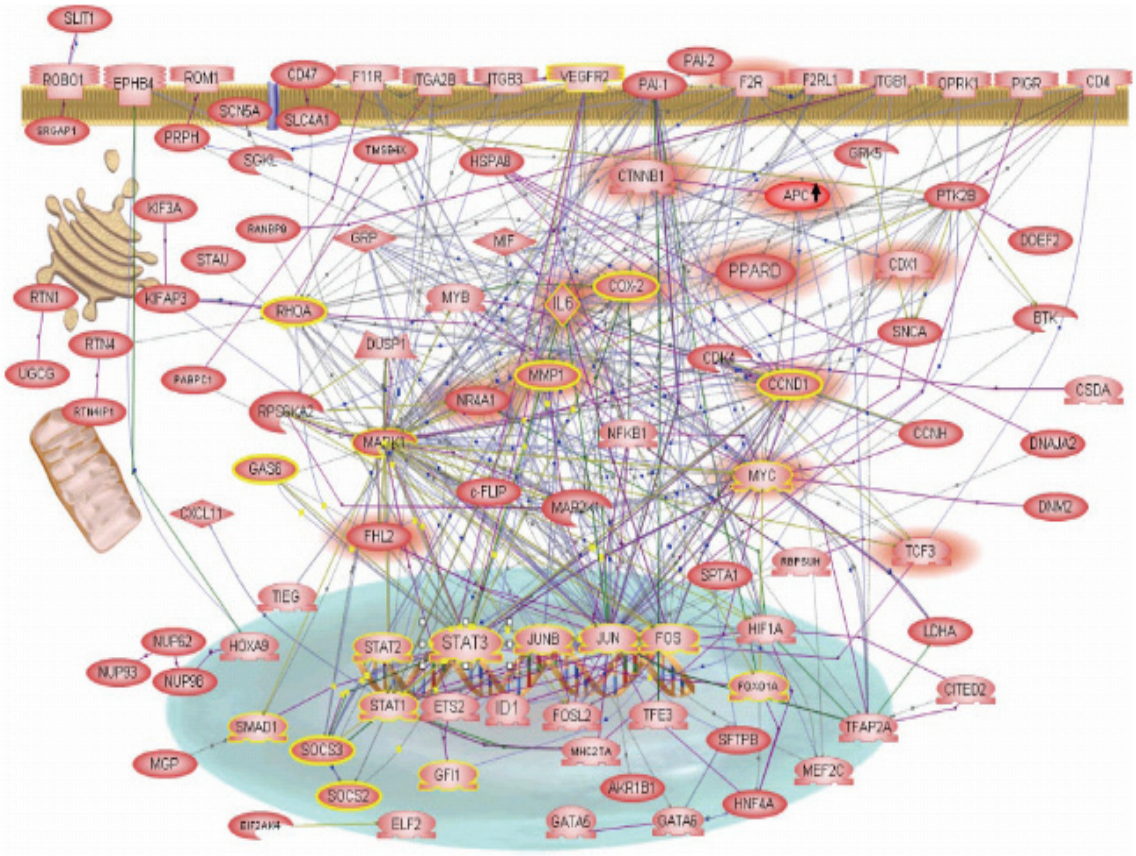

Fig. 1.9 – The Angiogenic Signaling Network - from Abdollahi (Abdollahi et al., 2007)

Overexpression of ang-1 has been documented in various types of human tumours including glioblastoma, neuroblastoma and lung cancer but others studies have suggested a selective loss of ang-1 expression during tumour progression (Metheny-Barlow & Li, 2003). Depending on the tumour model, stabilization of blood vessels by ang-1 may either promote tumour angiogenesis or reduce tumour growth, possibly by making EC unresponsive to further angiogenic factors (Metheny-Barlow & Li, 2003).

Hypoxia results in increased levels of ang-1 and ang-2 in tumours, although ang-2 is elevated to a far greater extent. Tait (Tait & Jones, 2004) collected angiopoietin expression data from 56 publications in order to determine a consensus expression profile. They found that although ang-1 and ang-2 are both upregulated in tumours, ang-2 is more frequently upregulated than ang-1 or Tie-2. Ang-2 seems to be particularly increased in highly vascular tumours. Ang-1 expression is generally restricted to tumour cells, whereas ang-2 is also found in EC.

Overexpression of ang-2 leads to a more invasive tumour. Colorectal tumours transfected with ang-2 grew significantly larger and heavier in nude mice compared to those transfected with the ang-1 construct or the vector alone (Ahmad et al., 2001b).

PDGF

PDGF was first identified in a search for serum factors that stimulate the proliferation of arterial smooth muscle cells (Ross et al., 1974). The PDGF family has been shown to drive cellular responses including proliferation, survival, migration, and the deposition of extracellular matrix and tissue remodelling factors.

The PDGF signalling network consists of four ligands, PDGF-A, B, C, and D, and two receptors, PDGFRα and PDGFRβ (**Fig.1.10**)(Hoch & Soriano, 2003). PDGFs are receptor tyrosine kinases, and the PDGF family is closely related to the VEGF family.

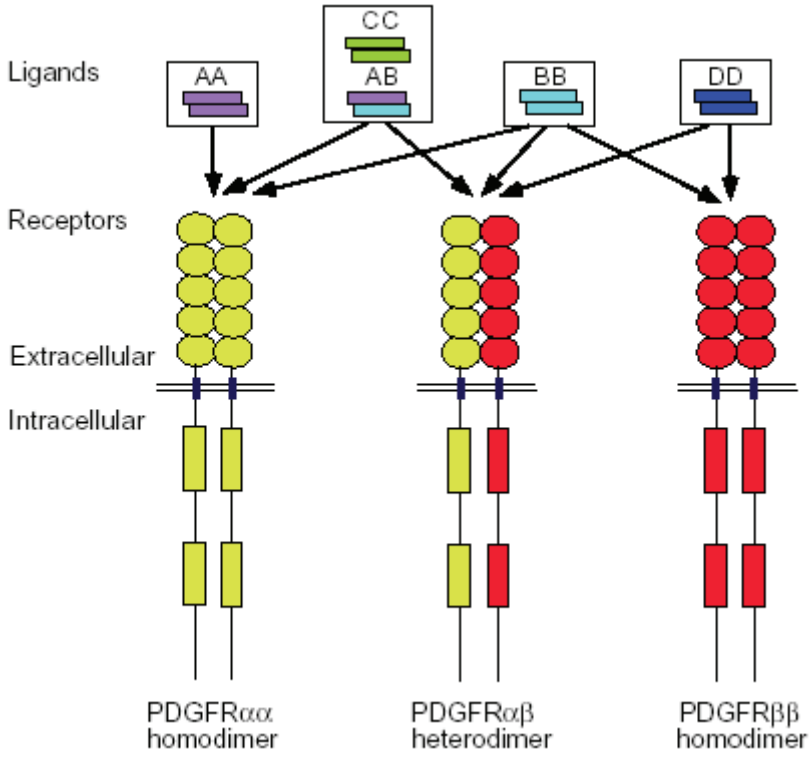

Fig. 1.10 – PDGF / PDGFR Binding Interactions (Hoch & Soriano, 2003)

PDGFB and PDGFRβ have essential roles in the recruitment of VSMC and pericytes to newly formed blood vessels, whereas PDGFA and PDGFRα have essential roles in numerous processes, including CNS, neural crest and organ development (Betsholtz, 2000; Karlsson et al., 2000; Leveen et al., 1994). PDGF-B can also induce intratumoural lymphangiogenesis and lymphatic metastasis by a VEGFR-3 independent mechanism

(Vincent & Rafii, 2004). PDGFB has an essential role in recruitment of pericytes to newly formed vessels. PDGFB and PDGFR-β deficient mice have a lack of pericytes that leads to microvascular aneurysms and lethal microhaemorrhages (Lindahl et al., 1997).

CD61 (β3-Integrin)

Integrins are cell-surface adhesion receptors that play an important role in mediating numerous physiological processes, including inflammation, migration, adhesion and proliferation. Integrins are composed of α and β subunits, which form heterodimers. Eight β and 18 α subunits have been described to date, and form 24 distinct integrins (Zhao et al., 2004). Each integrin performs specific functions depending upon the ligand-binding specificity (**Table 1.5**). Angiogenesis depends on specific molecular interactions between vascular cells and components of the extracellular matrix.

Subunits		Ligands
β_1†	α_1	Collagens, laminin
	α_2	Collagens, laminin
	α_3†	Fibronectin, laminin
	α_4	Fibronectin; VCAM-1
	α_5	Fibronectin
	α_6†	Laminin
	α_7	Laminin
	α_V	Fibronectin, vitronectin
β_2	α_L	ICAM-1, ICAM-2
	α_M	C3b, fibrinogen, factor X; ICAM-1
	α_X	Fibrinogen, C3b
β_3†	α_{IIb}	Fibrinogen, fibronectin, von Willebrand factor, vitronectin, thrombospondin
	α_V	Same as $\beta_3\alpha_{IIb}$; also osteopontin, collagen

**The integrins are grouped in subfamilies sharing a common β subunit. Ligands shown in red are vascular ligands; all others are proteins in the extracellular matrix.*
†These subunits can have multiply spliced isoforms with different cytosolic domains.

Table 1.5 Integrin Diversity & Binding Specificity (Stouffer & Smyth, 2003)

The β_3-integrin family consists of $\alpha_{IIb}\beta_3$ (glycoprotein IIb/IIIa), found on platelets and megakaryocytes, which has an essential role in haemostasis, and the more widely distributed $\alpha_v\beta_3$, found on endothelial cells, smooth muscle cells, platelets, lymphocytes, neutrophils, macrophages and osteoclasts (Eliceiri & Cheresh, 1999).

Endothelial cells exposed to growth factors, or those undergoing angiogenesis in tumours, express high levels of $\alpha_v\beta_3$ (Eliceiri & Cheresh, 1999). The expression of $\alpha_v\beta_3$ on activated endothelial cells suggests that this integrin may have an important function during angiogenesis (Cai & Chen, 2006; Cowden Dahl et al., 2005; Lamar et al., 2007; Nam et al., 2005; Wang et al., 2006). Disruption of $\alpha_v\beta_3$ with antibody (LM609) disrupts blood vessel formation in mouse retina (Drake et al., 1995). These antagonists disturb the growth and maturation of new blood vessels without detectably influencing the preexisting blood vessels. Systemic administration of $\alpha_v\beta_3$ antagonists to animals with ongoing angiogenesis shows blood vessels containing high levels of apoptotic endothelial cells (Eliceiri & Cheresh, 1999). The humanised form of the anti-$\alpha_v\beta_3$ monoclonal antibody LM609 (Vitaxin) has shown promise in early clinical trials.

Magnetic Resonance Imaging (MRI)

A brief overview of MRI is presented in **Appendix 1**

Dynamic Contrast Enhanced MRI

Introduction

DCE-MRI, using low-molecular-weight (<1 kDa) gadolinium-based paramagnetic contrast media, is an attractive technique for assessing the vascular physiology of tumours, by combining good anatomical detail with the ability to quantify vascular parameters. The rate at which contrast medium passes from the intravascular space to the extravascular extracellular space and then back to the intravascular space over time after bolus injection differs between normal tissue and tumour tissue and can be assessed qualitatively and quantitatively. MRI has the advantage of a good intrinsic signal-to-noise ratio, but quantification of tissue contrast agent concentrations is challenging, because there is no simple relation between signal-intensity change and contrast-medium concentration, especially for large vessels. Changes in signal intensity are dependent on many factors, including native tissue relaxation rates, contrast-agent dose, rate of injection, chosen imaging sequence and parameters, and machine gain and scaling factors (Goh et al., 2007). For kinetic parameter quantification to be feasible, careful calibration of contrast concentration with signal intensity has to be done to establish the exact relation between these two entities over the measured range of values.

Theory

DCE-MRI involves the rapid acquisition of a set of T1-weighted images through the tumour as an intravenous bolus of contrast agent is injected. The change in signal intensity over time following contrast injection can be analysed with mathematical models (Tofts, 1997). Quantitative kinetic parameters are derived which provide information about tumour microcirculation as they are indirectly related to perfusion, vascular permeability and vessel surface area (d'Arcy, 2006).

The theory underlying the use of DCE-MRI to measure physiological parameters such as tissue blood flow and permeability is based on the Kety equation for a freely diffusible tracer.

$$C_t(T) = EF\int_0^T C_a e^{\frac{-EF}{\lambda}(T-t)}dt \qquad (1)$$

where E is the extraction fraction, F is blood flow rate (ml whole blood per g of tissue per minute), λ is the tissue-blood partition coefficient of the substance, C_a is the arterial blood concentration and C_t is the tissue concentration. This can be adapted for intravenous bolus injection of an extracellular tracer such as Gd-DTPA (Tofts et al., 1999):

$$C_t(T) = K^{trans}\int_0^T C_p(t)e^{-k_{ep}(T-t)}dt \qquad (2)$$

where C_p is arterial plasma concentration of Gd-DTPA, K^{trans} is the volume transfer constant for Gd-DTPA from the vessel into the extracellular extravascular space (EES), and k_{ep} is the rate constant for the transfer of Gd-DTPA from the EES back into the plasma. From the above two equations,

$$K^{trans} = EF\rho(1-Hct) \qquad (3)$$

where ρ is tissue density (g/ml) and Hct is haematocrit. K^{trans} has several physiological interpretations depending on the balance between capillary permeability to Gd-DTPA and blood flow rate in the tissue of interest. In tissues with highly permeable vessels, where flux across the endothelium is flow limited, E is close to 1 so K^{trans} is equal to the blood plasma flow rate per unit volume of tissue (ml plasma per ml tissue per minute):

$$K^{trans} = F\rho(1 - Hct) \tag{4}$$

Adapting Renkin's equation (Renkin, 1959) for extraction fraction for a freely diffusible tracer to an extracellular tracer,

$$E = 1 - e^{-\frac{PS}{F(1-Hct)}} \tag{5}$$

where PS is the permeability (P) vessel surface area (S) product. Therefore, when PS<<F, as in tissues such as brain with low vessel permeability, flux across the endothelium is permeability limited,

$$E = \frac{PS}{F(1 - Hct)} \tag{6}$$

and K^{trans} is equal to the permeability surface area product per unit volume of tissue:

$$K^{trans} = PS\rho \tag{7}$$

In tumours there will be heterogeneity of vessel permeability, and K^{trans} will be determined by a combination of flow, permeability and vessel surface area. The ratio of K^{trans} to k_{ep} gives the volume of EES per unit volume of tissue, v_e, otherwise known as the Gd-DTPA leakage space:

$$v_e = \frac{K^{trans}}{k_{ep}} \tag{8}$$

This model assumes an instantaneous bolus, instant mixing of Gd-DTPA within the blood and within the leakage space after transfer from the vessel, and ignores the contribution of intravascular tracer to the tissue concentration.

Unlike CT imaging, the change in signal intensity on the MR image does not reflect contrast agent concentration directly but rather is a map of the effect of Gd-DTPA on the relaxation times of hydrogen nuclei present in the tissue. Therefore it is difficult to compare non-quantitative results from different institutions as different sequences,

machines and injection procedures will produce different changes in signal intensity for the same change in contrast agent concentration (Parker et al., 1997). For quantitative analysis (to obtain comparable results between institutions) and tracer kinetic model application, measurement of tissue contrast agent concentration is required (appendix 1).

T_1-weighted DCE-MRI kinetic parameters

The T_1-weighted quantitative parameters derived for the work presented in this thesis are $IAUGC_{60}$ (the initial 60s area under the Gd-DTPA concentration vs time curve) and the kinetic parameters obtained from the Tofts model (Tofts & Kermode, 1991): the transfer constant for Gd-DTPA from plasma to tumour extracellular space, K^{trans} (and back again k_{ep}) and the volume of the EES or leakage space, v_e.

IAUGC

The IAUGC (units: mM.min or mM.s) is usually calculated for the first 60 or 90 seconds following Gd-DTPA injection (Evelhoch, 1999; Evelhoch et al., 2004). It cannot be related simply to tumour physiology, but has the advantage of being a quantitative parameter that is obtained without mathematical modelling or knowledge of the arterial input function (AIF). As such, changes in pixels that are excluded from the mathematical modelling analysis are evaluated by the IAUGC parameter. It is a measure of how much contrast agent is taken up by the tumour in the first 60 or 90s post-Gd-DTPA injection and is influenced by tumour blood flow rate and tumour vessel permeability. IAUGC values can be easily and robustly calculated for individual pixels within a tumour region of interest. An average IAUGC value for the whole tumour can then be determined. **Figure 1.11** below shows the derivation of IAUGC. By using AUC from the Gd-DTPA concentration time curve rather than from the signal intensity time curve, the problem of dependence of signal enhancement on tissue T1 levels is avoided. The larger vascular contribution to the tissue Gd-DTPA concentration time curve in liver spleen and kidney means that the initial AUC parameter in these tissues has a greater contribution from blood volume than in muscle or tumour. Thus the same DCE-MRI parameter in these different tissues reflects a different combination of blood flow, vessel permeability to Gd-DTPA and blood volume.

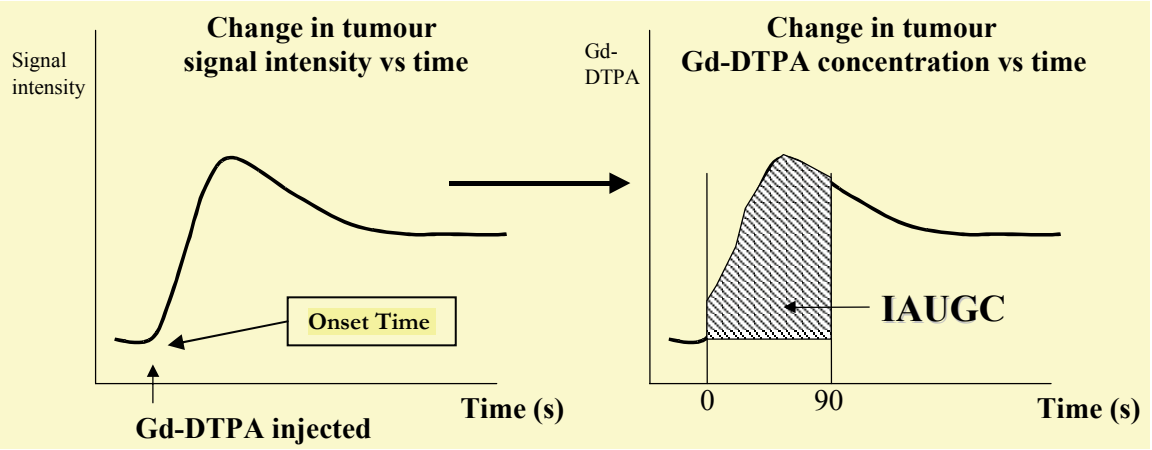

Fig. 1.11 - Diagram to show derivation of $IAUGC_{90}$

K^{trans} and v_e

The transfer constants for Gd-DTPA diffusion into the tumour EES from blood plasma (K^{trans}) and back again (k_{ep}) can be calculated using Tofts' mathematical model (**Figure 1.12**) (Tofts et al., 1999; Tofts & Kermode, 1991). This is an adaptation of the Kety model, which was developed to describe the uptake of a freely diffusible inert tracer from the plasma to tissue EES (Kety, 1960a; Kety, 1960b). The main differences between the Tofts and Kety models are that Gd-DTPA is not a freely diffusible tracer (which is a requirement of the Kety model) and that the transfer constants elicited are expressed per unit volume rather than per unit gram of tissue.

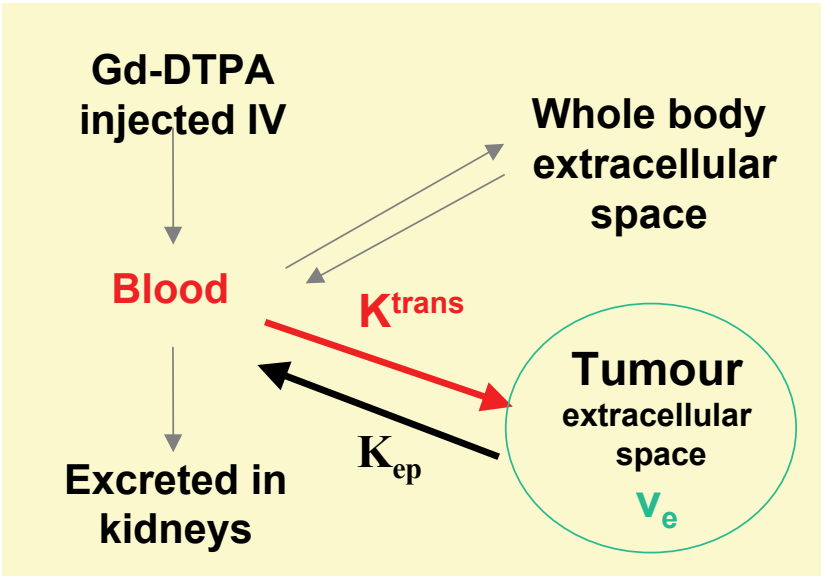

Fig. 1.12 - Diagram to show Toft's model for Gd-DTPA uptake kinetics.

K^{trans} (and k_{ep}) have both blood flow rate and permeability components as Gd-DTPA is not freely diffusible and their biological meaning is dependent on the balance between capillary

permeability and blood flow in the tissue of interest (Tofts, 1997; Tofts et al., 1999). In high permeability tissues, K^{trans} is equal to the blood plasma flow per unit volume of tissue. In low permeability tissues, such as in the brain, it is equal to the permeability surface area product between the blood plasma and the EES per unit volume of tissue (Tofts, 1997). In liver metastases the situation is likely to be somewhere between these two extremes.

There are many assumptions in the Tofts model so these parameters should be regarded as the *'apparent'* blood flow rate/permeability and leakage space (Parker et al., 1997). As the values of K^{trans} and v_e that are derived are based on Gd-DTPA concentration, comparisons between different studies and different MRI centres can be made.

Techniques for assessing the effects of VDAs

The effects of VDAs can be assessed using DCE-MRI, perfusion CT, contrast enhanced microbubble ultrasound, and with PET. DCE-MRI is the most established technique, with the greatest volume of data available. Mount Vernon Hospital have pioneered developments in the use of MRI to assess the VDAs, and the team there have great experience in the technique, hence it was the modality of choice for us. The Phase I CA4P UK study also used PET (at Hammersmith Hospital) to assess CA4P effects (see previous section). There is increasing data with perfusion CT, and we use this technique in Chapter 4 to look for late effects of CA4P. CT obviously involves a radiation dose to the patient, in contrast to MRI, but it is readily available and gives a direct measure of arterial input. MRI involves no radiation, but the dynamic parameters are calculated using models based on an arterial input estimate. Newer MRI scanners however are much faster and so this issue is gradually being resolved.

MRI in the assessment of VDAs

T_1-weighted DCE-MRI has been used to investigate the acute effects of the VDAs CA4P (Beauregard et al., 2001; Beauregard et al., 2002; Beauregard et al., 1998; Galbraith et al., 2003; Maxwell et al., 2002), DMXAA (Beauregard et al., 2002) & ZD6126 (Evelhoch et al., 2004; Robinson et al., 2003a) in animal models. Acute reductions in semi-quantitative and/or quantitative parameters are seen within 24 hours of treatment in a range of tumour types. Similar results were seen in phase I clinical trials of VDAs which used change in DCE-MRI parameters as biomarkers for the anti-vascular effects of CA4P (Dowlati et al.,

2002; Galbraith et al., 2003; Stevenson et al., 2003), DMXAA (Galbraith et al., 2002b), & ZD6126 (Evelhoch et al., 2004).

As K^{trans} has both blood flow and permeability components, reduction in K^{trans} cannot be directly equated to the acute blood flow shutdown seen with CA4P. However, the use of DCE-MRI to assess response to VDAs has been validated by Maxwell (Maxwell et al., 2002) and Padhani (Padhani, 2005; Padhani et al., 2007; Padhani & Leach, 2005). Changes in K^{trans} in response to CA4P in a rat carcinosarcoma model matched changes in blood flow rate measured using uptake of radiolabelled ^{125}iodoantipyrine (IAP). Reductions in absolute tumour blood flow rate at 4 and 24 hours as measured by IAP correlated with reductions in K^{trans}(and IAUGC) as measured by DCE-MRI. Although the size of the decrease seen in K^{trans} was smaller than that seen in tumour blood flow rate, the time course and dose-dependency patterns were very similar. Reductions in v_e were also seen, with no significant change in k_{ep}. Treatment with CA4P may alter Gd-DTPA kinetics such that, in this situation, blood flow rate is the dominant influence on K^{trans}.

The pattern and time course of changes in K^{trans} seen in a Phase I trial of CA4P was similar to that seen in animal models (Galbraith et al., 2003) indicating the appropriateness of using K^{trans} as a surrogate marker of vascular response to treatment. This view has been endorsed by a specialist panel meeting under the auspices of Cancer Research UK - who considered the measurement and analysis methodology requirements for robust application of DCE-MRI to anti-vascular clinical trials (Leach et al., 2003). BOLD-MRI has also been used to monitor the acute effects of anti-vascular agents (Robinson et al., 2003b).

DCE-MRI analysis was undertaken in six patients following a single dose of ZD6126 every three weeks (three patients at 56mg/m^2, two patients at 80mg/m^2 and one patient at 112mg/m^2) (DelProposto Z 2002). The overall tumour $IAUGC_{60}$ decreased to 13 – 84% of the baseline value 6 hours after ZD6126 administration in all but one subject (56mg/m^2). As expected, the effects were most noticeable in the tumour core. The IAUGC increased to baseline within 24h in three of the five patients with an initial decrease, but remained below baseline for two patients even after 18 – 21 days (DelProposto Z 2002). Robinson (Robinson et al., 2007) has demonstrated the potential of susceptibility contrast MRI with ultrasmall superparamagnetic iron oxide contrast agents to provide a quantitative imaging biomarker of fractional tumour blood volume to assess response to ZD6126.

A significant amount of experience has now been gained with DCE-MRI, and reproducibility between serial dynamic scans obtained daily in patients has been excellent (Evelhoch et al., 2001; Galbraith et al., 2002a; Taylor et al., 2004a; Taylor et al., 2004b; Taylor et al., 2006). CO and LVEF can now be measured during MRI scans, leading to better understanding of changes in kinetic parameters.

Dynamic Perfusion CT

Introduction

Dynamic contrast enhanced CT, also known as perfusion CT, describes the use of CT to capture physiological parameters that reflect the vasculature within tumours and other tissues following conventional iodinated contrast agent administration (Miles, 2002). Following intravenous injection contrast agent passes from the intravascular to EES, at a rate determined by the rate of tissue delivery, vessel surface area, and the leakiness of these vessels. There is subsequent return of contrast from the EES to vessels over time, and contrast is eventually excreted by the kidneys. Differences in contrast agent kinetics between normal tissue and tumour can be exploited to provide tissue-specific information.

By performing perfusion CT in the early phase (first pass and delayed phase) following a bolus injection of intravenous contrast agent and measuring the change in vascular and tissue contrast enhancement from the series of CT images obtained over time, it is possible to estimate both semi-quantitative (e.g. peak enhancement, maximum slope of enhancement and time to peak enhancement) and quantitative vascular parameters (e.g. perfusion, blood volume, and vascular leakage as expressed by extraction fraction or permeability surface area product).

The technique was first described in 1979 only 8 years after the introduction of CT into clinical practice; Leon Axel proposed a method for determining tissue perfusion from dynamic contrast enhanced CT data (Axel, 1980). Due to the computer processing requirements it took until the 1990s before perfusion CT could be performed with conventional CT rather than electron beam systems, thereby broadening the technique's availability (Miles et al., 1991; Miles et al., 1993).

Mathematical Modeling

Mathematical modeling techniques employed during Perfusion CT are summarized in **Appendix 4**.

Acquisition Techniques

A typical perfusion CT acquisition includes a series of sequential images obtained during the first pass of the bolus of contrast agent through the vascular system At this time the contrast material is predominantly intravascular which allows assessment of perfusion, blood volume and transit time. The delayed extravascular phase (>60sec) allows assessment of vascular leakage. In order to assess the contrast enhancement change over time at least one non contrast-enhanced baseline image is needed. By subtracting the baseline dataset from the remaining contrast enhanced datasets on a pixel by pixel or regional basis, the resulting temporal changes in contrast enhancement within the input vessel and for the tissue of interest may be displayed as attenuation-time curves. Direct application of mathematical modeling techniques to the enhancement data is possible as there is a direct linear relationship between enhancement change and iodine concentration. Absolute quantification of perfusion is possible and has been hailed as an advantage of CT.

The manner in which contrast is administered is also an important consideration. When using compartmental analysis to obtain perfusion values, a short sharp bolus is necessary because the validity of the method requires that peak arterial concentration occurs prior to the time of maximal increase in tissue enhancement. Thus, compartmental analysis methods need a relatively small bolus (40–50 ml) administered with higher injection rates of 5-10ml/s. Rates higher than 10 ml/s do not appear to produce further benefit due to buffering in the venous system. Typical acquisition parameters are shown in **Table 1.6.**

Comparison With MRI

In comparison with DCE-MRI, Perfusion CT is more straightforward to implement, provides direct quantification of vascular parameters, and demonstrates good spatial resolution. The ionizing radiation burden associated with a perfusion CT acquisition protocol is determined by the number of images in the sequence and the tube current (mAs) used for each image. A greater number of images results in more data points on the time–attenuation curve, and therefore higher quality perfusion measurements but a larger

patient dose. A larger tube current results in less photon noise within each image and greater certainty in the attenuation measurement at each time point but again imposes a greater patient dose.

Table 1.6 - Typical perfusion CT and DCE-MRI Acquisition Parameters (Goh & Padhani, 2006)

	MDCT Single Level (2D)	MDCT Volume (3D)	T1 DCE-MRI (2D/3D)	T2* DCE-MRI (2D)
Contrast Agent	>300mg/ml iodine	>300mg/ml iodine	0.5mmol/ml gadolinium	0.5mmol.ml gadolinium
Dose	0.5ml/kg	1.0ml/kg	0.1mmol/kg	≥0.2mmol/kg
Typical Volume	40mls	100mls	10 – 15mls	25 – 35mls
Injection Rate	3 – 5mls/sec bolus	2mls/sec infusion	3mls/sec bolus	4 – 6mls/sec bolus
Acquisition Type	Single Level	Multiple Helical	Single Level	Single Level
Slice Thickness	4 – 5mm	Whole Tumour	2 – 8mm	2 – 8mm
Data Sampling	1s for 1 – 2min	5s for 1 – 2min	5 – 12s for 5 – 12min	1 – 2s for 1 – 2min
Signal to Noise Ratio	Low	Low	Very High	Low
Signal Change Observed / Magnitude of Effect	Increase/Small	Increase/Small	Increase/Large	Decrease/Small
Analysis Technique	Deconvolution, Distributed Parameter Model	Patlak Analysis	General Multicompartment Pharmacokinetic Model(e.g.Tofts)	Central Volume Theorem
Parameter Typically Measured	Blood Flow Blood Volume Mean Transit Time Permeability	Permeability Relative Blood Volume	Transfer Constants Leakage Space Blood Volume Blood Flow	Relative Blood Flow Relative Blood Volume Mean Transit Time

To date, no studies have compared the performance of perfusion CT and DCE-MRI in tumour assessment, although a recent study compared them in the evaluation of solitary pulmonary nodules and concluded that there were no significant differences (Kim et al., 2004). There are anatomic regions where perfusion CT is preferable, mainly due to the presence of artefacts that would interfere with MRI evaluations. These include the upper abdomen, the mediastinum and at the pulmonary hila. Phase-encoded artefacts arising from vascular pulsatility, exaggerated by concentrated contrast medium, would render DCE-MRI potentially uninterpretable.

Perfusion CT for tumour assessment

CT is widely used in oncologic imaging, and perfusion studies can be incorporated relatively easily into routine examinations. The rationale for using CT for assessing tumour perfusion and blood volume is that these parameters are generally increased in malignant tissue reflecting the greater MVD found in tumours. Similarly vascular permeability, as tumour blood vessels are abnormally permeable to circulating molecules, including contrast media. To date perfusion CT has been validated against a variety of other techniques, and has been correlated against histologic markers of angiogenesis in lung, renal and colorectal cancer (Cenic et al., 1999; Gillard et al., 2000; Jinzaki et al., 2000; Tateishi et al., 2002; Yi et al., 2004).

Perfusion CT has been used for therapeutic assessment in a variety of cancers including rectal, lung and oropharyngeal cancer (Gandhi et al., 2006; Meijerink et al., 2007; Ng et al., 2007; Willett et al., 2004) and to monitor radiotherapy effects in rectal cancer (Bellomi et al., 2007; Rudisch et al., 2002; Sahani et al., 2005), prostate cancer (Harvey et al., 2001), and as a predictor of response in head and neck cancer (Hermans et al., 1997; Hermans et al., 2003). MDCT has also been used in lymphoma (Dugdale et al., 1999), and hepatic metastatic disease (Leggett et al., 1997; Sheafor et al., 2000a). In a series of 107 patients with indeterminate pulmonary nodules(IPN), Swensen (Swenson et al., 1996) was able to distinguish benign from malignant nodules using simple measurements of peak enhancement on CT. Peak enhancement (Miles, 1999) was also shown to correlate with histological assessments of MVD. A subsequent multicentre trial of 356 patients demonstrated a sensitivity of 98% and specificity 58% for IPN enhancement values in the diagnosis of malignancy (Swenson et al., 2000). Similarly Perfusion CT has been shown to be better than standard morphological criteria for differentiating colorectal cancer and diverticular disease (Goh et al., 2006).

Perfusion CT for hepatic assessment: a special case

As approximately three-quarters of the blood supply is derived from the portal vein in the normal liver rather than from the hepatic artery, modelling to derive quantitative vascular parameters ideally has to take this into account. In the 1990s Miles described a technique to assess hepatic perfusion. Using a dynamic single-section technique with temporal resolution imaging of 3–7sec, enhancement-time curves were generated for a ROI placed over the liver, aorta, and spleen (Miles et al., 1993). By assuming that peak splenic

enhancement marked the beginning of dominant PVP, hepatic parenchymal enhancement was resolved into arterial and portal venous components. Hepatic arterial and PVP values were calculated by dividing the slopes of the rise in attenuation during the arterial and portal venous phases of liver enhancement, respectively, by peak aortic enhancement. A hepatic perfusion index (HPI) was derived by dividing the calculated arterial perfusion by the sum of arterial and portal perfusion values (Miles et al., 1993). In 1995, Blomley (Blomley et al., 1995) revised this approach by subtracting the arterial phase hepatic enhancement (modeled after splenic enhancement) from the original hepatic enhancement curve to derive a "corrected" hepatic enhancement curve. PVP was calculated by dividing the slope of the rise in attenuation during the portal phase of liver enhancement by peak portal venous or splenic venous enhancement (Blomley et al., 1995). These slope-ratio methods of deriving perfusion indices have dominated the field of hepatic imaging (Blomley et al., 1995; Leggett et al., 1997; Miles et al., 1993), but tracer kinetic (Van Beers et al., 2001) and linear system approaches have also been applied to perfusion CT imaging of the liver (Cuenod et al., 2001). The slope method has been validated for the measurement of hepatic perfusion, including separate estimation of arterial and portal components (Bader et al., 1998; Blomley et al., 1995; Miles et al., 1993; Tsushima et al., 1999). However, simple use of the maximal rate of portal phase enhancement and an arterial rather than portal venous input function has been shown to result in underestimation of portal perfusion.

In the presence of metastatic disease, relative increases in hepatic arterial perfusion have been found on a global basis. Perfusion CT can also reveal occult hepatic metastases undetected by conventional CT (Cuenod et al., 2001; Platt et al., 1997; Sheafor et al., 2000b). CT measurements of hepatic perfusion amongst patients with colon cancer have been shown to provide risk stratification that is superior to the Dukes' classification (Miles et al., 2004).

Radioimmunotherapy (RIT)

Introduction

RIT is a form of cancer therapy that entails the use of molecular vectors to deliver radionuclides to tumours. The molecular vectors must have biological specificity for the target and are antibody-based whether intact, fragments or engineered constructs. Beta-emitting radionuclides are by far the most commonly used clinically. In principle it is the

ability to deliver enhanced radiation dose to systemic, and especially occult, disease that is their main theoretical advantage.

With targeted RIT, doses depend on such factors as the level of expression of cell surface or membrane transport proteins, metabolic pathways, vascular supply, capillary permeability and cellular conformation. The interaction between targeting agents and their biological targets can be divided into four factors:

1) Specificity: The main theoretical advantage - Enhanced levels of therapy can be delivered to tumours even if they are too small to be detected by imaging. This ability is compromised by cross-reactivity with other cell types, non-specific accumulation of radiolabeled molecules or metabolites in excretory pathways, and irradiation of normal tissues by activity in the systemic circulation.

2) Non-uniformity: The uptake of targeting agents in tumours is characteristically heterogeneous. This may be due to mechanisms such as elevated interstitial fluid pressure within tumours or to binding site barriers. A heterogeneous radionuclide distribution gives rise to a non-uniform dose distribution with the degree of correspondence determined by the range of emissions from the radionuclide (Humm JL, 1995; Yorke ED, 1993).

3) Potency: This is influenced by the nature of particulate emissions (alpha, beta or Auger electrons), the cellular conformation and radiobiological characteristics of the tumour and the uniformity of the dose distribution.

4) Range: Ionizing particles emitted as a consequence of nuclear decay have a finite range. This has the potential advantage that radionuclides do not have to be internalized or in contact with every tumour cell in order to deliver effective treatment. Tumour cells in regions with restricted radionuclide uptake may be sterilized by "bystander effect" radiation from activity in other parts of the tumour. The amount of bystander effect depends on the spatial configuration of tumour cells and the emission range of the radionuclide. The finite emission range also means that radionuclides present in the blood pool can produce incidental irradiation of the entire body and particularly the bone marrow.

Basic dosimetric and radiobiological factors

A large number of beta-emitting radionuclides have potential clinical application. From the point of view of radiation dosimetry the most important parameters of a radionuclide are its energy emission spectrum and half-life, $T_{1/2}$. If the number of radionuclide atoms per unit mass is N and the energy emitted per disintegration is E, then the absorbed dose-rate is proportional to $NE/T_{1/2}$ for conditions of electronic equilibrium. The ratio $E/T_{1/2}$ is thus a useful indicator of the intrinsic radiotherapeutic potency of the radionuclide. **Table 1.7** shows $E/T_{1/2}$ for a number of β-emitting radionuclides.

Radionuclide	$T_{1/2}$(day)	$E/T_{1/2}$(keV/day)	Optimal size(mm)
^{32}P	14.3	49	18 – 30
^{33}P	25.4	3	<0.2 - 1.0
^{47}Sc	3.35	49	2.0 - 3.8
^{67}Cu	2.58	60	1.6 - 2.8
^{77}As	1.62	140	3.6 - 6.0
^{90}Y	**2.67**	**352**	**28 – 42**
^{105}Rh	1.47	104	2.0 - 3.6
^{109}Pd	0.56	780	6 – 9
^{111}Ag	7.45	47	7 – 13
^{121}Sn	1.13	101	1.0 - 2.0
^{131}I	***8.02***	***24***	***2.6 - 5.0***
^{142}Pr	0.80	1012	24 – 34
^{143}Pr	13.6	23	6 – 11
^{149}Pm	2.21	162	8 – 12
^{153}Sm	1.95	138	2.8 - 5.0
^{159}Gd	0.77	403	6 – 9
^{166}Ho	1.12	620	18 – 25
^{177}Lu	6.71	22	1.2 - 3.0
^{186}Re	3.78	90	7 – 12
^{188}Re	0.71	1096	23 – 32
^{194}Ir	0.80	1003	24 – 34
^{199}Au	3.14	45	0.4 - 1.2

Table 1.7 - Physical Properties of Medical Radionuclides

In targeted therapy, the absorbed dose-rates experienced by both tumours and normal organs vary with time and are generally more complex than in other forms of radiation

therapy. This is caused by biological processes of accumulation and clearance superimposed on a background of physical decay.

The size dependency of tumour response

If the tumour sphere is large in comparison to the emission range, most of the emitted energy is absorbed and the absorbed fraction will be close to one. If the tumour sphere is small in comparison to the range, a proportion of the emitted energy will escape and the absorbed fraction may be significantly less than one (**Figure 1.13**).

Fig. 1.13 - Calculated values of the absorbed fraction (ϕ) as a function of sphere diameter for a selection of radionuclides with different emission spectra (Bardiès M, 1994)

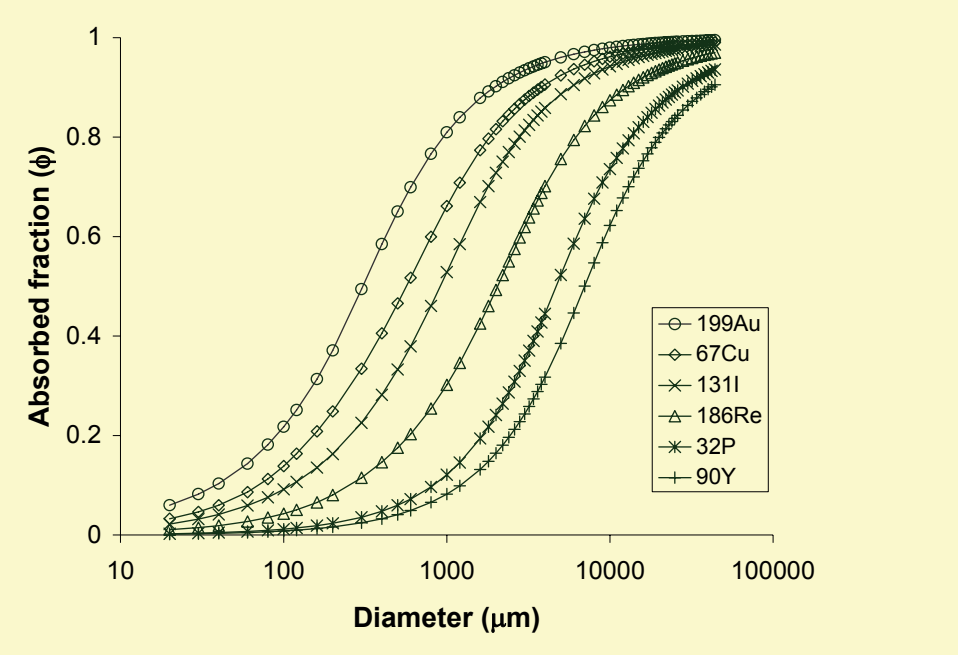

Data such as these enable the probability of tumour cure to be modelled as a function of tumour size for targeted therapies (O'Donoghue JA, 1995). In this simple model of tumour response it is assumed that tumours are spherical and are composed of a mixture of spherical tumour cells and an unspecified intercellular matrix of unit density material.

The relationship between tumour size and cure probability derived from this model is shown in **Figure 1.14** for ^{131}I. This is based on the assumption that clonogenic cell density and activity per unit mass are size-independent. Each curve corresponds to a different value of initial activity per gram of tumour. The model suggests that there will be a certain tumour size where the probability of cure is maximized. In the case of ^{131}I this occurs at a tumour diameter of around 3.5mm. The difference is caused by the reduction in energy absorption, and consequently absorbed dose, as tumours get smaller. Corresponding

relationships for other radionuclides have the same general shape, but the position of the maximum value depends on the details of the emission spectrum. Optimal tumour sizes for higher energy emitters are larger than for lower energy emitters. This is summarized in **Table 1.7** for a selection of radionuclides.

Fig. 1.14 - Relationship between tumour size and cure probability for ^{131}I. From O'Donoghue & Hopkins – Biologically Targeted Radionuclide Therapy – Biomodelling In Clinical Radiation Oncology

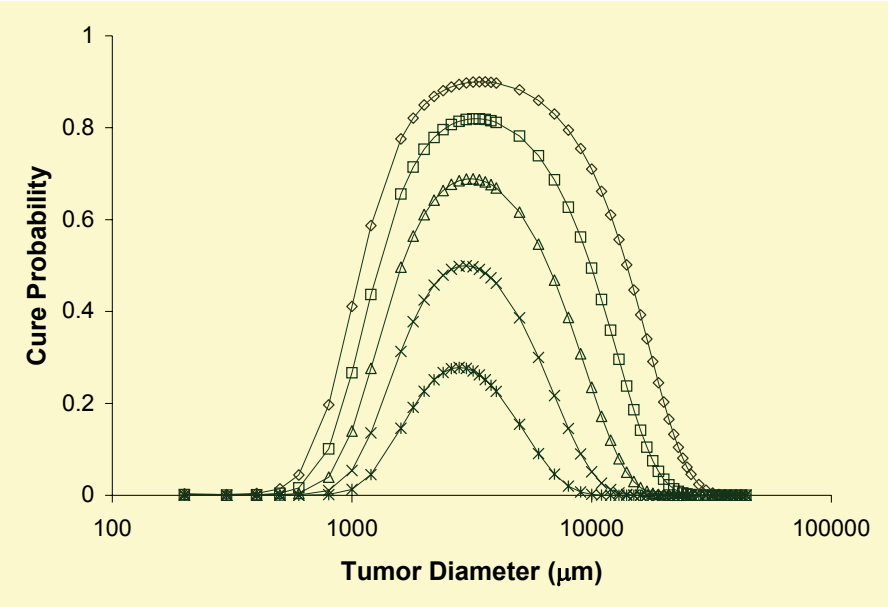

A5B7

RIT is effective in patients, particularly in the treatment of lymphoma, and encouraging responses have also been seen in the treatment of solid tumours (Boerman et al., 2007; Boswell & Brechbiel, 2007; Dearling & Pedley, 2007; Karagiannis, 2007; Napier MP, 1998; Park & Press, 2007).

A5B7 is a murine IgG anti-CEA monoclonal antibody that can be shown to localise in human colon carcinoma xenografts (Pedley, 1987). A5B7 is most effective at the tumour rim but has poor penetration of the tumour centre (Flynn AA, 1999) whereas CA4P is most effective in the tumour centre with sparing of the tumour rim (Dark et al., 1997). Also, trapping of radiolabelled antibody in the tumour by CA4P enhances the effect of RIT (Pedley B, personal communication, 2005). Therefore, the combination of RIT and CA4P is a promising therapeutic strategy for patients with advanced gastrointestinal carcinoma.

A5B7 is utilised to specifically target CEA positive cells. ^{131}I is a radioisotope with a beta emission capable of killing tumour cells over a range of up to 40 cell diameters and a gamma emission of 364keV, which is suitable for imaging with a gamma camera for quantitative analysis of normal tissue and tumour biodistribution. Radioimmunotherapy with ^{131}I-A5B7 has been shown to result in significant tumour growth delays in animal tumour models (Pedley et al., 1996)

A phase I/II study of RIT with ^{131}I-A5B7 was performed in patients with CEA expressing metastatic colorectal carcinoma (Lane D, 1994). 10 patients received RIT with ^{131}I-A5B7. Cyclosporin was administered to prevent the formation of Human Anti-mouse Antibodies (HAMA) and to allow repeated therapy. The MTD was established at 2400MBq/m^2 with DLT of thrombocytopenia and neutropenia. Cyclosporin was thought to be responsible for the other toxicities experienced, including nausea, vomiting and mild abnormalities in liver and renal function tests (Ledermann JA, 1991). Localisation of the radiolabelled antibody to tumour was demonstrated by quantitative gamma camera imaging. The mean half-life of ^{131}I-A5B7 in blood was 28.6h and in tumour was 59.5h. One PR was seen in a patient with a lung metastasis.

If small volume solid tumours are treated with RIT then higher response rates than those reported by Lane et al are seen. A phase I/II study of patients with colorectal cancer with total tumour bulk ≤2.5cm produced a complete or partial response rate of 26% with an additional 39% patients having stabilisation of previously rapidly progressing disease for up to 18 months (Behr T, 1999). These data suggest that, particularly in small volume disease, which has relatively little hypovascular component, RIT alone may be as effective as current conventional chemotherapy, with the advantage of having more tolerable side effects such as reduced gastrointestinal mucosal toxicity.

Pre-clinical efficacy studies of the combination of ^{131}I-A5B7 and CA4P were performed in a xenograft model, using the SW1222 human colon adenocarcinoma implanted in the flanks of nude mice. ^{131}I-A5B7 was administered intravenously at a dose of 7.4MBq. 200mg/kg of CA4P was given intraperitoneally 48h after the RIT. 5 out of 6 mice (85%) that received the combination showed complete tumour eradication that continued to be sustained until the experiment was terminated after 9 months (Pedley et al., 2001). No viable tumour cells were subsequently found at the implantation site of the cured mice. The only tumour to regrow did so after 97 days. CA4P alone had no effect on tumour growth compared to the controls, and ^{131}I-A5B7 alone produced tumour growth inhibition of

approximately 35 days, but all tumours subsequently regrew – **Fig. 1.15** (Pedley et al., 2001).

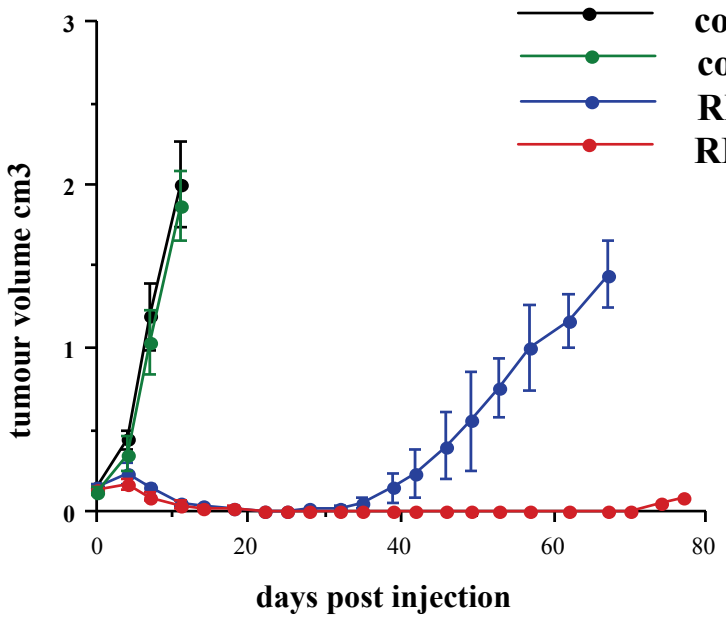

Figure 1.15 – A5B7/CA4P Phase I Trial in Mice
(Pedley et al., 2001)

Single agent CA4P has no effect on tumour growth delay in nude mice. A5B7 alone

Biodistribution studies show that administering CA4P 48 hours after ^{131}I-A5B7 results in trapping of the radioantibody within the tumour. Tumours retain an average of 90% greater radioantibody after CA4P administration compared with controls receiving radioantibody alone (Pedley et al., 2001). This retention appears most marked around the periphery of the tumour. The biodistribution of radioantibody in normal tissues remains unaffected by the addition of CA4P. Similar results were obtained when ^{131}I-A5B7 was combined with DMXAA (Pedley et al., 1996). It is therefore likely that ^{131}I-A5B7 and CA4P are working in a complementary and synergistic manner on different areas of the tumour.

There are three possible mechanisms:

1) Additive killing of the tumour centre by CA4P and the rim by ^{131}I-A5B7
2) Enhancement of the effect of ^{131}I-A5B7 by increased retention of radioantibody following CA4P-induced vessel collapse
3) A combination of 1 and 2, with option 3 being the most probable.

The basis for this hypothesis is that CA4P induced vascular collapse will trap radioantibody in the tumour, providing the CA4P is administered long enough after radioantibody to allow for biodistribution into the tumour. As CA4P has a much smaller effect on normal vasculature, the trapping phenomenon appears specific to tumours. Whether this phenomenon actually leads to any significant clinical benefit is debateable.

References

Abdollahi, A., Schwager, C., Kleeff, J., Esposito, I., Domhan, S., Peschke, P., Hauser, K., Hahnfeldt, P., Hlatky, L., Debus, J., Peters, J.M., Friess, H., Folkman, J. & Huber, P.E. (2007). Transcriptional network governing the angiogenic switch in human pancreatic cancer. *Proc Natl Acad Sci U S A*, **104,** 12890-5.

Abramsson, A., Lindblom, P. & Betsholtz, C. (2003). Endothelial and nonendothelial sources of PDGF-B regulate pericyte recruitment and influence vascular pattern formation in tumors. *J Clin Invest*, **112,** 1142-51.

Ahmad, S.A., Liu, W., Jung, Y.D., Fan, F., Reinmuth, N., Bucana, C.D. & Ellis, L.M. (2001a). Differential expression of angiopoietin-1 and angiopoietin-2 in colon carcinoma. A possible mechanism for the initiation of angiogenesis. *Cancer*, **92,** 1138-43.

Ahmad, S.A., Liu, W., Jung, Y.D., Fan, F., Wilson, M., Reinmuth, N., Shaheen, R.M., Bucana, C.D. & Ellis, L.M. (2001b). The effects of angiopoietin-1 and -2 on tumor growth and angiogenesis in human colon cancer. *Cancer Res*, **61,** 1255-9.

Airley, R., Loncaster, J., Davidson, S., Bromley, M., Roberts, S., Patterson, A., Hunter, R., Stratford, I. & West, C. (2001). Glucose transporter glut-1 expression correlates with tumor hypoxia and predicts metastasis-free survival in advanced carcinoma of the cervix. *Clin Cancer Res*, **7,** 928-34.

Akagi, K., Ikeda, Y., Sumiyoshi, Y., Kimura, Y., Kinoshita, J., Miyazaki, M. & Abe, T. (2002). Estimation Of Angiogenesis With Anti-CD105 Immunostaining In The Process Of Colorectal Cancer Development. *Surgery*, **131,** S109 - S113.

Anderson, H.L., Yap, J.T., Miller, M.P., Robbins, A., Jones, T. & Price, P.M. (2003). Assessment of pharmacodynamic vascular response in a phase I trial of combretastatin A4 phosphate. *J Clin Oncol*, **21,** 2823-30.

Astra Zeneca Pharmaceuticals (Macclesfield , U. Toprol-XL product information.

Axel, L. (1980). Cerebral blood flow determination by rapid-sequence computed tomography: theoretical analysis. *Radiology*, **137,** 679-86.

Bach, F., Uddin, F.J. & Burke, D. (2007). Angiopoietins in malignancy. *Eur J Surg Oncol*, **33,** 7-15.

Bader, T.R., Herneth, A.M., Blaicher, W., Steininger, R., Muhlbacher, F., Lechner, G. & Grabenwoger, F. (1998). Hepatic perfusion after liver transplantation: noninvasive measurement with dynamic single-section CT. *Radiology*, **209,** 129-34.

Baguley, B.C., Zhuang, L. & Kestell, P. (1997). Increased plasma serotonin following treatment with flavone-8-acetic acid, 5,6-dimethylxanthenone-4-acetic acid, vinblastine, and colchicine: relation to vascular effects. *Oncol Res*, **9,** 55-60.

Bardiès M, C.J. (1994). Absorbed doses for internal radiotherapy from 22 beta-emitting radionuclides: beta dosimetry of small spheres. *Phys Med Biol*, **39,** 961 - 981.

Bazett, H.C. (1920). An Analysis Of The Time Relations Of Electrocardiograms. *Heart*, **7,** 353 - 367.

Beauregard, D.A., Hill, S.A., Chaplin, D.J. & Brindle, K.M. (2001). The susceptibility of tumors to the antivascular drug combretastatin A4 phosphate correlates with vascular permeability. *Cancer Res*, **61,** 6811-5.

Beauregard, D.A., Pedley, R.B., Hill, S.A. & Brindle, K.M. (2002). Differential sensitivity of two adenocarcinoma xenografts to the anti-vascular drugs combretastatin A4 phosphate and 5,6-dimethylxanthenone-4-acetic acid, assessed using MRI and MRS. *NMR Biomed*, **15,** 99-105.

Beauregard, D.A., Thelwall, P.E., Chaplin, D.J., Hill, S.A., Adams, G.E. & Brindle, K.M. (1998). Magnetic resonance imaging and spectroscopy of combretastatin A4 prodrug-induced disruption of tumour perfusion and energetic status. *Br J Cancer*, **77,** 1761-7.

Beerepoot, L.V., Radema, S.A., Witteveen, E.O., Thomas, T., Wheeler, C., Kempin, S. & Voest, E. (2006). Phase I Clinical Evaluation Of Weekly Administration of the Novel Vascular Targeting Agent, ZD6126, In Patients With Solid Tumors. *J Clin Oncol*, **24,** 1491 - 1498.

Behr T, L.T., Canelo R, Wormann B, Hiddemann W, Ringe B, Becker H, Becker W. (1999). Radioimmunotherapy Of Small Volume Disease Of Colorectal Cancer: Results Of A Clinical Phase I/II Trial (abstract). *Eur J Cancer*, **35,** S51.

Bellomi, M., Petralia, G., Sonzogni, A., Zampino, M.G. & Rocca, A. (2007). CT perfusion for the monitoring of neoadjuvant chemotherapy and radiation therapy in rectal carcinoma: initial experience. *Radiology*, **244,** 486-93.

Benjamin, L.E., Hemo, I. & Keshet, E. (1998). A plasticity window for blood vessel remodelling is defined by pericyte coverage of the preformed endothelial network and is regulated by PDGF-B and VEGF. *Development*, **125,** 1591-8.

Betsholtz, C. (2000). Functions Of Platelet Derived Growth Factor And Its Receptors Deduced From Gene Inactivation In Mice. *Journal Of Clinical Ligand Assay*, **23,** 206 - 213.

Blakey, D.C., Westwood, F.R., Walker, M., Hughes, G.D., Davis, P.D., Ashton, S.E. & Ryan, A.J. (2002). Antitumor activity of the novel vascular targeting agent ZD6126 in a panel of tumor models. *Clin Cancer Res*, **8,** 1974-83.

Blomley, M.J., Coulden, R., Dawson, P., Kormano, M., Donlan, P., Bufkin, C. & Lipton, M.J. (1995). Liver perfusion studied with ultrafast CT. *J Comput Assist Tomogr*, **19,** 424-33.

Boehm, T., Folkman, J., Browder, T. & O'Reilly, M.S. (1997). Antiangiogenic therapy of experimental cancer does not induce acquired drug resistance. *Nature*, **390,** 404-7.

Boerman, O.C., Koppe, M.J., Postema, E.J., Corstens, F.H. & Oyen, W.J. (2007). Radionuclide therapy of cancer with radiolabeled antibodies. *Anticancer Agents Med Chem*, **7,** 335-43.

Borre, M., Bentzen, S.M., Nerstrom, B. & Overgaard, J. (1998). Tumour Cell Proliferation And Survival In Patients With Prostate Cancer Followed Expectantly. *J Urol*, **159,** 1609 - 1614.

Boswell, C.A. & Brechbiel, M.W. (2007). Development of radioimmunotherapeutic and diagnostic antibodies: an inside-out view. *Nucl Med Biol*, **34,** 757-78.

Burrows, F.J., Derbyshire, E.J., Tazzari, P.L., Amlot, P., Gazdar, A.F., King, S.W., Letarte, M., Vitetta, E.S. & Thorpe, P.E. (1995). Up-regulation of endoglin on vascular endothelial cells in human solid tumors: implications for diagnosis and therapy. *Clin Cancer Res*, **1,** 1623-34.

Burrows, F.J. & Thorpe, P.E. (1993). Eradication of large solid tumors in mice with an immunotoxin directed against tumor vasculature. *Proc Natl Acad Sci U S A*, **90,** 8996-9000.

Cai, W. & Chen, X. (2006). Anti-angiogenic cancer therapy based on integrin alphavbeta3 antagonism. *Anticancer Agents Med Chem*, **6,** 407-28.

Cenic, A., Nabavi, D.G., Craen, R.A., Gelb, A.W. & Lee, T.Y. (1999). Dynamic CT Measurement of Cerebral Blood Flow : A Validation Study. *AJNR*, **20,** 63 - 73.

Chantrain, C.F., Henriet, P., Jodele, S., Emonard, H., Feron, O., Courtoy, P.J., DeClerck, Y.A. & Marbaix, E. (2006). Mechanisms of pericyte recruitment in tumour angiogenesis: a new role for metalloproteinases. *Eur J Cancer*, **42,** 310-8.

Chaplin, D.J. & Dougherty, G.J. (1999). Tumour vasculature as a target for cancer therapy. *Br J Cancer*, **80 Suppl 1,** 57-64.

Chaplin, D.J. & Horsman, M.R. (1994). The influence of tumour temperature on ischemia-induced cell death: potential implications for the evaluation of vascular mediated therapies. *Radiother Oncol*, **30,** 59-65.

Chaplin, D.J., Horsman, M.R. & Siemann, D.W. (2006). Current development status of small-molecule vascular disrupting agents. *Curr Opin Investig Drugs*, **7,** 522-8.

Chaplin, D.J., Pettit, G.R. & Hill, S.A. (1999). Anti-vascular approaches to solid tumour therapy: evaluation of combretastatin A4 phosphate. *Anticancer Res*, **19,** 189-95.

Chaplin, D.J., Pettit, G.R., Parkins, C.S. & Hill, S.A. (1996). Antivascular approaches to solid tumour therapy: evaluation of tubulin binding agents. *Br J Cancer Suppl*, **27,** S86-8.

Ching, L.M., Cao, Z., Kieda, C., Zwain, S., Jameson, M.B. & Baguley, B.C. (2002). Induction of endothelial cell apoptosis by the antivascular agent 5,6-Dimethylxanthenone-4-acetic acid. *Br J Cancer*, **86,** 1937-42.

Ching, L.M., Goldsmith, D., Joseph, W.R., Korner, H., Sedgwick, J.D. & Baguley, B.C. (1999). Induction of intratumoral tumor necrosis factor (TNF) synthesis and hemorrhagic necrosis by 5,6-dimethylxanthenone-4-acetic acid (DMXAA) in TNF knockout mice. *Cancer Res*, **59,** 3304-7.

Cliffe, S., Taylor, M.L., Rutland, M., Baguley, B.C., Hill, R.P. & Wilson, W.R. (1994). Combining bioreductive drugs (SR 4233 or SN 23862) with the vasoactive agents flavone acetic acid or 5,6-dimethylxanthenone acetic acid. *Int J Radiat Oncol Biol Phys*, **29,** 373-7.

Cooney, M.M., Radivoyevitch, T., Dowlati, A., Overmoyer, B., Levitan, N., Robertson, K., Levine, S.L., DeCaro, K., Buchter, C., Taylor, A., Stambler, B.S. & Remick, S.C. (2004). Cardiovascular safety profile of combretastatin a4 phosphate in a single-dose phase I study in patients with advanced cancer. *Clin Cancer Res*, **10,** 96-100.

Cooney, M.M., van Heeckeren, W., Bhakta, S., Ortiz, J. & Remick, S.C. (2006). Drug insight: vascular disrupting agents and angiogenesis--novel approaches for drug delivery. *Nat Clin Pract Oncol*, **3,** 682-92.

Cooper, R., Sarioglu, S., Sokmen, S., Fuzun, M., Kupelioglu, A., Valentine, H., Gorken, I.B., Airley, R. & West, C. (2003). Glucose transporter-1 (GLUT-1): a potential marker of prognosis in rectal carcinoma? *Br J Cancer*, **89,** 870-6.

Corbett, T.H., Bissery, M.C., Wozniak, A., Plowman, J., Polin, L., Tapazoglou, E., Dieckman, J. & Valeriote, F. (1986). Activity of flavone acetic acid (NSC-347512) against solid tumors of mice. *Invest New Drugs*, **4,** 207-20.

Cowden Dahl, K.D., Robertson, S.E., Weaver, V.M. & Simon, M.C. (2005). Hypoxia-inducible factor regulates alphavbeta3 integrin cell surface expression. *Mol Biol Cell*, **16,** 1901-12.

Cuenod, C., Leconte, I., Siauve, N., Resten, A., Dromain, C., Poulet, B., Frouin, F., Clement, O. & Frija, G. (2001). Early changes in liver perfusion caused by occult metastases in rats: detection with quantitative CT. *Radiology*, **218,** 556-61.

d'Arcy, J.A., Collins, D.J. , Padhani A.R. , Walker-Samuel S. , Suckling J. , Leach M.O. (2006). Informatics in Radiology. Magnetic Resonance Imaging Workbench: Analysis and Visualisation of Dynamic Contrast Enhanced MR Imaging Data. *Radiographics*, **26,** 621 - 632.

Dachs, G.U., Steele, A.J., Coralli, C., Kanthou, C., Brooks, A.C., Gunningham, S.P., Currie, M.J., Watson, A.I., Robinson, B.A. & Tozer, G.M. (2006). Anti-vascular agent Combretastatin A-4-P modulates hypoxia inducible factor-1 and gene expression. *BMC Cancer*, **6,** 280.

Dark, G.G., Hill, S.A., Prise, V.E., Tozer, G.M., Pettit, G.R. & Chaplin, D.J. (1997). Combretastatin A-4, an agent that displays potent and selective toxicity toward tumor vasculature. *Cancer Res*, **57,** 1829-34.

Davis, P.D., Dougherty, G.J., Blakey, D.C., Galbraith, S.M., Tozer, G.M., Holder, A.L., Naylor, M.A., Nolan, J., Stratford, M.R., Chaplin, D.J. & Hill, S.A. (2002). ZD6126: a novel vascular-targeting agent that causes selective destruction of tumor vasculature. *Cancer Res*, **62,** 7247-53.

Dearling, J.L. & Pedley, R.B. (2007). Technological advances in radioimmunotherapy. *Clin Oncol (R Coll Radiol)*, **19,** 457-69.

DelProposto Z , L.P., Latif Z et al. (2002). MRI evaluation of the effects of the vascular targeting agent ZD6126 on tumor vasculature. *Proc Am Soc Clin Oncol*, **21,** Abstr 440.

Dowlati, A., Robertson, K., Cooney, M., Petros, W.P., Stratford, M., Jesberger, J., Rafie, N., Overmoyer, B., Makkar, V., Stambler, B., Taylor, A., Waas, J., Lewin, J.S., McCrae, K.R. & Remick, S.C. (2002). A phase I pharmacokinetic and translational study of the novel vascular targeting agent combretastatin a-4 phosphate on a single-dose intravenous schedule in patients with advanced cancer. *Cancer Res*, **62,** 3408-16.

Drake, C.J., Cheresh, D.A. & Little, C.D. (1995). An Antagonist Of alpha v beta 3 integrin Prevents Maturation Of Blood Vessels During Embryonic Neovascularisation. *J Cell Sci*, **108,** 2655 - 2661.

Dugdale, P.E., Miles, K.A. & Bunce, I.H. (1999). CT Measurement of Perfusion And Permeability Within Lymphoma Masses And Its Ability To Assess Grade, Activity And Chemotherapeutic Response. *J Comput Assist Tomogr*, **23,** 540 - 547.

Eberhard, A., Kahlert, S., Goede, V., Hemmerlein, B., Plate, K.H. & Augustin, H.G. (2000). Heterogeneity of angiogenesis and blood vessel maturation in human tumors: implications for antiangiogenic tumor therapies. *Cancer Res*, **60,** 1388-93.

Eliceiri, B.P. & Cheresh, D. (1999). The Role Of alpha-v Integrins During Angiogenesis: Insights Into Potential Mechanisms Of Actiuon And Clinical Development. *J Clin Invest*, **103,** 1227 - 1230.

Evelhoch, J., LoRusso, P., Latif, Z., Morton, P., Wolf, W., McKinley, M., Waterton, J. & Barge, A. (2001). Reproducibility of dynamic contrast enhanced (DCE-MRI) assessment of tumor vascularity. *Proc Am Soc Clin Oncol*, **20,** Abstract 399.

Evelhoch, J.L. (1999). Key factors in the acquisition of contrast kinetic data for oncology. *J Magn Reson Imaging*, **10**.

Evelhoch, J.L., LoRusso, P.M., He, Z., DelProposto, Z., Polin, L., Corbett, T.H., Langmuir, P., Wheeler, C., Stone, A., Leadbetter, J., Ryan, A.J., Blakey, D.C. & Waterton, J.C. (2004). Magnetic resonance imaging measurements of the response of murine and human tumors to the vascular-targeting agent ZD6126. *Clin Cancer Res*, **10,** 3650-7.

Farrington-Rock, C., Crofts, N.J., Doherty, M.J., Ashton, B.A., Griffin-Jones, C. & Canfield, A.E. (2004). Chondrogenic and adipogenic potential of microvascular pericytes. *Circulation*, **110,** 2226-32.

Ferrara, N. (2004). Vascular endothelial growth factor: basic science and clinical progress. *Endocr Rev*, **25,** 581-611.

Flynn AA, G.A., Boxer GM, Casey JL, Pedley RB, Begent RHJ. (1999). The Measurement Of Uniformity Of Radiolabelled AnA Novel Technique Using Radioluminography, For tibody Distribution In A Colorectal Cancer Xenograft Model. *International Journal of Radiation Oncology Biology And Physics*, **43,** 183 - 189.

Folberg, R., Hendrix, M.J. & Maniotis, A.J. (2000). Vasculogenic mimicry and tumor angiogenesis. *Am J Pathol*, **156,** 361-81.

Folkman, J. (1971). Tumour Angiogenesis : Therapeutic Implications. *N Engl J Med*, **285,** 1182 - 1186.

Fontanini, G., Faviana, P., Lucchi, M., Boldrini, L., Mussi, A., Camacci, T., Mariani, M.A., Angeletti, C.A., Basolo, F. & Pingitore, R. (2002). A high vascular count and overexpression of vascular endothelial growth factor are associated with unfavourable prognosis in operated small cell lung carcinoma. *Br J Cancer*, **86,** 558-63.

Fridericia, L.S. (1920). Die Systolendauer Im Electrokardiogramm Bei Normalen Menchan Und Bei Herzdranken. *Acta Med. Scand.*, **53,** 469 - 486.

Gadgeel SM , L.P., Wozniak AJ , Wheeler C. (2002). A dose escalation study of the novel vascular targeting agent ZD6126 in patients with solid tumours. *Proc Am Soc Clin Oncol*, **21,** Abstr 438.

Galbraith, S.M., Chaplin, D.J., Lee, F., Stratford, M.R., Locke, R.J., Vojnovic, B. & Tozer, G.M. (2001). Effects of combretastatin A4 phosphate on endothelial cell morphology in vitro and relationship to tumour vascular targeting activity in vivo. *Anticancer Res*, **21,** 93-102.

Galbraith, S.M., Lodge, M.A., Taylor, N.J., Rustin, G.J., Bentzen, S., Stirling, J.J. & Padhani, A.R. (2002a). Reproducibility of dynamic contrast-enhanced MRI in human muscle and tumours: comparison of quantitative and semi-quantitative analysis. *NMR Biomed*, **15,** 132-42.

Galbraith, S.M., Maxwell, R.J., Lodge, M.A., Tozer, G.M., Wilson, J., Taylor, N.J., Stirling, J.J., Sena, L., Padhani, A.R. & Rustin, G.J. (2003). Combretastatin A4 phosphate has tumor antivascular activity in rat and man as demonstrated by dynamic magnetic resonance imaging. *J Clin Oncol*, **21,** 2831-42.

Galbraith, S.M., Rustin, G.J., Lodge, M.A., Taylor, N.J., Stirling, J.J., Jameson, M., Thompson, P., Hough, D., Gumbrell, L. & Padhani, A.R. (2002b). Effects of 5,6-dimethylxanthenone-4-acetic acid on human tumor microcirculation assessed by dynamic contrast-enhanced magnetic resonance imaging. *J Clin Oncol*, **20,** 3826-40.

Gandhi, D., Chepeha, D.B., Miller, T., Carlos, R.C., Bradford, C.R., Karamchandani, R., Worden, F., Eisbruch, A., Teknos, T.N., Wolf, G.T. & Mukherji, S.K. (2006). Correlation between initial and early follow-up CT perfusion parameters with endoscopic tumor response in patients with advanced squamous cell carcinomas of the oropharynx treated with organ-preservation therapy. *AJNR Am J Neuroradiol*, **27,** 101-6.

Ganss, R. (2006). Tumor stroma fosters neovascularization by recruitment of progenitor cells into the tumor bed. *J Cell Mol Med*, **10,** 857-65.

Gaya, A.M. & Rustin, G.J. (2005). Vascular disrupting agents: a new class of drug in cancer therapy. *Clin Oncol (R Coll Radiol)*, **17,** 277-90.

Gee, M.S., Procopio, W.N., Makonnen, S., Feldman, M.D., Yeilding, N.M. & Lee, W.M. (2003). Tumor vessel development and maturation impose limits on the effectiveness of anti-vascular therapy. *Am J Pathol*, **162,** 183-93.

Gerhardt, H. & Betsholtz, C. (2003). Endothelial-pericyte interactions in angiogenesis. *Cell Tissue Res*, **314,** 15-23.

Gillard, J.H., Minhas, P.S. & Hayball, M.P.e.a. (2000). Assessment of Quantitative Cerebral Perfusion Imaging With H2(15)O PET. *Neurol Res*, **22,** 457 - 464.

Glade Bender, J., Cooney, E.M., Kandel, J.J. & Yamashiro, D.J. (2004). Vascular remodeling and clinical resistance to antiangiogenic cancer therapy. *Drug Resist Updat*, **7,** 289-300.

Goede, V., Schmidt, T., Kimmina, S., Kozian, D. & Augustin, H.G. (1998). Analysis of blood vessel maturation processes during cyclic ovarian angiogenesis. *Lab Invest*, **78,** 1385 - 1394.

Goh, V., Halligan, S., Gartner, L., Bassett, P. & Bartram, C.I. (2006). Quantitative colorectal cancer perfusion measurement by multidetector-row CT: does greater tumour coverage improve measurement reproducibility? *Br J Radiol*, **79,** 578-83.

Goh, V. & Padhani, A.R. (2006). Imaging Tumour Angiogenesis: Functional Assessment Using MDCT or MRI? *Abdom Imaging*, **31,** 194 - 199.

Goh, V., Padhani, A.R. & Rasheed, S. (2007). Functional imaging of colorectal cancer angiogenesis. *Lancet Oncol*, **8,** 245-55.

Griggs, J., Brindle, K.M., Metcalfe, J.C., Hill, S.A., Smith, G.A., Beauregard, D.A. & Hesketh, R. (2001a). Potent anti-metastatic activity of combretastatin-A4. *Int J Oncol*, **19,** 821-5.

Griggs, J., Hesketh, R., Smith, G.A., Brindle, K.M., Metcalfe, J.C., Thomas, G.A. & Williams, E.D. (2001b). Combretastatin-A4 disrupts neovascular development in non-neoplastic tissue. *Br J Cancer*, **84,** 832-5.

Griggs, J., Metcalfe, J.C. & Hesketh, R. (2001c). Targeting tumour vasculature: the development of combretastatin A4. *Lancet Oncol*, **2,** 82-7.

Grosios, K., Holwell, S.E., McGown, A.T., Pettit, G.R. & Bibby, M.C. (1999). In vivo and in vitro evaluation of combretastatin A-4 and its sodium phosphate prodrug. *Br J Cancer*, **81,** 1318-27.

Grosios, K., Loadman, P.M., Swaine, D.J., Pettit, G.R. & Bibby, M.C. (2000). Combination chemotherapy with combretastatin A-4 phosphate and 5-fluorouracil in an experimental murine colon adenocarcinoma. *Anticancer Res*, **20,** 229-33.

Haerslev, T., Jacobsen, G.K. & Zedeler, K. (1996). Correlation Of Growth Fraction By Ki-67 And Proliferating Cell Nuclear Antigen (PCNA) Immunohistochemistry With Histopathological Parameters And Prognosis In Primary Breast Carcinomas. *Breast Cancer Res Treat*, **37,** 101 - 113.

Hanahan, D. & Folkman, J. (1996). Patterns and emerging mechanisms of the angiogenic switch during tumorigenesis. *Cell*, **86,** 353-64.

Harvey, C.J., Blomley, M.J., Dawson, P., Morgan, J.A., Dooher, A., Deponte, J., Vernon, C.C. & Price, P. (2001). Functional CT imaging of the acute hyperemic response to radiation therapy of the prostate gland: early experience. *J Comput Assist Tomogr*, **25,** 43-9.

Hawighorst, T., Skobe, M., Streit, M., Hong, Y.K., Velasco, P., Brown, L.F., Riccardi, L., Lange-Asschenfeldt, B. & Detmar, M. (2002). Activation of the tie2 receptor by angiopoietin-1 enhances tumor vessel maturation and impairs squamous cell carcinoma growth. *Am J Pathol*, **160,** 1381-92.

Hermans, R., Lambin, P. & van den Bogaert, W. (1997). Non Invasive Tumour Perfusion Measurement By Dynamic CT: Preliminary Results. *Radiother Oncol*, **44,** 159 - 162.

Hermans, R., Meijerink, M. & van den Bogaert, W. (2003). Tumour Perfusion Rate Determined Non Invasively By Dynamic CT Predicts Outcome In Head & Neck Cancer After Radiotherapy. *Int J Radiat Oncol Biol Phys*, **57,** 1351 - 1356.

Heslin, M.J., Cordon-Cardo, C., Lewis, J.J., Woodruff, J.M. & Brennan, M.F. (1998). Ki-67 Detected By MIB-1 Predicts Distant Metastasis And Tumour Mortality In Primary, High Grade Extremity Soft Tissue Sarcoma. *Cancer*, **83,** 490 - 497.

Hicklin, D.J. & Ellis, L.M. (2005). Role of the vascular endothelial growth factor pathway in tumor growth and angiogenesis. *J Clin Oncol*, **23,** 1011-27.

Hill, S.A., Chaplin, D.J., Lewis, G. & Tozer, G.M. (2002a). Schedule dependence of combretastatin A4 phosphate in transplanted and spontaneous tumour models. *Int J Cancer*, **102,** 70-4.

Hill, S.A., Toze, G.M., Pettit, G.R. & Chaplin, D.J. (2002b). Preclinical evaluation of the antitumour activity of the novel vascular targeting agent Oxi 4503. *Anticancer Res*, **22,** 1453-8.

Hoch, R.V. & Soriano, P. (2003). Roles Of PDGF In Animal Development. *Development*, **130,** 4769 - 4784.

Hori, K. & Saito, S. (2003). Microvascular mechanisms by which the combretastatin A-4 derivative AC7700 (AVE8062) induces tumour blood flow stasis. *Br J Cancer*, **89,** 1334-44.

Horsman, M.R., Christensen, K.L. & Overgaard, J. (1992). Relationship between the hydralazine-induced changes in murine tumor blood supply and mouse blood pressure. *Int J Radiat Oncol Biol Phys*, **22,** 455-8.

Horsman, M.R., Ehrnrooth, E., Ladekarl, M. & Overgaard, J. (1998). The effect of combretastatin A-4 disodium phosphate in a C3H mouse mammary carcinoma and a variety of murine spontaneous tumors. *Int J Radiat Oncol Biol Phys*, **42,** 895-8.

Horsman, M.R. & Murata, R. (2002). Combination of vascular targeting agents with thermal or radiation therapy. *Int J Radiat Oncol Biol Phys*, **54,** 1518-23.

Huang, X., Molema, G., King, S., Watkins, L., Edgington, T.S. & Thorpe, P.E. (1997). Tumor infarction in mice by antibody-directed targeting of tissue factor to tumor vasculature. *Science*, **275,** 547-50.

Humm JL, M.R., Lu XQ, Yang Y, Bump K, Beresford B, Chin LM. (1995). The spatial accuracy of cellular dose estimates obtained from 3D reconstructed serial tissue autoradiographs. *Phys. Med. Biol*, **40,** 163 - 180.

Iyer, S., Chaplin, D.J., Rosenthal, D.S., Boulares, A.H., Li, L.Y. & Smulson, M.E. (1998). Induction of apoptosis in proliferating human endothelial cells by the tumor-specific antiangiogenesis agent combretastatin A-4. *Cancer Res*, **58,** 4510-4.

Jacobsen, J., Rasmuson, T., Grankvist, K. & Ljungberg, B. (2000). Vascular Endothelial Growth Factor As A Prognostic Factor In Renal Cell Carcinoma. *J Urol*, **163,** 343 - 347.

Jain, R.K. (2003). Molecular regulation of vessel maturation. *Nat Med*, **9,** 685-93.

Jameson M , T.P., Baguley B , Evans B , Harvey V , Porter D , McCrystal M , Kestell P. (2000). Phase I Pharmacokinetic and Pharmacodynamic Study of 5,6-Dimethylxanthenone-4-Acetic Acid (DMXAA), a Novel Anti Vascular Agent. *Proc Am Soc Clin Oncol***,** Abstract 705.

Jameson, M.B., Baguley, B.C., Kestell, P., Zhao, L., Paxton, J.W., Thompson, P.I. & Waller, S. (2007). Pharmacokinetics of 5,6-dimethylxanthenone-4-acetic acid (AS1404), a novel vascular disrupting agent, in phase I clinical trial. *Cancer Chemother Pharmacol*, **59,** 681-7.

Jameson, M.B., Thompson, P.I., Baguley, B.C., Evans, B.D., Harvey, V.J., Porter, D.J., McCrystal, M.R., Small, M., Bellenger, K., Gumbrell, L., Halbert, G.W. & Kestell, P. (2003). Clinical aspects of a phase I trial of 5,6-dimethylxanthenone-4-acetic acid (DMXAA), a novel antivascular agent. *Br J Cancer*, **88,** 1844-50.

Jinzaki, M., Tanimoto, A. & Mukai, M.e.a. (2000). Double Phase Helical CT Of Small Renal Parenchymal Neoplasms : Correlation With Pathologic Findings And Tumour Angiogenesis. *J Comput Assist Tomogr*, **24,** 835 - 842.

Joseffson, A., Wikstrom, P., Granfors, T., Egevad, L., Karlberg, L., Stattin, P. & Bergh, A. (2005). Tumor Size, Vascular Density And Proliferation As Prognostic Markers In Gleeson 6 & 7 Prostate Tumors In Patients With Long Follow-Up And Non-Curative Treatment. *Eur Urol***,** In Press.

Kakolyris, S., Fox, S.B., Koukourakis, M., Giatromanolaki, A., Brown, N., Leek, R.D., Taylor, M., Leigh, I.M., Gatter, K.C. & Harris, A.L. (2000). Relationship of vascular maturation in breast cancer blood vessels to vascular density and metastasis, assessed by expression of a novel basement membrane component, LH39. *Br J Cancer*, **82,** 844-51.

Kanthou, C. & Tozer, G.M. (2002). The tumor vascular targeting agent combretastatin A-4-phosphate induces reorganization of the actin cytoskeleton and early membrane blebbing in human endothelial cells. *Blood*, **99,** 2060-9.

Karagiannis, T.C. (2007). Comparison of different classes of radionuclides for potential use in radioimmunotherapy. *Hell J Nucl Med*, **10,** 82-8.

Karlsson, L., Lindahl, P., Heath, J.K. & Betsholtz, C. (2000). Abnormal Gastrointestinal Development In PDGF-A and PDGFR-alpha Deficient Mice Implicates A Novel Mesenchymal Structure With Putative Instructive Properties In Villus Morphogenesis. *Development*, **127,** 3457 - 3466.

Kerr, D.J. & Kaye, S.B. (1989). Flavone acetic acid--preclinical and clinical activity. *Eur J Cancer Clin Oncol*, **25,** 1271-2.

Kety, S. (1960a). Blood-tissue exchange methods. Theory of blood-tissue exchange and its application to measurement of blood flow. *Meth Med Res*, **8**.

Kety, S. (1960b). Measurement of local blood flow by the exchange of an inert, diffusible substance. *Meth Med Res*, **8,** 228 - 236.

Kim, J.H., Kim, H.J. & Lee, K.H. (2004). Solitary Pulmonary Nodules: A Comparative Study Evaluating Contrast Enhanced Dynamic MR Imaging And CT. *J Comput Assist Tomogr*, **28,** 766 - 775.

Kirla, R., Salminen, E.K., Huhtala, S., Nuutinen, J.M., Talve, L., Haapasalo, H. & Kalimo, H. (2000). Prognostic Value Of The Expression Of Tumour Suppressor Genes p53, p21, p16 and Rb, and Ki-67 Labelling In High Grade Astrocytomas Treated With Radiotherapy. *J Neuro Oncol*, **46,** 71 - 80.

Lamar, J.M., Iyer, V. & Dipersio, C.M. (2007). Integrin alpha3beta1 Potentiates TGFbeta-Mediated Induction of MMP-9 in Immortalized Keratinocytes. *J Invest Dermatol*.

Landuyt, W., Ahmed, B., Nuyts, S., Theys, J., Op de Beeck, M., Rijnders, A., Anne, J., van Oosterom, A., van den Bogaert, W. & Lambin, P. (2001). In vivo antitumor effect of vascular targeting combined with either ionizing radiation or anti-angiogenesis treatment. *Int J Radiat Oncol Biol Phys*, **49,** 443-50.

Lane D, E.K., Begent R, Hope-Stone L, Green A, Casey J, Keep P, Kelly A, Ledermann J, Glaser M, Hilson A. (1994). Radioimmunotherapy Of Metastatic Colorectal Tumours With Iodine-131 Labelled Antibody To Carcinoembryonic Antigen : Phase I/II Study With Comparative Biodistribution Of Intact And F(ab)2 Antibodies. *Br J Cancer*, **70,** 521 - 525.

Lash, C.J., Li, A.E., Rutland, M., Baguley, B.C., Zwi, L.J. & Wilson, W.R. (1998). Enhancement of the anti-tumour effects of the antivascular agent 5,6-dimethylxanthenone-4-acetic acid (DMXAA) by combination with 5-hydroxytryptamine and bioreductive drugs. *Br J Cancer*, **78,** 439-45.

Leach, M., Brindle, K., Evelhoch, J., Griffiths, J., Horsman, M., Jackson, A., Judson, I., Knopp, M., Maxwell, R., McIntyre, D., Padhani, A., Price, P., Rathbone, R., Rustin, G., Tofts, P., Tozer, G., Vennart, W., Waterton, J., Williams, S. & Workman, P. (2003). Assessment of anti-angiogenic and anti-vascular therapeutics using Magnetic Resonance Imaging: recommendations for appropriate methodology for clinical trials. *Proc ISMRM*, **Toronto, Canada,** Abstract 1238.

Ledermann JA, B.R., Massof C, Kelly AMB, Adam T, Bagshawe KD. (1991). A Phase I Study Of Repeated Therapy With Radiolabelled Antibody To Carcinoembryonic Antigen Using Intermittent Or Continuous Administration Of Cyclosporin A To Suppress The Immune Response. *Int. J. Cancer*, **47,** 659 - 664.

Leggett, D.A., Kelley, B.B., Bunce, I.H. & Miles, K.A. (1997). Colorectal cancer: diagnostic potential of CT measurements of hepatic perfusion and implications for contrast enhancement protocols. *Radiology*, **205,** 716-20.

Leveen, P., Pekny, M., Gebre-Medhin, S., Swolin, B., Larsson, E. & Betsholtz, C. (1994). Mice Deficient For PDGF-B Show Renal, Cardiovascular and Haematological Abnormalities. *Genes Dev*, **8,** 1875 - 1887.

Li, L., Rojiani, A. & Siemann, D.W. (1998). Targeting the tumor vasculature with combretastatin A-4 disodium phosphate: effects on radiation therapy. *Int J Radiat Oncol Biol Phys*, **42,** 899-903.

Lin, C.M., Ho, H.H., Pettit, G.R. & Hamel, E. (1989). Antimitotic natural products combretastatin A-4 and combretastatin A-2: studies on the mechanism of their inhibition of the binding of colchicine to tubulin. *Biochemistry*, **28,** 6984-91.

Lindahl, P., Johansson, B.R., Leveen, P. & Betsholtz, C. (1997). Pericyte loss and microaneurysm formation in PDGF-B-deficient mice. *Science*, **277,** 242-5.

Linderholm, B., Lindh, B., Tavelin, B., Grankvist, K. & Henriksson, R. (2000). p53 and vascular-endothelial-growth-factor (VEGF) expression predicts outcome in 833 patients with primary breast carcinoma. *Int J Cancer*, **89,** 51-62.

Lippert, J.W., 3rd. (2007). Vascular disrupting agents. *Bioorg Med Chem*, **15,** 605-15.

Lode, H.N., Moehler, T., Xiang, R., Jonczyk, A., Gillies, S.D., Cheresh, D.A. & Reisfeld, R.A. (1999). Synergy between an antiangiogenic integrin alphav antagonist and an antibody-cytokine fusion protein eradicates spontaneous tumor metastases. *Proc Natl Acad Sci U S A*, **96,** 1591-6.

LoRusso S, G.S., Wozniak A, et al. (2001). A Phase I dose escalation trial of ZD6126, a novel vascular targeting agent, in patients with cancer refractory to other treatments. *Proc AACR-NCI-EORTC*, Abstr 36.

Mahadevan, V., Malik, S.T., Meager, A., Fiers, W., Lewis, G.P. & Hart, I.R. (1990). Role of tumor necrosis factor in flavone acetic acid-induced tumor vasculature shutdown. *Cancer Res*, **50,** 5537-42.

Malcontenti-Wilson, C., Chan, L., Nikfarjam, M., Muralidharan, V. & Christophi, C. (2007). Vascular targeting agent Oxi4503 inhibits tumor growth in a colorectal liver metastases model. *J Gastroenterol Hepatol*.

Maniotis, A.J., Folberg, R., Hess, A., Seftor, E.A., Gardner, L.M., Pe'er, J., Trent, J.M., Meltzer, P.S. & Hendrix, M.J. (1999). Vascular channel formation by human melanoma cells in vivo and in vitro: vasculogenic mimicry. *Am J Pathol*, **155,** 739-52.

Mauceri, H.J., Hanna, N.N., Beckett, M.A., Gorski, D.H., Staba, M.J., Stellato, K.A., Bigelow, K., Heimann, R., Gately, S., Dhanabal, M., Soff, G.A., Sukhatme, V.P., Kufe, D.W. & Weichselbaum, R.R. (1998). Combined effects of angiostatin and ionizing radiation in antitumour therapy. *Nature*, **394,** 287-91.

Maxwell, R.J., Wilson, J., Prise, V.E., Vojnovic, B., Rustin, G.J., Lodge, M.A. & Tozer, G.M. (2002). Evaluation of the anti-vascular effects of combretastatin in rodent tumours by dynamic contrast enhanced MRI. *NMR Biomed*, **15,** 89-98.

Mayer, A., Hockel, M., Wree, A. & Vaupel, P. (2005). Microregional Expression Of Glucose Transporter 1 And Oxygenation Status : Lack Of Correlation In Locally Advanced Cervical Cancers. *Clin Cancer Res*, **11,** 2768 - 2773.

McDonald, D.M., Munn, L. & Jain, R.K. (2000). Vasculogenic mimicry: how convincing, how novel, and how significant? *Am J Pathol*, **156,** 383-8.

McKeage, M.J., Fong, P., Jeffery, M., Baguley, B.C., Kestell, P., Ravic, M. & Jameson, M.B. (2006). 5,6-Dimethylxanthenone-4-acetic acid in the treatment of refractory tumors: a phase I safety study of a vascular disrupting agent. *Clin Cancer Res*, **12,** 1776-84.

Meijerink, M.R., van Cruijsen, H., Hoekman, K., Kater, M., van Schaik, C., van Waesberghe, J.H., Giaccone, G. & Manoliu, R.A. (2007). The use of perfusion CT for the evaluation of therapy combining AZD2171 with gefitinib in cancer patients. *Eur Radiol*, **17,** 1700-13.

Metheny-Barlow, L.J. & Li, L.Y. (2003). The enigmatic role of angiopoietin-1 in tumor angiogenesis. *Cell Res*, **13,** 309-17.

Miles, K.A. (1999). Tumour Angiogenesis And Its Relation To Contrast Enhancement On CT: A Revie. *Eur J Radiol*, **30,** 198 - 205.

Miles, K.A. (2002). Functional CT In Oncology. *Eur J Cancer*, **38,** 2079 - 2084.

Miles, K.A., Colyvas, K., Griffiths, M.R. & Bunce, I.H. (2004). Colon Cancer: Risk Stratification Using Perfusion CT. *Eur Radiol*, **14,** 129.

Miles, K.A., Hayball, M. & Dixon, A.K. (1991). Colour perfusion imaging: a new application of computed tomography. *Lancet*, **337,** 643-5.

Miles, K.A., Hayball, M.P. & Dixon, A.K. (1993). Functional images of hepatic perfusion obtained with dynamic CT. *Radiology*, **188,** 405-11.

Moilanen, E., Thomsen, L.L., Miles, D.W., Happerfield, D.W., Knowles, R.G. & Moncada, S. (1998). Persistent induction of nitric oxide synthase in tumours from mice treated with the anti-tumour agent 5,6-dimethylxanthenone-4-acetic acid. *Br J Cancer*, **77,** 426-33.

Moon, W.S., Park, H.S., Yu, K.H., Jang, K.Y., Kang, M.J., Park, H. & Tarnawski, A.S. (2006). Expression of angiopoietin 1, 2 and their common receptor Tie2 in human gastric carcinoma: implication for angiogenesis. *J Korean Med Sci*, **21,** 272-8.

Morikawa, S., Baluk, P., Kaidoh, T., Haskell, A., Jain, R.K. & McDonald, D.M. (2002). Abnormalities in pericytes on blood vessels and endothelial sprouts in tumors. *Am J Pathol*, **160,** 985-1000.

Murata, R., Siemann, D.W., Overgaard, J. & Horsman, M.R. (2001). Improved tumor response by combining radiation and the vascular-damaging drug 5,6-dimethylxanthenone-4-acetic acid. *Radiat Res*, **156,** 503-9.

Nam, J.O., Jeong, H.W., Lee, B.H., Park, R.W. & Kim, I.S. (2005). Regulation of tumor angiogenesis by fastatin, the fourth FAS1 domain of betaig-h3, via alphavbeta3 integrin. *Cancer Res*, **65,** 4153-61.

Napier MP, B.R. (1998). Radioimmunotherapy of Gastrointestinal Cancer. In *Cancer Radioimmunotherapy*, P, R. (ed) pp. 333 - 388. Harwood Academia, Boston.

Nelkin, B.D. & Ball, D.W. (2001). Combretastatin A-4 and doxorubicin combination treatment is effective in a preclinical model of human medullary thyroid carcinoma. *Oncol Rep*, **8,** 157-60.

Ng QS, C.D., Milner J, Meer K, Saunders MI, Hoskin PJ. (2005). Phase Ib Trial Of Combretastatin A4 Phosphate (CA4P) In Combination With Radiotherapy (RT) : Initial Clinical Results. *Proc ASCO*, **Abstract 3117**.

Ng, Q.S., Goh, V., Carnell, D., Meer, K., Padhani, A.R., Saunders, M.I. & Hoskin, P.J. (2007). Tumor antivascular effects of radiotherapy combined with combretastatin a4 phosphate in human non-small-cell lung cancer. *Int J Radiat Oncol Biol Phys*, **67,** 1375-80.

O'Byrne, K.J., Koukourakis, M.I., Giatromanolaki, A., Cox, G., Turley, H., Steward, W.P., Gatter, K. & Harris, A.L. (2000). Vascular endothelial growth factor, platelet-derived endothelial cell growth factor and angiogenesis in non-small-cell lung cancer. *Br J Cancer*, **82,** 1427-32.

O'Donoghue JA, B.M., Wheldon TE. (1995). Relationships between tumor size and curability for uniformly targeted therapy with b-emitting radionuclides. *J Nucl Med*, **36,** 1902 - 1909.

Oliver, R.J., Woodwards, R.T., Sloan, P., Thakker, N.S., Stratford, I.J. & Airley, R.E. (2004). Prognostic value of facilitative glucose transporter Glut-1 in oral squamous cell carcinomas treated by surgical resection; results of EORTC Translational Research Fund studies. *Eur J Cancer*, **40,** 503-7.

Padhani, A.R. (2005). Where are we with imaging oxygenation in human tumours? *Cancer Imaging*, **5,** 128-30.

Padhani, A.R., Krohn, K.A., Lewis, J.S. & Alber, M. (2007). Imaging oxygenation of human tumours. *Eur Radiol*, **17,** 861-72.

Padhani, A.R. & Leach, M.O. (2005). Antivascular cancer treatments: functional assessments by dynamic contrast-enhanced magnetic resonance imaging. *Abdom Imaging*, **30,** 324-41.

Park, S.I. & Press, O.W. (2007). Radioimmunotherapy for treatment of B-cell lymphomas and other hematologic malignancies. *Curr Opin Hematol*, **14,** 632-8.

Parker, G., Suckling, J., Tanner, S., Padhani, A., Revell, P., Husband, J. & Leach, M. (1997). Probing tumor microvascularity by measurement, analysis and display of contrast agent uptake kinetics. *J Magn Reson Imaging*, **7,** 564 - 574.

Patterson, D. & Rustin, G. (2007). Phase I Evaluation Of OXi4503, A Vascular Disrupting Agent, In Patients With Solid Tumours. In *NCRI Annual Conference*.

Pedley, R.B., Boden, J.A., Boden, R., Boxer, G.M., Flynn, A.A., Keep, P.A. & Begent, R.H. (1996). Ablation of colorectal xenografts with combined radioimmunotherapy and tumor blood flow-modifying agents. *Cancer Res*, **56,** 3293-300.

Pedley, R.B., Boden JA, Keep PA, Harwood PJ, Green AJ, Rogers GT. (1987). Relationship Between Tumour Size & Uptake Of Radiolabelled Anti-CEA Antibody In A Colon Tumour Xenograft. *Eur J Nucl Med*, **13,** 197 - 202.

Pedley, R.B., El-Emir, E., Flynn, A.A., Boxer, G.M., Dearling, J., Raleigh, J.A., Hill, S.A., Stuart, S., Motha, R. & Begent, R.H. (2002). Synergy between vascular targeting agents and antibody-directed therapy. *Int J Radiat Oncol Biol Phys*, **54,** 1524-31.

Pedley, R.B., Hill, S.A., Boxer, G.M., Flynn, A.A., Boden, R., Watson, R., Dearling, J., Chaplin, D.J. & Begent, R.H. (2001). Eradication of colorectal xenografts by combined radioimmunotherapy and combretastatin a-4 3-O-phosphate. *Cancer Res*, **61,** 4716-22.

Pedley, R.B., Sharma, S.K., Boxer, G.M., Boden, R., Stribbling, S.M., Davies, L., Springer, C.J. & Begent, R.H. (1999). Enhancement of antibody-directed enzyme prodrug therapy in colorectal xenografts by an antivascular agent. *Cancer Res*, **59,** 3998-4003.

Pettit, G.R., Singh, S.B., Hamel, E., Lin, C.M., Alberts, D.S. & Garcia-Kendall, D. (1989). Isolation and structure of the strong cell growth and tubulin inhibitor combretastatin A-4. *Experientia*, **45,** 209-11.

Pettit, G.R., Temple, C., Jr., Narayanan, V.L., Varma, R., Simpson, M.J., Boyd, M.R., Rener, G.A. & Bansal, N. (1995). Antineoplastic agents 322. synthesis of combretastatin A-4 prodrugs. *Anticancer Drug Des*, **10,** 299-309.

Philpott, M., Ching, L.M. & Baguley, B.C. (2001). The antitumour agent 5,6-dimethylxanthenone-4-acetic acid acts in vitro on human mononuclear cells as a co-stimulator with other inducers of tumour necrosis factor. *Eur J Cancer*, **37,** 1930-7.

Platt, J.F., Francis, I.R., Ellis, J.H. & Reige, K.A. (1997). Liver Metastases: Early Detection Based On Abnormal Contrast Material Enhancement At Dual Phase Helical CT. *Radiology*, **205,** 49 - 53.

Pollack, A., DeSilvio, M., Khor, L.Y., Li, R., Al-Saleem, T., Hammond, M.E., Venkatesan, V., Lawron, C.A., Roach, M., Shipley, W.U., Hanks, G.E. & Sandler, H.M. (2004). Ki-67 Staining Is A Strong Predictor Of Distant Metastasis And Mortality For Men With Prostate Cancer Treated With Radiotherapy And Androgen Deprivation: Radiation Therapy Oncology Group Trial 92-02 (RTOG92-02). *J Clin Oncol*, **22,** 2133 - 2140.

Pruijn, F.B., van Daalen, M., Holford, N.H. & Wilson, W.R. (1997). Mechanisms of enhancement of the antitumour activity of melphalan by the tumour-blood-flow inhibitor 5,6-dimethylxanthenone-4-acetic acid. *Cancer Chemother Pharmacol*, **39,** 541-6.

Raben, D., Bianco, C., Damiano, V., Bianco, R., Melisi, D., Mignogna, C., D'Armiento, F.P., Cionini, L., Bianco, A.R., Tortora, G., Ciardiello, F. & Bunn, P. (2004). Antitumor activity of ZD6126, a novel vascular-targeting agent, is enhanced when combined with ZD1839, an epidermal growth factor receptor tyrosine kinase inhibitor, and potentiates the effects of radiation in a human non-small cell lung cancer xenograft model. *Mol Cancer Ther*, **3,** 977-83.

Radema SA , B.L., Witteveen PO at al. (2002). Clinical evaluation of the novel vascular targeting agent ZD6126 : assessment of toxicity and surrogate markers of vascular damage. *Proc Am Soc Clin Oncol*, **21,** Abstr 439.

Renkin, E.M. (1959). Transport of potassium-42 from blood to tissue in isolated mammalian skeletal muscles. *Am J Physiol*, **197,** 1205-10.

Rewcastle, G.W., Atwell, G.J., Li, Z.A., Baguley, B.C. & Denny, W.A. (1991). Potential antitumor agents. 61. Structure-activity relationships for in vivo colon 38 activity among disubstituted 9-oxo-9H-xanthene-4-acetic acids. *J Med Chem*, **34,** 217-22.

Rhee, J. & Hoff, P.M. (2005). Angiogenesis inhibitors in the treatment of cancer. *Expert Opin Pharmacother*, **6,** 1701-11.

Risau, W. (1997). Mechanisms of angiogenesis. *Nature*, **386,** 671-4.

Robinson, S., McIntyre, D., Checkley, D., Tessier, J., Howe, F., Griffiths, J., Ashton, S., Ryan, A., Blakey, D. & Waterton, J. (2003a). Tumour dose response to the antivascular agent ZD6126 assessed by magnetic resonance imaging. *Br J Cancer*, **88,** 1592 - 1597.

Robinson, S., Rijken, P., Howe, F., McSheehy, P., Van Der Sanden, B., Heerschap, A., Stubbs, M., Van Der Kogel, A. & Griffiths, J. (2003b). Tumor vascular architecture and function evaluated by non-invasive susceptibility MRI methods and immunohistochemistry. *J Magn Reson Imaging*, **17,** 445 - 454.

Robinson, S.P., Howe, F.A., Griffiths, J.R., Ryan, A.J. & Waterton, J.C. (2007). Susceptibility Contrast Magnetic Resonance Imaging Determination of Fractional Tumor Blood Volume: A Noninvasive Imaging Biomarker of Response to the Vascular Disrupting Agent ZD6126. *Int J Radiat Oncol Biol Phys*, **69,** 872-9.

Ross, R., Glomset, J., Kariya, B. & Harker, L. (1974). A Platelet Dependent Serum Factor That Stimulates The Proliferation Of Arterial Smooth Muscle Cells In Vitro. *Proc Natl Acad Sci U S A*, **71,** 1207 - 1210.

Rudisch, A.R., De Vries, A. & Kremser, C. (2002). CT Assessment of Microcirculation And Haemodynamics In Malignant Rectal Neoplasms: Validation And Initial Clinical Experience. *Eur Radiol*, **12 (suppl 1),** 114.

Rustin, G.J., Bradley, C., Galbraith, S., Stratford, M., Loadman, P., Waller, S., Bellenger, K., Gumbrell, L., Folkes, L. & Halbert, G. (2003a). 5,6-dimethylxanthenone-4-acetic acid (DMXAA), a novel antivascular agent: phase I clinical and pharmacokinetic study. *Br J Cancer*, **88,** 1160-7.

Rustin, G.J., Galbraith, S.M., Anderson, H., Stratford, M., Folkes, L.K., Sena, L., Gumbrell, L. & Price, P.M. (2003b). Phase I clinical trial of weekly combretastatin A4 phosphate: clinical and pharmacokinetic results. *J Clin Oncol*, **21,** 2815-22.

Rustin GJ , N.P., Boxall J, Saunders L, Ganesan TS, Shreeves GE. (2005). A Phase Ib Trial Of Combretastatin A4 Phosphate (CA4P) In Combination With Carboplatin Or Paclitaxel Chemotherapy In Patients With Advanced Cancer. *Proc ASCO*, **Abstract 3103**.

Sahani, D.V., Kalva, S.P., Hamberg, L.M., Hahn, P.F., Willett, C.G., Saini, S., Mueller, P.R. & Lee, T.Y. (2005). Assessing tumor perfusion and treatment response in rectal cancer with multisection CT: initial observations. *Radiology*, **234,** 785-92.

Salmon, H.W., Mladinich, C. & Siemann, D.W. (2006). Evaluations of vascular disrupting agents CA4P and OXi4503 in renal cell carcinoma (Caki-1) using a silicon based microvascular casting technique. *Eur J Cancer*, **42,** 3073-8.

Salmon, H.W. & Siemann, D.W. (2006). Effect Of The Second Generation Vascular Disrupting Agent OXi4503 On Tumor Vascularity. *Clin Cancer Res*, **12,** 4090 - 4094.

Sauter, E.R., Nesbit, M., Watson, J.C., Klein-Szanto, A., Litwin, S. & Herlyn, M. (1999). Vascular endothelial growth factor is a marker of tumor invasion and metastasis in squamous cell carcinomas of the head and neck. *Clin Cancer Res*, **5,** 775-82.

SC, R. (2002). Vascular Targeting : Clinical Experience. *Horizons In Cancer Therapeutics: From Bench To Bedside*, **3,** 16 - 23.

Scholzen, T. & Gerdes, J. (2000). The Ki-67 Protein: From The Known And The Unknown. *J Cell Physiol*, **182,** 311 - 322.

Senger, D.R., Galli, S.J., Dvorak, A.M. & al., e. (1983). Tumour Cells Secrete A Vascular Permeability Factor That Promotes Accumulation Of Ascites Fluid. *Science*, **219,** 983 - 985.

Sheafor, D.H., Killius, J.S. & Paulson, E.K. (2000a). Hepatic Parenchymal Enhancement During Triple Phase Helical CT: Can It Be Used To Predict Which Patients With Breast Cancer Will Develop Hepatic Metastases. *Radiology*, **214,** 875 - 880.

Sheafor, D.H., Killius, J.S., Paulson, E.K., DeLong, D.M., Foti, A.M. & Nelson, R.C. (2000b). Hepatic parenchymal enhancement during triple-phase helical CT: can it be used to predict which patients with breast cancer will develop hepatic metastases? *Radiology*, **214,** 875-80.

Shim, W.S., Ho, I.A. & Wong, P.E. (2007). Angiopoietin: a TIE(d) balance in tumor angiogenesis. *Mol Cancer Res*, **5,** 655-65.

Siemann, D.W., Mercer, E., Lepler, S. & Rojiani, A.M. (2002). Vascular targeting agents enhance chemotherapeutic agent activities in solid tumor therapy. *Int J Cancer*, **99,** 1-6.

Siemann, D.W. & Rojiani, A.M. (2002). Enhancement of radiation therapy by the novel vascular targeting agent ZD6126. *Int J Radiat Oncol Biol Phys*, **53,** 164-71.

Siemann, D.W. & Rojiani, A.M. (2005). The vascular disrupting agent ZD6126 shows increased antitumor efficacy and enhanced radiation response in large, advanced tumors. *Int J Radiat Oncol Biol Phys*, **62,** 846-53.

Siemann, D.W. & Shi, W. (2003). Targeting the tumor blood vessel network to enhance the efficacy of radiation therapy. *Semin Radiat Oncol*, **13,** 53-61.

Siemann, D.W., Shi, W. (2004). Efficacy of Combined Antiangiogenic and Vascular Disrupting Agents In Treatment of Solid Tumours. *Int J Radiation Oncology Biol Phys*, **60,** 1233 - 1240.

Siim, B. (2004). The DMXAA Experience. *Proc 2nd International Conference On Vascular Targeting, Miami, Florida***,** Abstract 5.

Simon, R., Freidlin, B., Rubinstein, L., Arbuck, S.G., Collins, J. & Christian, M.C. (1997). Accelerated titration designs for phase I clinical trials in oncology. *J Natl Cancer Inst*, **89,** 1138-47.

Smith, G.P., Calveley, S.B., Smith, M.J. & Baguley, B.C. (1987). Flavone acetic acid (NSC 347512) induces haemorrhagic necrosis of mouse colon 26 and 38 tumours. *Eur J Cancer Clin Oncol*, **23,** 1209-11.

Stevenson, J.P., Rosen, M., Sun, W., Gallagher, M., Haller, D.G., Vaughn, D., Giantonio, B., Zimmer, R., Petros, W.P., Stratford, M., Chaplin, D., Young, S.L., Schnall, M. & O'Dwyer, P.J. (2003). Phase I trial of the antivascular agent combretastatin A4 phosphate on a 5-day schedule to patients with cancer: magnetic resonance imaging evidence for altered tumor blood flow. *J Clin Oncol*, **21,** 4428-38.

Stouffer, G.A. & Smyth, S.S. (2003). Effects Of Thrombin On Interactions Between Beta-3-Integrins And Extracellular Matrix In Platelets And Vascular Cells. *Arterioscler Thromb Vasc Biol*, **23,** 1971 - 1978.

Sullivan, R. & Graham, C.H. (2007). Hypoxia-driven selection of the metastatic phenotype. *Cancer Metastasis Rev*, **26,** 319-31.

Swenson, S., Brown, L.R., Colby, T.V. & al., e. (1996). Lung Nodule Enhancement At CT : Prospective Findings. *Radiology*, **201,** 447 - 455.

Swenson, S., Viggiano, R.W., Midthun, D.E. & al., e. (2000). Lung Nodule Enhancement At CT: Multicenter Study. *Radiology*, **214,** 73 - 80.

Tait, C.R. & Jones, P.F. (2004). Angiopoietins in tumours: the angiogenic switch. *J Pathol*, **204,** 1-10.

Tanaka, S., Sugimachi, K., Yamashita, Y., Shirabe, K., Shimada, M. & Wands, J.R. (2003). Angiogenic switch as a molecular target of malignant tumors. *J Gastroenterol*, **38 Suppl 15,** 93-7.

Tateishi, U., Nishihara, H., Tsukamoto, A., Morikawa, S., Tamaki, N. & Miyasaka, K. (2002). Lung Tumours Evaluated With FDG-PET And Dynamic CT: The Relationship Between Vascular Density And Glucose Metabolism. *J Comput Assist Tomogr*, **26,** 185 - 190.

Taylor, N., Lankester, K., Ah-See, M.-L., Stirling, J., Rustin, G., Makris, A., D'Arcy, J., Walker-Samuel, S., Leach, M. & Padhani, A. (2004a). Reproducibility of T1 and T2* weighted dynamic contrast-enhanced MRI: a multiparametric comparison of breast and abdominal tumours. *Proc ISMRM***,** Abstract 1975.

Taylor, N.J., d'Arcy, A.J., Walker-Samuel, S., Collins, D.J., Knowles, B., Stirling, J.J., Wallace, T., Koh, D.M., Tang, A., Lee, C., Leach, M.O., Rustin, G.J. & Padhani, A. (2004b). Effect of Vascular Input Functions on Reproducibility of DCE-MRI Studies of Tumours. In *ISMRM*.

Taylor, N.J., d'Arcy, J.A., Walker-Samuel, S., Lankester, K.J., Collins, D.J., Knowles, B., White, D.L., Miaux, Y., Suhy, J., Guermazi, A., Stirling, J.J., Wallace, T., Koh, D.-M., Tang, A., Lee, C., Rustin, G.J.S., Leach, M.O. & Padhani, A.R. (2006). Single and multi-centre DCE-MRI reproducibility in Phase I clinical trials. In *Proc. I.S.M.R.M* pp. Abstract 766: 14th Annual Meeting.

Thomsen, L.L., Ching, L.M., Zhuang, L., Gavin, J.B. & Baguley, B.C. (1991). Tumor-dependent increased plasma nitrate concentrations as an indication of the antitumor effect of flavone-8-acetic acid and analogues in mice. *Cancer Res*, **51,** 77-81.

Thorpe, P.E. (2004). Vascular targeting agents as cancer therapeutics. *Clin Cancer Res*, **10,** 415-27.

Thorpe, P.E., Chaplin, D.J. & Blakey, D.C. (2003). The first international conference on vascular targeting: meeting overview. *Cancer Res*, **63,** 1144-7.

Tofts, P.S. (1997). Modeling tracer kinetics in dynamic Gd-DTPA MR imaging. *J Magn Reson Imaging*, **7,** 91 - 101.

Tofts, P.S., Brix, G., Buckley, D.L., Evelhoch, J.L., Henderson, E., Knopp, M.V., Larsson, H.B., Lee, T.Y., Mayr, N.A., Parker, G.J., Port, R.E., Taylor, J. & Weisskoff, R.M. (1999). Estimating kinetic parameters from dynamic contrast-enhanced T(1)-weighted MRI of a diffusable tracer: standardized quantities and symbols. *J Magn Reson Imaging*, **10,** 223-32.

Tofts, P.S. & Kermode, A.G. (1991). Measurement of the blood-brain barrier permeability and leakage space using dynamic MR imaging. 1. Fundamental concepts. *Magn Reson Med*, **17,** 357 - 367.

Tokunaga, T., Oshika, Y., Abe, Y., Ozeki, Y., Sadahiro, S., Kijima, H., Tsuchida, T., Yamazaki, H., Ueyama, Y., Tamaoki, N. & Nakamura, M. (1998). Vascular endothelial growth factor (VEGF) mRNA isoform expression pattern is correlated with liver metastasis and poor prognosis in colon cancer. *Br J Cancer*, **77,** 998-1002.

Tolcher AW , F.L., Celio P , Hammond LA , Patnaik A , Hill M , Verat-Follet C , Haacke M , Besenval M , Rowinsky EK. (2003). Phase I , pharmacokinetic, and DCE-MRI correlative study of AVE8062A, an antivascular combretastatin analogue, administered weekly for 3 weeks every 28 days. *Proc Am Soc Clin Oncol*, **22,** Abstract 834.

Tozer, G.M. (2003). Measuring tumour vascular response to antivascular and antiangiogenic drugs. *Br J Radiol*, **76 Spec No 1,** S23-35.

Tozer, G.M., Kanthou, C. & Baguley, B.C. (2005). Disrupting tumour blood vessels. *Nat Rev Cancer*, **5,** 423-35.

Tozer, G.M., Kanthou, C., Parkins, C.S. & Hill, S.A. (2002). The biology of the combretastatins as tumour vascular targeting agents. *Int J Exp Pathol*, **83,** 21-38.

Tozer, G.M., Prise, V.E., Wilson, J., Cemazar, M., Shan, S., Dewhirst, M.W., Barber, P.R., Vojnovic, B. & Chaplin, D.J. (2001). Mechanisms associated with tumor vascular shut-down induced by combretastatin A-4 phosphate: intravital microscopy and measurement of vascular permeability. *Cancer Res*, **61,** 6413-22.

Tozer, G.M., Prise, V.E., Wilson, J., Locke, R.J., Vojnovic, B., Stratford, M.R., Dennis, M.F. & Chaplin, D.J. (1999). Combretastatin A-4 phosphate as a tumor vascular-targeting agent: early effects in tumors and normal tissues. *Cancer Res*, **59,** 1626-34.

Tozer, G.M. & Shaffi, K.M. (1993). Modification of tumour blood flow using the hypertensive agent, angiotensin II. *Br J Cancer*, **67,** 981-8.

Tsushima, Y., Blomley, J.K., Kusano, S. & Endo, K. (1999). The portal component of hepatic perfusion measured by dynamic CT: an indicator of hepatic parenchymal damage. *Dig Dis Sci*, **44,** 1632-8.

Van Beers, B.E., Leconte, I., Materne, R., Smith, A.M., Jamart, J. & Horsmans, Y. (2001). Hepatic perfusion parameters in chronic liver disease: dynamic CT measurements correlated with disease severity. *AJR Am J Roentgenol*, **176,** 667-73.

Varghese HJ, M.L., Groom AC, Ellis CG, Ryan A, MacDonald IC, Chambers AF. (2004). In Vivo Videomicroscopy Reveals Differential Effects of the Vascular Targeting Agent ZD6126 and the Anti-Angiogenic Agent ZD6474 On Vascular Function In A Liver Metastasis Model. *Angiogenesis*, **7,** 157 - 164.

Vincent, L. & Rafii, S. (2004). Vascular frontiers without borders: multifaceted roles of platelet-derived growth factor (PDGF) in supporting postnatal angiogenesis and lymphangiogenesis. *Cancer Cell*, **6,** 307-9.

Vrignaud, P. (2004). In Vivo Synergy Between Cytotoxic Agents And AVE8062A, A Tumour Vascular Targeting Agent. *Proc 2nd International Conference On Vascular Targeting, Miami, Florida***,** Abstract 8.

Wang, Y., Jin, G., Miao, H., Li, J.Y., Usami, S. & Chien, S. (2006). Integrins regulate VE-cadherin and catenins: dependence of this regulation on Src, but not on Ras. *Proc Natl Acad Sci U S A*, **103,** 1774-9.

Wildiers, H., Ahmed, B., Guetens, G., De Boeck, G., de Bruijn, E.A., Landuyt, W. & van Oosterom, A.T. (2004). Combretastatin A-4 phosphate enhances CPT-11 activity independently of the administration sequence. *Eur J Cancer*, **40,** 284-90.

Willett, C.G., Boucher, Y., di Tomaso, E., Duda, D.G., Munn, L.L., Tong, R.T., Chung, D.C., Sahani, D.V., Kalva, S.P., Kozin, S.V., Mino, M., Cohen, K.S., Scadden, D.T., Hartford, A.C., Fischman, A.J., Clark, J.W., Ryan, D.P., Zhu, A.X., Blaszkowsky, L.S., Chen, H.X., Shellito, P.C., Lauwers, G.Y. & Jain, R.K. (2004). Direct evidence that the VEGF-specific antibody bevacizumab has antivascular effects in human rectal cancer. *Nat Med*, **10,** 145-7.

Wilson, W.R., Li, A.E., Cowan, D.S. & Siim, B.G. (1998). Enhancement of tumor radiation response by the antivascular agent 5,6-dimethylxanthenone-4-acetic acid. *Int J Radiat Oncol Biol Phys*, **42,** 905-8.

Winter, S.F., Acevedo, V.D., Gangula, R.D., Freeman, K.W., Spencer, D.M. & Greenberg, N.M. (2007). Conditional activation of FGFR1 in the prostate epithelium induces angiogenesis with concomitant differential regulation of Ang-1 and Ang-2. *Oncogene*, **26,** 4897-907.

Yi, C.A., Lee, K.S., Kim, E.A., Han, J., Kim, H., Kwon, O.J., Jeong, Y.J. & Kim, S. (2004). Solitary pulmonary nodules: dynamic enhanced multi-detector row CT study and comparison with vascular endothelial growth factor and microvessel density. *Radiology*, **233,** 191-9.

Yorke ED, W.L., Demidecki AJ, Heidorn DB, Roberson PL, Wessels BW. (1993). Multicellular dosimetry for beta-emitting radionuclides: Autoradiography, thermoluminescent dosimetry and three-dimensional dose calculations. *Med Phys*, **20,** 543 - 550.

Younes, M., Brown, R.W., Stephenson, M., Gondo, M. & Cagle, P.T. (1997). Overexpression Of Glut-1 and Glut-3 In Stage I Non Small Cell Lung Carcinoma Is Associated With Poor Survival. *Cancer*, **80,** 1046 - 1051.

Younes, M., Juarez, D., Lechago, L.V. & Lerner, S.P. (2001). Glut 1 expression in transitional cell carcinoma of the urinary bladder is associated with poor patient survival. *Anticancer Res*, **21,** 575-8.

Young, S.L. & Chaplin, D.J. (2004). Combretastatin A4 phosphate: background and current clinical status. *Expert Opin Investig Drugs*, **13,** 1171-82.

Zhao, L., Ching, L.M., Kestell, P., Kelland, L.R. & Baguley, B.C. (2005). Mechanisms of tumor vascular shutdown induced by 5,6-dimethylxanthenone-4-acetic acid (DMXAA): Increased tumor vascular permeability. *Int J Cancer*, **116,** 322-6.

Zhao, R., Alokkumar, S.P. & Stouffer, G.A. (2004). Beta-3-Integrin Cytoplasmic Binding Proteins. *Arch Immunol Ther Exp*, **52,** 348 - 355.

Zwi, L.J., Baguley, B.C., Gavin, J.B. & Wilson, W.R. (1994). Correlation between immune and vascular activities of xanthenone acetic acid antitumor agents. *Oncol Res*, **6,** 79-85.

Chapter 2

A Phase Ib Trial of Radioimmunotherapy with ^{131}Iodine-Labelled A5B7 Anti-CEA Antibody in Combination with Combretastatin-A4-Phosphate In Advanced Gastrointestinal Carcinomas.

Abstract

In pre-clinical models the combination of RIT with ^{131}I-A5B7 and the VDA CA4P was synergistic, curing 5/6 mice with CEA-positive colon carcinoma xenografts. The antibody attaches to the tumour periphery with poor penetration of the core because of relative hypoxia and its high molecular weight. CA4P, a tubulin-binding small molecule vascular disruptive agent, leads to central tumour vascular shutdown with relative sparing of the periphery. Previous single agent phase I trials have defined the MTD for ^{131}I-A5B7 at 2400MBq/m^2 and CA4P between 60-68mg/m^2. We performed a trial to determine DLT, MTD and efficacy of this combination in patients with advanced gastrointestinal cancer. The initial drug doses were set 25% below MTD of single agent studies. Patients had advanced gastrointestinal adenocarcinoma, CEA 10-1000μg/L, disease measurable by RECIST, QTc ≤450ms, no cardiac arrhythmia/ischaemia and adequate haematology/biochemistry. Disease had to be suitable for evaluation by DCE-MRI. All patients received a test dose of CA4P up to 2 weeks prior to day 1, to document blood flow response. The starting dose was 1800MBq/m^2 of ^{131}I-A5B7 given on day 1 and 45mg/m^2 CA4P given 48 and 72 hours post A5B7, and then weekly for up to seven weeks. Between October 2003 and April 2007 88 patients were screened, and twelve patients treated; eleven colorectal and one pancreatic adenocarcinoma, mean age 63(32-77), WHO PS 0(6) and 1(6). 2/6 patients at the first dose level had DLTs (grade 4 neutropenia) attributed to ^{131}I-A5B7. The dose was reduced to 1600MBq/m^2 and CA4P escalated to 54mg/m^2. Again, 2/6 patients had DLTs attributable to ^{131}I-A5B7 (grade 4 neutropaenia), and one patient had grade 3 ataxia attributable to CA4P. Other toxicities were manageable and included infusion reactions, pyrexia, thrombocytopenia (up to grade 3), QTc prolongation within the normal range - mean 10ms at 4h($2p=0.0016$), hypertension - mean increase in systolic BP 12mmHg at 1h($2p<0.0001$), tachycardia - mean increase in HR 10bpm at 3h($2p<0.0001$), nausea, fatigue, tumour pain and pruritis. Of ten evaluable patients 1 had SD and 9 had PD, confirmed by FDG-PET in four. CA4P and A5B7 pharmacokinetics were similar to previous studies. SPECT confirmed tumour antibody uptake in all 5 patients studied. This is the first clinical trial reporting on the combination of RIT and a VDA; each therapy component was shown to function but with dose-limiting myelosuppression from the combination at 66% of the single agent antibody MTD (Gaya et al., 2008).

Introduction

Colorectal cancer is the second leading cause of cancer death in the UK, with approximately 35000 new cases per year (CR-UK figures). Conventional systemic treatment modalities remain ineffective at curing patients with metastatic disease, although significant advances have been made using combination chemotherapy, pre-operative chemoradiotherapy, biological therapies, and hepatic surgery. Five year overall survival is now approaching 50%, however there remains a need for novel therapies.

Carcinoembryonic antigen (CEA) is a membrane bound glycoprotein that is expressed by most gastrointestinal tumours; normal expression is usually limited to the luminal surface of the gastrointestinal tract. CEA represents a good target for RIT. The mouse monoclonal antibody A5B7 was raised against CEA (Harwood et al., 1986) and localises to human colon carcinoma xenografts (Pedley, 1987). A5B7 was purified from supernatant culture by protein A chromatography and ion-exchange chromatography (Ledermann et al., 1988), and radiolabelled with ^{131}I using the N-bromosuccinamide method (Adam, 1989). This method has a labelling efficiency of 88-94% without loss of immunoreactivity (Lane et al., 1994). ^{131}I is a beta emitter capable of destroying tumour cells over a range of 40 cell diameters. The isotope also releases gamma radiation of 364keV, which is suitable for imaging with a gamma camera for quantitative analysis of normal tissue and tumour biodistribution. There was a 10% response rate in advanced colorectal cancer patients with single agent ^{131}I-A5B7 (Lane et al., 1994). MTD was 2400MBq/m^2 and DLT were neutropenia and thrombocytopenia.

Pre-clinical studies have confirmed the antivascular activity of the tubulin binding VDA CA4P (Chaplin et al., 1996) and it has completed single agent Phase I trials in the UK and USA (Dowlati et al., 2002; Rustin et al., 2003; Stevenson et al., 2003) and **Chapter 1**. MTD was 60 – 68mg/m^2 and DLT was ataxia. Cardiovascular toxicity was seen in patients with active ischaemic heart disease or uncontrolled hypertension. Although central vascular shutdown was detected by DCE-MRI, minimal antitumour activity was seen due to regrowth from the tumour periphery.

A5B7 is most effective at the tumour rim but is a large molecule and has poor penetration of the hypoxic tumour centre (Flynn AA, 1999). CA4P is most effective at destroying the tumour core with sparing of the peripheral rim (Dark et al., 1997). In addition, trapping of

radiolabelled antibody in the tumour by CA4P enhances the effect of RIT (Pedley B, personal communication,2005). When this combination was administered to mice, cure was achieved in 5/6 animals whereas CA4P alone was ineffective and RIT merely delayed tumour growth (Pedley et al., 2001).

There were also limitations to the design of the study. Yttrium has a better affinity for carrier molecules than iodine, with higher specific activity, less dissociation and better stability. Patients could also be subjected to biopsies to determine histologically vascular damage and tumour necrosis following CA4P, and allow for direct immunohistochemical studies. The starting dose of CA4P was also below the activity level of 50 mg/m^2. A5B7 was non humanised meaning it could only realistically be given as a single dose due to the development of HAMA. Clinically, for example in the treatment of lymphoma, radioantibodies are given in multiple doses.

Combining A5B7 RIT with CA4P may therefore be a promising therapeutic strategy in which the action of the two agents is complimentary. We undertook a phase 1b dose escalation trial to define the MTD & DLT of the combination with toxicity as the primary endpoint. This study (PH1-092) was sponsored by CR-UK, CTA Number 21106/0002/001, EudraCT Number 2004-004788-31

Methods

Study Objectives

1) Define DLTs and MTD
2) Gain preliminary evidence of efficacy of the combination.
3) Pharmacokinetic and pharmacodynamic assessments.

Study Design

This was a phase I dose-escalation trial sponsored by CR-UK. The study was conducted at Mount Vernon Hospital, Northwood and the Royal Free Hospital, London. The study was approved by participating hospitals' ethical review boards, and all patients provided written informed consent.

It was proposed that the combination of ^{131}I-A5B7 and CA4P should not result in major additional toxicity over that experienced by each agent individually. This was based on the

different toxicity profiles and mechanism of action of each agent, and pre-clinical studies confirming no additional toxicity. The starting dose of each drug (1800MBq/m^2 A5B7 and 45mg/m^2 CA4P) was 25% below MTD in the Phase I single agent studies (Lane et al., 1994; Rustin et al., 2003). CA4P was to be escalated by 20% to 54mg/m^2 (above the activity threshold of 50 mg/m^2). A5B7 was to be dose escalated initially in 2 steps up to the single agent MTD of 2400 mg/m^2.

Up to two weeks before A5B7 treatment two DCE-MRI scans were performed at Mount Vernon Hospital for repeatability analysis prior to a single intravenous CA4P infusion, and a further scan 4h post-CA4P to assess changes in vascular kinetic parameters (**Chapter 3**). A5B7 treatment was administered as an inpatient on day 1, and CA4P on days 3 and 4 before hospital discharge, then as an outpatient weekly from d11 until disease progression was documented or other withdrawal criteria were met. A5B7 treatment could be repeated after d57 if no HAMA developed. In the absence of DLT, three patients were to be treated at each dose level. Adverse events were the primary endpoint.

All patients were evaluable for safety. Patients who received one cycle of combination treatment were evaluable for response. One cycle of combination treatment was defined as a single dose ^{131}I-A5B7 plus 3 doses of CA4P (first dose up to two weeks before ^{131}I-A5B7, second and third doses on d3 and 4 after ^{131}I-A5B7). Any patient not receiving this minimum number of infusions was replaced. Adverse events and other symptoms were graded according to the NCI Common Toxicity Criteria v2.0. A minimum time interval of four weeks had to elapse between the first patient being treated on a previous dose level and entry of a new patient at the next dose level, to take into consideration experience gained at the lower dose level.

The study commenced recruitment in October 2003 and was set to continue for 24 months. It was initially expected that the accrual rate would be 1-2 patients per month for a total of 30-40 patients to be recruited.

Patient Selection

Patients with histologically confirmed gastrointestinal adenocarcinoma not amenable to standard therapy or refractory to conventional therapy were eligible for this study. Other eligibility criteria included a plasma CEA 10-1000 μg/L; disease measurable by RECIST criteria (Therasse et al., 2000); QTc interval ≤450ms and no evidence of cardiac arrhythmia

or ischaemia; disease assessable by DCE-MRI and no contraindication to MRI scanning; age ≥18 years; life expectancy ≥3 months; WHO performance status 0/1; adequate bone marrow function with neutrophils ≥1.5 x 10^9/L, haemoglobin ≥9g/dl, platelets ≥100 x 10^9/L; adequate clotting with INR ≤1.3, normal plasma potassium and magnesium levels and EDTA creatinine clearance ≥50mls/min; adequate hepatic function with plasma bilirubin ≤ twice upper limit of normal (ULN), ALT or AST ≤ twice ULN (or 5x ULN in the presence of liver metastases). To be suitable for DCE-MRI the tumour had to be ≥2cm diameter and away from areas of major vascular pulsation such as the heart, mediastinum or aorta.

Patients were excluded if they had a history of ischaemic heart disease, congestive heart failure or significant cardiac arrhythmia; uncontrolled hypertension (defined as BP consistently greater than 150/100 despite medication); ECG evidence of clinically significant pathology or QTc >450ms; taking any drug known to prolong the QTc interval; conditions associated with QTc prolongation; major thoracic or abdominal surgery in the preceding four weeks; symptomatic brain metastasis; autoimmune disorders, inflammatory bowel disease or ≥ grade 2 peripheral neuropathy; previous radical radiotherapy; hepatitis B,C or HIV; positive HAMA; previous anti-cancer therapy within four weeks.

Treatment Administration

Unlabelled CA4P was supplied by OXiGene Inc to the CR-UK formulations unit where it was labelled and released. CA4P was supplied as a sterile lyophilized cake in amber glass vials containing 90mg of CA4P as free acid with 10% additional overfill. CA4P was stored in the dark to prevent conversion to the less active *trans* isomer. The drug was reconstituted with 10-11 ml sterile water (depending on the batch) for injection and further diluted with 100-150 ml of normal saline, and was administered IV over 10 minutes protected from light. Particulate matter was removed by administration through a 5 micron line filter.

A5B7 was produced by the Biotherapeutics Development Unit of CR-UK, formulated in isotonic phosphate buffered saline and stored at 4°C. A fixed dose of 10mg A5B7 was radiolabelled with ^{131}I in the department of medical physics at the Royal Free Hospital using the N-bromosuccinamide method. The % iodine incorporation of the labelled product was measured by thin layer chromatography and the CEA binding by a CEA

column. A5B7 was administered within 4hrs via an indwelling central venous catheter in 50ml 0.9% saline over 30-40 minutes using a syringe driver.

Routine pre-medication was not mandatory prior to CA4P but if significant toxicity occurred with the first dose pre-medication with dexamethasone 8mg IV and metaclopramide 10mg IV was recommended prior to subsequent cycles. If systolic BP was >180 mmHg on two readings following CA4P glyceryl trinitrate 0.3mg was given sublingually or amlodipine 10mg orally. No routine allergic prophylaxis was offered prior to A5B7; however hydrocortisone 100mg and chlorpheniramine 10mg IV were administered if clinically necessary.

Potassium iodide 60mg three times daily for 8 days was commenced 48h before A5B7 to block thyroid ^{131}I uptake.

The first CA4P dose was administered within 14 days of ^{131}I-A5B7 to assess DCE-MRI response. On Day 1, patients received ^{131}I-A5B7 infusion at the Royal Free Hospital. The patients were kept in protective isolation and appropriate radioprotection procedures were followed. CA4P was given on d3 and 4 as this timing has been shown to increase trapping of ^{131}I-A5B7 within tumours (B Pedley, Personal Communication 2005). The patient was sent home when radiation levels had fallen within acceptable limits. Weekly CA4P was then administered until disease progression or other withdrawal criteria were met. Treatment limits were for platelets to be above $50x10^9$/L, and neutrophils above $0.5x10^9$/L. If below these parameters, CA4P treatment was delayed until recovery.

Patients were assessed by RECIST criteria for response on d29 and 57 (Therasse et al., 2000). If the patient developed HAMA, repeat treatment would be with CA4P alone at weekly intervals. If the patient remained negative for HAMA, the combination treatment could be repeated. Providing no DLT occurred in any of the three patients per cohort, doses were increased as shown in **Table 2.1**. If one DLT was seen three additional patients could be recruited to that dose level. If two out of three to six patients experienced DLT, three more patients would be treated at a lower dose level to define MTD. Patients were followed up for eight weeks after the last administration of study drug, or until all drug-related toxicity had returned to baseline.

Table 2.1 – Dose Escalation Strategy

Dose Cohort	CA4P Dose mg/m^2 *	^{131}I-A5B7 RIT Dose (MBq/m^2)
1	45 (50)	1800
2	55 (60.5)	
3		2100
4		2400
A[1]	54 (60)	1600
B[1]	63 (70)	

*Figure in brackets is the salt dose (higher) with the actual free acid dose approximately 10% lower.
1 – Dose cohorts A and B were subsequently introduced to replace cohorts 2 – 4 due to DLT (Grade 4 neutropenia) seen in two patients in dose cohort 1. Dose cohorts 2 – 4 were abandoned (see discussion).

At the MTD, the trial was to consist of two stages: First, 14 evaluable patients would be entered. If there were no responses the trial would be terminated. If there were one or more responses in the first 14 patients, 11 additional patients would be added in the second stage. This scheme ensured that if the drug was active in 20% or more patients, the chance of erroneously rejecting the drug after the first 14 patients was 0.044 (80% power, α=0.05).

Study Procedures and Observations

Medical history, physical exam, performance status, ECG, chest X-ray, urinalysis, calculated creatinine clearance, pregnancy test (if appropriate), HAMA, haematology, biochemistry (renal,liver,glucose,clotting,thyroid,CEA,Ca19.9), baseline RECIST CT/MRI assessment (within 4 weeks of study), and PET scan (optional) were performed prior to study entry.

Vital signs (heart rate, blood pressure, temperature) were obtained prior to administration of CA4P and at ½,1,2,3,4,5 and 6h. Vital signs monitoring was continued hourly if clinically indicated. Vital signs were also recorded prior to administration of ^{131}I-A5B7, at the end of the infusion, & at 1,2,3 and 4h after the infusion. Three pre-treatment ECGs were obtained at least 5 minutes apart before each infusion of CA4P, and post-CA4P at 1,2, and 4h. Following the 1st four doses of CA4P an optional full blood count was also taken 4h post infusion. SPECT scans were performed 4h post ^{131}I-A5B7 and at 24,48,72 & 96 hours post infusion. Further assessments were as set out in **Tables 2.2 and 2.3**

Pharmacokinetic Sampling

CA4P pharmacokinetics was performed up to 14 days prior to A5B7 infusion prior to DCE-MRI scanning. Samples were taken immediately before completion of CA4P

infusion, and at 5, 30, 45, 60, 120 & 240 minutes after the end of infusion. Blood samples were kept on ice. Blood was centrifuged at 3000 rpm as soon as possible after collection at 4^0C for 10-15 min, and not stored longer than 30 minutes at 4^0C. Following separation, 2 x 500µl plasma aliquots were removed and stored at -70^0C.

The fluorescence method of Stratford (Stratford & Dennis, 1999) was used. CA4P and CA4 levels were quantified by HPLC on a system from Waters comprising a 2695 Separations module, 2996 photodiode array detector and W474 fluorescence detector. The resulting concentration/time data was analysed using a non-compartmental method, plotted by Stratford et al using Microcal '*Origin'* software, and fitted using non-linear least squares regression analysis to determine the half-life.

1ml ^{131}I-A5B7 blood PK samples were taken into an EDTA tube pre-administration, 5min after completion of the infusion, and at 4, 24, 48, 72 & 96h post infusion. Samples were kept in an approved radioactive storage area until they had decayed to appropriate levels for ^{131}I activity analysis. Radioactivity was measured using a Packard Cobra 11th Series Auto gamma counter. The time of measurement was recorded and a decay correction applied as appropriate to calculate the percentage injected dose/kg blood at each time point. Antibody distribution and dosimetry was determined using SPECT analysis. Planar imaging was performed on an ADAC Vertex Plus Dual Headed gamma camera. Reconstruction of SPECT images was iterative with scatter and attenuation correction applied. ROI analysis was performed on tumour, liver, lung, spleen, blood/heart and kidney. This resulted in a calculation of decay corrected % injected dose of radioactivity/kg in each of these organs.

Dose Limiting Toxicity

DLT was defined as any of the following, considered probably or definitely related to therapy: QTc prolongation ≥500ms, >Grade 2 ventricular/supraventricular arrhythmia, grade 3/4 non-haematologic toxicity (except: alopecia grade 3, nausea grade 3/4, diarrhoea or vomiting (in patients who hadn't received optimal anti-emetics or anti-diarrhoeals), grade 3 tumour pain, grade 3 hypertension (controlled by antihypertensives), neutrophils <500 cells/mm^3 for ≥5 consecutive days or febrile neutropenia with neutrophils <1000 cells/mm^3, platelets <10,000 cells/mm^3 for >5 consecutive days or a bleeding episode requiring platelet transfusion, haemoglobin <8.0g/dl, grade ≥2 neurotoxicity. Non tolerated dose was defined as the dose when any of the above drug-related toxicities

occurred in 2 of up to 6 patients. MTD was defined as the highest dose level of CA4P administered with A5B7, at which one or fewer patients experienced DLT.

End-of-Study Assessments

To ensure that adverse events had resolved, the following were performed at least 30 days after the final dose of study drug: Performance status; physical examination; weight; vital signs; full blood count; biochemical profile; urinalysis; ECG; adverse event analysis.

TABLE 2.2 Study Assessments	Within 1 week DCE-MRI	Within 24 hours 1st CA4P dose	Within 48 hours 1st CA4P dose	1st CA4P dose	Day (-2)	Day 1	Day 3	Day 4	Day 11	Day 18	Day 25	Day 29	Day 32	Day 39	Day 46	Day 53	Day 57
Written Informed Consent	x within 28 days																
Medical History	x																
Symptom History							x	x	x	x	x		x	x	x	x	
Assessment of QTc affecting medication	x																
Physical examination	x					x	x	x	x	x	x		x	x	x	x	
Register CR-UK	x																
Vital signs				x		x	x	x	x	x	x		x	x	x	x	
BSA/Weight	x					x											
Admit to ward						x											
Discharge from ward								x									
Urinalysis	x					x											
ECG	x			x			x	x	x	x	x		x	x	x	x	
CXR	x																
WHO PS	x								x	x	x		x	x	x	x	
Creatinine Clearance	x																
Serum pregnancy test	x																
Haematology (pre-dose)	x					x		x	x	x	x		x	x	x	x	
Haematology (4h post CA4P)				x			x	x	x	x	x						
Biochemistry	x					x		x	x	x	x		x	x	x	x	
Clotting	x																
Tumour markers	x within 14 days					x							x			x	
Thyroid function	x within 14 days												x			x	
HAMA	x within 12 wks												x			x	
CT/MRI disease assessments	x within 28 days											x					x
FDG-PET and blood glucose	(x) within 21 days									(x)		(x)					(x)
DCE-MRI		x	x	x													
CA4P infusion				x			x	x	x	x	x		x	x	x	x	
CA4P PK				x													
A5B7 infusion						x											
131I-A5B7 PK						x											
SPECT scans						x	x	x									
Potassium Iodide					x	x	x	x									

(x) = Optional

Treatment with 131I-A5B7/CA4P in combination													
TABLE 2.3 Assessments Cycle 2	**Day 60**	**Day 62** *(Day (-2))*	**Day 64** *(Day 1)*	**Day 66** *(Day 3)*	**Day 67** *(Day 4)*	**Day 74** *(Day 11)*	**Day 81** *(Day 18)*	**Day 88** *(Day 25)*	**Day 92** *(Day 29)*	**Day 95** *(Day 32)*	**Day 102** *(Day 39)*	**Day 109** *(Day 46)*	**Day 116** *(Day 53)*	**Day 120** *(Day 57)*
Symptom History			x	x	x	x	x	x		x	x	x	x	
Physical Exam			x	x	x	x	x	x		x	x	x	x	
WHO PS			x	x	x	x	x	x		x	x	x	x	
Vital signs			x	x	x	x	x	x		x	x	x	x	
ECG			x	x	x	x	x	x		x	x	x	x	
Radiological assessment									x					x
Haematology			x	x	x	x	x	x		x	x	x	x	
Biochemistry			x	x	x	x	x	x		x	x	x	x	
HAMA			x			x	x	x		x	x	x	x	
Tumour markers										x			x	
Thyroid function										x			x	
Potassium Iodide		x	x	x	x									
A5B7 infusion			x											
A5B7 PK			x											
SPECT scans			x	x	x									
CA4P infusion				x	x	x	x	x		x	x	x	x	
Treatment with CA4P alone														
Assessments	**Day 60**	**Day 62** *(Day (-2))*	**Day 64** *(Day 1)*	**Day 66** *(Day 3)*	**Day 67** *(Day 4)*	**Day 74** *(Day 11)*	**Day 81** *(Day 18)*	**Day 88** *(Day 25)*	**Day 92** *(Day 29)*	**Day 95** *(Day 32)*	**Day 102** *(Day 39)*	**Day 109** *(Day 46)*	**Day 116** *(Day 53)*	**Day 120** *(Day 57)*
Symptom History	x				x	x	x	x		x	x	x	x	
Physical Exam	x				x	x	x	x		x	x	x	x	
WHO PS	x				x	x	x	x		x	x	x	x	
Vital signs	x				x	x	x	x		x	x	x	x	
ECG	x				x	x	x	x		x	x	x	x	
Radiological assessment									x					x
Haematology	x				x	x	x	x		x	x	x	x	
Biochemistry	x				x	x	x	x		x	x	x	x	
Tumour markers										x			x	
CA4P infusion	x				x	x	x	x		x	x	x	x	

Results

Between January 2004 and April 2007, 88 patients were screened and twelve enrolled. Reasons for screening failure included patient unsuitable for DCE-MRI (19), patient refusal (11), CEA negative or >1000 (9), WHO PS>1 (9), no RECIST assessable disease (5), cardiac ischaemia or arrhythmia (5), previous radical radiotherapy (4), abnormal biochemistry (4), and other reasons (10).

Mean age was 63 (range 32–77). There were 7 males and 5 females. Eleven patients had metastatic colorectal adenocarcinoma, and one metastatic pancreatic adenocarcinoma. Performance status was WHO 0 (6) and 1 (6). Results are presented primarily for patients 1–7, recruited during my time as clinical research fellow, although I have included data for subsequent patients where available. **Tables 2.4, 2.5 and 2.6** illustrate the demographics, underlying diagnosis and previous treatment of the patients.

Recruitment

Recruitment initially proceeded as anticipated. However, following two cases of grade 4 neutropenia in the first six-patient cohort (1800MBq/m^2 A5B7, 45mg/m^2 CA4P), the study was suspended as a major protocol amendment was required to reduce the A5B7 dose to 1600MBq/m^2. The CA4P dose was escalated to 54mg/m^2 as it was felt the myelosuppression seen was due to ^{131}I-A5B7 in a group of heavily pre-treated patients. In addition CA4P at 45mg/m^2 was felt to be below the threshold to see any significant vascular effect (Galbraith et al., 2003). The amendments were approved by CR-UK, main Research ethics Committee and the MHRA, but resulted in significant delays to patient accrual.

Table 2.4 – Patient Diagnosis & Recruitment

Patient ID	Age / Sex	Histology at Diagnosis & Sites of Metastases at Study Entry	Previous Cancer Treatment
01	59F	Adenocarcinoma rectum,local recurrence,liver mets,ascites	Pelvic chemoradiation to 36 Gy for local recurrence (stopped due to toxicity) with concomitant 5FU/Mitomycin C .Liver mets 06/03 6 cycles FOLFOX(PD)
02	72F	Adenocarcinoma of caecum,liver, lung,bone,(brain) mets	FOLFOX x 6 12/01, FOLFIRI 12 cycles 4/02,RFA Liver 10/02,ADEPT 4/03,RFA Liver 7/03,RFA Lung & Liver 10/03,RT Rt hip & T/Spine 12/03
03	57F	Adenocarcinoma sigmoid colon,liver mets	Irinotecan/5FU 5 cycles 6/03 , Oxaliplatin/5FU 4 cycles 9/03
04	65M	Adenocarcinoma sigmoid colon,liver,lung mets	Weekly 5FU/FA x 30 (11/01) Irinotecan x 5 (10/02) ,ADEPT (6/03)
05	70M	Adenocarcinoma ascending colon,liver mets	FOLFOX x 5 PD
06	32F	Adenocarcinoma of caecum, peritoneal,para-aortic,Iliac nodes	De Gramont x 12 (1/03), Completion panproctocolectomy - Laparotomy (open & shut - carcinomatosis) 9/2003, Oxaliplatin + de Gramont x 9 (10/03)
07	72M	Adenocarcinoma of rectum,liver,lung mets	Weekly 5FU/FA x 24 (11/03) Liver resection 7/04 ,Oxaliplatin + 5FU 4 cycles 12/04
08	77M	Rectal adenocarcinoma with liver & lung metastases	Pelvic chemoradiation 45Gy +Capecitabine (01/05), weekly 5FU x 26 (06/05)
09	66F	Adenocarcinoma of pancreas with liver metastases	Gemcitabine x 6 (08/05)
10	61M	Rectal adenocarcinoma with liver metastases	Rectal RT (05/97), 5FU/FA x 6 (NK/97), Oxaliplatin/5FU x 8 (03/00), Liver resection (11/01), Rectal RT (05/04), Irinotecan/5FU x 6 (07/04), Irinotecan x 8 (06/05)& x 4 (03/06), Cetuximab x 8 (06/05) & x 4 (03/06)
11	58M	Colorectal adenocarcinoma with liver & lung metastases	Sigmoid colectomy (07/05), FOLFOX x 8 (11/05), FOLFIRI x 4 (08/06)
12	63M	Rectal adenocarcinoma with adrenal and bone metastases	Liver resection + 5FU/FA pre & post resection (NK/00), Irinotecan/Capecitabine (NK/02), Oxaliplatin/Capecitabine (07/05), IMRT to para-aortics (NK/05)

RFA = Radiofrequency ablation, FOLFOX = Oxaliplatin with the de Gramont infusional & bolus 5FU/Folinic Acid regimen, FOLFIRI = Irinotecan with the de Gramont infusional & bolus 5FU/Folinic Acid regimen, ADEPT = Antibody Dependent Enzyme Prodrug Therapy Phase I Study. N/A – Data for patients 08 – 12 not available from central database at time of writing

Further significant delays to accrual occurred with the introduction of the European Union Clinical Trials Directive (2004). As the A5B7 radiolabelling was considered an on-site manufacturing process, an application for an Investigational Medicinal Product (IMP) license from the MHRA had to be processed. During this time a new radiopharmacist was recruited and trained at the Royal Free Hospital.

Table 2.5 – Amount Of Trial Drug Received & Reason Patients Removed From Study

Patient ID	Dose Cohort	Number of A5B7 Infusions Received	Number of CA4P Infusions Received	A5B7 Activity (MBq/m^2)	Dose of CA4P (mg/m^2)	Day Withdrawn From Study	Reason Patient Withdrawn From Study
01	1*	1	4	1800	45	18	PD Liver & ascites. Haematuria. DLT Grade 4 Neutropenia
02		1	5			25	New brain/lung mets. SD liver
03		1	4			18	PD Liver.concern over ECG ischaemia
04		2**	16			95	PD Liver
05		1	6			29	PD Liver
06		1	10			57	PD Peritoneal mass. DLT G4 neutropenia
07	A*	1	3	1600	54	11	SAE ataxia & hypotension. Hickman line sepsis
08		1	8			46	Progressive disease. DLT G4 neutropenia
09		1	3			4	Cardiac Ischaemia & hypertension. PD.
10		0	1	-		1	Not evaluable. Consent withdrawn
11		1	5	1600		29	PD liver
12		1	7			32	PD – New brain mets DLT – G4 neutropenia

*Dose cohorts explained in Table 2.1
**2nd A5B7 Infusion only received if HAMA negative by ELISA at Day 53 assessment.
PD = Progressive disease by RECIST criteria, SD = Stable disease, SAE = Serious Adverse Event, DLT = Dose Limiting Toxicity

Toxicity

The following **Table 2.6** illustrates the drug related toxicity seen. Other than myelosuppression, toxicity was manageable. The majority of SAE's were not drug related. Myelosuppression did not result in excess morbidity because the gastrointestinal mucosa was intact. This is a feature of the haematological toxicity associated with RIT. Conventional systemic therapy can lead to septicaemia when myelosuppressed if there is gastrointestinal mucositis. The grade 4 neutropenia seen in patient 01 meant cohort 1 was expanded to six patients. However the occurrence of a second case necessitated the revised dose levels A&B (**Table 2.1**). Two further cases of grade 4 neutropenia occurred in cohort A. It was felt that reducing the dose of A5B7 and/or CA4P further would be unlikely to result in an active combination, and the trial was terminated early.

Table 2.6 – Drug Related Toxicity patients 1 - 6

System	CTC Toxicity Criteria	A5B7/CA4P Related (No. Episodes)			
		Grade 1	Grade 2	Grade 3	Grade 4
Blood / Bone Marrow	Anaemia	3	5	0	0
	Leucopenia	2	0	2	2
	Lymphopenia	1	5	3	0
	Neutropenia	0	3	0	2
	Thrombocytopenia	4	0	3	0
Metabolic	Hypermagnesaemia	0	0	0	0
	Hypomagnesaemia	1	0	0	0
	Hypoalbuminaemia	3	0	0	0
	Hyperkalaemia	1	0	0	0
Coagulation	High APTT	1	0	0	0
	High Prothrombin time	1	0	0	0
Cardiovascular	ECG Changes	1	0	0	0
	QTc Prolongation (normal Range)	1	0	0	0
	Sinus Tachycardia	10	0	0	0
	Sinus Bradycardia	4	0	0	0
	Hypertension	14	1	0	0
	Hypotension	4	0	0	0
Constitutional Symptoms	Fever	11	0	0	0
	Rigors	4	0	0	0
	Sweating	5	0	0	0
	Fatigue	1	2	0	0
Dermatology	Pruritis	6	0	0	0
Endocrine	Low TSH	1	0	0	0
	Hypothyroidism	1	0	0	0
Gastrointestinal	Nausea	3	0	0	0
	Vomiting	1	0	0	0
	Diarrhoea	3	0	0	0
	Stomatitis	1	0	0	0
	Constipation	1	0	0	0
	Anorexia	0	1	0	0
	Taste Disturbance	1	0	0	0
Hepatic	Hepatomegaly	1	0	0	0
Neurology	Sensory Peripheral Neuropathy	1	0	0	0
Pain	Tumour Pain	4	2	0	0
	Liver Pain (Tumour)	4	1	0	0
	Hip Pain	0	1	0	0
	Abdo Pain	0	1	0	0
	Pelvic Pain	1	0	0	0
	Chest Pain (muscular)	1	0	0	0
	Headache	1	0	0	0

Vital Signs

Temperature

The following **Figures 2.1–2.4**, illustrate changes in vital signs following A5B7 or CA4P. Pyrexia following infusion was common, in 4/7 patients, as high as 39°C. Two patients felt unwell with rigors. This phenomenon was felt to be a hypersensitivity immune reaction to the foreign antibody, and has been seen with other non-humanised & partially humanised monoclonal antibody biological therapies e.g. Rituximab, Trastuzumab, Cetuximab (Lenz, 2007). Very modest rises in core temperature were also seen following CA4P.

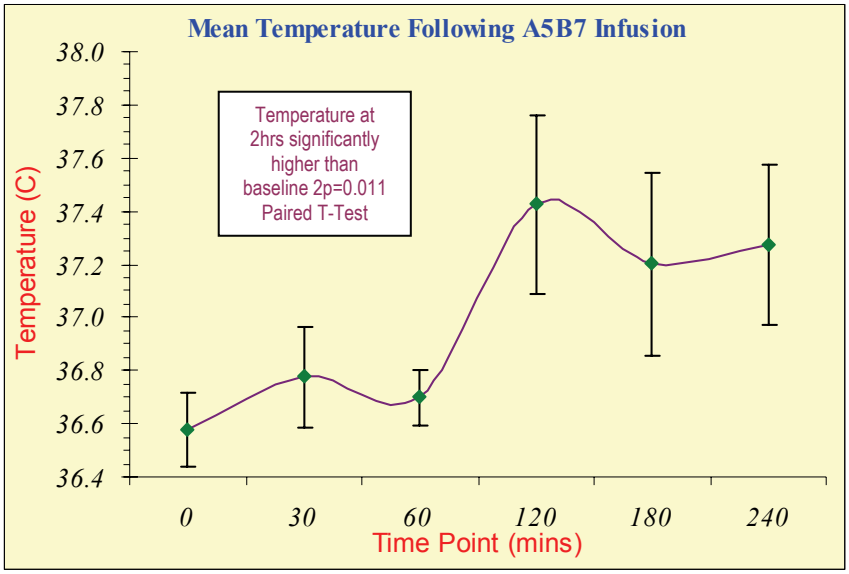

Figures 2.1 (above) & 2.2 (below)

Core Temperature Following A5B7 and CA4P Infusion (n=7 patients, 1800MBq/m² A5B7 and 45 mg/m² CA4P in the first 6). Mean ± Standard Error

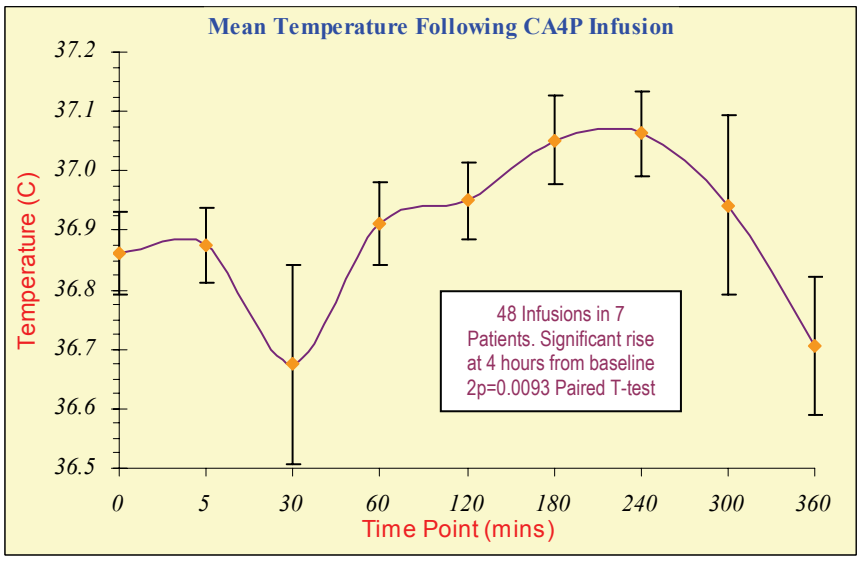

Blood Pressure

Changes seen in HR/BP following A5B7 probably relate to the infusion reaction. BP change at 3h from baseline is significant 2p=0.011. The changes following CA4P are as previously described by Rustin (Rustin et al., 2003). A BP rise is seen because of alterations in peripheral resistance with a compensatory increase in HR at 4 hours. For CA4P HR at 3h against baseline, and BP at 1h against baseline, highly significant rises seen 2p<0.0001

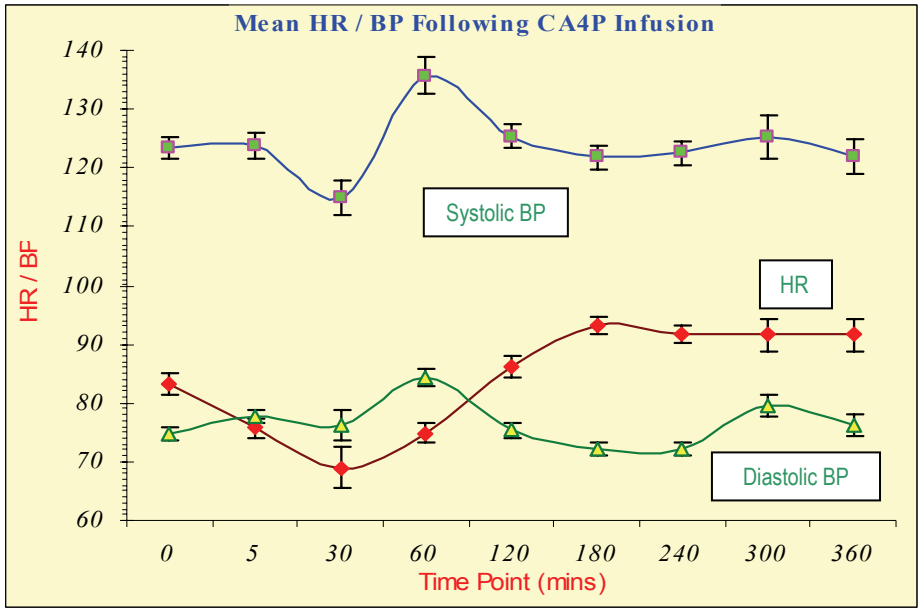

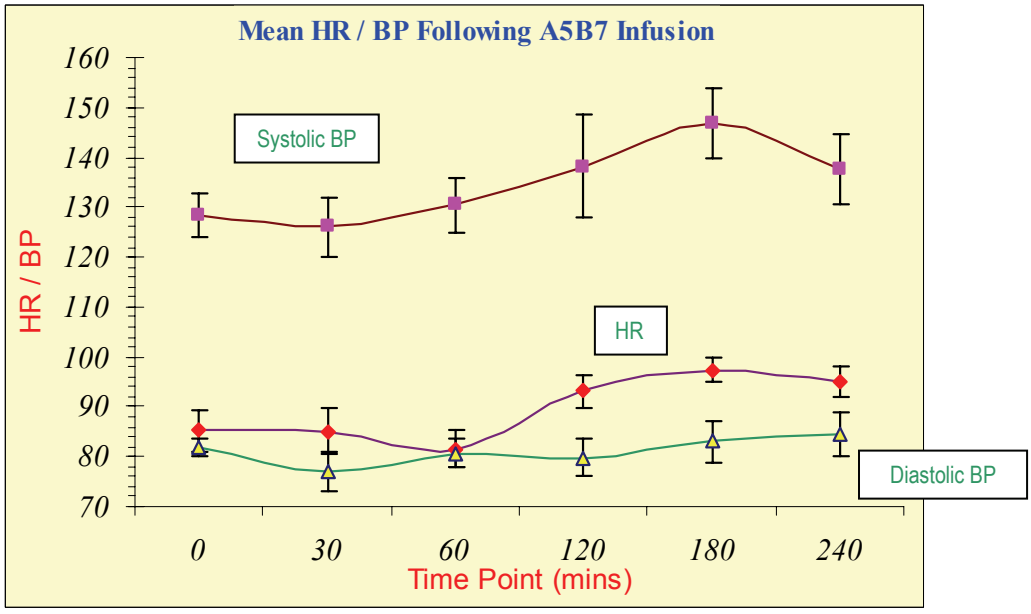

Figures 2.3 & 2.4

Heart Rate & BP Following A5B7 or CA4P Infusion (n=7 patients) Mean ± Standard Error

ECG Changes

QTc prolongation within the normal range has previously been described following CA4P infusion and is presented below for this study in **Figure 2.5**. There is significant QTc prolongation at 4h by 11ms (2p=0.0016). The aetiology is reviewed in **Chapter 1** and also see UKCTC-207 Study (**Chapter 6**).

Figure 2.5 - QTc Interval Following CA4P Infusion (n=7 patients) Mean ± Standard Error

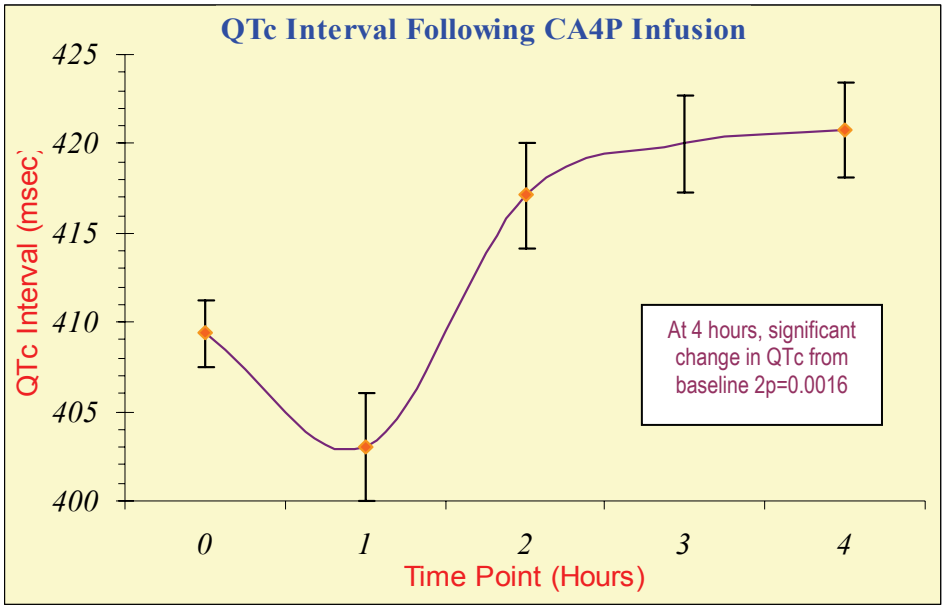

Haematological Toxicity

This is illustrated in **Figures 2.6–2.7**. Significant falls in neutrophil counts were seen 32 days following A5B7 (2p=0.036). The significant rise in neutrophil count 4h following CA4P (2p=0.016) (**Figure 2.8**) is likely to be an inflammatory response to the vascular endothelial assault. This rise was also documented in the UK Phase I study of CA4P and is resolved by 24h (Rustin et al., 2003). In the Rustin study, significant falls in lymphocytes were also seen 4h after CA4P administration. Our result (**Figure 2.9**), which included only the first seven patients, did not achieve statistical significance (2p=0.18). **Figures 2.10–2.11** illustrate the thrombocytopenia and neutropenia seen in patient 06.

Figures 2.6 & 2.7 – Thrombocytopenia & Myelosuppression following A5B7 Infusion (n=7). 1800MBq/m² A5B7 administered on day 1 in first 6 patients, 1600MBq/m² patient 7. Mean ± Standard Error

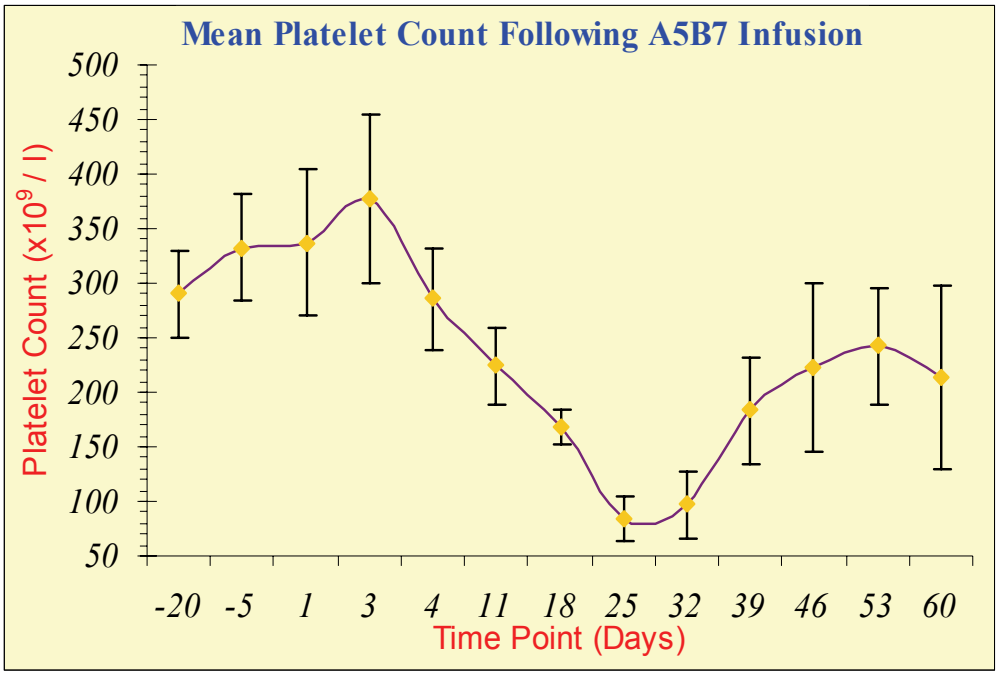

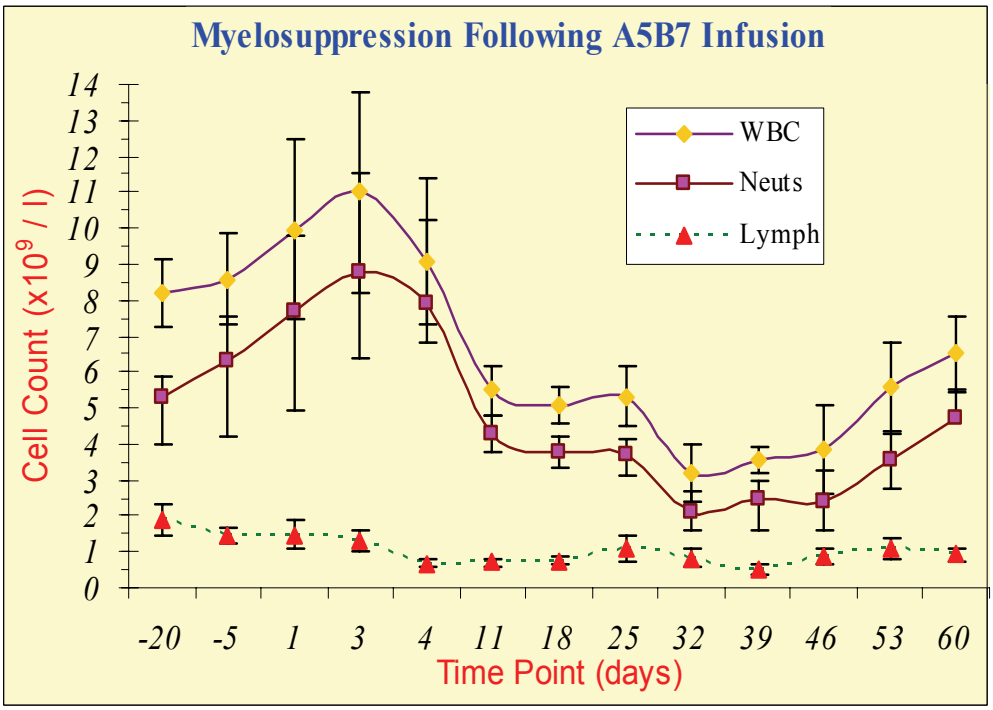

Figure 2.8 - Neutrophil Count 4 hours Following CA4P Infusion (n=7)

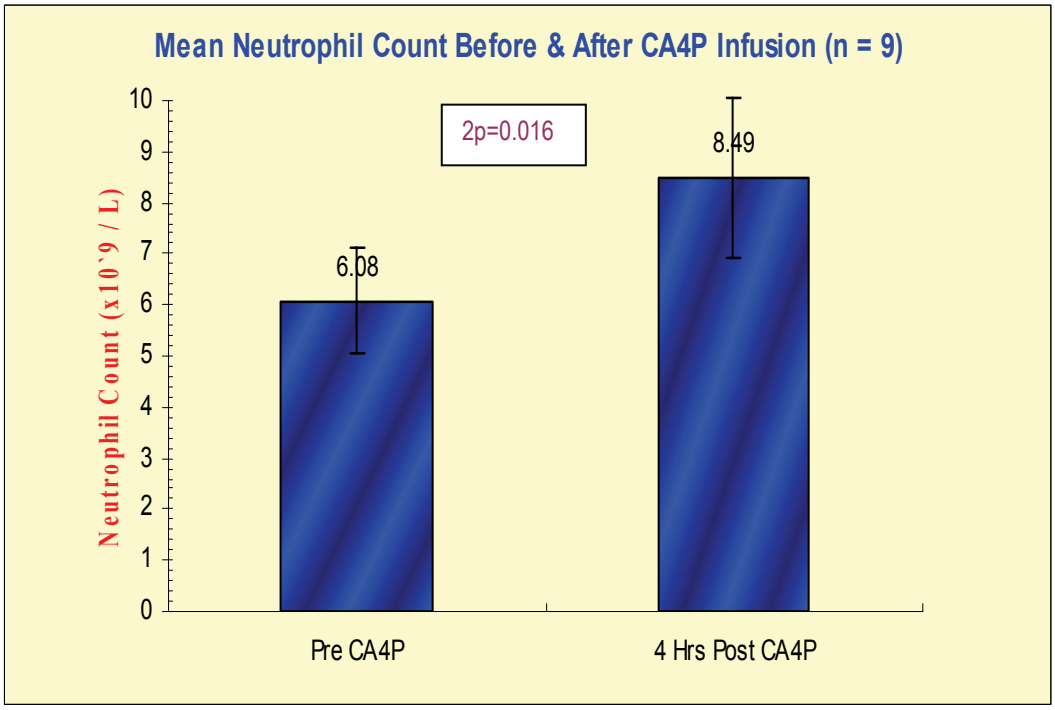

Figure 2.9 - Lymphocyte Count 4 hours Following CA4P Infusion (n=7). Mean ± SE

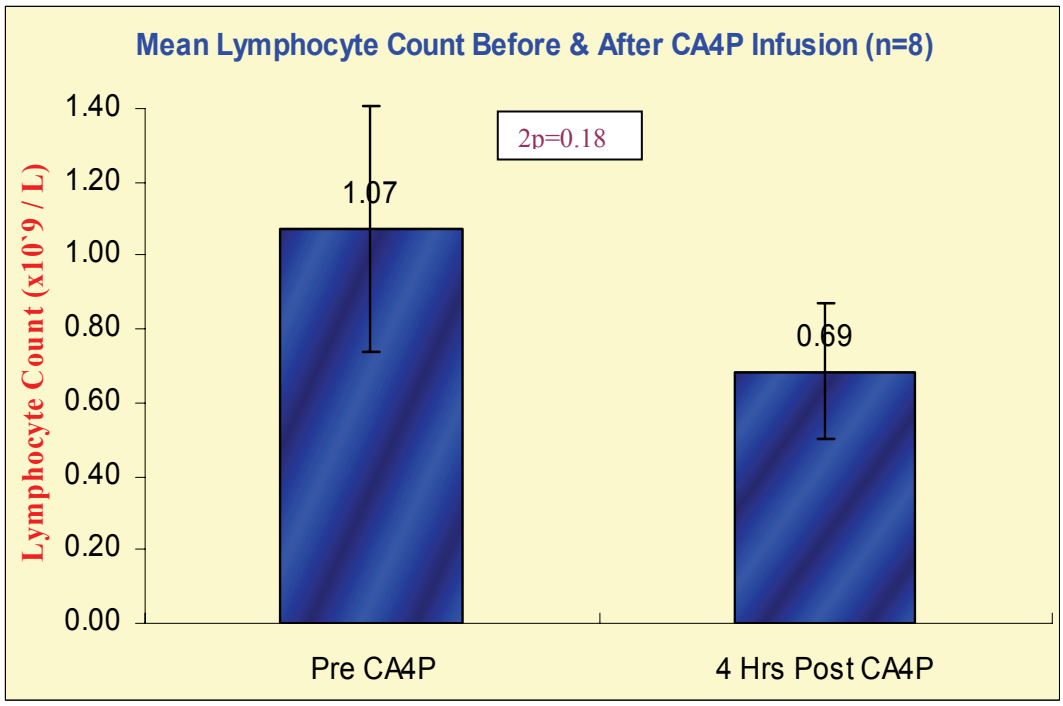

Figures 2.10 – 2.11 – Patient 6, WBC and platelets Following A5B7. Data chosen to illustrate delayed and dose-limiting grade 4 neutropenia and grade 3 thrombocytopenia lasting for a week following 1800MBq/m² A5B7. Growth factors were not administered. Recovery was uncomplicated without pyrexia. CA4P was witheld until recovery. Arrow indicates drug infusion.

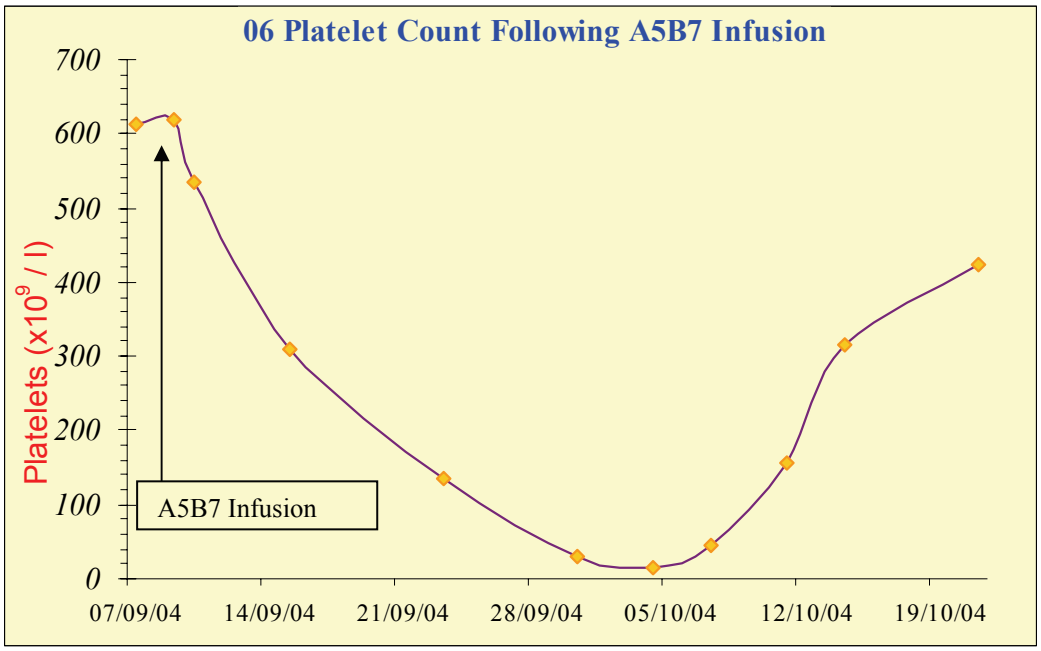

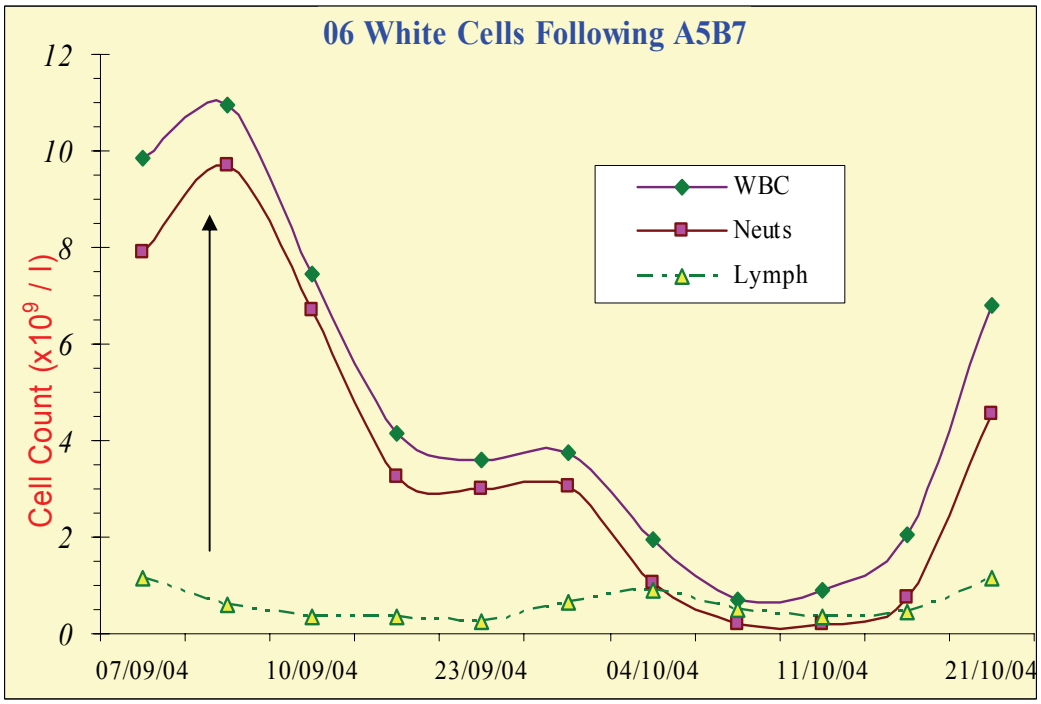

Tumour Markers

Figures 2.12 & 2.13 – Serum CEA & Ca19.9 Following Combination Treatment - Tracking of patient tumour markers throughout study. A minor response was seen in patient 06

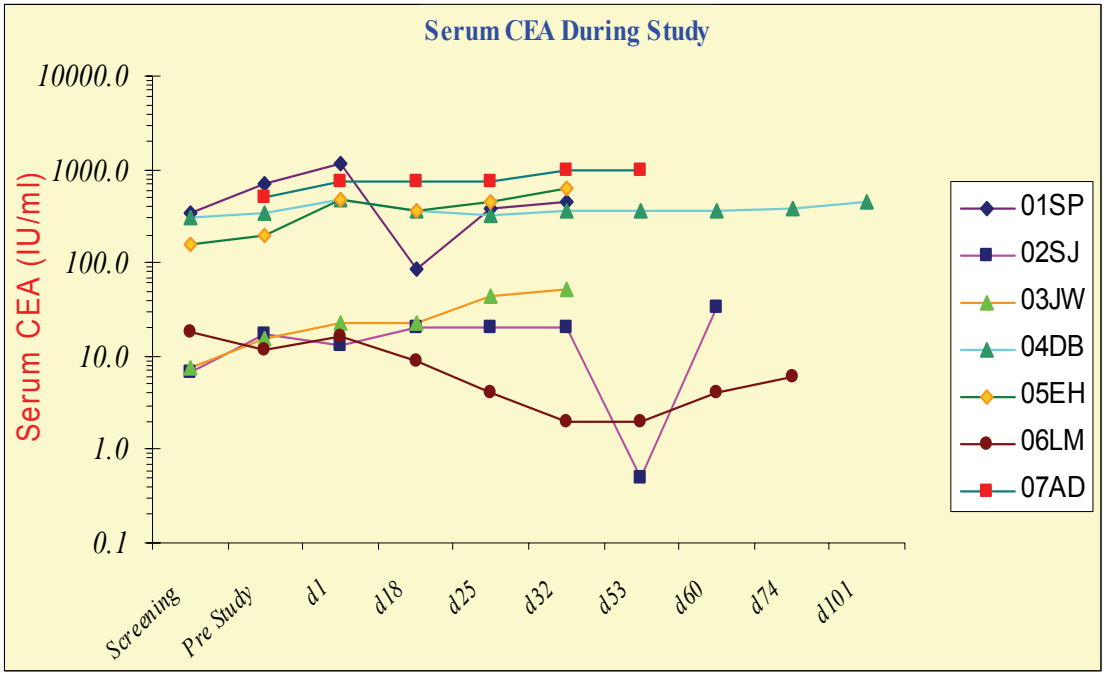

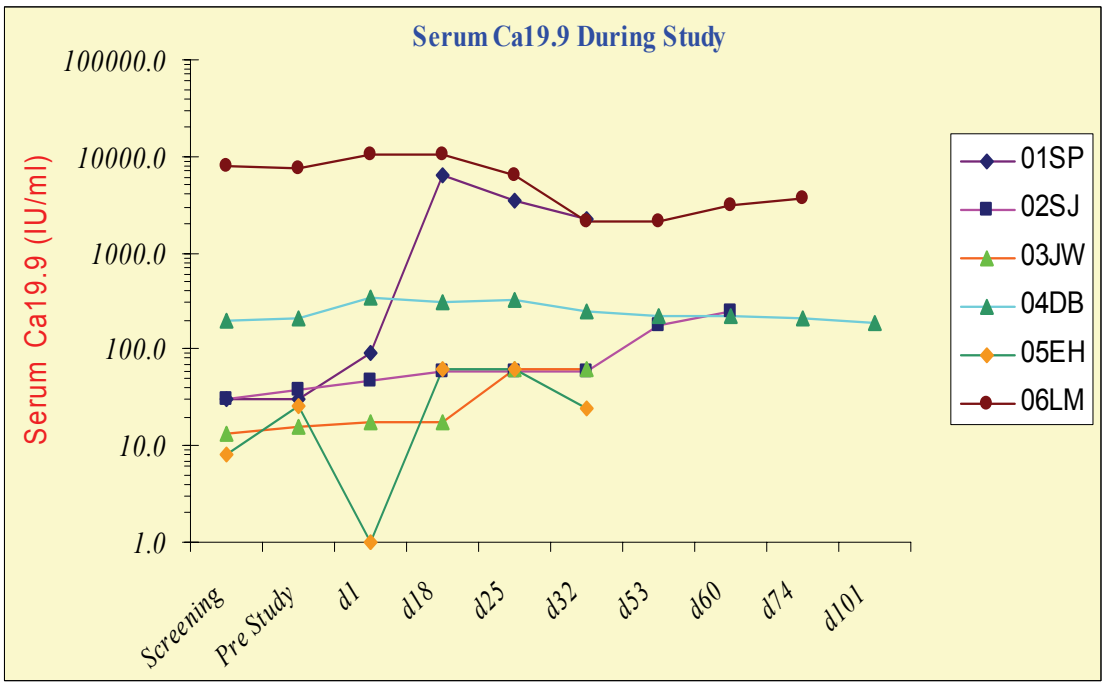

ECG Changes

Patient 03 was removed from the study on safety grounds on March 19th 2004 following ECG changes, which were deemed 'possibly related' to CA4P. The history of events is illustrated in **figures 2.14 a-g**. The pre-study screening ECG A showed no evidence of T-wave inversion. There was left ventricular hypertrophy by voltage criteria present in leads v4 to v6 (red arrow); however this was entirely consistent with known longstanding hypertension, which was well controlled. There was no evidence of significant ischaemic heart disease, which would exclude her from the study. ECG B, d3 Pre-CA4P illustrates anterior T-wave inversion in leads v2 and v3. The patient was completely asymptomatic. This ECG was reviewed by a cardiologist prior to CA4P, who confirmed a degree of undiagnosed coronary artery disease; this was not felt significant enough to warrant further immediate investigation. The infusion proceeded without incident although the patient was hypertensive. Two hours post CA4P (ECG C), the ischaemic ECG changes had resolved. Four hours post CA4P (ECG D) T wave inversion had reappeared in v2 (arrow), but not V_3, without patient symptoms.

On day 11, baseline ECG E shows T wave inversion present in the anterior leads. A repeat ECG (not shown) had normal T-waves, so CA4P was administered. One hour after CA4P (ECG F) T wave inversion was again present in anterior leads. The patient was asymptomatic, and cardiac enzymes (CPK and Troponin C) were negative for an acute cardiac event. Because of the poor prognosis from her underlying metastatic cancer, it was felt inappropriate to proceed with further investigation. The patient was withdrawn from the study for her own safety. Six hours post CA4P (ECG G) T-wave inversion was still present. Although the T-wave inversion appeared intermittent and random, it could not be excluded that CA4P exacerbated the changes. Following these episodes, a protocol amendment was passed to allow prophylactic antihypertensive treatment for patients experiencing grade 2 rises in BP following CA4P

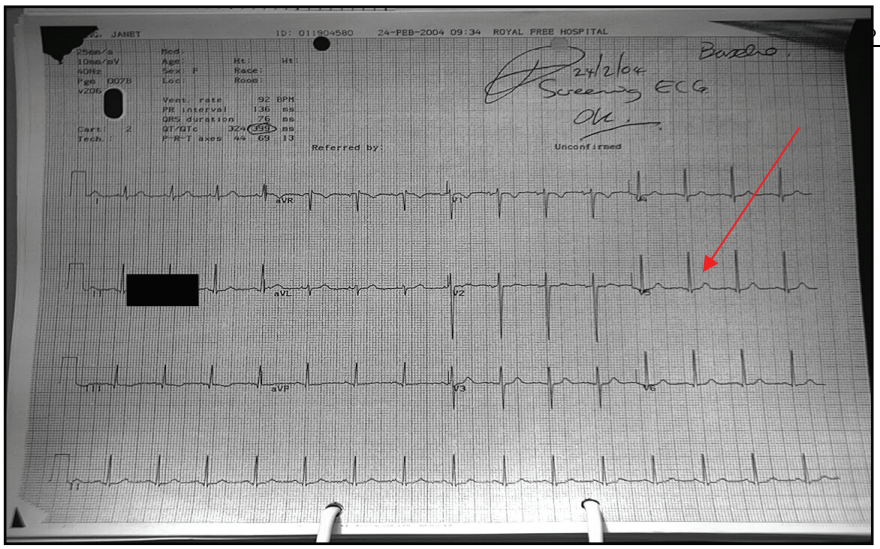

A

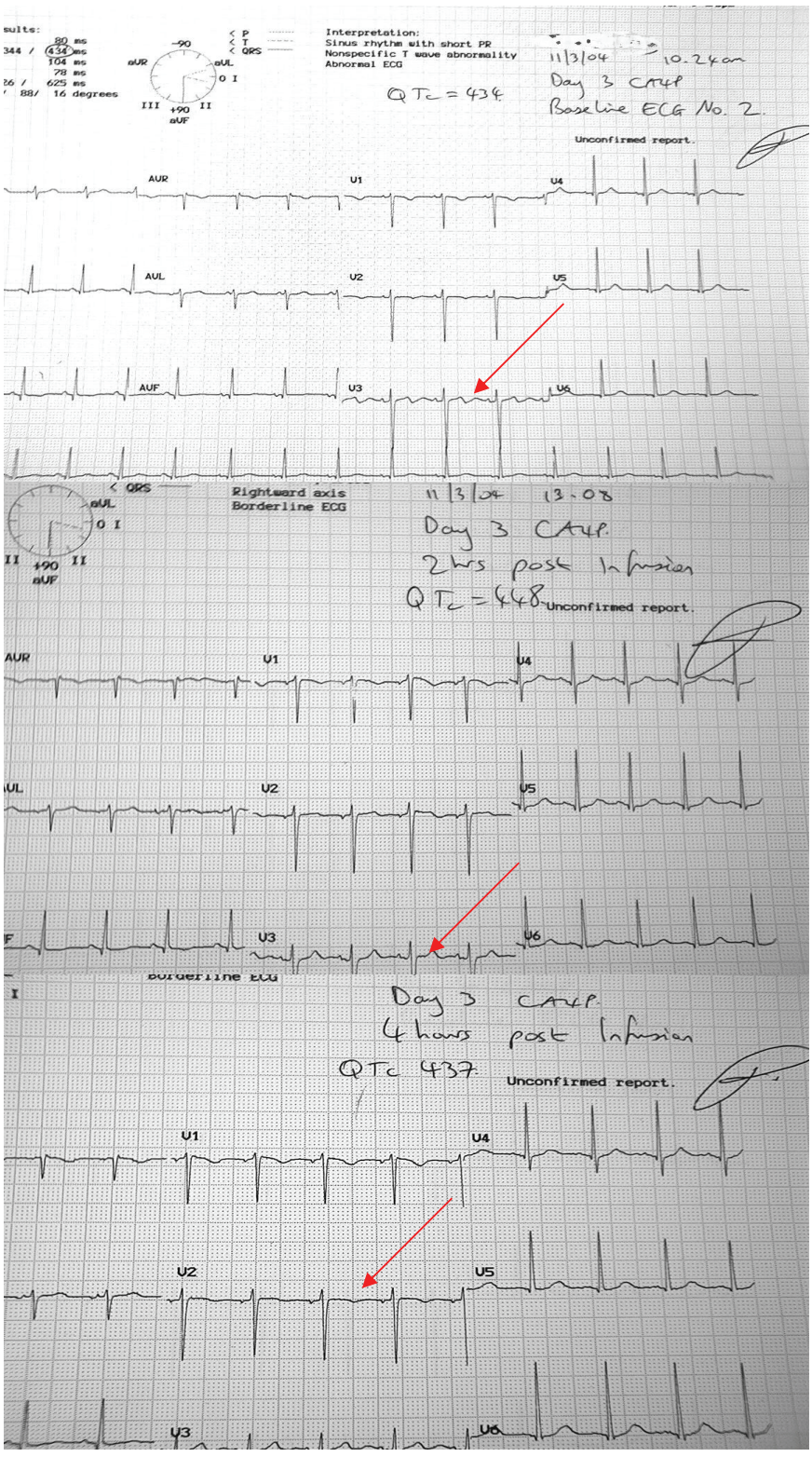

B

C

D

Figure 2.14 A – G – ECG Changes In Patient 03

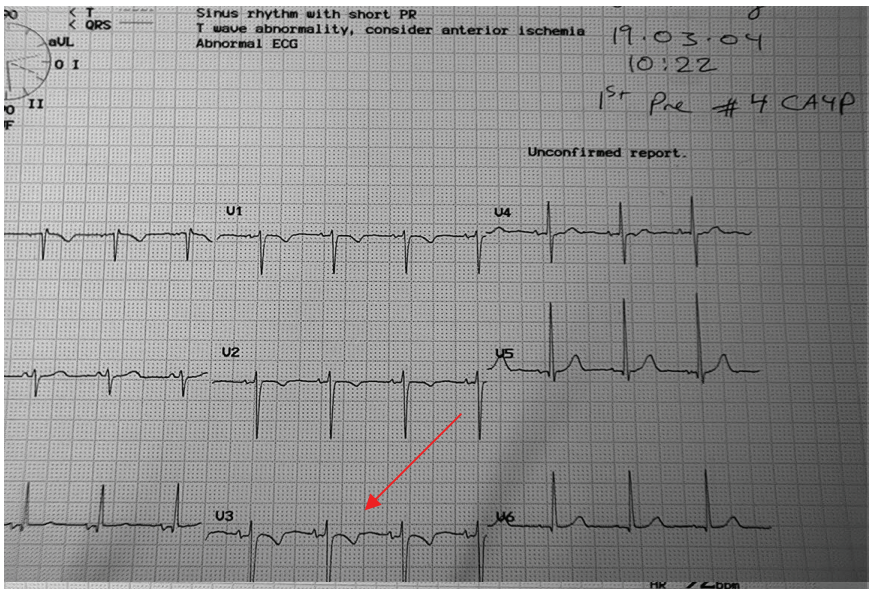
Sinus rhythm with short PR
T wave abnormality, consider anterior ischemia
Abnormal ECG
19.03.04
10:22
1st Pre #4 CA4P
Unconfirmed report.
V1
V4
V2
V5
V3
V6

E

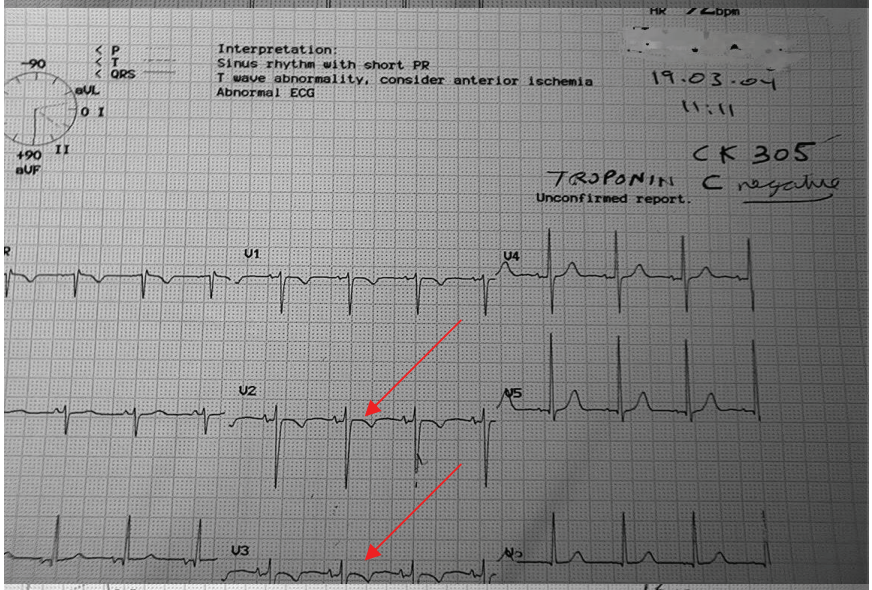
Interpretation:
Sinus rhythm with short PR
T wave abnormality, consider anterior ischemia
Abnormal ECG
19.03.04
11:11
CK 305
TROPONIN C negative
Unconfirmed report.
V1
V4
V2
V5
V3

F

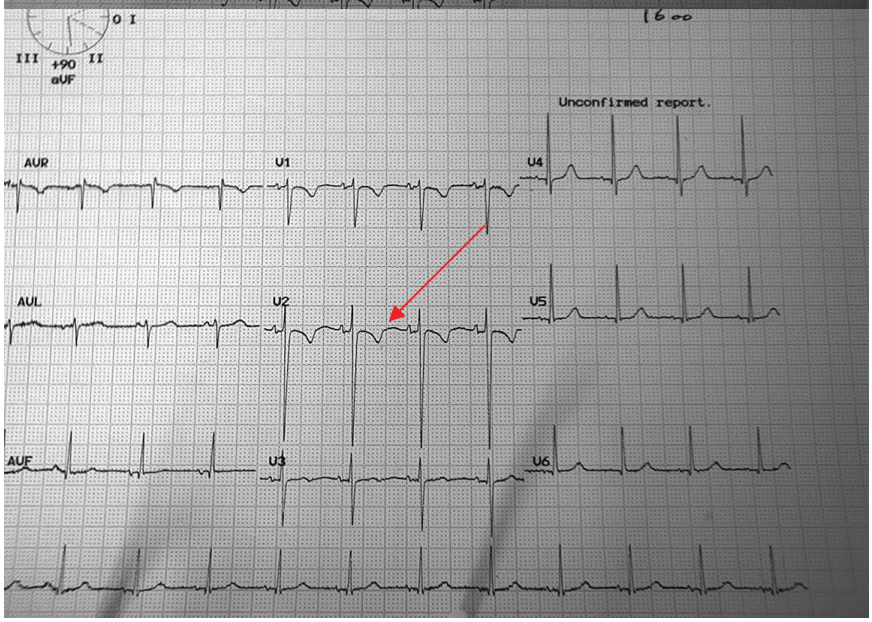
1600
Unconfirmed report.
AVR
V1
V4
AVL
V2
V5
AVF
V3
V6

G

Response Assessment

In the eleven patients who received A5B7 and CA4P there was one case of stable disease (patient 04) and one minor response seen in patient 06 at d29, best overall RECIST SD. A pelvic node reduced in size by >50% however other marker lesions were of similar size (**figure 2.15)**. These responses were short lived and a total of ten patients were withdrawn from the study due to progressive disease.

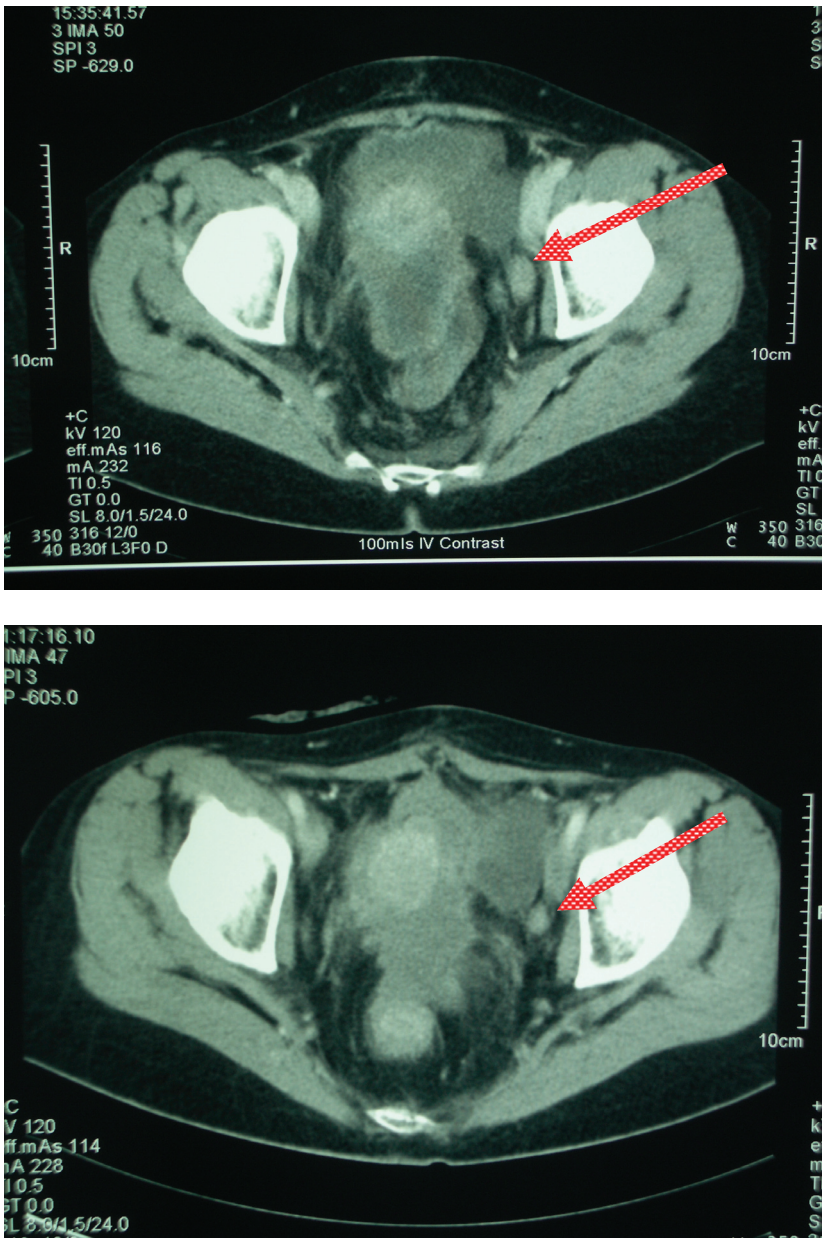

Figure 2.15a,b- Patient 06 Pre-Study & Day 29 CT Scan

Following A5B7 and six CA4P infusions a response was seen in this target lesion (an enlarged pelvic lymph node), however the overall RECIST response was stable disease.

Pharmacokinetics

The pharmacokinetic data was analysed by Dr Mike Stratford at the Gray Cancer Institute and is summarised in **Table 2.7**.

Table 2.7 – Summary Pharmacokinetic Data (Courtesy of Dr M Stratford) The pharmacokinetic parameters determined for CA4P included the maximum observed plasma concentration (C_{max}), the area under the plasma concentration time curve (AUC), initial and terminal elimination half-life ($T_{½}$), mean residence time (MRT), clearance (CL), and steady-state volume of distribution (Vss). For CA4, C_{max}, AUC and $T_{½}$ were determined, and in addition, time to reach C_{max} (T_{max}).

patient	CA4P dose mg/m²	Infusion time (h)	CA4P$_{max}$* (µM)	CA4P AUC µmol.h.l^{-1}	clearance l.h^{-1}.m²	AUMC µmol.h².l^{-1}	MRT (h)	Vdss l.m²	CA4$_{max}$ µM	T$_{max}$ h	CA4 AUC µmol.h.l^{-1}
01	45	0.17	N/A	N/A	N/A	N/A	N/A	N/A	N/A	N/A	N/A
02			23.8	10.1	11.3	3.05	0.217	2.44	2.13	0.27	2.51
03			13.1	4.34	26.2	0.885	0.119	3.11	2.81	0.23	1.75
04			22.1	6.74	16.9	1.58	0.151	2.54	1.63	0.25	2.15
05			27.9	7.02	16.2	1.72	0.160	2.59	1.73	0.25	1.96
06			27.8	7.88	14.4	2.11	0.183	2.64	5.41	0.27	4.04
Mean			**22.9**	**7.22**	**17.0**	**1.87**	**0.166**	**2.67**	**2.74**	**0.25**	**2.48**
Std dev			**6.05**	**2.08**	**5.58**	**0.79**	**0.037**	**0.26**	**1.56**	**0.02**	**0.91**
07	54	0.30	28.9	8.91	15.3	3.35	0.226	3.46	1.39	0.35	2.04
08		0.17	30.6	8.89	15.3	2.49	0.195	2.99	4.11	0.30	3.10
09			31.8	7.97	17.1	1.85	0.147	2.52	2.97	0.27	4.14
10			35.3	8.43	16.2	1.89	0.139	2.25	4.23	0.20	2.67
11			28.9	8.09	16.9	2.09	0.173	2.92	4.70	0.18	4.65
12			30.5	10.4	13.1	3.88	0.288	3.78	1.28	0.17	1.39
Mean			**31.0**	**8.78**	**15.6**	**2.59**	**0.195**	**2.99**	**3.11**	**0.25**	**3.00**
Std dev			**2.4**	**0.88**	**1.45**	**0.84**	**0.056**	**0.57**	**1.49**	**0.07**	**1.24**

* - peak CA4P concentration extrapolated from fit back to end of infusion if sample not taken then
PK parameters for patient #1 not calculated due to contamination of the immediate post-infusion sample with dosing solution

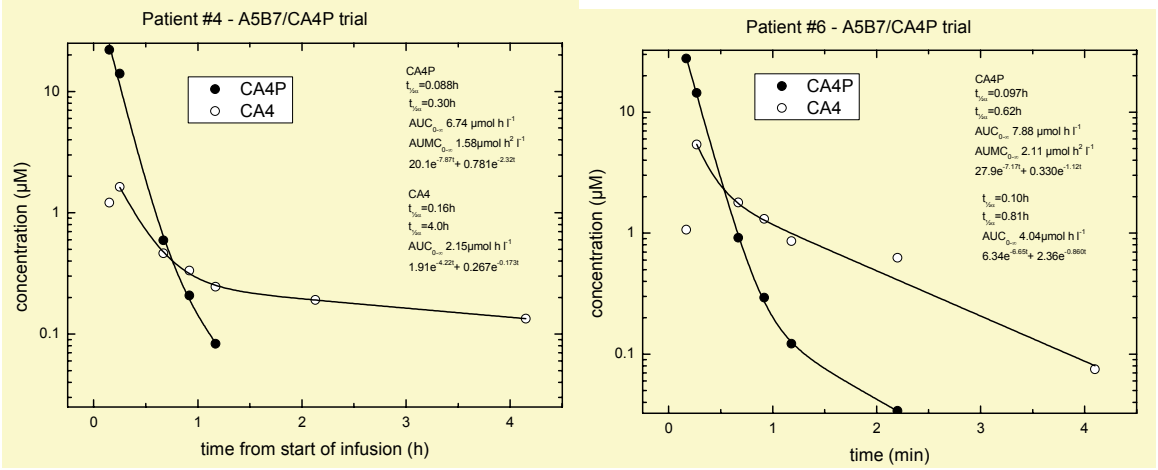

Figures 2.16a,b – CA4P Clearance - Patients 04 & 06 (Courtesy of Dr M Stratford, Gray Cancer Institute)

CA4P pharmacokinetics were in agreement with previous data (Rustin et al., 2003). Data for 01 was omitted from the analysis as the sample immediately after CA4P infusion was taken from the same intravenous line as the drug, giving an artificially high reading; It is not possible to fit the CA4P data to either a monophasic or biphasic model without the end of infusion time point, because it is so rapidly cleared. Clearance curves are presented for patient 04 and 06 (**Figure 2.16 a,b**).

CA4P is rapidly hydrolysed by plasma and tissue esterases to the active CA4, with a mean initial half-life of 5 min. In all cases, the maximum plasma CA4P was observed in the first sample taken post-start of infusion. There were no significant differences in $T_{½}$, Cl or Vss between the two doses used, with terminal $T_{½}$ at the lower and higher doses of 0.36 ± 0.22 h and 0.45 ± 0.15 h, clearance 29.4 ± 7.21 $L.h^{-1}$ and 25.7 ± 13.5 $L.h^{-1}$, and Vss 4.69 ± 0.67 L and 4.71 ± 2.59 L respectively. As expected, there was an increase in the AUC of the parent CA4P (22 %) and active CA4 (21 %) at the higher dose consistent with the 20 % higher dose used. The rapid activation to CA4 was reflected in the time to reach peak CA4 concentration; in the majority of cases, this occurred in the first post-end of infusion sample, although in four patients, the highest level was seen at the same time as the peak CA4P, immediately at the end of the infusion. This included Patient 07 who received the longer 18 min infusion. CA4 was cleared from plasma with a half-life of 2.24 ± 1.19 h and 1.92 ± 0.69 h at the lower and higher doses of CA4P respectively.

SPECT imaging also confirmed no delayed excretion of radioisotope as a result of CA4P infusion. Excretion half life was 26 hrs. SPECT graphs and analysis (**Figures 2.17–2.20**) are included courtesy of Dr J Violet (University of London).

SPECT ANALYSIS

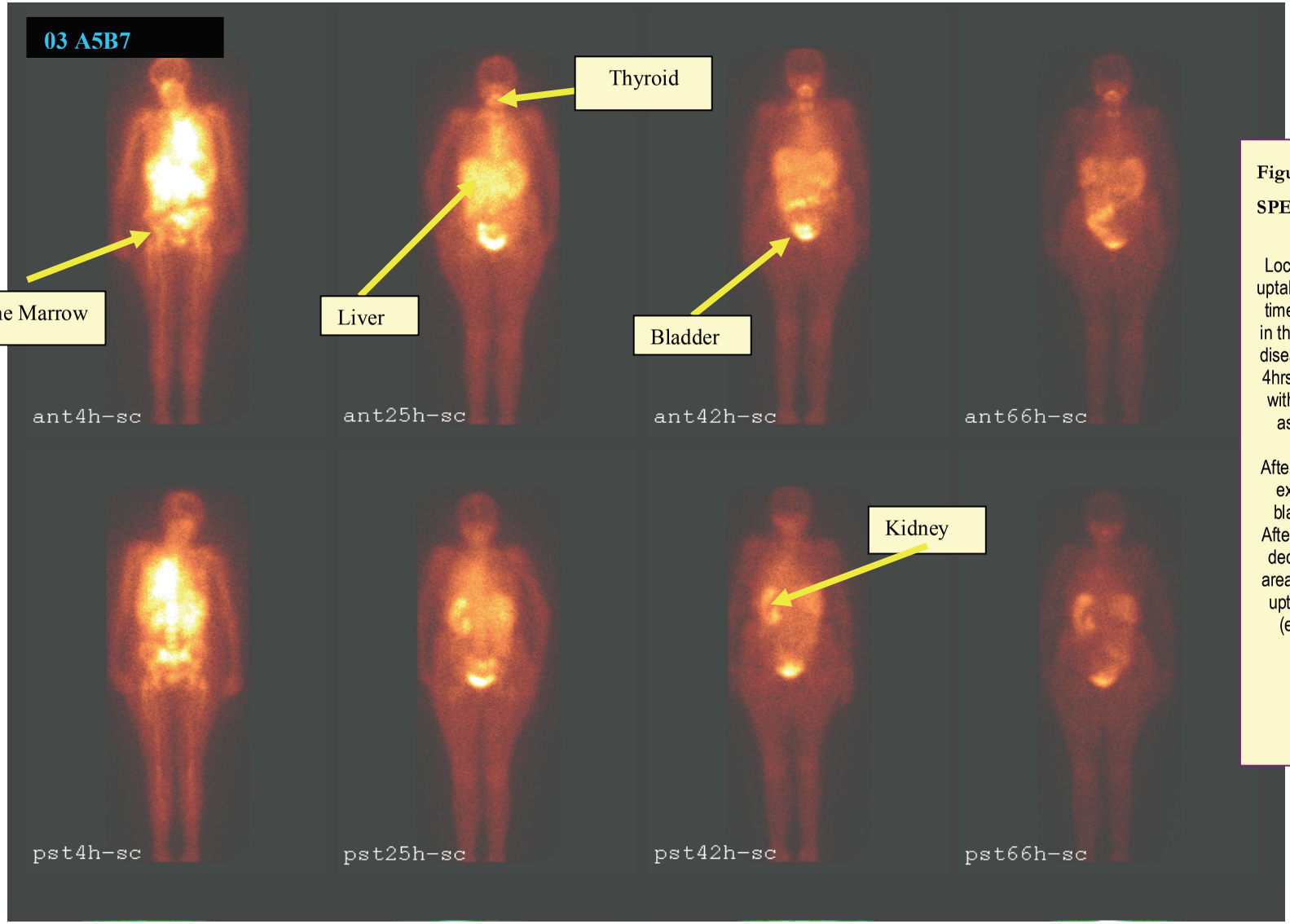

Figure 2.17

SPECT Scans patient 03

Localisation of ^{131}-I-A5B7 antibody uptake within patient and decay over time. Localisation is predominantly in the liver (known site of metastatic disease) and bladder (excretion). At 4hrs there is also some localisation within the chest and bone marrow as detected using the Gamma-Camera.
After 25 hours localisation is almost exclusively in tumour(liver) with bladder excretion clearly visible. After 42hrs & 66hrs the isotope has decayed however still localised to areas of tumour. Note some thyroid uptake at 25,42 and 66hrs. Renal (excretion) shown on posterior views.

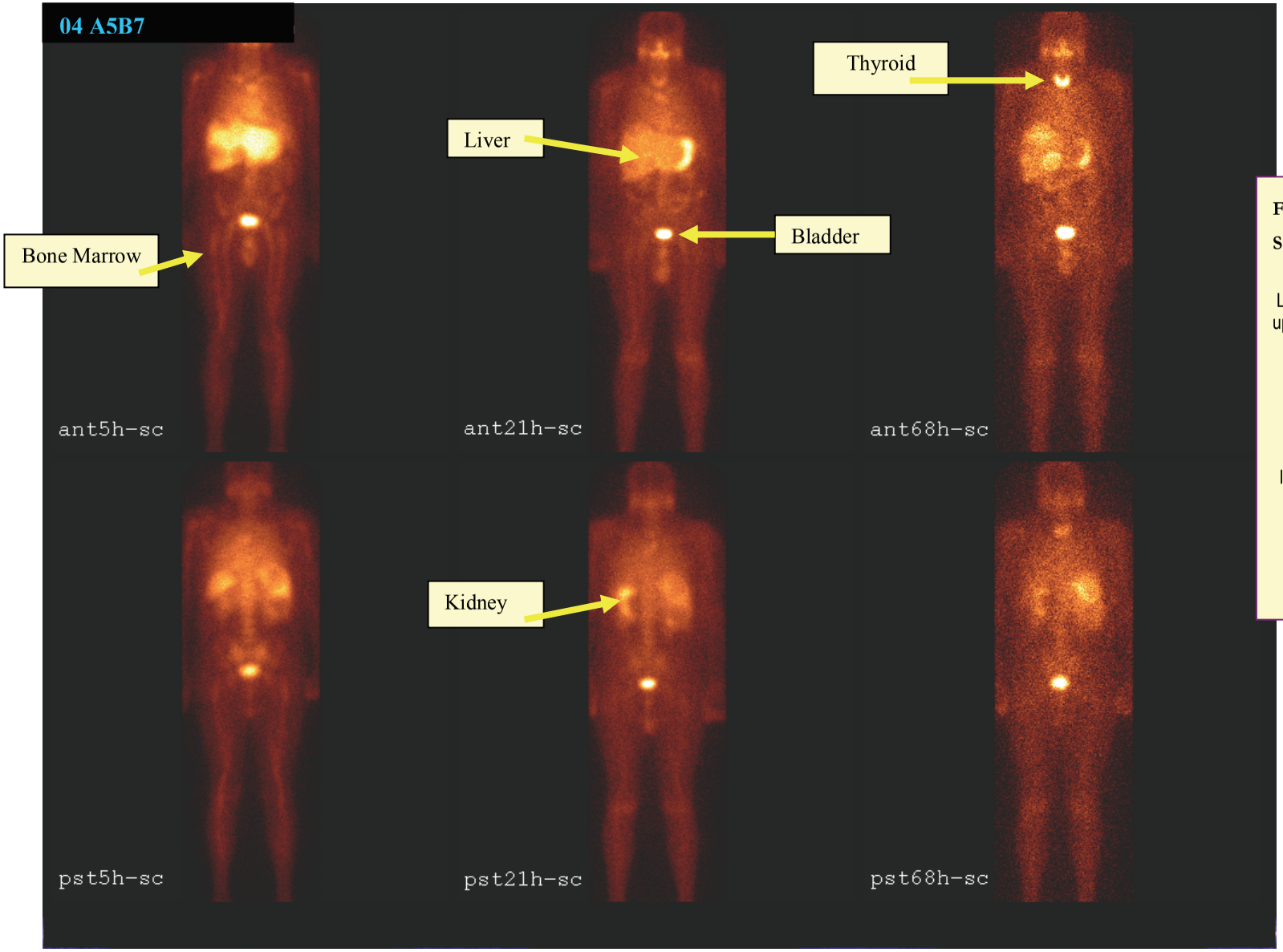

Figure 2.18

SPECT Scans patient 04

Localisation of 131-I-A5B7 antibody uptake within patient and decay over time. Localisation was predominantly in the liver (known site of metastatic disease) and bladder(excretion). At 5hrs there was also some localisation within the bone marrow. After 21 hours localisation was almost exclusively in tumour(liver). After 68hrs the isotope had decayed however still localised to areas of tumour. Note some thyroid uptake at 21 and 68 hrs.

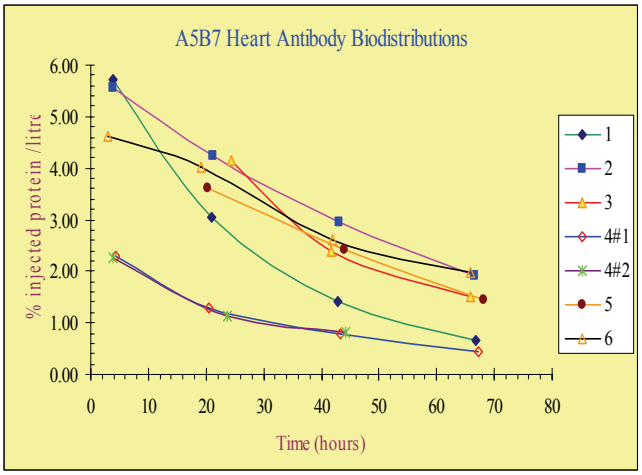

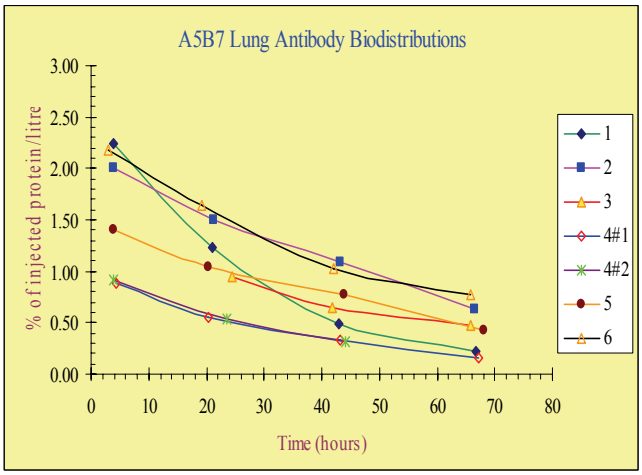

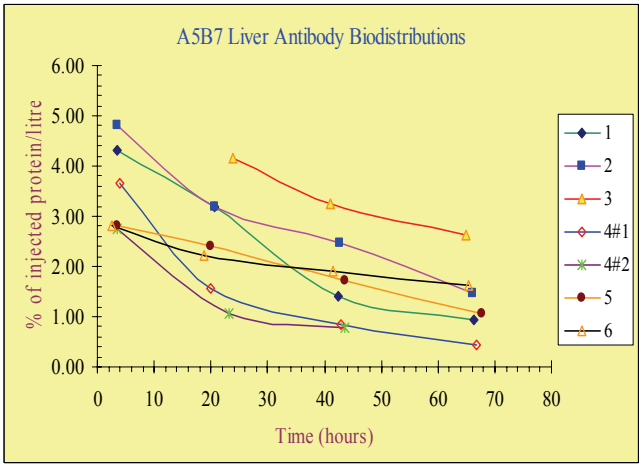

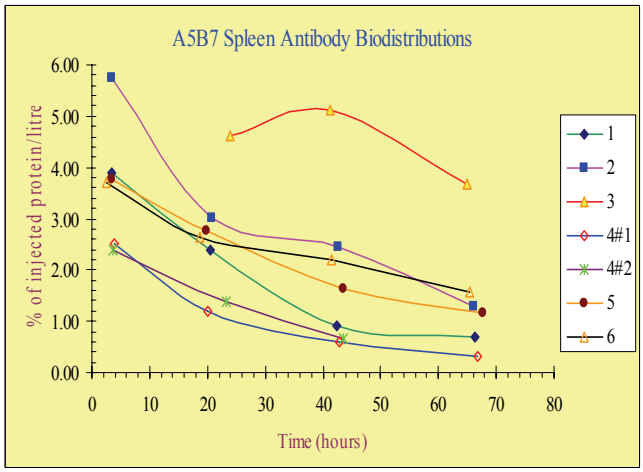

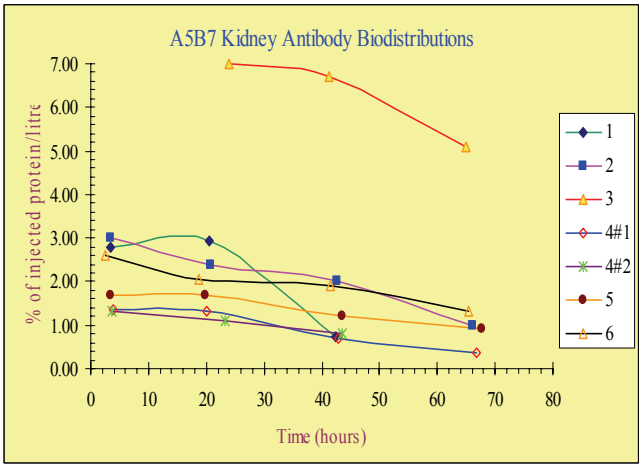

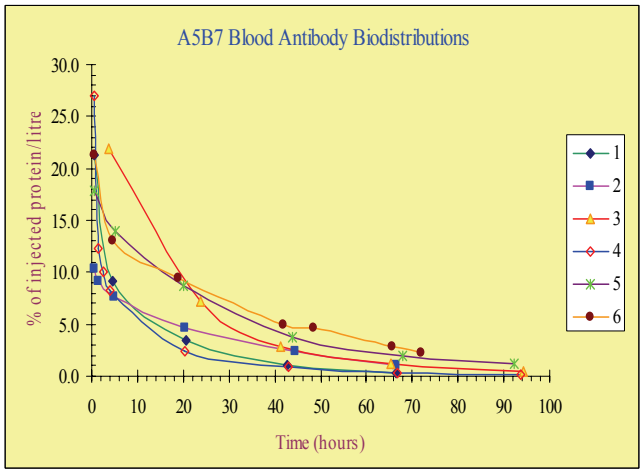

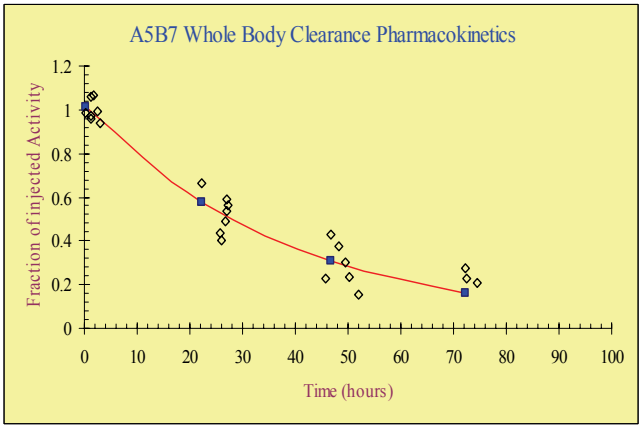

Figure 2.19 a – g - SPECT Analysis

A5B7 Organ Antibody Biodistributions. Blood clearance faster due to absorption into tissues. Note patient 3 – renal excretion delayed. Clearances as expected, with no extended antibody retention. No evidence of radioantibody trapping within tumour by CA4P

Heart A0 = 4.507 T1/2 = 36.470 Lung A0 = 1.743 T1/2 = 31.484 Liver A0 = 4.865 T1/2 = 20.020 Spleen A0 = 3.766, T1/2 = 44.750 Kidney A0 = 3.767, T1/2 = 44.750 Blood A0 = 15.865, T1/2 = 15.479 Whole Body Effective A0 = 1.02, effective t1/2 = 26.86 , Residence time = 39.51 MBq.hr Courtesy of Dr John Violet, University of London

Figure 2.20 A5B7 Tissue & Tumour Dosimetry. The normal tissue and tumour dose is presented as the decay corrected % injected dose of radioactivity/kg for 12 ^{131}I-A5B7 administrations in 11 patients (Patient 4 received 2 doses, patient 10 withdrew from study before A5B7). In all normal tissues there was a progressive fall in dose at each time point but in the tumour there is evidence of retention of radiation up to the final time point consistent with selective targeting.

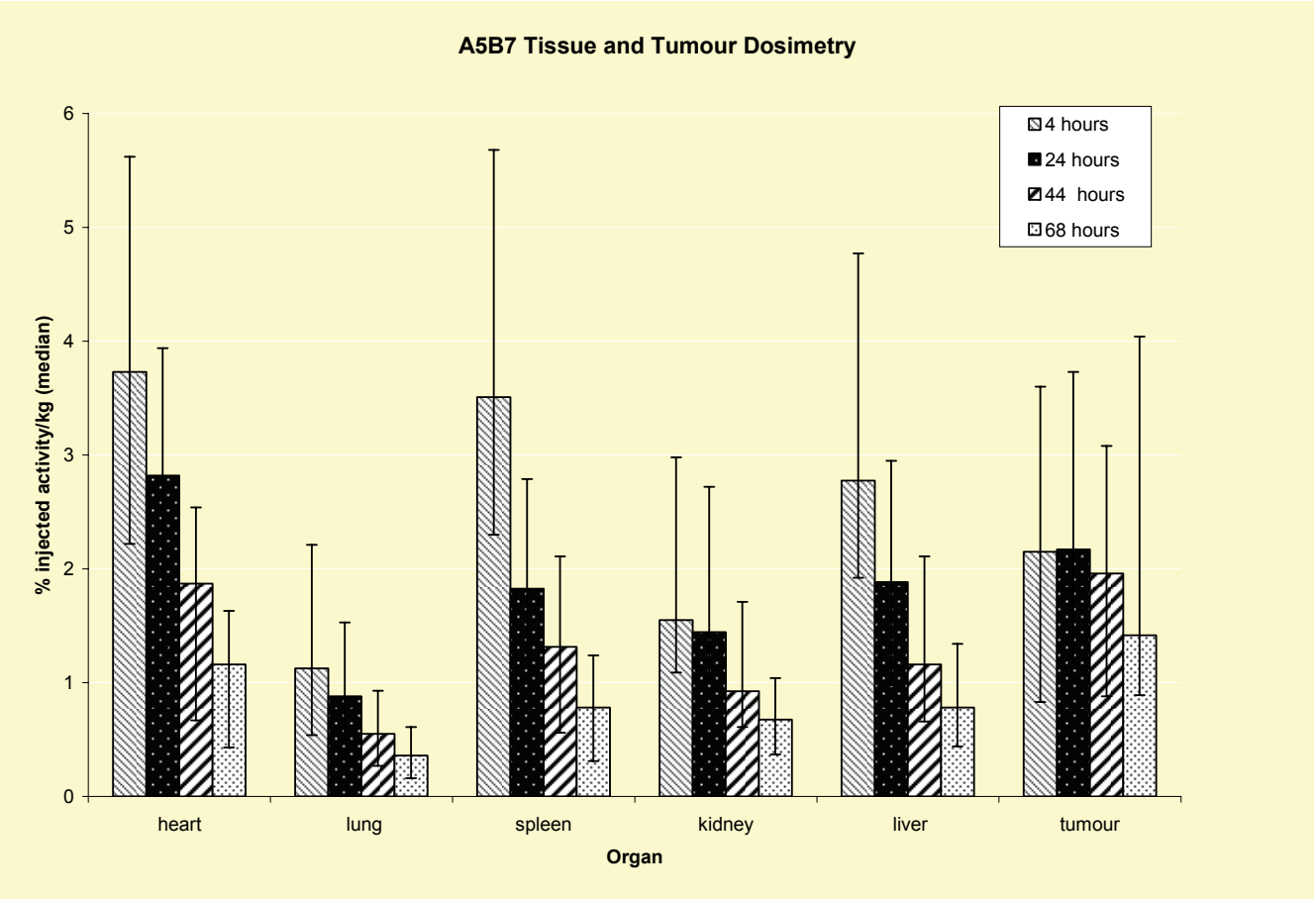

Discussion

The combination of CA4P at 54mg/m^2 with A5B7 at 1600MBq/m^2 is safe, but with dose limiting myelosuppression, and shows little indication of activity so far in heavily pretreated patients with gastrointestinal cancer (Gaya AM et al,2008). The absence of gastrointestinal mucositis (a feature of RIT associated myelosuppression) results in a significantly lower rate of sepsis following neutropenia. In Lane's study (Lane et al., 1994) the haematological toxicity seen was manageable. We calculated the starting A5B7 radiation activity of 1800MBq/m^2 25% below Lane's MTD. In previous studies of A5B7, thrombocytopenia has been dose limiting, either in single or repeated dose trials (Ledermann JA, 1991). The bone marrow suppression is most likely caused by perfusion of marrow by blood containing radiolabelled antibody, and by gamma emissions from isotope residing in neighbouring organs.

In 1994, 5-Fluorouracil was the only effective chemotherapeutic agent for metastatic colorectal cancer, given less intensively than today's combination treatment, so patients recruited had greater bone marrow reserve. Most of our patients had received intensive multiple combination chemotherapy regimens or pelvic radiotherapy (**Table 2.4**) which may explain the increased haematological toxicity. However, patients experiencing grade 4 neutropenia had not been more heavily pre-treated.

There may have been interactions between CA4P and A5B7 which caused profound myelosuppression. CA4P can delay renal clearance of drugs due to reduced renal blood flow following infusion, however this is short lived. In a study by Bilenker (Bilenker JH 2003) CA4P was given immediately prior to carboplatin chemotherapy leading to delayed renal excretion and dose limiting thrombocytopenia at what would otherwise have been a safe dose of carboplatin. In this study we administered CA4P 48h following A5B7; SPECT analysis showed uptake of A5B7 was predominantly localised to tumour and that excretion was not delayed by CA4P.

A Phase I/II study of RIT with ^{131}I-A5B7 was performed at the Royal Free Hospital in patients with CEA expressing metastatic colorectal carcinoma (Lane et al., 1994). Ten patients received RIT with ^{131}I-A5B7. Cyclosporin was administered to prevent the formation of HAMA and to allow repeated therapy. The maximum tolerated dose was established at 2400MBq/m^2 with dose limiting toxicity of thrombocytopenia and

neutropenia. Clinical responses were seen in 10% of patients. Cyclosporin was thought to be responsible for the other toxicities experienced, including nausea, vomiting and mild abnormalities in liver and renal function tests (Ledermann JA, 1991). The mean half lives for tumour & blood clearance of A5B7 were 59.5 & 28.6 hours respectively, which agree with our data. Localisation of the radiolabelled antibody to tumour was demonstrated by quantitative gamma camera imaging. One partial response was seen in a patient with a lung metastasis.

If small volume solid tumours are treated with RIT then higher response rates than those reported by Lane are seen. A Phase I/II study of patients with colorectal cancer with total tumour bulk ≤2.5cm produced a complete or partial response rate of 26% with an additional 39% patients having stabilisation of previously rapidly progressing disease for up to 18 months (Behr et al., 1999a; Behr et al., 1999b). These data suggest that, particularly in small volume disease, which has relatively little hypovascular component, RIT, alone, may be as effective as current conventional chemotherapy, with the advantage of often having fewer side-effects.

Blood pressure control was felt to be central to managing the cardiovascular effects of CA4P after the experience with patient 03. Patients with baseline hypertension were more prone to cardiovascular fluctuation, probably as a result of damaged vascular endothelium (**Chapter 6**). Aggressive hypertension management has prevented any further cardiac toxicity to date. Patient 07 experienced ataxia, a known neurological DLT of CA4P, and dose cohort A was therefore expanded to six patients. Premedication with dexamethasone before CA4P may reduce the risk of neurological DLT in addition to hypertension and allow higher CA4P doses to be administered (G Rustin, Personal Communication 2007). Whether this will reduce the effectiveness of the drug is not known. Other common toxicities of A5B7 (infusion reaction, pyrexia) and CA4P (tumour pain, fatigue, pruritis, nausea, QTc prolongation) were short lived, manageable and as previously documented (Gaya & Rustin, 2005).

The CA4P dose in the Phase I preclinical A5B7 study was 200 $mg.kg^{-1}$ (Pedley et al., 2001). The equivalent dose in humans can be estimated using either a conversion factor (Chodera & Feller, 1978) or comparison of pharmacokinetic data such as AUC for the active metabolite CA4 (Rustin et al., 2003). Either way, the human equivalent dose is ten times the mouse MTD of CA4P (Rustin et al., 2003). Clearly this dose could not be safely

administered to humans and results from the differing mammalian physiologies and intraperitoneal administration.

Indirect evidence that a clinically relevant dose of CA4P should be effective in combination with A5B7 comes from a comparison of the effect of three dose levels on tumour antibody retention (Lankester K 2004). SW1222 tumour-bearing mice received a dose of A5B7 and then either 30,100, or 200 mg.kg^{-1} intraperitoneal CA4P 48 hours later, or no further treatment in the control group. All three doses significantly increased antibody retention in tumour (increases of 71%,78% and 90% against control for 30,100 and 200 mg.kg^{-1} respectively) but not in normal tissues (Lankester, 2005; Lankester et al., 2007) and RB Pedley, Personal Communication 2004. The percentage increases were not significantly different between the three treatment groups. Although 30mg.kg^{-1} CA4P produced only a transient decrease in tumour vascular function it still increased radioantibody retention in tumour significantly. This dose however is more clinically relevant for human study. Exactly why this occurs is not known, but possibly some vessels are permanently destroyed by CA4P so antibody has less chance of escaping from tumour.

Pre-clinical efficacy studies of the combination of ^{131}I-A5B7 and CA4P were performed in a xenograft model, using the SW1222 human colon adenocarcinoma implanted in the flanks of nude mice. ^{131}I-A5B7 was administered IV at a dose of 7.4MBq (40μg antibody). 200mg/kg of CA4P was given intraperitoneally 48h after radiolabelled antibody. 5/6 mice (85%) that received the combination showed complete tumour eradication that continued to be sustained until the experiment was terminated after 9 months (Pedley et al., 2001). No viable tumour cells were subsequently found at the implantation site of the cured mice. The only tumour to regrow did so after 97 days. CA4P alone when administered to the mice had no effect on tumour growth compared to the controls, and ^{131}I-A5B7 alone produced tumour growth inhibition of approximately 35 days, but all tumours subsequently regrew (Pedley et al., 2001).

Following a meeting with the sponsor CR-UK in June 2007 the trial was suspended by consensus agreement. DLT had been reached at the first and a subsequently revised dose level. It was agreed that the treatment was tolerable with hints of activity, and that the DLT definition may need revision. It was also proposed to omit DCE-MRI from subsequent patients to increase accrual rate as proof of mechanism had been documented. A proposal was put forward to treat a total of 14 patients at dose level A as per the protocol (including five already recruited at dose level A). Due to the ataxia seen at 54mg/m^2 CA4P the

sponsor felt this dose was too high, despite data showing it to be safe and well tolerated in over 100 patients in other studies. Dexamethasone pre-medication has also been shown to reduce the incidence of ataxia and other neurological side effects of CA4P (G Rustin, personal communication, 2007). It was felt a CA4P dose lower than this was unlikely to be clinically active and a decision was made by the sponsor and chief investigators to close the study.

The A5B7/CA4P combination may be optimised further and explored as more effective and less toxic therapy with certain refinements. A humanized form of the antibody, allowing repeated smaller doses (<1600MBq/m^2), could be used in less heavily pretreated patients with smaller metastases which would maximize the ^{131}I call kill. The performance of our radioantibody, as illustrated in **figure 2.20**, was variable. There are theoretical dosimetric advantages to using ^{90}Yttrium labeled antibody, including stronger binding, which may enhance the effectiveness of the combination. Combining the RIT with an alternative VDA such as OXi4503, ten times more potent, may also improve the therapeutic ratio. Our patient population was relatively frail and heavily pretreated. The combination may have a greater chance of success in 1st line metastatic colorectal cancer.

Conclusions (Gaya et al., 2008)

1) The combination of CA4P at 54mg/m^2 with A5B7 at 1600MBq/m^2 has dose limiting myelosuppression in the absence of gastrointestinal mucositis in this patient cohort..
2) The cardiovascular effects of CA4P can be controlled by careful patient selection and aggressive management of hypertension.
3) The combination shows little activity in heavily pretreated patients with gastrointestinal cancer. Out of twelve patients, one short lived case of stable disease and a minor response was seen.
4) Toxicity was manageable. Most SAE's were not drug related, and there were no unexpected or new toxicities with the combination therapy.
5) Pharmacokinetic and SPECT studies of CA4P and A5B7 are similar to previous single agent studies, and confirm no evidence of antibody retention at these doses.
6) There is no evidence of A5B7 trapping within tumour.
7) DCE-MRI confirmed CA4P vascular shutdown in patients at 45 and 54 mg/m^2 (**Chapter 3**).

8) MTD was not determined due to closure of the study following dose limiting myelosuppression.
9) The dose for further study would currently be 1600MBq/m^2 A5B7 and 54mg/m^2 CA4P.
10) Due to limitations in the design of the study it is not certain that the objectives have definitely been met, hence the suggestions for further study. Alternative study designs have been discussed.

References

Adam, T. (1989). Radioiodination for therapy. *Ann Clin Biochem*, **26 (Pt 3),** 244-5.

Behr, T.M., Memtsoudis, S., Vougioukas, V., Liersch, T., Gratz, S., Schmidt, F., Lorf, T., Post, S., Wormann, B., Hiddemann, W., Ringe, B. & Becker, W. (1999a). Radioimmunotherapy of colorectal cancer in small volume disease and in an adjuvant setting: preclinical evaluation in comparison to equitoxic chemotherapy and initial results of an ongoing phase-I/II clinical trial. *Anticancer Res*, **19,** 2427-32.

Behr, T.M., Salib, A.L., Liersch, T., Behe, M., Angerstein, C., Blumenthal, R.D., Fayyazi, A., Sharkey, R.M., Ringe, B., Becker, H., Wormann, B., Hiddemann, W., Goldenberg, D.M. & Becker, W. (1999b). Radioimmunotherapy of small volume disease of colorectal cancer metastatic to the liver: preclinical evaluation in comparison to standard chemotherapy and initial results of a phase I clinical study. *Clin Cancer Res*, **5,** 3232s-3242s.

Bilenker JH , S.J., Rosen MA , Gallagher M , Flaherty KT , Algazy K , Sun W , Schnall M , O'Dwyer PJ. (2003). Phase Ib trial of combretastatin A4 Phosphate (CA4P) in combination with carboplatin in patients with advanced cancer. *Proc Am Soc Clin Oncol*, **22,** Abstract 889.

Chaplin, D.J., Pettit, G.R., Parkins, C.S. & Hill, S.A. (1996). Antivascular approaches to solid tumour therapy: evaluation of tubulin binding agents. *Br J Cancer Suppl*, **27,** S86-8.

Chodera, A. & Feller, K. (1978). Some Aspects Of Pharmacokinetic And Biotransformation Differences In Humans And Mammal Animals. *Int J Clin Pharmacol Biopharm*, **16,** 357 - 360.

Dark, G.G., Hill, S.A., Prise, V.E., Tozer, G.M., Pettit, G.R. & Chaplin, D.J. (1997). Combretastatin A-4, an agent that displays potent and selective toxicity toward tumor vasculature. *Cancer Res*, **57,** 1829-34.

Dowlati, A., Robertson, K., Cooney, M., Petros, W.P., Stratford, M., Jesberger, J., Rafie, N., Overmoyer, B., Makkar, V., Stambler, B., Taylor, A., Waas, J., Lewin, J.S., McCrae, K.R. & Remick, S.C. (2002). A phase I pharmacokinetic and translational study of the novel vascular targeting agent combretastatin a-4 phosphate on a single-dose intravenous schedule in patients with advanced cancer. *Cancer Res*, **62,** 3408-16.

Flynn AA, G.A., Boxer GM, Casey JL, Pedley RB, Begent RHJ. (1999). The Measurement Of Uniformity Of Radiolabelled AnA Novel Technique Using Radioluminography, For tibody Distribution In A Colorectal Cancer Xenograft Model. *International Journal of Radiation Oncology Biology And Physics*, **43,** 183 - 189.

Galbraith, S.M., Maxwell, R.J., Lodge, M.A., Tozer, G.M., Wilson, J., Taylor, N.J., Stirling, J.J., Sena, L., Padhani, A.R. & Rustin, G.J. (2003). Combretastatin A4 phosphate has tumor antivascular activity in rat and man as demonstrated by dynamic magnetic resonance imaging. *J Clin Oncol*, **21,** 2831-42.

Gaya, A., Dancey, G., Stratford, M., Othman, S., Ricamara, M., Sharma, S., Boxall, J., Poupard, L., Violet, J., Green, A., Padhani, A., Rustin, G.J., Begent, R. & Meyer, T. (2008). A Phase I/II Trial of Radioimmunotherapy (RIT) with 131Iodine-Labelled A5B7 Anti-CEA Antibody (131I-A5B7) in Combination with Combretastatin-A4-Phosphate (CA4P) In Advanced Gastrointestinal Carcinomas'. *J Clin Oncol*, **26,** abstract 14517.

Gaya, A.M. & Rustin, G.J. (2005). Vascular disrupting agents: a new class of drug in cancer therapy. *Clin Oncol (R Coll Radiol)*, **17,** 277-90.

Harwood, P.J., Britton, D.W., Southall, P.J., Boxer, G.M., Rawlins, G. & Rogers, G.T. (1986). Mapping epitope characteristics on carcinoembryonic antigen. *Br J Cancer*, **54,** 75-82.

Lane, D., Eagle , K., Begent, R., Hope-Stone, L., Green, A., Casey, J., Keep, P., Kelly, A., Ledermann, J., Glaser, M. & Hilson, A.J. (1994). Radioimmunotherapy Of Metastatic Colorectal Tumours With Iodine-131 Labelled Antibody To Carcinoembryonic Antigen : Phase I/II Study With Comparative Biodistribution Of Intact And F(ab)2 Antibodies. *Br J Cancer*, **70,** 521 - 525.

Lankester, K. (2005). Magnetic Resonance Imaging And The Development Of Vascular Targeted Treatments For Cancer. In *Gray Cancer Institute, Northwood, Middlesex, UK* pp. pp31. University of London, Faculty of Oncology: London.

Lankester K , P.B. (2004). Acute Anti Vascular Effects Of Combretastatin A4 Phosphate (CA4P) On The SW1222 Tumour As Measured By Dynamic Contrast Enhanced MRI (DCE-MRI). Abstract.

Lankester, K.J., Maxwell, R.J., Pedley, R.B., Dearling, J.L., Qureshi, U.A., El-Emir, E., Hill, S.A. & Tozer, G.M. (2007). Combretastatin A-4-phosphate effectively increases tumor retention of the therapeutic antibody, 131I-A5B7, even at doses that are sub-optimal for vascular shut-down. *Int J Oncol*, **30,** 453-60.

Ledermann, J.A., Begent, R.H., Bagshawe, K.D., Riggs, S.J., Searle, F., Glaser, M.G., Green, A.J. & Dale, R.G. (1988). Repeated antitumour antibody therapy in man with suppression of the host response by cyclosporin A. *Br J Cancer*, **58,** 654-7.

Ledermann JA, B.R., Massof C, Kelly AMB, Adam T, Bagshawe KD. (1991). A Phase I Study Of Repeated Therapy With Radiolabelled Antibody To Carcinoembryonic Antigen Using Intermittent Or Continuous Administration Of Cyclosporin A To Suppress The Immune Response. *Int. J. Cancer*, **47,** 659 - 664.

Lenz, H.J. (2007). Management and preparedness for infusion and hypersensitivity reactions. *Oncologist*, **12,** 601-9.

Pedley, R.B., Boden JA, Keep PA, Harwood PJ, Green AJ, Rogers GT. (1987). Relationship Between Tumour Size & Uptake Of Radiolabelled Anti-CEA Antibody In A Colon Tumour Xenograft. *Eur J Nucl Med*, **13,** 197 - 202.

Pedley, R.B., Hill, S.A., Boxer, G.M., Flynn, A.A., Boden, R., Watson, R., Dearling, J., Chaplin, D.J. & Begent, R.H. (2001). Eradication of colorectal xenografts by combined radioimmunotherapy and combretastatin a-4 3-O-phosphate. *Cancer Res*, **61,** 4716-22.

Rustin, G.J., Galbraith, S.M., Anderson, H., Stratford, M., Folkes, L.K., Sena, L., Gumbrell, L. & Price, P.M. (2003). Phase I clinical trial of weekly combretastatin A4 phosphate: clinical and pharmacokinetic results. *J Clin Oncol*, **21,** 2815-22.

Stevenson, J.P., Rosen, M., Sun, W., Gallagher, M., Haller, D.G., Vaughn, D., Giantonio, B., Zimmer, R., Petros, W.P., Stratford, M., Chaplin, D., Young, S.L., Schnall, M. & O'Dwyer, P.J. (2003). Phase I trial of the antivascular agent combretastatin A4 phosphate on a 5-day schedule to patients with cancer: magnetic resonance imaging evidence for altered tumor blood flow. *J Clin Oncol*, **21,** 4428-38.

Stratford, M.R. & Dennis, M.F. (1999). Determination of combretastatin A-4 and its phosphate ester pro-drug in plasma by high-performance liquid chromatography. *J Chromatogr B Biomed Sci Appl*, **721,** 77-85.

Therasse, P., Arbuck, S.G., Eisenhauer, E.A., Wanders, J., Kaplan, R.S., Rubinstein, L., Verweij, J., Van Glabbeke, M., van Oosterom, A.T., Christian, M.C. & Gwyther, S.G. (2000). New guidelines to evaluate the response to treatment in solid tumors. European Organization for Research and Treatment of Cancer, National Cancer Institute of the United States, National Cancer Institute of Canada. *J Natl Cancer Inst*, **92,** 205-16.

Chapter 3
Variability of DCE-MRI Response Between Patients and Between Lesions Following Infusion of CA4P

Abstract

Tumour blood flow is reduced after treatment with CA4P. We evaluated the heterogeneity of blood flow related DCE-MRI parameters between different patients and in lesions within patients. DCE-MRI measurements were performed before and four hours following CA4P alone on 12 patients in the A5B7 study. Measurement errors were estimated for patients (n=12) and their lesions (n=30), and changes in vascular kinetic variables after CA4P were documented. Statistically significant falls in tumour K^{trans} values were seen (mean -25.1%; range +63.5 to -100%; paired t-test 0.011). At baseline there was greater variability in K^{trans} between-patients compared to between-tumours[within-patients] (ratio 1.93). The variability in K^{trans} changes induced by CA4P was also greater between-patients than between-tumours[within-patients] (ratio 2.37). In conclusion, metastatic lesions within-patients are more similar compared to between-patients in DCE-MRI kinetic parameters both at baseline and in their response to CA4P. There were greater reductions in kinetic parameters at 54mg/m^2 CA4P versus 45mg/m^2 consistent with a threshold dose effect.

Introduction

T_1-weighted DCE-MRI has been used to investigate the acute effects of CA4P in phase I studies which use change in kinetic variables as biomarkers for the anti-vascular effects of CA4P (Dowlati et al.,2002; Galbraith et al.,2003; Stevenson et al.,2003). DCE-MRI studies have also been used to evaluate antiangiogenic drugs (O'Connor et al., 2007). DCE-MRI studies can define the biologically active dose and predict the efficacy of treatment on the basis of changes observed (Dowlati et al.,2002; Galbraith et al.,2003; Padhani,2003; Stevenson et al.,2003). Without exception, in all prior DCE-MRI phase I studies, single lesions were chosen for analysis on the implicit assumption that responses of chosen lesions would be representative of responses in all lesions within the same patient. Between-patient and intratumoural heterogeneity in DCE-MRI responses to CA4P are documented in these studies but the assumption of similarity at baseline and of responses of lesions within individual patients has not been formally investigated.

Methods

Patients and Therapy

Following ethics board approval we performed DCE-MRI scans on 12 patients taking part in a CR-UK sponsored Phase I trial of CA4P in combination with ^{131}I (A5B7) anti-CEA antibody in advanced gastrointestinal cancer (Study PH1/092 – **Chapter 2**). All patients gave written informed consent.

MRI procedures

MRI was performed on a 1.5 tesla Magnetom Symphony scanner (Siemens Medical Systems, Erlangen, Germany), using body coils. Scans were performed 48h (R1) and 24h (R2) before infusion of CA4P to obtain repeatability data, and a third scan 4h following CA4P (Rx1) to assess anti-vascular effects. At the start of each procedure T1 and T2-weighted anatomical images were performed in two orthogonal planes to select three suitable contiguous slices through the centre(s) of tumour(s). An experienced radiographer used bony landmarks and images from previous examinations to minimize positioning errors from day to day.

1) MRI data acquisition

1. Proton density-weighted (PD) images were acquired in the chosen plane and used with subsequent T1-weighted images to calculate T1-relaxation rates in the dynamic series. Parameters for the PD spoiled gradient-recalled echo (GRE) FLASH sequence were: FOV 350*350 mm, acquisition matrix 256*154 pixels reconstructed to 256^2, slice thickness 8mm, number of slices 3, TR 350ms, TE 4.76ms, α 20°, TA 4.29s, 5 signal averages, total time 21.5s.

2. The dynamic series consisted of 40 navigator-guided T1-weighted GRE FLASH images. Parameters were: FOV 350*350 mm, acquisition matrix 256*154 pixels reconstructed to 256^2, slice thickness 8mm, number of slices 3 acquired sequentially, TR 43ms, TE 4.76ms, α 50°, TA (one scan) 6s with 5s for breathing. Gadopentetate dimeglumine (Gd-DTPA, Magnevist®, Bayer-Schering Pharma, Newbury, UK) was the contrast agent used, injected intravenously using an automatic power injector ($0.1 mmol \cdot kg^{-1}$) at $4 ml \cdot s^{-1}$ initiated at the start of the fifth acquisition. Contrast medium was administered through an identically-sized cannula on each day. When imaging liver metastases, patients were required to breath-hold at the end of passive expiration during each dynamic acquisition, following instruction of a radiographer via an intercom system. System measurement gain and scaling factors were maintained between acquisition of the PD and T1-weighted dynamic series, to enable calculation of changing tissue T1-relaxivities and contrast agent concentrations at each time point of the dynamic acquisition (Parker et al., 1997).

2) Dynamic MRI analysis

We used Magnetic Resonance Imaging Workbench software (MRIW) for DCE-MRI analysis (Institute of Cancer Research, UK (d'Arcy, 2006)). Using information from anatomical and post-contrast T_1-weighted images, ROIs were drawn around tumour edges on all three scan slices by a radiologist who carefully excluded areas of artefact, necrosis, blood vessels and normal tissues. Metastases >2cm diameter with no partial volume averaging were chosen and up to five metastases per organ were analysed. Similar ROIs were used for all MR examinations in an individual patient, all of which were drawn at the same session to minimise intra-observer variability in ROI placement (Beresford et al., 2006). A control ROI was also drawn within skeletal muscle on the

central slice. MRIW software converts signal intensities of T_1-weighted DCE-MRI datasets into T_1-relaxation rates and then into Gd-DTPA concentrations for individual pixels at each of the 40 time points (Parker et al., 1997).

$IAUGC_{60}$ (Initial Area Under the Gadolinium Concentration time curve) was calculated over the first 60s from the onset of signal increase following injection of contrast (units: $mmol \cdot s^{-1}$). The changing tissue Gd-DTPA curve was fitted to a standard compartmental model (Kety, 1960; Tofts, 1997) to characterise the influx of Gd-DTPA into the tumour extracellular extravascular space (EES) and its venous efflux. Pixel-by-pixel values of transfer constant (K^{trans} - units min^{-1}), rate constant (k_{ep} - units min^{-1}) and leakage space (v_e - units %) were calculated. A literature-based pooled arterial input function (combined Fritz-Hansen/Weinmann) was used for the modelling (Walker-Samuel et al., 2006).

Using Microsoft Excel, the ROI pixel data was sorted. For tumour ROIs, pixels from all three scan slices were combined for analysis. Enhancing pixels which failed the modelling process (e.g. $K^{trans}>5$) were excluded, mainly due to non-physiological leakage space (v_e) estimates of >90%. Non-enhancing voxels (e.g. $K^{trans}=0$ or $IAUGC_{60}=0$) were retained to calculate median kinetic parameter estimates for each lesion evaluated. $IAUGC_{60}$ estimates did include enhancing pixels that failed the modelling process (i.e. not negative or zero values), **Table 3.1**. Pixel data from all slices per lesion were combined and median values were taken as representative of central tendency because histogram distributions of some kinetic parameters were skewed. The quality of the fit of the raw DCE-MRI data to the model functions is demonstrated in **figure 3.1**

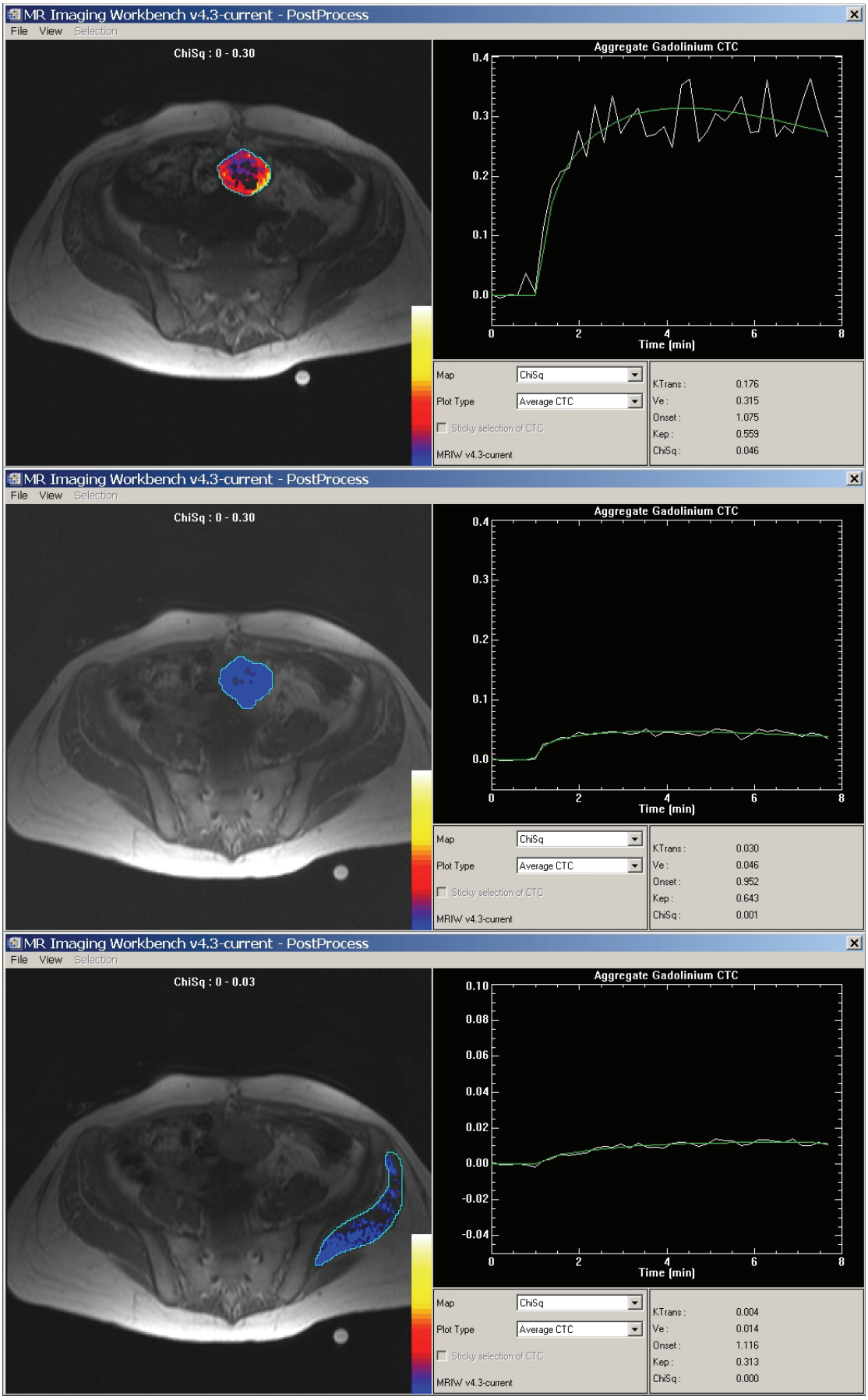

Figure 3.1 – Example of the quality of fit of the raw DCE-MRI data to model function. Patient 06 – Top screen dump day1, middle is 4 hours post CA4P and bottom screen dump shows muscle control data. The estimated parameters are given on screen with the Chi Square value showing the fit to the modelling function. The nearer to zero, the better the fit.

Table 3.1 – Tumour ROI Data Analysis – Proportion of non-enhancing pixels and modelling failures within ROIs. Data shown for patients 1 – 7.

Three Slices Through Tumour ROI – Combined Pixels								
Patient & Day	**Total Pixels in ROI (A)**	**$IAUGC_{60}$ = 0 (B)[1] (Non Enhancing)**	**$IAUGC_{60}$ = 0 & K^{trans} = 0[2]**	**$K^{trans} > 5$[3] (modelling failures)**	**$K^{trans} = 0$[4] (non enhancing)**	**Enhancing Pixels A-B**	**K^{trans} 0.01 – 5.005**	**K^{trans} 1.20 – 5.006**
01 R1	10679	13	8	863	7564	10666	2252	1469
01 R2	11075	61	58	1112	6606	11014	3296	2310
01 Rx1	11007	3	3	1054	6972	11004	2978	2391
02 R1	653*	14	14	16	255	639	368	139
02 R2	525*	1	1	24	216	524	284	121
02 Rx1	351*	0	0	88	53	351	210	121
03 R1	2630	2	2	411	173	2628	2044	1199
03 R2	2679	0	0	339	153	2679	2187	1396
03 Rx1	2744	10	1	18	41	2734	2675	1324
04 R1	4843	230	228	5	988	4613	3620	377
04 R2	4933	1481	1257	0	784	3452	2668	122
04 Rx1	4873	913	793	0	967	3960	2993	65
05 R1	2150	101	89	310	232	2049	1507	442
05 R2	1665	130	115	2	193	1535	1340	283
05 Rx1	1799	90	81	7	364	1709	1338	114
06 R1	2006	23	23	15	513	1983	1455	195
06 R2	1684	25	19	22	244	1659	1393	249
06 Rx1	1728	25	21	43	76	1703	1584	362
07 R1	1747	140	140	27	1492	1607	88	58
07 R2	1780	100	100	47	1504	1680	129	102
07 Rx1	1469	29	28	1	873	1440	566	28

1 – Non Enhancing Pixel Modelling Failures, 2 – Subgroup of 1 above, 3 – Enhancing Pixel Modelling Failures (high) 4 – Enhancing Pixel Modelling Failures (low), 5 – Enhancing Pixels Modelling OK Kt 0.01 – 5.00, 6 – Enhancing Pixels Modelling OK Kt 1.20 – 5.00 * - Slices 2 & 3 only suitable for analysis, Rx1 Slices 1 & 3

3) DCE-MRI Repeatability & Variance Components Analysis

The analysis was carried out on 30 tumours from 12 patients (**Table 3.2**) with the number of tumours per patient ranging from 1-5. The DCE-MRI data consisted of four kinetic parameters (K^{trans}, v_e, k_{ep} and $IAUGC_{60}$) in multiple lesions (1-5) per patient taken at three time points (R1, R2 and Rx1). For these data, the parameter values for each tumour cannot be treated as independent samples, as the behaviour of tumours within-patients share biological environments that are common. That is we expect some correlation between tumours within a particular patient both on baseline studies (R1, R2) and in therapy responses (Rx1). Bland and Altman's variance-components methods (Bland & Altman, 1996a; Bland & Altman, 1996b; Galbraith et al., 2002) were extended

to take into account the clustering of tumours within patients according to methods described by Rabe-Hesketh & Skrondal (Rabe-Hesketh & Skrondal, 2005). All statistical tests were two-tailed and p values ≤0.05 were considered significant.

Table 3.2 – Details of 30 metastatic lesions from 12 patients.

Patient ID	Age/ Sex	Primary tumour site and histology	CA4P Dose (mg/m²)	Lesion No.	Lesion size (cm)	Metastatic Lesion location
01	59F	Rectal adenocarcinoma	45	1	10.9	Liver - Left
				2	3.65	Liver - Right
				3	3.92	
02	72F	Caecal adenocarcinoma		1	3.5	
03	57F	Sigmoid adenocarcinoma		1	5.2	Liver - Right
				2	4.2	
				3	4.2	
				4	2.2	
				5	2.4	Liver - Left
04	65M	Sigmoid adenocarcinoma		1	7.8	Liver - Right
				2	6.5	
				3	8.1	
				4	7.8	
				5	5.7	
05	70M	Ascending colon adenocarcinoma		1	4.6	Liver - Right
06	32F	Caecal adenocarcinoma		1	4.6	Pelvic - peritoneal mass
07	72M	Rectal adenocarcinoma	54	1	4.5	Liver - Right
08	77M	Rectal adenocarcinoma		1	4.9	Liver - Right
				2	5.6	
				3	2.3	Liver - Left
				4	4.5	Liver - Right
09	66F	Pancreatic adenocarcinoma		1	4.2	Liver - Right
10	61M	Rectal adenocarcinoma		1	4.6	Liver - Right
				2	2.7	
				3	2.8	
11	58M	Colorectal adenocarcinoma		1	4.1	Liver - Left
				2	2.7	Liver - Right
				3	4.1	
12	63M	Rectal adenocarcinoma		1	7.9	Retroperitoneal node
				2	3.6	Bone

a) Repeatability of parameter measurements

This analysis estimated the variation between repeated measurements for the same tumour within each patient. That is, how far from the true value a single measurement was likely to be. The value depends on the quantity being measured, and the "between-tumours[within-patients]" variability is estimated as if it were the same for all. The standard-deviation of repeated measurements was obtained, and we would expect 68% of observations to fall within one standard deviation and 95% within 1.96 standard deviations from the true value. For this data a linear mixed model was used, designed for fitting random coefficients and multilevel models. Within the model, patients were treated as the grouping factor. This model allowed estimations of the between-patient variance and between-tumours[within-patients] variance to derive estimates of repeatability at the tumour level using pre-treatment parameter values. Estimation of variance components was derived using *xtmixed* in STATA version 9.2 (StataCorp LP, College Station, USA).

For both between-patient and between-tumours[within-patients] analyses, kinetic parameter values are expressed as means, standard deviations and interclass correlation coefficients (ICCs). The ICC is the average correlation coefficient across all possible orderings of the data when there is no obvious choice of X and Y axis for each of the pairs of measurements. The repeatability statistic (r) (also expressed as a percentage change (r%) is the threshold value below which the absolute difference between two measurements on the same patient/tumour (n=1) is expected to lie for 95% of paired observations (95% limits of agreement). From this, one can calculate for any number of patients/tumours the threshold value needed for a parameter to change at the 95% confidence level; that is, a real change rather than simply being due to measurement variability.

b) Estimates of variance components due to treatment effect

We also sought to demonstrate that the behaviour of tumours within a patient following CA4P are more highly correlated than the behaviour observed between different patients' tumours. We used a three-level model, adding a fixed treatment effect to the three-level model used for the repeatability analysis. The fixed treatment effect was nested within patients, and we used a similar linear mixed model (as above) to evaluate the data.

Results

1) Baseline variability and repeatability assessments

The baseline variability analyses for the four kinetic parameters for both between-patient and between-tumours[within-patients] analyses are given in **Table 3.3**. For the kinetic parameters K^{trans}, v_e and $IAUGC_{60}$, baseline values were more similar between-tumours[within-patients] than between-patient. This is illustrated in **Figure 3.2** where the baseline variability of the kinetic parameters K^{trans} and $IAUGC_{60}$ for the two repeatability examinations (R1 and R2) is illustrated. For the k_{ep} parameter, variability between-patient was similar to between-tumours[within-patients] (sd ratio = 1.05).

Table 3.3 - Estimates of between patient and between tumour variability and repeatability (N=12, observations=60). The analysis has allowed for a clustering of tumours within patients on each tumour measurement. Produced with David Wellsted & Sue Cliffe, University of Hertfordshire biostatistics Dept.

	Kinetic parameter			
	K^{trans}	**v_e**	**k_{ep}**	**$IAUGC_{60}$**
Patients (tumours)	12 (29)	12 (29)	12 (29)	12 (30)
Mean (tumours)	0.395 min^{-1}	0.416	0.938 min^{-1}	22.88 $mmol \cdot s^{-1}$
Variability				
sd (between-patient)	0.185	0.153	0.274	15.129
sd (between-tumours[within patients])	0.096	0.043	0.261	4.124
sd (error)	0.105	0.064	0.228	4.534
sd ratio (between-patients/between-tumours[within patients])	1.93	3.56	1.05	3.67
Repeatability (tumours)				
r	0.29 min^{-1}	0.18	0.63 min^{-1}	12.56 $mmol \cdot s^{-1}$
r%	73.6	42.6	67.3	54.9
CV	0.27	0.15	0.24	0.20
ICC	0.64	0.71	0.55	0.77

Figure 3.2 – Range and Repeatability for the Primary Endpoints K^{trans} and $IAUGC_{60}$. Patient ID on X-axis. Baseline values on the two repeatability examinations (R1 and R2) are more similar between-tumours[within-patients] than between-patients. Patients 11 & 12 had marked motion artefacts at one or more examinations.

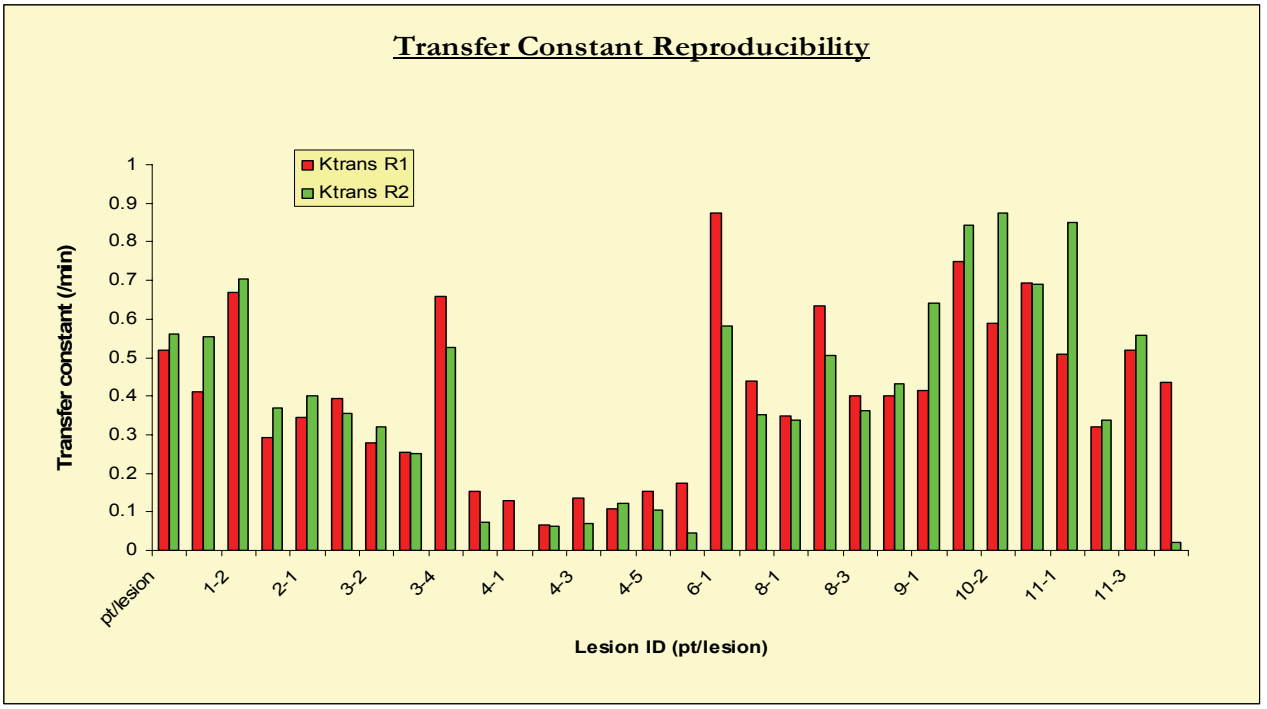

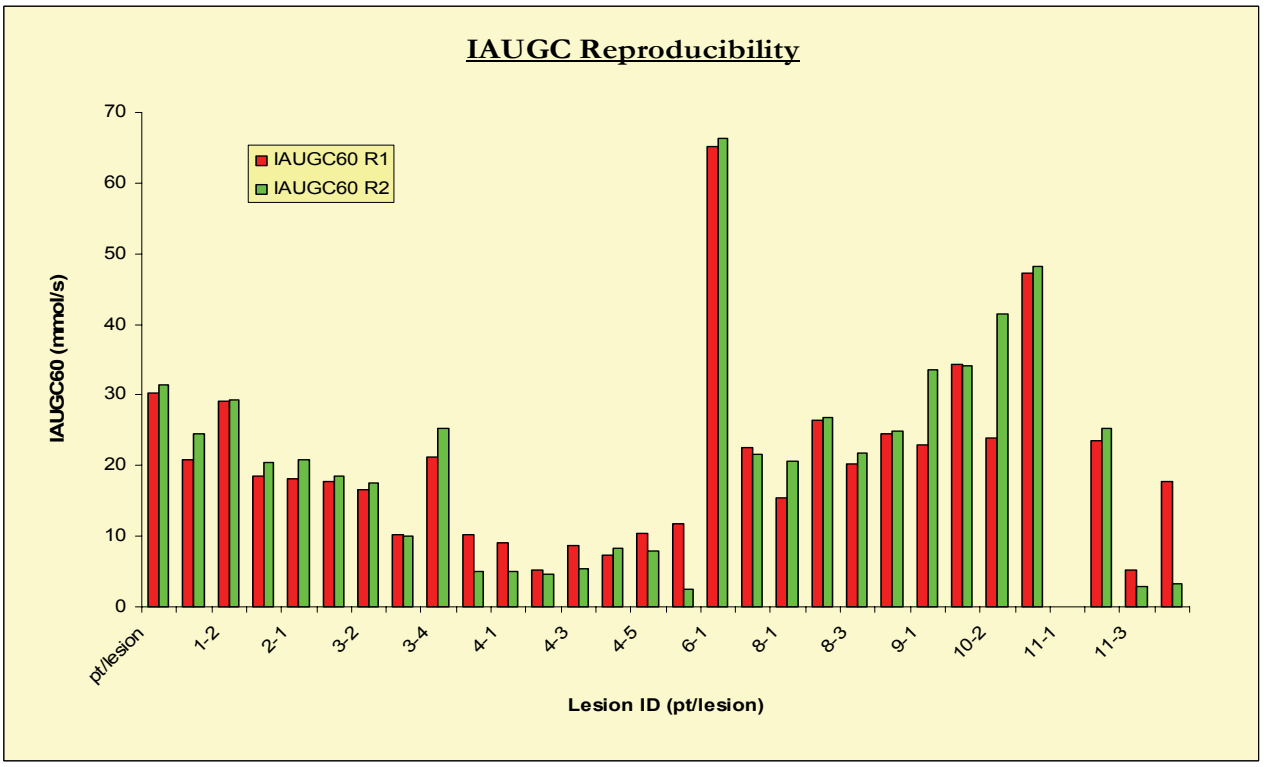

2) Response to therapy assessments

Reductions in enhancement within the lesion centre were observed visually in 9/30 tumours using parametric maps. Representative images for patient 03 are illustrated in **Figure 3.3**.

Treatment-induced changes in DCE-MRI kinetic parameters are given in **Table 3.4**. The mean values of the first and second repeatability examinations were taken to represent tumour baseline values against which to assess changes induced on the post-CA4P examination (Rx1). Highly statistically significant reductions were found in the kinetic parameters K^{trans}, k_{ep} and v_e (n=29). $IAUGC_{60}$ changes (n=30) only just reached significance because of one outlier point (patient 11, lesion 2 had marked lesion movement).

Comparisons of variability due to treatment (between-patients and between tumours[within-patients]) are also given in **Table 3.4**. For the kinetic parameters K^{trans}, v_e and $IAUGC_{60}$, therapy-induced changes are more similar between-tumours[within-patients] than between-patients (sd ratios >1). This is illustrated in **Figure 3.4** where the variabilities of response for the kinetic parameters K^{trans} and $IAUGC_{60}$ are shown. For the k_{ep} parameter, variability between patients was similar to between-tumours[within-patients] after therapy (sd ratio 1.23).

As an example, For K^{trans} lower 95% CI limit was -19% fall. 8/12 patients or 17/29 tumours had significant or borderline reductions at four hours. (**Figure 3.4)**

Figure 3.3 – Patient 03 Discrepancy Between Visual and Quantitative Analysis

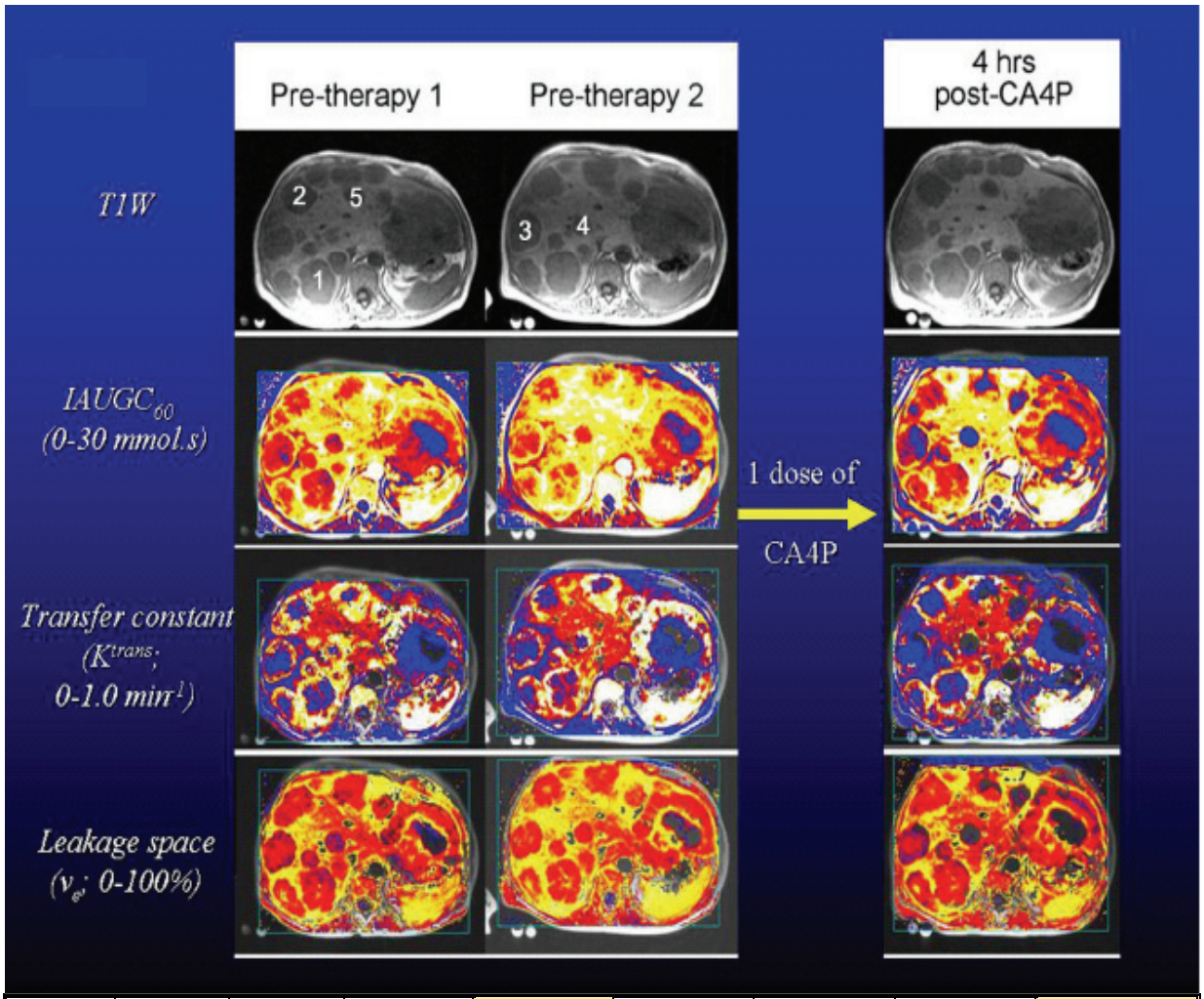

Lesion ID	K^{trans} d1	K^{trans} d2	K^{trans} d3	% Change	$IAUGC_{60}$ d1	$IAUGC_{60}$ d2	$IAUGC_{60}$ d3	% Change
03-01	0.346	0.3995	0.31275	-16.1	18.14	20.85	17.47	-10.39
03-02	0.393	0.3556	0.3043	-18.7	17.83	18.45	15.1	-16.74
03-03	0.2798	0.3198	0.2089	-30.3	16.52	17.62	11.6	-32.02
03-04	0.2528	0.25065	0.1361	-45.9	10.25	10.05	7.49	-26.15
03-05	0.65865	0.5252	0.48755	-17.6	21.18	25.22	20.91	-9.87

Rapid reduction in kinetic variables within tumour induced by CA4P at 45mg/m^2. Columns represent serial examinations acquired before treatment (48h and 24h before CA4P to assess baseline variability) and 4h after the first infusion. Rows show anatomical T1-weighted images (top row), maps of $IAUGC_{60}$ (2nd row), inflow transfer constant (K^{trans}; third row) and extra cellular leakage space EES (v_e; bottom row) acquired at the 3 imaging time points. Reduction in kinetic variables is observed as darker colours on $IAUGC_{60}$ and K^{trans} maps with the absence of morphological change. Note that there is little change in the leakage space (v_e) Note marked inter- and intratumoural heterogeneity with greatest anti-vascular effects within the centre of some lesions only. The changes visible on images are not necessarily reflected in the changes in quantitative parameter estimates in the table. Units of K^{trans} are min^{-1}

Figure 3.4 – Change in Primary Endpoints K^{trans} and $IAUGC_{60}$ following CA4P – Only values crossing the lower 95% CI line (marked on graph) are statistically and clinically significant (-19%), however there are widespread falls in variables in most patients following CA4P. Note also the greater falls in variables at 54mg/m² CA4P (patients 7 – 12) compared with 45mg/m² (patients 1-6). Patients 11,12 – Severe motion artefact. Patient ID and lesion number listed (e.g. 1-1 is patient 01, lesion 01)

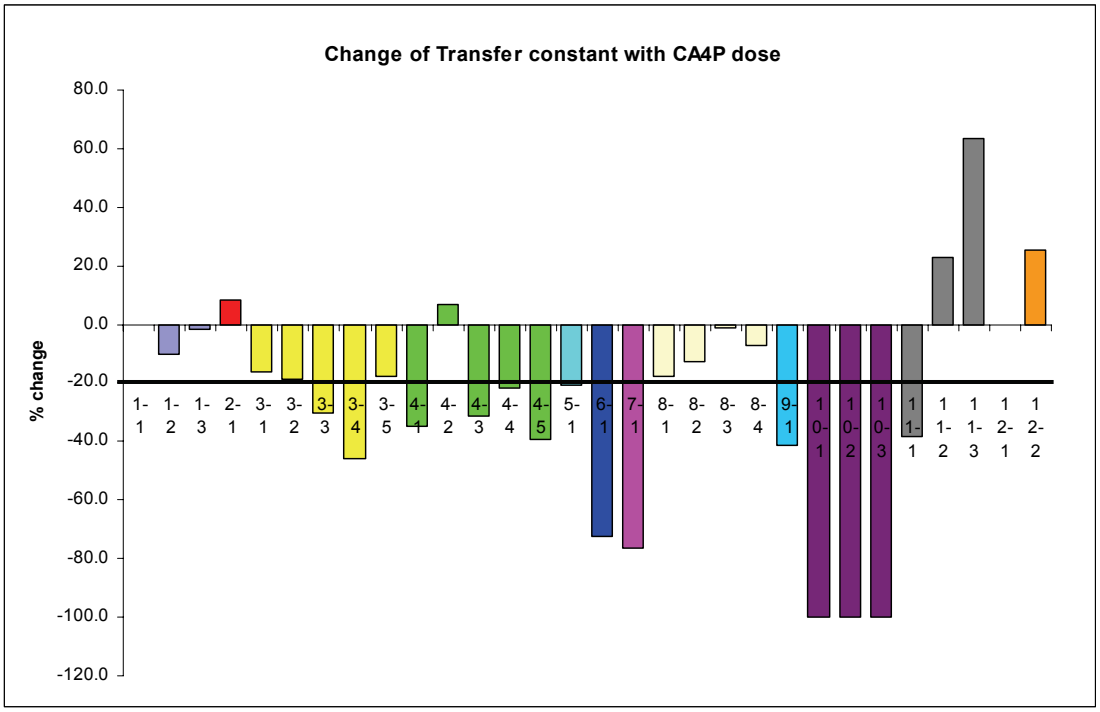

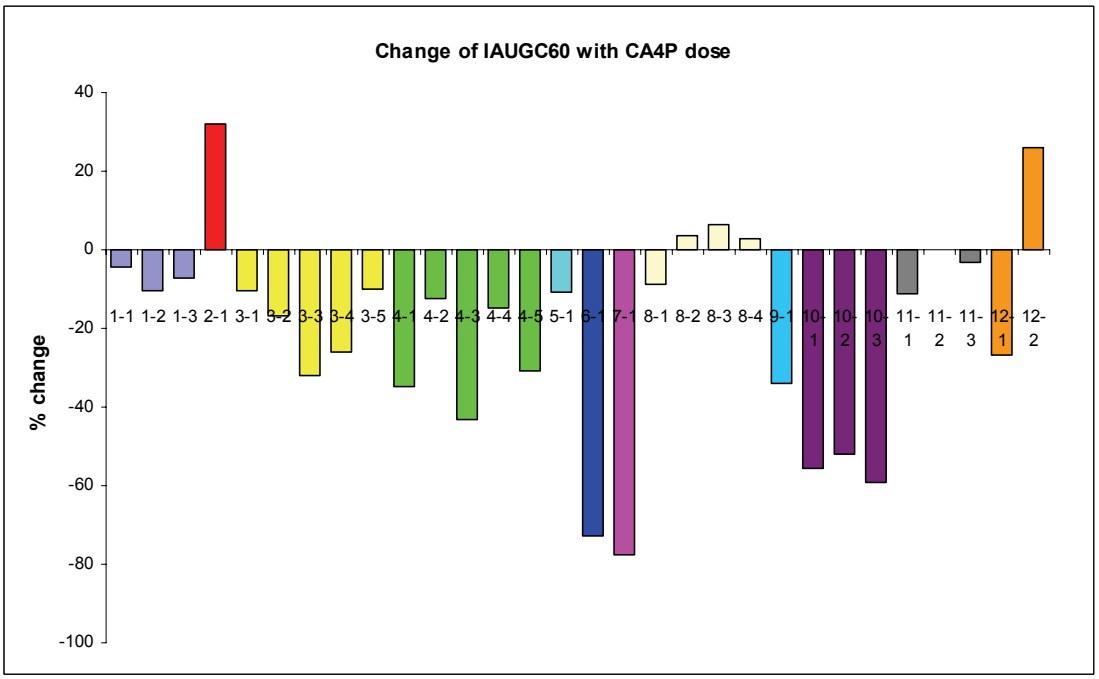

Table 3.4 - Treatment induced changes and comparisons of variability 4h after CA4P treatment (between-patients and between-tumours[within-patients])

	Kinetic parameter			
	K^{trans}	v_e	k_{ep}	$IAUGC_{60}$
Patients (tumours)	12 (29)	12 (29)	12 (29)	12 (30)
Treatment changes in tumours				
Mean (tumours)	0.395 min^{-1}	0.416	0.938 min^{-1}	22.88 $mmol{\cdot}s^{-1}$
Mean change after CA4P (Rx1)	-0.123	-0.079	-0.23	-3.68
95% CI	-0.05, -0.19	-0.03, -0.13	-0.10, -0.37	-0.22, -7.13
z	-3.50	-3.25	-3.33	-2.09
p	>0.001	0.001	0.001	0.04
Variability				
sd (between-patients)	0.151	0.144	0.26	11.30
sd (between-tumours[within-patients])	0.063	0.034	0.21	3.68
sd (error)	0.154	0.106	0.31	6.53
sd ratio (between-patients to between-tumours[within patients])	2.40	4.23	1.23	3.07

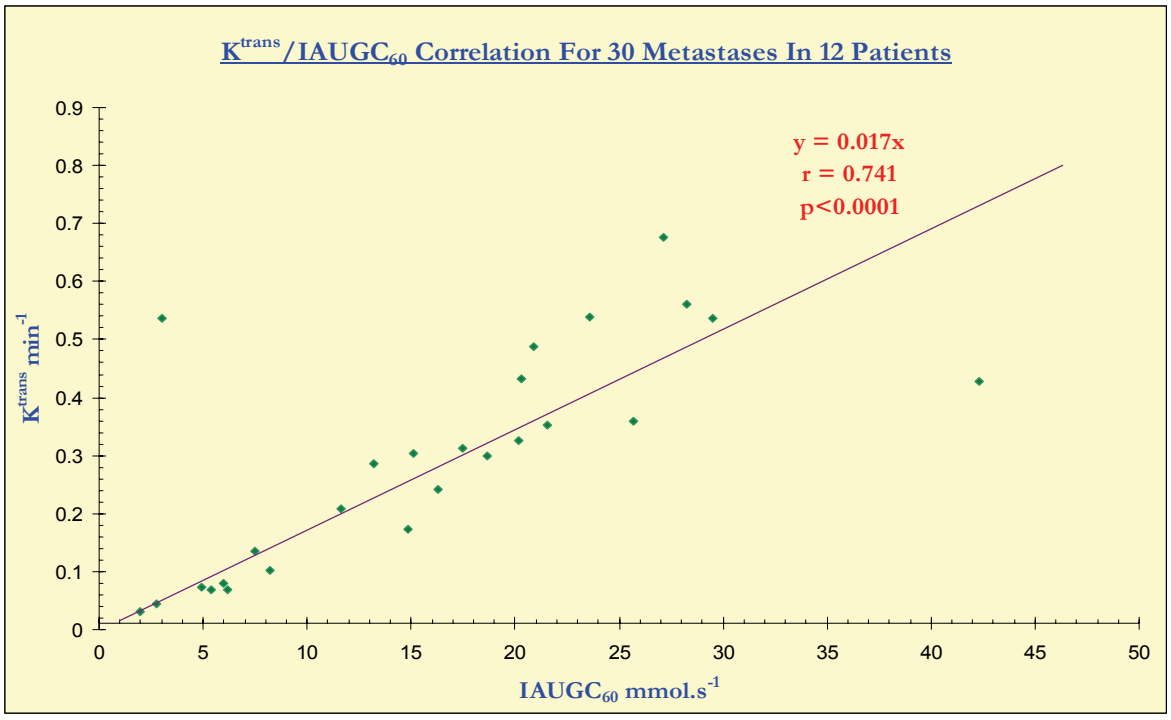

Fig. 3.5 – Relationship between K^{trans} & $IAUGC_{60}$. 26 points plotted, as 4 tumours did not have calculated values for both K^{trans} and $IAUGC_{60}$. Regression line shown, correlation r=0.741, a positive correlation between the two kinetic variables (p<0.0001). See discussion.

3) Dose Response of DCE-MRI Parameters to CA4P

No significant differences in between the 2 dose cohorts were seen. For K^{trans} at 45mg/m^2 CA4P (patients 1-6), the mean fall in K^{trans} four hours post CA4P was -21.6%, compared to -27.4% at the 54mg/m^2 dose (patients 7-12) (the 95% CI for a difference was -37.9 to 9.6%, 2p=0.246). For $IAUGC_{60}$ the values were -19.1% versus -22.3% (95% CI -17.1 to 23.5, 2p=0.747). For v_e the values were -8.9% and -20.8% (95% CI -33.0 to 9.0, 2p=0.251). For k_{ep} the values were -11.0% and -27.3% (95% CI -16.4 to 18.8%, 2p=0.897).

4) Control Tissue

In contrast, alterations in muscle dynamic MRI kinetic variables were variable, with no group changes seen outside of the 95% confidence limits at any time point (**Table 3.5**), proof in principle of a differential effect of CA4P on tumour and normal vasculature.

Table 3.5 – Muscle Kinetic Variable Analysis (MRIW 4.2.1), patients 1 – 7

Patient ID	Median K^{trans} R1	Median K^{trans} R2	Median K^{trans} Rx1	Median v_e R1	Median v_e R2	Median v_e Rx1	Median k_{ep} R1	Median k_{ep} R2	Median k_{ep} Rx1	Median $IAUGC_{60}$ R1	Median $IAUGC_{60}$ R2	Median $IAUGC_{60}$ Rx1
01	0.302	0.406	0.261	0.649	0.730	0.801	0.461	0.559	0.337	6.041	8.573	6.320
02	0.267	0.274	0.136	0.305	0.285	0.262	0.888	1.041	0.526	5.922	5.899	3.130
03	0.324	0.353	0.347	0.264	0.297	0.330	1.263	1.287	1.074	5.156	6.506	6.095
04	0.111	0.166	0.126	0.119	0.144	0.116	0.978	1.153	1.072	2.246	3.692	2.776
05	0.120	0.128	0.100	0.220	0.174	0.154	0.551	0.747	0.678	2.634	3.001	2.960
06	0.062	0.096	0.066	0.124	0.150	0.127	0.511	0.636	0.521	1.989	2.377	1.388
07	0.327	0.259	0.274	0.389	0.365	0.348	0.891	0.740	0.779	7.691	5.696	6.118

Discussion

Decreases in tumour MRI kinetic variables that are related to tumour flow and permeability are consistent with the known anti-vascular effects of CA4P (Galbraith et al., 2003; Dowlati et al., 2002; (Malcontenti-Wilson et al., 2001; Salmon & Siemann, 2007). Eight patients experienced significant falls in K^{trans} following CA4P. There were also statistically significant falls in v_e and k_{ep} in many patients.

In routine clinical practice when evaluating the effects of treatments on tumour size, multiple lesions are often chosen to determine the "average" change. However, DCE-MRI studies investigating the antivascular effects of vascular disrupting agents and antiangiogenic drugs in phase I have without exception, chosen single lesions for ROI analysis (O'Connor et al., 2007). The implicit assumption being made is that responses of chosen lesions are representative of responses in all lesions within the same patient. However heterogeneity of tumour DCE-MRI responses after CA4P, occurring between patients and intratumourally, has also been shown in previous preclinical and clinical work (Galbraith et al., 2003). The assumption of similar responses to CA4P, of lesions within individual patients had not been formally investigated.

We noted significant between-patient variability in DCE-MRI kinetic parameters both at baseline and 4h due to treatment with CA4P. We also noted that there was variability between-tumours[within-patients] both at baseline and due to treatment with CA4P. However between-patient variability was always greater than variability between-tumours[within-patients] for DCE-MRI parameters related to blood flow and vascular permeability (K^{trans} and $IAUGC_{60}$). Although between-tumours[within-patients] variability was smaller, it was quite marked for some patients; this may in part be related to motion artefacts particularly in patients 11 & 12.

These results concur with and further clarify previous DCE-MRI and PET studies on the actions of CA4P. Rustin et al have previously reported marked reductions in K^{trans} values, particularly in tumour centres, with some sparing of the peripheral rim. Significant reductions were seen in tumour K^{trans} in 6 of 16 patients treated at $\geq 52 mg/m^2$ (Galbraith et al.,2002; Rustin et al.,2003). No significant changes were seen in patients treated at 20-40 mg/m^2, which indicated a threshold dose for DCE-MRI effects (Dowlati et al.,2002;

Galbraith et al.,2003). Our data are also consistent with the work of Dowlati and Stevenson et al. (Dowlati et al.,2002; Galbraith et al.,2003; Stevenson et al.,2003).

We have evaluated the variability of response between-tumours in the same patient and we have shown that there is a tendency for tumours within-patients to behave similarly both at baseline and due to treatment after one dose of CA4P. This was seen in five of seven patients who had more than one tumour evaluated. This observation will require confirmation in larger patient cohorts and the recent move in DCE-MRI methodology towards three-dimensional/whole organ evaluations will provide the opportunity to undertake future studies in this regard.

An acute reduction in v_e may occur if the ability of Gd-DTPA to access the EES is reduced (Maxwell et al.,2002). In other cases, it is possible that early loss of cytokine production (e.g. VEGF) by tumour cells in response to chemotherapy or A5B7 results in a reduction of vascular permeability and interstitial fluid pressure that could reduce v_e. Such a change in permeability might not be detected by changes in K^{trans}, as K^{trans} is flow-dominated in tumours (Maxwell et al.,2002; Tofts,1997). Lankester et al (Lankester,2005) found K^{trans} was significantly correlated with k_{ep} but not with v_e, as expected. IAUGC correlated strongly with K^{trans} and strongly with v_e, reflecting its value as a 'summary' T1 parameter.

A positive correlation was found as expected and as previously described between K^{trans} and $IAUGC_{60}$ (**Figure 3.5**). IAUGC before peak enhancement should reflect transfer constant (wash-in rate) and be related to blood flow (Walker-Samuel et al.,2006 & AR Padhani, Personal Communication,2008). IAUGC is a mixed parameter and has a complex relationship with K^{trans}, v_e and k_{ep}. The range over which IAUGC is taken and the nature of the estimated AIF do not affect these relationships.

Limitations

There are a number of limitations of our study including the repeatability of the MRI procedures given that patient studies were performed on different days. These uncertainties can be partly taken into account by gauging responses in relation to the repeatability statistics which takes into account patient set-up errors, machine measurement variability and intrinsic tumour fluctuations of blood flow and

permeability. There are well known uncertainties with regard to the reliability of kinetic variable estimates derived from the application of tracer kinetic models to the DCE-MRI data. These derive from assumptions implicit in kinetic models and those for the measurement of tissue contrast agent concentration. For example, we have used a literature based description of the time-varying blood concentration of the contrast agent as the arterial input function, and the Tofts' model assumes that the supply of contrast medium is not flow limited, and that tissue blood volume contributes negligibly to signal intensity changes compared with that arising from contrast medium in the interstitial space. We have also used an established two-point T1 estimation technique (proton density and initial T1-weighted image) to calculate relaxation values; however there are alternative schemes for calculating these values that may be more or similarly accurate. However, it should be stated that the DCE-MRI techniques employed in this study have been used successfully to assess vascular response to a variety of therapies that affect tumour vasculature. Furthermore, three international consensus meetings have recognised that tissue contrast agent modelling remains a controversial area and have sought not to be prescriptive in this regard (Leach et al., 2005), recognizing that despite these complexities, quantitative DCE-MRI kinetic parameters can provide insights into underlying tissue pathophysiological processes, and that they are useful tools for decision making in pharmaceutical drug trials.

Conclusions

CA4P causes statistically significant reductions in tumour DCE-MRI kinetic variables related to blood flow and microvessel permeability at 4h, with no systematic decrease in CO, effectively excluding decreased CO as an explanatory factor. There is marked heterogeneity in tumour response between patients with smaller between tumours[within-patients] variability. New whole-organ DCE-MRI methodology will provide opportunities to undertake future studies comparing between-patients to intra-patient variability responses to antiangiogenic and vascular disruptive agents.

References

Beresford, M.J., Ah-See, M.-L., Padhani, A. et al (2005). Inter And Intra-Observer Variability Of DCE-MRI In Breast Cancer. In *Proc ISMRM*, Vol. 13. pp. 1863: Miami Beach, FL.

Bland, J. Altman, D. (1996a). Measurement Error. *BMJ*, **312,** 1654.

Bland, J. Altman, D. (1996b). Measurement Error Proportional To The Mean. *BMJ*, **313,** 744.

d'Arcy, J.A. Collins, D.J. Padhani A.R. et al (2006). Informatics in Radiology. MRIW: Analysis and Visualisation of DCE-MRI Data. *Radiographics*, **26,** 621 - 632.

Dowlati, A., Robertson, K., Cooney, M., et al (2002). A phase I pharmacokinetic and translational study of the novel VDA CA4P on a single-dose intravenous schedule in patients with advanced cancer. *Cancer Res*, **62,** 3408-16.

Fritz-Hansen, T., Rostrup, E., Larsson, H.B., et al (1996). Measurement of the arterial concentration of Gd-DTPA using MRI: a step toward quantitative perfusion imaging. *Magn Reson Med*, **36,** 225-31.

Galbraith, S.M., Lodge, M.A., Taylor, N.J.,et al (2002). Reproducibility of DCE-MRI in human muscle and tumours: comparison of quantitative and semi-quantitative analysis. *NMR Biomed*, **15,** 132-42.

Galbraith, S.M., Maxwell, R.J., Lodge, M.A., et al (2003). CA4P has tumor antivascular activity in rat and man as demonstrated by DCE-MRI. *J Clin Oncol*, **21,** 2831-42.

Hayes,C. Padhani,A. Leach,M.O.(2002) Changes In Tumour Vasc. Func. Using DCEMRI. *NMR Biomed*, **15,** 154 - 163.

Kety, S. (1960). Blood-tissue exchange. Theory of blood-tissue exchange and application to measurement of blood flow. *Meth Med Res*, **8**.

Lankester, K. (2005). MRI And The Development Of Vascular Targeted Treatments For Cancer. In *Gray Cancer Institute, Northwood, Middlesex, UK* pp. pp31. University of London, Faculty of Oncology: London.

Leach, M.O., Brindle, K., Evelhoch, J.L., et al (2005). The Assessment of Antiangiogenic And Antivascular Therapies In Early Stage Clinical Trials Using MRI: Issues And Recommendations. *Br J Cancer*, **92,** 1599 - 1610.

Maxwell, R.J., Wilson, J., Prise, V.E., et al. (2002). Evaluation of the anti-vascular effects of combretastatin in rodent tumours by DCE-MRI. *NMR Biomed*, **15,** 89-98.

Morgan, B., Thomas, A.L., Drevs, J., et al. (2003). DCE-MRI as a biomarker for the pharmacological response of PTK787/ZK 222584, an inhibitor of the VEGF receptor tyrosine kinases, in patients with advanced colorectal cancer and liver metastases: results from two phase I studies. *J Clin Oncol*, **21,** 3955-64.

O'Donnell, A., Padhani, A.R., Hayes, C. et al (2005). Phase I Study of the Angiogenesis Inhibitor SU5416 (Semaxanib) In Solid Tumors, Incorporating DCE-MRI Pharmacodynamic Endpoints. *Br J Cancer*, **93,** 876 - 883.

Padhani, A.R. (2003). MRI for assessing antivascular cancer treatments. *Br J Radiol*, **76 Spec No 1,** S60-80.

Parker, G., Suckling, J., Tanner, S., et al (1997). Probing tumor microvascularity by measurement, analysis and display of contrast agent uptake kinetics. *J Magn Reson Imaging*, **7,** 564 - 574.

Rustin, G.J., Galbraith, S.M., Anderson, H., et al (2003). Phase I clinical trial of weekly combretastatin A4 phosphate: clinical and pharmacokinetic results. *J Clin Oncol*, **21,** 2815-22.

Stevenson, J.P., Rosen, M., Sun, W., et al (2003). Phase I trial of the antivascular agent CA4P on a 5-day schedule to patients with cancer: MRI evidence for altered tumor blood flow. *J Clin Oncol*, **21,** 4428-38.

Taylor, N.J., Tunariu, N., Ah-See, M, et al (2007). Effects of AIF on DCE-MRI parameter estimates: analysis of parameter variability & model fitting in breast cancer patients. *Proc ISMRM*. Abstract 1975: 15th Meeting.

Tofts, P.S. (1997). Modeling tracer kinetics in dynamic Gd-DTPA MR imaging. *J Magn Reson Imaging*, **7,** 91 - 101.

Walker-Samuel, S., Leach, M.O. Collins, D.J. (2006). Evaluation of response to treatment using DCE-MRI: the relationship between IAUGC and quantitative pharmacokinetic analysis. *Phys Med Biol*, **51,** 3593-602.

Chapter 4

Late CA4P Effects Assessed By Liver Perfusion CT

Abstract

We describe the use of perfusion CT to measure arterial liver perfusion (ALP) and portal venous perfusion (PVP) in a small series of A5B7 patients with liver metastases. The objective was to determine whether there are long term changes in liver perfusion (weeks rather than hours) following CA4P. Four out of seven A5B7 patients (3 males,1 female,mean age 67) were suitable. A 2.4cm tumour volume was selected consisting of four contiguous 6mm slices. The dynamic study consisted of two end-expiration 30sec breathold acquisitions including both arterial and portal venous phases. Iodinated contrast was adminstered using a dual head pump injector. CT data was analysed using commercial perfusion software based on the 'slope method'. ROIs were placed within the aorta(for arterial input), portal vein(for PVP), spleen and liver to enable a smoothed arterial enhancement-time curve and corrected hepatic enhancement-time curve to be derived in an automated fashion, allowing parametric maps for ALP, PVP and hepatic perfusion index (HPI) to be produced, each pixel representing a parameter value. A ROI was then drawn freehand around the selected liver metastasis. This was repeated for each scan slice in which the lesion was visible and mean ALP, PVP and HPI were generated for each selected metastasis. No significant changes in liver perfusion were observed. This may be because CA4P has no late effects, disease progression, or the changes may be too small to observe with such a small sample in the presence of wide inter- and intrapatient variability.

Introduction

Results of current clinical trials indicate that conventional imaging strategies using tumour size (Gehan & Tefft,2000; Therasse et al.,2000) may not be suitable for monitoring the effects of anti-vascular drugs (Li,2000). Biological agents are often cytostatic and hence prolonged disease stability is a perfectly valid clinical endpoint. In these situations functional imaging such as perfusion CT can provide information on vascular tumour response at the physiological level. For example, a reduction in blood flow and blood volume after single administration of Bevacizumab (Willett et al.,2004), a reduction in blood volume after radiotherapy (Ng et al.,2007) and a reduction in hepatic perfusion after administration of AZD2171 and gefitinib (Meijerink et al.,2007).

This chapter discusses perfusion CT (reviewed in **Chapter 1** and **Appendix 4, page 240**) to measure ALP and PVP in a small series of A5B7 patients with macroscopic liver metastases. The objective was to determine whether there are long term changes in liver perfusion (over weeks rather than hours) following treatment with CA4P (Gaya et al.,2008).

Methods

Patients

Mount Vernon patients participating in the A5B7 study with liver metastases were identified and approached. They were given the option of having additional sequences performed following their routine tumour assessment CT scans, approximately 4h after the initial scan to allow time for contrast washout. Thus patients were scanned at baseline and d29 and d57 if still on-study.

Inclusion criteria

The patient must fulfil eligibility criteria for the A5B7 study (see **Chapter 2**); recruited by Mount Vernon Hospital; assessable liver metastases (masses at least 2cm diameter and away from areas of major vascular pulsation); spleen and aorta visible within the four contiguous slices chosen through liver (for modelling); patient able to breath-hold for 30sec; no known allergy to x-ray contrast media.

Exclusion criteria

Patients eligible for A5B7 could not undergo perfusion CT if they were having their assessment CT scans at the Royal Free Hospital; if they did not have assessable liver metastases; if they were unable to breath hold for 30sec; if there was a history of allergy to x-ray contrast media.

Perfusion CT Scan Protocol

Patients were scanned supine using a 4-slice multidetector CT (4-MDCT)(Lightspeed Plus, GE Healthcare). They were cannulated prior to the initial assessment scan with a 16-gauge cannula or greater. An abdominal study was performed initially without administration of intravenous contrast to identify the CT spatial coordinates of the liver metastases with the following parameters: 10-mm section thickness, 5-mm section interval, 30mm/sec table speed, 120kV, 180mA, 0.6-second rotation speed, 500mm scan field of view, and 512x512mm acquisition matrix.

A 2.4cm tumour volume was then selected consisting of four contiguous 6mm slices by a Consultant Radiologist with experience of perfusion imaging (VG). These slices included the spleen, aorta and a portal vein branch in addition to liver metastases to enable the software calculations to be made. The dynamic study consisted of two 30s breathold acquisitions thus including the arterial and portal venous phases. The first 30s acquisition was at a frequency of 1 acquisition/s, and the second 30s acquisition at a frequency of 1 acquisition/2s. There was a gap of 5s in between the two acquisitions for a breathing interval. Breatholding was at end expiration. Patients were coached before the scan to ensure compliance. Iodinated contrast (50ml of iobitridol(300mg iodine/ml(Xenetix 300,Guerbet)) was adminstered using

an automatic dual head pump injector (Injektron CT2, Medtron, USA) at 6ml/s followed by 20ml flush of normal saline at 6ml/s. The dynamic study was initiated 5s following contrast administration using the following parameters: Slice thickness 4x6mm, 120kV, current 150mA, 1.5mm detector width, acquisition matrix 512x512mm.

Image Analysis

The CT data was transferred to a dedicated workstation (Leonardo, Siemens Medical, Erlangen, Germany) and analysed using commercial perfusion software (Syngo-Body Perfusion CT, Siemens Medical, Erlangen, Germany) based on the slope method to calculate perfusion.

An assumption is made that the arterial time enhancement curve for the aorta in the field of view is the same, with a time shift, as that of the metastasis' feeding vessel. This assumption should hold where there is no stenosis between the feeding vessel and the vessel of the tumour and there is no significant circulation from collateral vessels or other circulation abnormalities. Hepatic arterial perfusion is calculated by dividing the initial slope of corrected hepatic parenchymal enhancement curve by peak aortic enhancement as described by Blomley (Blomley et al.,1995).

PVP is calculated by dividing the slope of the rise in attenuation during the PV phase of liver enhancement by peak portal venous enhancement. Hepatic perfusion index (HPI) is calculated as arterial liver perfusion (ALP) divided by the sum of arterial and PV perfusion (PVP).

A processing threshold of -50 to 150 HU was selected to optimize soft tissue visualisation. Regions of interest were placed within the aorta (for arterial input), portal vein (to enable for PVP), spleen and liver to enable a smoothed arterial enhancement-time curve and corrected hepatic enhancement-time curve to be derived in an automated fashion, allowing parametric maps for ALP, PVP and HPI to be produced, each pixel representing a parameter value. A

ROI was then drawn freehand around the selected liver metastasis using a cursor and mouse in order to generate a mean value of ALP, PVP and HPI for the metastasis which was recorded for each patient. This was repeated for each scan slice in which the lesion was visible and an overall value of ALP, PVP and HPI was generated for each selected metastasis by averaging values from the slices analysed. Each pixel location within the functional map corresponds to a single quantitative perfusion value resulting from the mathematical modelling of the data at that location (**Figures 4.1–4.4)**.

Results

Fig 4.1 – MIP (Maximum Intensity Projection) Jan 2004, Patient 01. This early image shows arterial enhancement only. Hepatic portal vein (HPV) has yet to opacify.

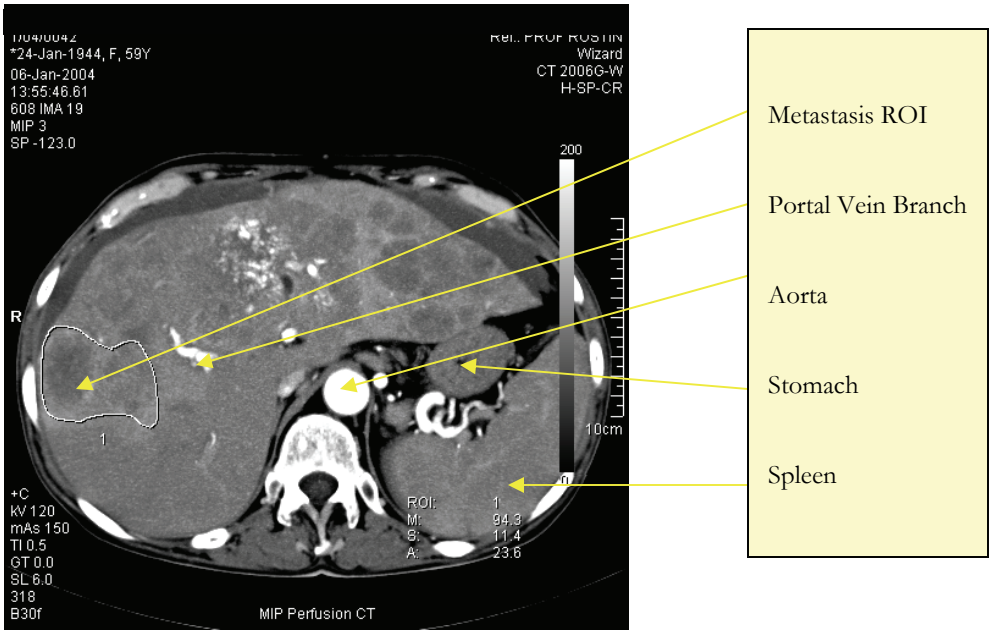

Fig 4.2a,b - ALP Jan 2004 and Feb 2004 Patient 01 – no significant changes. The colours represent ALP with the figure as shown on the scale (range -2 to 150ml/min/100ml)

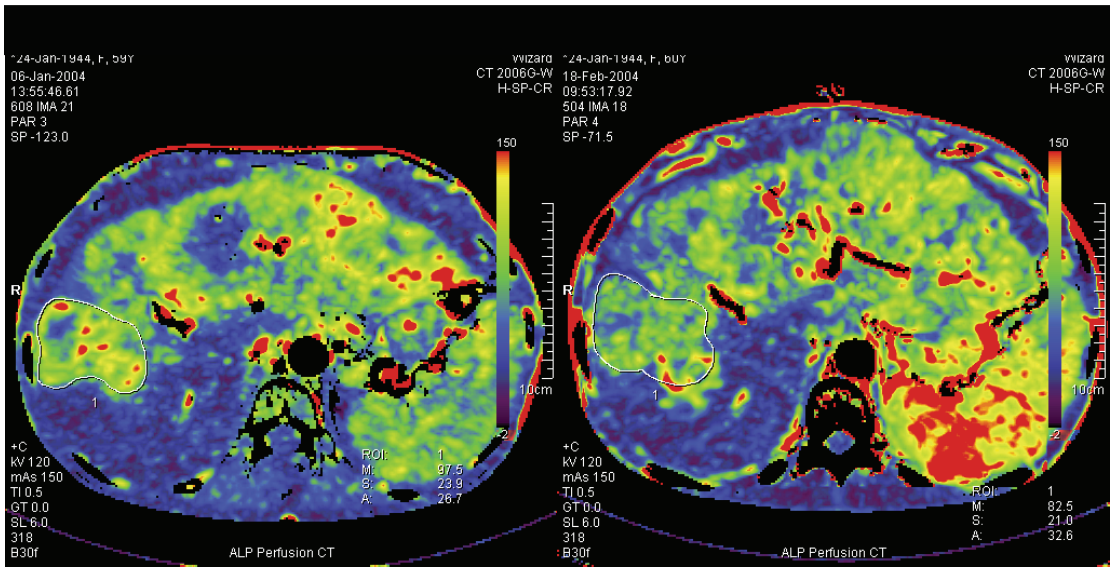

Fig 4.3a,b - PVP Perfusion CT Jan 2004 & Feb 2004 Patient 01 – Note increased PVP in Feb scan**.** The colours represent PVP as illustrated on the scale (range -2 to 250ml/min/100ml tissue)

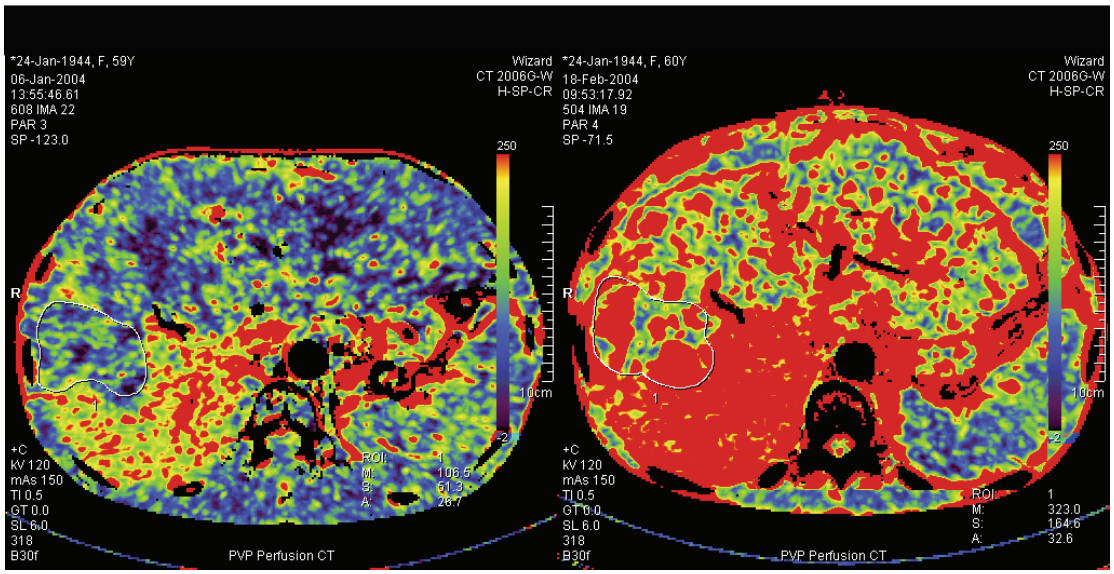

Fig 4.4a,b - HPI Perfusion CT Jan 2004 & Feb 2004 Patient 01. General decrease in HPI in Feb scan. Colours represent HPI as illustrated on the scale (range -2 to 80)

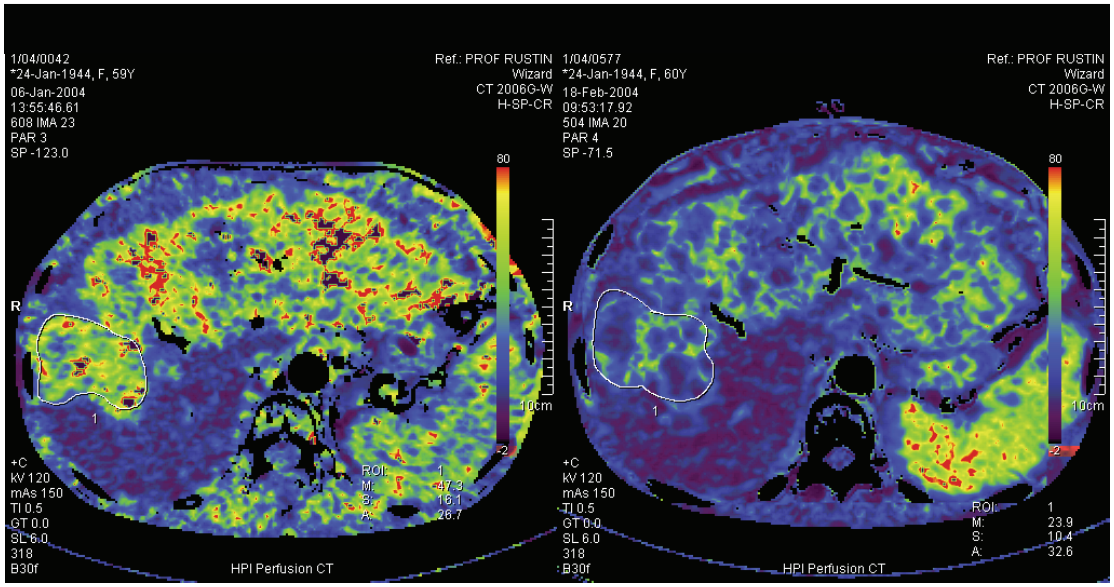

Seven patients were eligible and of these four underwent perfusion CT. Of the three remaining patients, one refused and withdrew consent, one did not have assessable liver disease, and the third was withdrawn by the chief investigator due to concerns over hypertension and cardiac ischaemia.

Of the four patients recruited, all had liver metastases from colorectal cancer. There were three males and one female. Average age was 67 years (range 60–73). All patients were eventually withdrawn from A5B7 for progressive disease although patient 04 was on study for 95 days. Four patients underwent seven perfusion CT scans (**Tables 4.1 & 4.2)**(patient 05 performance status deteriorated and could not cope with breath holding for the second scan).

No significant changes in liver perfusion were observed in this small group of four patients.

A5B7 ID	Date Scan	Slices (6mm)	Liver Site	Liver Segment	Lesion size (cm)	ALP	St Dev	ROI area mm²	PVP	St Dev	ROI area mm²	HPI	St Dev	ROI Area mm²
01	06/01/2004	2	Left lobe	2,3	9.2	98.6	23.8	25	105.5	52.2	25	50.2	15.4	25
	18/02/2004	2			13.6	87.5	22.9	73.5	236.2	102.3	73.5	29.7	10.4	73.5
04	05/04/2004	4	Right lobe	8,5,1	9.9	58.5	47.8	54.1	151.4	6.7	54.1	28.2	5.8	54.5
	10/05/2004	4			9.6	77.6	55.4	57.8	172	96.3	57.8	31	6.7	57.8
07	12/09/2005	2	Right lobe	7	4.1	86.5	27.2	16.8	1130.1	310.5	18.8	7.5	2.1	16.8
	17/10/2005	1			5.1	108.8	46.2	19.8	512.4	280.3	19.8	19.9	8.5	19.8
05	12/07/2004	1	Right lobe	8	6.3	57.1	21.7	29.7	263.5	145.8	29.7	19.1	4.8	29.7

ID	Normal lobe for comparison	ALP	SD	ROI area mm²	PVP	SD	ROI area mm²	HPI	SD	ROI area mm²
01	Right lobe	28.8	6.8	1.6	227	31.4	1.6	12.3	3.1	1.6
		26.8	5.1	1.6	308.3	63.7	1.6	8.2	2	1.6
04	Left lobe	54	14.4	3.5	220.6	27.4	3.5	19.7	3.9	3.5
		60.3	15.3	3.5	240.4	41.8	3.5	20.4	4.3	3.5
07 None available - previous left hepatic lobectomy and problems with patient movement										
05	Left lobe	58.9	11.4	0.9	2170.7	47.8	0.9	12.3	1.6	0.9

Tables 4.1 & 4.2 –Perfusion CT Results for the four patients studied: Top table(4.1) illustrates Perfusion CT results. Lower table(4.2) illustrates normal liver in the same group of patients for comparison. Results shown with standard deviation. There is wide interpatient and intrapatient variability, see discussion. ALP/PVP units are ml/min/100ml. Note the higher HPI in diseased liver. Patient 05 withdrawn from study before 2nd scan due to clinical deterioration and disease progression.

Discussion

No significant changes in liver perfusion were observed (Gaya A et al,2008). There were only small changes seen in ALP, but it should be noted ALP was higher in metastatic lesions than in normal tissue as expected. There was an increase in PVP in patient 01 and a corresponding fall in 07, of some considerable degree, but of uncertain clinical significance. HPI was higher in metastatic lesions than normal liver, with a fall in patient 01 and rise in 07. Both values were higher than and agree with the threshold ratios set by Perkins (Perkins et al.,1987). The ALP values are in agreement with the Miles & Blomley's publications which suggest values>50 ml/min/100 ml tissue in hepatic metastases (Blomley et al.,1995; Miles et al.,1993).

Tables 4.1 and 4.2 illustrate wide interpatient and intrapatient variability in measurement of liver perfusion. This variability has also been reported in dynamic MRI assessment of colorectal liver metastases (Padhani AR, Taylor NJ Personal Communication 2007). Certainly colorectal liver metastases can be extremely heterogeneous in their vascular supply, but there may be other reasons for this as well. Patient movement and respiration can lead to a reduction in the sensitivity of measurement. The reproducibility of ROI outlining between scans can also lead to intrapatient variability. If non-metastatic tissue is included in an ROI (e.g. necrosis, vessels) this will also reduce reproducibility (Taylor et al.,2006). The analysis software can also encounter modeling failures during processing however this should be constant between patients.

All patients were shown to have disease progression on study. CA4P is short-lived and its effects are not known to persist longer than 24h following infusion (Tozer et al.,1999). Thus it is probable that the results of this study reflect the patients' disease progression rather than any CA4P effect.

The availability of CT coupled with commercial perfusion software has made this method of assessment widely accessible to clinicians. Furthermore, reproducibility of the CT technique

(Blomley et al.,1995; Fiorella et al.,2004; Goh et al.,2005; Miles & Griffiths,2003) gives CT advantages over other imaging modalities that enable similar vascular assessments.

CT measurements of perfusion have been shown to be reproducible and have been validated against a range of reference methods (Blomley et al.,1993; Blomley et al.,1995; Cenic et al.,2000; Cenic et al.,1999; Gillard et al.,2001; Gillard et al.,2000; Miles et al.,1993). The increasing number of publications reporting a correlation between contrast enhancement parameters and histological measurements of angiogenesis, such as microvessel density (MVD), validates the use of perfusion CT as a marker of angiogenesis (Jinzaki et al.,2000; Swenson et al.,1996; Tateishi et al.,2001). To date, no consensus has emerged as to which perfusion CT technique is optimal for the assessment of tumour vascularity. The high image frequency required for first pass studies may restrict the volume of tissue that can be assessed even using MDCT or table toggling techniques (Roberts et al.,2001).

The relationship between angiogenesis and hepatic perfusion is complex. Hepatic metastases derive their blood supply almost exclusively from the arterial system; the portal circulation in surrounding liver can be affected by mechanical compression by enlarging metastases, by white cell margination within portal vessels adjacent to metastases and by circulating hormonal factors (Dugdale & Miles,1999). The physiological linkage between arterial and portal circulations is such that reduced portal flow is associated with increased arterial flow, which complicates the situation further. Histological studies have shown that unlike primary tumours, greater vascularisation of hepatic metastases is associated with a better prognosis (Mooteri et al.,1996). This association is reflected by perfusion CT findings amongst patients with hepatic metastases. Increased arterial perfusion, particularly in the periphery of the metastasis, is associated with a longer survival (Miles et al.,1998), whereas a small series of patients with hepatic metastases from colon cancer has suggested that low portal perfusion throughout the liver (below 0.22 ml/min/ml) is associated with progressive disease and a poor response to chemotherapy (Leggett et al.,1997; Sommerfield et al.,1999).

Absolute measurement of perfusion is dependent on the cardiac output(CO) at the time of measurement. To normalize perfusion values Miles (Miles et al.,2001) proposed the standardized perfusion value(SPV) as the perfusion scaled by the whole body perfusion, expressed as CO over weight. CO may be determined from the arterial input time attenuation curve provided the dose of contrast material is known.

CT perfusion studies have been performed at a range of energies and beam intensities, from 120kV at 210mA to 80kV and 80mA. Wintermark (Wintermark et al.,2000) compared the use of 80 and 120kV at 200mA on cerebral contrast material enhancement using pre and post enhancement images after a bolus of contrast material. 80kV gave increased enhancement, greater contrast between white and grey material and lowered the radiation dose by a factor of 2.8 compared with 120kV. The difference in noise between 80kV and 120kV images was not significant. However, the CT perfusion was not calculated from this data. The slope method requires good contrast material enhancement with minimum noise in those images used to calculate perfusion. However, it generally has a shorter acquisition time and may be able to use acquisition parameters with a greater radiation dose per image. There will always be a trade off between radiation dose and increased temporal resolution.

In patients with known liver metastatic disease, increased ALP has been shown by using CT perfusion imaging with the slope-ratio analytic methods described by Miles (Miles et al.,1993) and Blomley (Blomley et al.,1995). Blomley et al reported a value of 43mL/min/100mL, and Miles (Miles et al.,1993) reported that of 50mL/min/100mL in patients with known metastatic disease versus values of 19mL/min/100mL and 17mL/min/100mL, respectively, in healthy control groups. Leggett (Leggett et al.,1997) also demonstrated increased arterial perfusion (25mL/ min/100mL) in 9/11 patients with colorectal liver metastases examined by using CT perfusion with slope methods. The relationship between an elevated HPI value and overt metastatic disease has been well established (Leveson et al.,1985; Leveson et al.,1983; Perkins et al.,1987). Perkins (Perkins et al.,1987) determined a hepatic perfusion index threshold value of 0.37; at values above this level, metastatic disease should be suspected.

Several authors have studied the effect of liver metastases on perfusion indices (Blomley et al.,1995; Miles et al.,1993; Miles et al.,1998) using functional CT. Miles (Miles & Kelley,1997) measured capillary permeability in abdominal lymph nodes and Leggett examined the effect of occult metastases on hepatic perfusion (Leggett et al.,1997). Surprisingly, little work has been published so far on the response of tumours to therapy (Bellomi et al.,2007; Dugdale & Miles,1999; Hayano et al.,2007; Kiessling et al.,2004; Makari et al.,2007; Meijerink et al.,2007; Ng et al.,2007; Rumboldt et al.,2005; Sahani et al.,2005; Willett et al.,2005).

Conclusions

These results do not suggest that further late time-point studies are worthwhile as there was no hint of alterations at these time points. This may be because CA4P has no late effects, it may be due to disease progression, or the changes may be too small to observe with such a small sample in the presence of wide interpatient and intrapatient variability (Gaya et al.,2008). The quantitative data produced by perfusion CT makes it an attractive modality for assessing acute perfusion changes, however this has to be balanced against the radiation doses involved. Faster MRI scanners now allow direct measurement of arterial input and this is therefore likely to be the way forward.

References

Bellomi, M., Petralia, G., Sonzogni, A., Zampino, M.G. & Rocca, A. (2007). CT perfusion for the monitoring of neoadjuvant chemotherapy and radiation therapy in rectal carcinoma: initial experience. *Radiology*, **244,** 486-93.

Blomley, M.J., Coulden, R., Bufkin, C., Lipton, M.J. & Dawson, P. (1993). Contrast bolus dynamic computed tomography for the measurement of solid organ perfusion. *Invest Radiol*, **28 Suppl 5,** S72-7; discussion S78.

Blomley, M.J., Coulden, R., Dawson, P., Kormano, M., Donlan, P., Bufkin, C. & Lipton, M.J. (1995). Liver perfusion studied with ultrafast CT. *J Comput Assist Tomogr*, **19,** 424-33.

Cenic, A., Nabavi, D.G. & Craen, R.A. (2000). A CT Method To Measure Haemodynamics In Brain Tumours: Validation And Application Of Cerebral Blood Flow Maps. *AJNR*, **21,** 462 - 470.

Cenic, A., Nabavi, D.G., Craen, R.A., Gelb, A.W. & Lee, T.Y. (1999). Dynamic CT Measurement of Cerebral Blood Flow : A Validation Study. *AJNR*, **20,** 63 - 73.

Dugdale, P.E. & Miles, K.A. (1999). Hepatic metastases: the value of quantitative assessment of contrast enhancement on computed tomography. *Eur J Radiol*, **30,** 206-13.

Fiorella, D., Heiserman, J., Prenger, E. & Partovi, S. (2004). Assessment of the reproducibility of postprocessing dynamic CT perfusion data. *AJNR Am J Neuroradiol*, **25,** 97-107.

Gaya, A., Taylor, N.J., Stirling, J.J., Rustin, G.J., Padhani, A. & Goh, V. (2008). Early & Late Tumour Vasculature Changes Following the Vascular Disruptive Agent (VDA) Combretastatin-A4-Phosphate (CA4P) Using Dynamic Contrast Enhanced MRI (DCE-MRI) and Perfusion CT. In *ESGAR* pp. Abstract 31227: Istanbul, Turkey.

Gehan, E.A. & Tefft, M.C. (2000). Will there be resistance to the RECIST Criteria? *J Natl Cancer Inst*, **92,** 179-81.

Gillard, J.H., Antoun, N.M., Burnet, N.G. & Pickard, J.D. (2001). Reproducibility of quantitative CT perfusion imaging. *Br J Radiol*, **74,** 552-5.

Gillard, J.H., Minhas, P.S., Hayball, M.P., Freer, C.E., Mathews, J.C., Miles, K.A. & Pickard, J.D. (2000). Assessment of quantitative computed tomographic cerebral perfusion imaging with H2(15)O PET. *Neurol Res*, **22,** 457-64.

Goh, V., Halligan, S., Hugill, J.A., Bassett, P. & Bartram, C.I. (2005). Quantitative assessment of colorectal cancer perfusion using MDCT: inter- and intraobserver agreement. *AJR Am J Roentgenol*, **185,** 225-31.

Hayano, K., Okazumi, S., Shuto, K., Matsubara, H., Shimada, H., Yanagawa, N. Ochiai, T. (2007). Perfusion CT can predict the response to chemoradiation therapy and survival in esophageal SCC: Initial results. *Oncol Rep*, **18,** 901-8.

Jinzaki, M., Tanimoto, A. & Mukai, M.e.a. (2000). Double Phase Helical CT Of Small Renal Parenchymal Neoplasms : Correlation With Pathologic Findings And Tumour Angiogenesis. *J Comput Assist Tomogr*, **24,** 835 - 842.

Kiessling, F., Boese, J., Corvinus, C., Ederle, J.R., Zuna, I., Schoenberg, S.O., Brix, G., Schmahl, A., Tuengerthal, S., Herth, F., Kauczor, H.U. & Essig, M. (2004). Perfusion CT in patients with advanced bronchial carcinomas: a novel chance for characterization and treatment monitoring? *Eur Radiol*, **14,** 1226-33.

Leggett, D.A., Kelley, B.B., Bunce, I.H. & Miles, K.A. (1997). Colorectal cancer: diagnostic potential of CT measurements of hepatic perfusion and implications for contrast enhancement protocols. *Radiology*, **205,** 716-20.

Leveson, S.H., Wiggins, P.A., Giles, G.R., Parkin, A. & Robinson, P.J. (1985). Deranged liver blood flow patterns in the detection of liver metastases. *Br J Surg*, **72,** 128-30.

Leveson, S.H., Wiggins, P.A., Nasiru, T.A., Giles, G.R., Robinson, P.J. & Parkin, A. (1983). Improving the detection of hepatic metastases by the use of dynamic flow scintigraphy. *Br J Cancer*, **47,** 719-21.

Li, W.W. (2000). Tumor angiogenesis: molecular pathology, therapeutic targeting, and imaging. *Acad Radiol*, **7,** 800-11.

Makari, Y., Yasuda, T., Doki, Y., Miyata, H., Fujiwara, Y., Takiguchi, S., Matsuyama, J., Yamasaki, M., Hirao, T., Koyama, M.K., Nakamuara, H. & Monden, M. (2007). Correlation between tumor blood flow assessed by perfusion CT and effect of neoadjuvant therapy in advanced esophageal cancers. *J Surg Oncol*, **96,** 220-9.

Meijerink, M.R., van Cruijsen, H., Hoekman, K., Kater, M., van Schaik, C., & Manoliu, R.A. (2007). The use of perfusion CT for the evaluation of therapy combining AZD2171 with gefitinib in cancer patients. *Eur Radiol*, **17,** 1700-13.

Miles, K.A. & Griffiths, M.R. (2003). Perfusion CT: a worthwhile enhancement? *Br J Radiol*, **76,** 220-31.

Miles, K.A., Griffiths, M.R. & Fuentes, M.A. (2001). Standardized perfusion value: universal CT contrast enhancement scale that correlates with FDG PET in lung nodules. *Radiology*, **220,** 548-53.

Miles, K.A., Hayball, M.P. & Dixon, A.K. (1993). Functional images of hepatic perfusion obtained with dynamic CT. *Radiology*, **188,** 405-11.

Miles, K.A. & Kelley, B.B. (1997). CT Measurements Of Capillary Permeability With Nodal Masses: A Potential Technique For Assessing The Activity Of Lymphoma. *Br J Radiol*, **70,** 74 - 79.

Miles, K.A., Leggett, D.A., Kelley, B.B., Hayball, M.P., Sinnatamby, R. & Bunce, I. (1998). In vivo assessment of neovascularization of liver metastases using perfusion CT. *Br J Radiol*, **71,** 276-81.

Mooteri, S., Rubin, D., Leurgans, S. & al., e. (1996). Tumour Angiogenesis In Primary And Metastatic Colorectal Cancers. *Dis Colon Rectum*, **39,** 1073 - 1080.

Ng, Q.S., Goh, V., Milner, J., Padhani, A.R., Saunders, M.I. & Hoskin, P.J. (2007). Acute tumor vascular effects following fractionated radiotherapy in human lung cancer: In vivo whole tumor assessment using volumetric perfusion computed tomography. *Int J Radiat Oncol Biol Phys*, **67,** 417-24.

Perkins, A.C., Whalley, D.R., Ballantyne, K.C. & Hardcastle, J.D. (1987). Reliability of the hepatic perfusion index for the detection of liver metastases. *Nucl Med Commun*, **8,** 982-9.

Roberts, H.C., Roberts, T.P., Smith, W.S., Lee, T.J., Fischbein, N.J. & Dillon, W.P. (2001). Multisection dynamic CT perfusion for acute cerebral ischemia: the "toggling-table" technique. *AJNR Am J Neuroradiol*, **22,** 1077-80.

Rumboldt, Z., Al-Okaili, R. & Deveikis, J.P. (2005). Perfusion CT for head and neck tumors: pilot study. *AJNR Am J Neuroradiol*, **26,** 1178-85.

Sahani, D.V., Kalva, S.P., Hamberg, L.M., Hahn, P.F., Willett, C.G., Saini, S., Mueller, P.R. & Lee, T.Y. (2005). Assessing tumor perfusion and treatment response in rectal cancer with multisection CT: initial observations. *Radiology*, **234,** 785-92.

Sommerfield, N.W.B., Miles, K.A., Dugdale, P.E., Leggett, D.A. & Bunce, I.H. (1999). Colorectal Cancer: Progressive Disease Is Associated With Altered Liver Perfusion On Functional CT. In *50th Annual Meeting Of the Royal Australia And New Zealand College Of Radiologists* pp. Abstract 56.

Swenson, S., Brown, L.R., Colby, T.V. & al., e. (1996). Lung Nodule Enhancement At CT : Prospective Findings. *Radiology*, **201,** 447 - 455.

Tateishi, U., Nishihara, H., Watanabe, S., Morikawa, T., Abe, K. & Miyasaka, K. (2001). Tumor angiogenesis and dynamic CT in lung adenocarcinoma: radiologic-pathologic correlation. *J Comput Assist Tomogr*, **25,** 23-7.

Taylor, N.J., d'Arcy, J.A., Walker-Samuel, S., Lankester, K.J., Collins, D.J., Knowles, B., White, D.L., Miaux, Y., Suhy, J., Guermazi, A., Stirling, J.J., Rustin, G.J.S., Leach, M.O. & Padhani, A.R. (2006). Single and multi-centre DCE-MRI reproducibility in Phase I clinical trials. In *Proc. I.S.M.R.M* pp. Abstract 766: 14th Annual Meeting.

Therasse, P., Arbuck, S.G., Eisenhauer, E.A., Wanders, J., & Gwyther, S.G. (2000). New guidelines to evaluate the response to treatment in solid tumors. European Organization for Research and Treatment of Cancer, National Cancer Institute of the United States, National Cancer Institute of Canada. *J Natl Cancer Inst*, **92,** 205-16.

Tozer, G.M., Prise, V.E., Wilson, J., Locke, R.J., Vojnovic, B., Stratford, M.R., Dennis, M.F. & Chaplin, D.J. (1999). Combretastatin A-4 phosphate as a tumor vascular-targeting agent: early effects in tumors and normal tissues. *Cancer Res*, **59,** 1626-34.

Willett, C.G., Boucher, Y., di Tomaso, E., Duda, D.G., A.X., Blaszkowsky, L.S., Chen, H.X., Shellito, P.C., Lauwers, G.Y. & Jain, R.K. (2004). Direct evidence that the VEGF-specific antibody bevacizumab has antivascular effects in human rectal cancer. *Nat Med*, **10,** 145-7.

Willett, C.G., Boucher, Y., Duda, D.G., di Tomaso, E., Shellito, P.C., Mino-Kenudson, M. & Lauwers, G.Y. (2005). Surrogate markers for antiangiogenic therapy and dose-limiting toxicities for bevacizumab with radiation and chemotherapy: continued experience of a phase I trial in rectal cancer patients. *J Clin Oncol*, **23,** 8136-9.

Wintermark, M., Maeder, P., Verdun, F.R., Thiran, J.P., Valley, J.F., Schnyder, P. & Meuli, R. (2000). Using 80 kVp versus 120 kVp in perfusion CT measurement of regional cerebral blood flow. *AJNR Am J Neuroradiol*, **21,** 1881-4.

Chapter 5 – Cardiac Output Changes Following CA4P

Abstract

It has been suggested that tumour vascular shutdown following administration of VDAs is due to a reduction in systemic cardiac output (CO) and tissue blood delivery, i.e. not a wholly tumour specific local effect. In order to confirm or refute this hypothesis 12 patients taking part in the A5B7 trial had CO measured by MRI using phase contrast sequences through the ascending aorta before and 4h following infusion of CA4P at 45–54mg/m^2. Regions of interest (ROI) were drawn on the margins of the ascending aorta on the 40 phases obtained and stroke volume (SV) calculated using Argus flow software. As heart rate (HR) was measured before each scan CO could be calculated as the product of HR and forward SV. There was a mean increase in CO of 14.0% (range -6.9% to 47.3%, increased CO in 8/11 assessable patients, p=0.026) 4h following CA4P, yet DCE-MRI analysis confirmed significant tumour vascular shutdown in several patients, and reductions in the kinetic variables K^{trans} and $IAUGC_{60}$ in most. There is no evidence for reductions in CO as a cause for reduced tumour K^{trans} after CA4P, effectively excluding a central effect for the reduced kinetic variables seen in tumours.

Introduction

Phase contrast MRI is a well established non-invasive technique for measurement of CO (Diddier et al.,2000). It is based on the principle that the phase of flowing spins relative to stationary spins along a magnetic gradient changes proportionally to flow velocity. The absolute velocity is calculated at any given time during the cardiac cycle at specified locations in the plane of acquisition for each pixel within the ROI. The instantaneous flow volume for each time frame during a cardiac cycle is calculated as the product of cross-sectional area of the vessel (proximal ascending aorta in our case) and spatial mean velocity (the average velocity for all the pixels in the cross-sectional area). Integration of all instantaneous flow volumes throughout the cardiac cycle yields the flow volume per heart beat, also called the SV, which when muliplied by HR gives the CO. This technique has been evaluated both *in vitro* and *in vivo* by several investigators and shown to provide an accurate measurement of SV and CO both through the aorta and the pulmonary artery (Higgins et al.,1992; Mohiaddin & Pennell,1998).

Transient alterations in HR and BP are common following CA4P. It has been suggested that the reduction in tumour blood flow detected by DCE-MRI kinetic variable alterations after 4h could be due to a reduction in CO (Anderson et al.,2003; Galbraith et al.,2003) i.e. not a wholly tumour specific effect.

The objective of this study was to determine whether any significant CO changes are seen 4h following infusion of CA4P in the presence of tumour vascular shutdown, in order to confirm or refute this hypothesis.

Methods

Following ethics board approval, all 12 patients from the A5B7 trial were consented for CO measurement and DCE-MRI.

MRI imaging procedures

MRI was performed on a 1.5 tesla Magnetom Symphony Scanner (Siemens Medical, Erlangen, Germany), using a surface phased array coil. An ECG-gated phase contrast sequence to calculate CO, and DCE-MRI were performed 48h (R1) and 24h (R2) prior to, and 4h following infusion of CA4P (Rx1). The DCE-MRI data is discussed in **Chapter 3**.

Phase contrast sequences were performed through the proximal ascending aorta just above the sino-tubular junction whilst at rest. Scans were obtained in through-plane (perpendicular to the long axis of aorta) with retrospective ECG gating using the following parameters: Field of view 320*240 mm; Acquisition matrix 256*179; TR=68ms; TE=4.8; TA=56s; Flip angle 30° and slice thickness 6 mm. Velocity encoding was kept at 150cm/s and increased further if aliasing was detected. ROIs were drawn on the margins of the ascending aorta on the 40 phases obtained and the following parameters were calculated using Argus flow software (Siemens Medical, Erlangen, Germany): Peak velocity (cm/s), average velocity (cm/s), total forward SV (ml/s), reverse volume (ml/s), and net forward volume (ml/s) (**Figure 5.1**).

Figure 5.1 a-f - Procedure for obtaining CO with ECG gated MRI: Oblique tru-FISP sequence images (a & b) through the aortic root demonstrating the plane of acquisition of phase-contrast images at sino-tubular junction (c & d). Magnitude (c) and phase images (d) of the phase contrast sequence with the ROI drawn around the aortic wall. (e) demonstrates the time-velocity curve of blood flow through the cardiac cycle, whilst (f) gives the different parameters of velocity and flow calculated by the software.

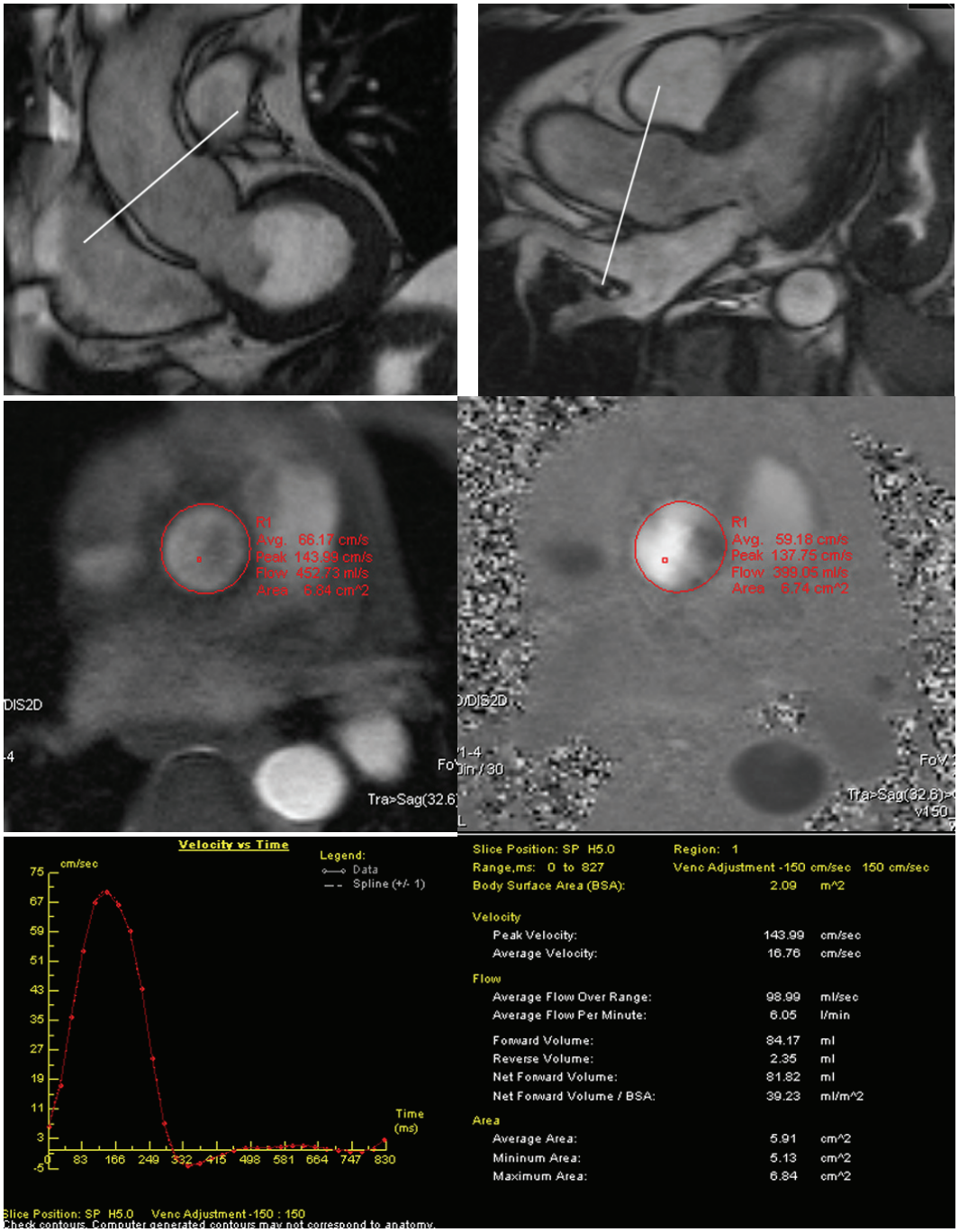

CO was calculated as the product of HR and SV (net forward volume). Three patients who did not have HR measured at the time of the MRI had the value taken either from the CA4P vital signs table 4h post-infusion, or the population group mean was used.

Results

11/12 patients successfully completed at least one pre- and one post-CA4P cardiac MRI. **Table 5.1** illustrates CO 48h and 24h pre-CA4P and 4h post-CA4P, demonstrated graphically in **Figure 5.2**. In 8/11 cases there was a rise in CO 4h following CA4P (p=0.026, 2-tailed group t-test). The mean CO increase was 14.0% (range 0.7% to 47.3%). 3/11 cases showed a small fall in CO (range -6.9% to -0.5%). The statistical significance was maintained no matter which method was used to estimate missing HR data (vital signs table or group mean HR during MRI). **Figure 3.3** (**Chapter 3**) illustrates changes in the DCE-MRI kinetic parameters K^{trans} and $IAUGC_{60}$ 4h following CA4P. Falls in these parameters were widespread although only a few reached statistical significance (patients 6, 7, 10). This is consistent with a global reduction of tumour perfusion following CA4P, in the face of increased CO in 8/11 patients.

Table 5.1 – CO Measurement Pre & Post-CA4P

Patient ID	Scan No.	HR	Peak Vel (cm/s)	Av. Vel (cm/s)	Av. flow (ml/s)	Forward Vol ml	Rev vol. ml	Net forward vol (ml)	CO (L/min)	Mean CO R1 & R2	CO Rx1 (Post CA4P)	% Change In CO Rx1
01	R1	95	121.51	9.78	107.28	68.13	2.69	65.44	6.47			+6.5
	R2	95	124.61	8.68	95.16	63.81	2.9	60.9	6.06			
	Rx1	102	107.23	9	99.53	64.67	4.25	60.42	6.60	6.27	6.60	
02	R1	62	104.81	5.9	74.84	72.74	1.71	71.02	4.51			+23.0
	R2	61	116.9	5.5	71.7	69.5	1.2	68.2	4.24			
	Rx1	90	108.6	8.6	89.6	59.8	1.9	58	5.38	4.37	5.38	
03	R1	108	86.3	8	67.6	39.2	1.4	37.3	4.23			+11.7
	R2	102	82.1	8.8	75.8	43.6	1.7	41.9	4.45			
	Rx1	117	101.2	8.8	77.8	43.5	2	41.5	5.09	4.34	5.09	
04	R1	78	85.11	11.54	83.47	66.34	1.73	64.6	5.17			+17.1
	R2	78	103.5	11.82	88.46	66.04	2.88	63.16	5.15			
	Rx1	85	109.5	14.35	103.46	71.02	3.56	67.48	6.04	5.16	6.04	
06	R1	89	93.8	11.7	93.8	72.9	0.3	72.7	6.49			+0.77

	R2	89	82.6	12.7	96.4	73.4	1.2	72.5	6.53			
	Rx1	86	95.6	13.85	106.6	76.3	1.6	74.7	6.56	6.51	6.56	
05	R1	67	100.2	10.6	96	86.2	1	85.2	5.78			+29.3
	R2	60	92.5	10.8	96.1	89.9	1.4	88.5	5.39			
	Rx1	82	105.5	13.1	118.6	88	1	87	7.22	5.58	7.22	
07	R1	75	89.7	9.4	61.5	50.4	1.73	48.6	3.78			+31.7
	R2	76	87.4	8.4	62.5	51.62	2.21	49.41	3.92			
	Rx1	110	94.3	10.8	73.3	46.1	4.26	41.85	5.07	3.85	5.07	
08	R1	57	90.6	8.2	70.6	80.7	1.3	79.5	4.60			-6.9
	R2	61	82.3	7.1	61.5	69.3	5.8	63.5	4.23			
	Rx1	69	86.3	7.9	66.5	59.5	4.1	55.4	4.11	4.41	4.11	
09	R1	75	118.7	10.1	60.5	46.6	1.3	45.2	3.50			-0.55
	R2	80	113.7	10	62.5	47.8	1.1	46.7	3.82			
	Rx1	102	112.9	10.5	60.5	36.4	1.6	34.9	3.71	3.66	3.71	
10	N/A	N/A	N/A	N/A	N/A	N/A	N/A	N/A	N/A	N/A	N/A	N/A
11										5.37	7.91	+47.3
12										5.2	4.9	-5.77

CO – Cardiac Output (litres/min). CO data extracted by Dr Tarun Mittal. R1 and R2 - baseline studies 1 and 2. Rx1 - examination 4h after 1st dose of CA4P. N/A – Patient not scanned. CO – Cardiac Output, measured in litres/min

Figure 5.2 – Cardiac Output Changes Following CA4P

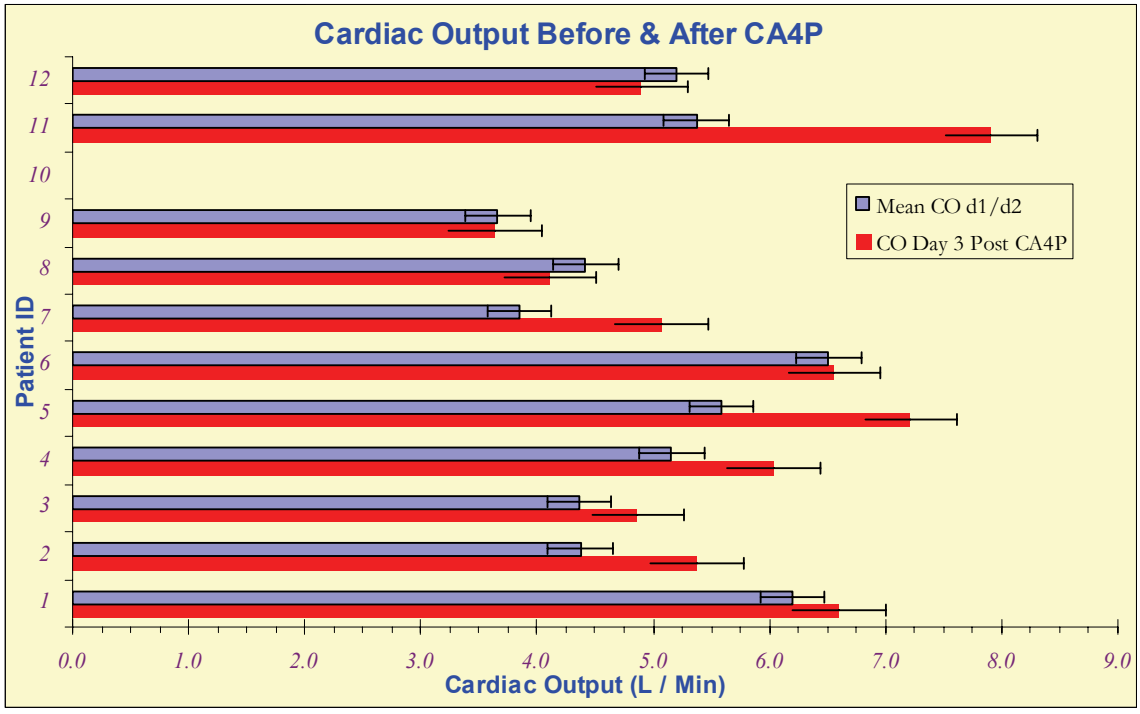

Bars show group standard error of the mean, p=0.026 significant increase in CO following CA4P using HR data from the vital signs table (2-tailed t-test). Using the population average HR instead, p=0.039. CO calculated from HR multiplied by net forward SV divided by 1000 giving CO units of litres/min for patients 1 - 12.

Discussion

Taking all eleven cases as a cohort there was a statistically significant rise in systemic CO 4h following CA4P. The statistical significance was maintained no matter which method was used to estimate the missing HR data (A5B7 CRF at 4hrs post CA4P or group mean).

Interestingly, patients 8, 9 and 12, who experienced small falls in CO following CA4P were all treated with the higher 54mg/m^2 dose, which has been shown to have a greater effect on tumour vasculature (**Chapter 3, Figure 3.3,** (Galbraith et al.,2003)). As CA4P dose increases towards the maximum tolerated (~70mg/m^2) there may be a greater effect on systemic vasculature leading to the DLTs experienced (cerebellar ataxia, cardiac ischaemia) (Tozer et al.,1999).

Following CA4P a significant fall in HR is seen, most prominent at 1h (**Figure 5.3**) (Rustin GJ 2005) as BP increases. After 4h there is overcompensation with a corresponding increase in HR and fall in BP. All vital signs normalise by 24h (Rustin et al.,2003). The CO rise 4h post-CA4P may reflect the rise in HR seen at this time, without a corresponding decrease in SV. In the UK Phase I CA4P study (Rustin et al.,2003), mean BP increase at doses ≥52 mg/m^2 was 8–10% over the first hour followed by a mean BP decrease of 6–7% at 4h. Microtubule depolymerisation is known to affect vasomotor tone and total peripheral resistance. So although CA4P has effects on the systemic vasculature at four hours the reductions seen in MRI kinetic variables are unlikely to be mediated directly by these systemic effects.

Figure 5.3 – Change in Vital Signs Following CA4P. From the UKCTC-207 study (**Chapter 6**) (Rustin GJ 2005) There is a fall in HR of mean 7 bpm 1h post CA4P with a corresponding increase in mean heart rate of 9 bpm above baseline at 4h. The BP changes are the opposite, with a rise at 1h and corresponding falls at 4h.

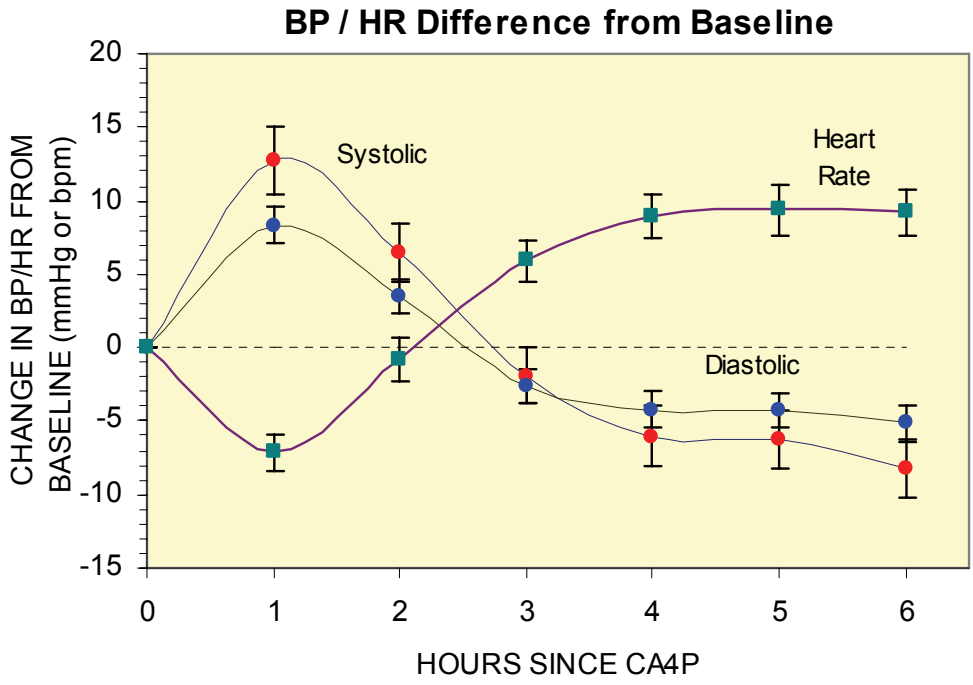

Galbraith reported that HR dropped during MRI whilst during PET it increased and suggested that the effects on CO at the examination times in the PET and DCE-MRI studies may therefore have been different. There was no reduction in SV seen in the PET study, indicating that the observed changes in HR were reflected in the CO change (Galbraith et al.,2003). Anderson et al reported that at doses of CA4P above 40mg/m^2 BP was significantly increased within the first hour after infusion and was associated with a decreased HR but no change in SV. However, this coincided with a significant decrease in CO demonstrated by PET (Anderson et al.,2003). There was no significant difference in CO pre-CA4P administration versus 24h post-CA4P. However, the rapid 10% decrease in CO to all tissues most likely results from increased peripheral vascular resistance caused by CA4P.

There is an apparent paradox, with conflicting data as to the degree and nature of CO change following CA4P. Our study has helped resolve this issue, although the full

explanation is likely to be a combination of differing time points and measurement techniques. We would like to perform CO measurement 1h post CA4P to determine if the HR drop at 1h also corresponds to a decrease in CO.

The effects of 10mg/kg CA4P on mean arterial BP and blood flow rate to the p22 rat carcinosarcoma and selected normal tissues have been measured (Prise et al.,2002; Tozer,2003). Blood flow rate was measured using the tissue uptake of radiolabelled iodo-antipyrine. Comparison of MABP and skeletal muscle blood flow results suggested that the initial hypertensive effect of CA4P was due to vasoconstriction in muscle. CA4P caused a 100-fold decrease in blood flow to tumour, with a much smaller reduction in blood flow to spleen, skeletal muscle and brain. No significant reduction was observed in heart, kidney and intestine (Tozer et al.,1999). Data such as these clearly demonstrate the potential of CA4P for selective tumour vascular shutdown, and there may be tissue specific differences in CA4P vascular response. CA4P exerts its anti-vascular effect preferentially on tumour vessels which are structurally and phenotypically very different to normal vessels (Gaya & Rustin,2005).

The alteration in tumour blood flow following CA4P is much greater than that seen with drugs affecting systemic haemodynamics. Limited changes in tumour blood flow in rats have been seen with hypertensive agents such as angiotensin II (Tozer & Shaffi,1993), but only at doses that caused much larger changes in systemic BP and HR than CA4P. Also, larger reductions were seen in normal tissue blood flow. Reduced tumour blood flow has also been observed after treatment with high doses of the vasodilator hydralazine (Horsman et al.,1992), which reduced systemic BP by 50%.

Conclusion

This new MRI CO data clarifies the central effects of CA4P at the 4h time point becaue it shows that any early (approximately 30-60 mins) decreases in CO (as noted by the PET data) are reversed by 4h.

References

Anderson, H.L., Yap, J.T., Miller, M.P., et al (2003). Assessment of pharmacodynamic vascular response in a phase I trial of CA4P. *J Clin Oncol*, **21,** 2823-30.

Diddier, D., Ratib, O., Lerch, R. et al (2000). Detection and quantification of valvular heart disease with dynamic cardiac MR imaging. *Radiographics*, **20,** 1279 - 1299.

Galbraith, S.M., Maxwell, R.J., Lodge, M.A., et al (2003). CA4P has tumor antivascular activity in rat and man as demonstrated by dynamic MRI. *J Clin Oncol*, **21,** 2831-42.

Gaya, A.M. Rustin, G.J. (2005). VDAs: a new class of drug in cancer therapy. *Clin Oncol (R Coll Radiol)*, **17,** 277-90.

Higgins , C.B., Caputo, G., Wendland, M.F. et al (1992). Measurement of blood flow and perfusion in the cardiovascular system. *Invest Radiol*, **27,** 66 - 71.

Horsman, M.R., Christensen, K.L. Overgaard, J. (1992). Relationship between the hydralazine-induced changes in murine tumor blood supply and mouse blood pressure. *Int J Radiat Oncol Biol Phys*, **22,** 455-8.

Mohiaddin, R.H. Pennell, D.J. (1998). MR blood flow measurement: clinical application in the heart and circulation. *Cardiol Clin*, **16**.

Prise, V.E., Honess, D.J., Stratford, M.R., et al (2002). The vascular response of tumor and normal tissues in the rat to the VDA CA4P, at clinically relevant doses. *Int J Oncol*, **21,** 717-26.

Rustin, G.J., Galbraith, S.M., Anderson, H., et al (2003). Phase I clinical trial of weekly CA4P: clinical and pharmacokinetic results. *J Clin Oncol*, **21,** 2815-22.

Rustin GJ , N.P., Boxall J, Saunders L, et al (2005). A Phase Ib Trial Of CA4P With Carboplatin/Paclitaxel Chemotherapy In Patients With Advanced Cancer. *Proc ASCO*, **Abstract 3103**.

Tozer, G.M. (2003). Measuring tumour vascular response to antivascular and antiangiogenic drugs. *Br J Radiol*, **76 Spec No 1,** S23-35.

Tozer, G.M., Prise, V.E., Wilson, J., et al (1999). CA4P as a tumour VDA: early effects in tumors and normal tissues. *Cancer Res*, **59,** 1626-34.

Tozer, G.M. Shaffi, K.M. (1993). Modification of tumour blood flow using the hypertensive agent, angiotensin II. *Br J Cancer*, **67,** 981-8.

Chapter 6

A Phase Ib trial of CA4P in Combination with Carboplatin and/or Paclitaxel Chemotherapy in Patients with Advanced Cancer (UKCTC-207)

Abstract

Animal studies confirm the VDA CA4P has increased activity combined with conventional anti-cancer therapies. We describe a Phase Ib dose escalation trial in patients with advanced cancer, to establish the optimal schedule, DLT, MTD and recommended Phase II dose(RP2D) of combining CA4P with carboplatin and/or paclitaxel, and gather preliminary data on anti-tumour efficacy. On day one of each 21-day cycle patients received CA4P over 10min escalating from 27 – 72mg/m^2, followed twenty hours later by either a 60min infusion of carboplatin AUC 4-5 and/or a 3hr infusion of paclitaxel (135 – 175mg/m^2). Forty six patients received 179 cycles of treatment. Mean age was 58(24–77) with 28 females and 18 males. The most frequent primary tumour sites were ovarian(18), melanoma(6), colorectal(5), renal(5), and lung(3). WHO PS at study entry was 0(13), 1(27), and 2(6). Most patients were heavily pre-treated with chemotherapy. Pharmacokinetic data confirmed no delayed excretion of cytotoxic drug following CA4P and changes in vital signs were similar to previous CA4P studies. Side effects of CA4P were mild, mainly CTC grade 1 fatigue, tumour pain, flushing, pruritis, headache and hypertension. Haematological toxicity was mild in contrast to a previous study due to cytotoxic administration following renal recovery from the CA4P effect. DLT was cerebellar ataxia at 72mg/m^2 CA4P. The MTD and RP2D are 63mg/m^2 CA4P, carboplatin AUC5 and paclitaxel 175mg/m^2. Overall RECIST assessment showed 16%PR, 54%SD and 30%PD. Of 18 patients with ovarian cancer, half had a Ca125 response >50%. Of 13 RECIST assessable ovarian patients there were 3PR and 6SD. Of five platinum resistant ovarian patients there were two cases of RECIST SD and one Ca125 response. The triplet combination is now being studied in a Phase II trial for platinum resistant ovarian cancer.

Introduction

Phase I trials of CA4P have demonstrated minimal single agent activity, and have confirmed that it has vascular disruptive activity according to dynamic contrast MRI and PET imaging (Anderson et al., 2003; Dowlati et al., 2002; Galbraith et al., 2003; Rustin et al., 2003; Stevenson et al., 2003). DLT's were seen above 60mg/m^2. Enhanced activity was seen when CA4P was combined with chemotherapy or radiotherapy in animal studies (Chaplin & Dougherty, 1999; Grosios et al., 2000; Wildiers et al., 2004). CA4P had greatest effect on the tumour core whilst conventional therapy was active against the tumour rim.

Following ethics committee approval we embarked on a Phase I study of CA4P+carboplatin and CA4P+paclitaxel, progressing to assessment of the triplet combination.

Methods

Study Objectives

1) To establish the optimal schedule, DLT, MTD and RP2D of combining CA4P with carboplatin, paclitaxel, or both.
2) To gather preliminary data on anti-tumour efficacy of the combinations.

Patient selection

Patients with histological confirmation of cancer, not amenable to standard therapy or refractory to conventional therapy were eligible for this study. Other eligibility requirements included having RECIST measurable disease or being evaluable by serial Ca125 measurements; WHO performance status 0-2; life expectancy ≥4 months; age ≥18 years; adequate bone marrow function with: a) neutrophil count >1500 cells/mm^3; b) Platelet count >100,000 cells/mm^3; adequate hepatic function: a) total bilirubin <1.5mg/dl, b) ALT and AST <2.5x upper limit of normal; adequate renal function with glomerular filtration rate measured by EDTA clearance ≥50ml/min; on no other anti-cancer therapy for 4 weeks; no active concurrent malignancies except cone biopsied in situ carcinoma of cervix, or adequately treated basal or squamous carcinoma of skin.

Patients were excluded if they had brain metastases, serious infection or other non-malignant illness, ≥grade 2 neuropathy, major surgery within 4 weeks, prior radical radiotherapy or evidence of vascular damage from radiotherapy, a history of peripheral or cardiovascular disease or arrhythmias, uncontrolled hypertension, or on anticoagulation apart from low dose warfarin for maintenance of central line patency.

Study Design

This was an open label phase I dose-escalation trial. The study was conducted at three sites – Mount Vernon Hospital, UK; The Churchill Hospital, Oxford, UK; and the Henry Ford Hospital, Detroit, Michigan, USA. The study was approved by participating hospitals' ethical review boards, and all enrolled patients provided written informed consent.

Entry into the treatment arms was non-randomised and left to the clinician's discretion. This ensured the most appropriate treatment given the type of cancer, therapeutic history and potential side-effect profile was offered to each patient, although statistically an element of bias was introduced. The starting dose levels were chosen approximately 20 - 25% below accepted single agent doses for the cytotoxic agents – i.e. Carboplatin AUC4, and Paclitaxel 135 mg/m^2. For CA4P, 45 mg/m^2 was felt to be the lowest dose that had a reasonable chance of activity in combination with cytotoxic agents. In the carboplatin arm, the starting CA4P dose level was 20% below this at 36 mg/m^2 and in the paclitaxel arm 40% below at 27 mg/m^2 (because of the increased haematological toxicity expected in this arm). The likelihood of significant interactions between CA4P and the cytotoxic agents was however felt to be low on the basis of previous combination studies (see Chapter 1).

Treatment was administered on an inpatient basis and repeated every 21 days. Patients continued to receive treatment until disease progression was documented or to a maximum of 6 cycles or until other withdrawal criteria were met. In the absence of DLT in one patient, up to 5 patients were treated at each dose level. Subsequent dose levels were not opened until three patients at the previous dose level had completed administration of course 2. Once the MTD was defined in 3 patients with carboplatin and three patients with paclitaxel, the MTD dose of CA4P was assessed in combination

with both paclitaxel and carboplatin. Adverse events were the primary study endpoint. All patients who received any study drug were evaluable for safety. Adverse events and other symptoms were graded according to the NCI CTC v3.0.

Treatment Administration

CA4P was supplied as a sterile lyophilized cake in amber glass vials containing 90mg of CA4P as free acid with 10% additional overfill. The drug was reconstituted with 10ml of sterile water for injection and further diluted with 100-150ml of normal saline. The carboplatin and paclitaxel were prepared from commercially available vials containing sterile aqueous solution, which was diluted with 500mL of 5% dextrose and 500mL normal saline respectively.

On Day 1 of each 21-day cycle, patients received a 10min infusion of CA4P. Routine pre-medication was not mandatory but if significant toxicity occurred with the first cycle pre-medication with dexamethasone 8mg IV and metaclopramide 10mg IV was suggested prior to subsequent cycles. If systolic blood pressure was >180mmHg on two readings following CA4P glyceryl trinitrate 0.3mg was given sublingually or amlodipine 10mg orally. On Day 2, 18-22 hours after the CA4P, patients received a 60-minute infusion of carboplatin or a 3h infusion of paclitaxel. This scheduling was chosen on the basis of the significant toxicity seen in Bilenker's study (Bilenker JH 2003). Providing no DLT occurred in any of the three patients per cohort, doses were increased as shown in **Table 6.1**. Once it had been ascertained that no DLTs were seen at a CA4P dose of 54mg/m^2 (above the threshold dose for CA4P activity from previous studies) in either of the doublet arms, patients were then treated with the triplet combination at doses shown in **Table 6.1**. If a DLT was seen three additional patients could be recruited to that dose level. The triplet consisted of CA4P on day 1, followed 18-22 hours later by a 3h infusion of paclitaxel then a 60-minute infusion of carboplatin.

Dose Limiting Toxicities

DLT was defined as any of the following events, considered to be probably or definitely related to combination study therapy: QTc prolongation ≥500 ms, >Grade 2 ventricular arrhythmia, grade 3/4 non-haematologic toxicity (except: fatigue/asthenia, nausea and/or vomiting), toxicity resulting in treatment delay >14 days, absolute neutrophil

count <500 cells/mm^3 for >5 consecutive days or febrile neutropenia with neutrophil count <1000 cells/mm^3, thrombocytopenia <25,000 cells/mm^3 or bleeding episode requiring platelet transfusion, grade 2 or worse neuropathy which did not recover to grade 1 within 14 days after scheduled re-treatment, or any grade toxicity requiring patient removal from the study in the judgement of investigators.

The MTD was defined as the maximum dose level of CA4P, administered in combination with carboplatin and paclitaxel, at which one or fewer patients experienced a DLT. The dose level below that at which one or more DLTs were seen was expanded to 6 patients and if no DLT's were seen became the RP2D.

Treatment Assessment

Upon enrolment in the study, patients underwent a complete medical history, physical examination and biochemical assessment. Thereafter, laboratory assessments were performed weekly. Tumour evaluations were done at screening and then every two cycles. Criteria for response were based on RECIST and response of Ca125 was based on definitions agreed by the Gynaecologic Cancer Intergroup (Rustin, 2003; Therasse et al., 2000). Patients were removed from the study on disease progression.

Table 6.1a - Dose Escalation Schedule for CA4P/Carboplatin

Dose Level	CA4P(free acid dose) mg/m²	Carboplatin AUC
1	36	4
2	45	
3		5
4	54	

Table 6.1b - Dose Escalation Schedule for CA4P/Paclitaxel

Dose Level	CA4P (free acid dose) mg/m²	Paclitaxel Dose mg/m²
1	27	135
2		175
3	36	
4	45	
5	54	

Table 6.1c - Dose Escalation Schedule for CA4P/Carboplatin/Paclitaxel

Dose Level	CA4P(free acid dose) mg/m²	Carboplatin AUC	Paclitaxel Dose mg/m²
1	54	5	175
2	63		
3	72		

* The last three subjects treated at MTD continued into the Phase II study.

Study Procedures and Observations

Full blood count, biochemistry profile, adverse event assessment, performance status, physical examination, and vital signs were all performed prior to drug administration. Post CA4P, vital signs (HR,BP, temperature, respiratory rate) were obtained at 1, 2, 3, 4, 5 and 6h for all cycles. On Day 1 of each cycle, three pre-treatment ECGs were obtained at least 5min apart. ECGs were obtained post-administration of CA4P at the following time points: 1, 2, 3, 4, 5 and 6h for cycles 1/2; and 2 and 4 hours for subsequent cycles. If no abnormalities in the QTc interval were present after 4 cycles, monitoring was reduced to one pre-treatment, one at one hour post-treatment and two hours post-treatment.

End-of-Study Assessments

To ensure that drug-related adverse events had resolved, the following assessments were performed at least 30 days after the final dose of study drug for all patients: Performance

status; physical examination; weight; vital signs; full blood count; biochemical profile; urinalysis; ECG; adverse event analysis.

Pharmacokinetic analyses

Plasma samples were taken for carboplatin or paclitaxel pharmacokinetics at the following time points, to assess whether excretion of cytotoxic was delayed by the administration of CA4P: at the start and end of the CA4P infusion; prior to cytotoxic drug infusion; for carboplatin, samples were also taken 5min prior to the end of the 60min infusion & 1, 2 & 4 hours post infusion; for paclitaxel, samples were also taken halfway through and at the end of the 3h infusion & ½, 1, 2 & 3 hours post infusion. Urine collections for carboplatin pharmacokinetics were performed from 0–3h, 3–6h and 6–30h from the start of carboplatin infusion.

Results

Between 27/6/03 and 1/11/05 46 patients were enrolled. Median age was 58 (range 24-77). There were 28 females and 18 males and their tumour types are listed in **Table 6.2**. ECOG performance status at study entry was 0 (13), 1 (27), 2 (6). A total of 179 cycles were given to 46 patients, with 15 completing all 6 cycles. Seventeen withdrew due to tumour progression, 3 due to early death, 5 because of toxicity and 6 for other reasons. Patients' previous cancer treatment is illustrated in **Table 6.3**, and the sites and measurements of marker lesions in **Table 6.4**. Patient responses to treatment are illustrated in **Tables 6.5 – 6.7**.

Table 6.2 – Subject Details

Primary Tumour Origin	Number Of Patients
Ovary	17
Melanoma	6
Colorectal	5
Renal	5
Lung	3
Oesophagus	2
Thyroid	2
GIST	1
Neuroendocrine	1
Cholangiocarcinoma	1
Leiomyosarcoma Uterus	1
Testicular	1
Fallopian Tube	1

N=46

Table 6.3 – Subjects' Previous Cancer Treatment

Trial No.	Treatment History Prior To Study
01	TAH+BSO 10/00, Carbox4,Docetaxel/Gemcitabine x 4 11/00-5/01 (SCOTROC2), cisplatin+etoposide 11/01, caelyx 12/02
02	Docetaxel+Carbo 5/00, Carbo 4/02-6/02, Cisplat+Etoposide 9/02-10/02, Altretamine 7/01-11/02, etoposide 11/02-1/03
03	TAH+BSO+Omentectomy 6/99, Carboplatin x2 Taxol x2 Topotecan x2 7/99-12/99 (sequential trial), Taxol/carbo 1/01-5/01, Carboplatin/taxotere 10/02-2/03
04	Carbo x4 12/01-3/02, taxol x6 4/02-7/02, Tamoxifen 7/02-9/02, cisplatin + etoposide 9/02-11/02, etoposide 12/02, talc pleurodesis 1/03, caelyx 2/03 - 3/03, Gem/carbo 3/03 - 6/03
05	TAH+BSO+Oment 11/97, Carbox5 3/99-7/99, carbo x 6 10/01-1/02, biliary stent 4/02, cisplat+etoposide 5/02-6/02, etoposide 7/02-8/02
06	BSO+ Omentectomy 3/01 , Taxol/Carbo 4/01-9/01, Topotecan 9/02-1/03, Carbo 3/03-4/03, Cisplatin 5/03-6/03
07	BSO+Omentectomy 3/02, Carbo x 6 3/02-7/02, Cisplatin+Taxotere x 5 12/02-1/03, Tamoxifen 1/03-9/03
08	Sigmoid colectomy 1/02, 5FU/FA 3/02, Oxaliplatin+de Gramont 3/02 - 8/02, Capecitabine 5/03 - 8/03
09	TAH+BSO+Omentectomy 5/01, Carboplatin x4 & Docetaxel/Gemcitabine x 4 (SCOTROC2) 6/01 - 12/01, Carboplatin 9/02 - 7/03, cisplatin+etoposide 9/03 - 10/03
10	surgery Lt arm 7/99 , Lt axilla dissection 6/02, DTIC 5/03 - 7/03 , BIBF 1120 8/03 - 11/03
11	Gemcitabine + Cisplatin 10/03 - 12/03
12	Oxaliplatin + 5FU 11/99, Rt hemihepatectomy 2/00, de Gramont 4/00 - 9/00, Irinotecan 4/01(stopped), Oxaliplatin 6/01 - 10/01, Xeloda 10/02 - 2/03, Xeloda 8/03 - 1/04
13	BSO+Right Hemicolectomy 4/95, Carboplatin 5/95-9/95, Taxol+Carboplatin 3/96-6/96, TAH 6/96, Hexalen 1/97, Carboplatin 9/97-11/97, Topotecan 6/98-8/98, Cisplatin + Etoposide 11/98 - 1/99, Gemcitabine Carboplatin 11/99-2/00, Taxotere+Carboplatin 6/00-9/00, Caelyx+Carboplatin 5/01-8/01, Tamoxifen 1/02-12/02, Carboplatin 1/03-4/03
14	10/99 Left Orchidectomy, POMACE 11/99-1/00, Para-aortic lymphadenectomy 1/00, TIP 8/02-10/02, thorascopic resection 12/02, etoposide+stem cell harvest +ABMT 2/03, thorascopic resection 8/03, Taxol Gemcitabine Carboplatin 12/03-1/04, thorascopic resection 2/04
15	Right Nephrectomy 9/01, IFN+IL-2+5FU (RE04 trial) 2/03-4/03
16	OEO2 trial Cisplatin/5FU 9/01 – 10/01, Oesophagogastrectomy 11/01, Capecitabine 11/03 - 3/04
17	TAH+BSO 1989, Carboplatin 12/89-4/90, Carboplatin 8/99-11/99, Phase I Tazorotene 10/00-12/00, cisplatin 2/01-3/01, etoposide 2/01-6/01, Taxol 8/02-9/02 , Tamoxifen 12/02-6/04
18	TAH+BSO 4/99, Carboplatin 5/99-8/99, Taxol+Carboplatin 9/03-12/03, Tamoxifen 4/04-8/04
19	Anterior resection 11/01, 5FU+FA 2/02-8/02, Right hepatectomy 12/02, Failed liver resection 6/03, Irinotecan 7/03-11/03, FOLFOX 3/04-6/04
20	7/03 Radiotherapy 20Gy/5#, MVP 6/03-7/03, Gemcitabine+Carboplatin 9/04
21	TAH+BSO 9/03, doxorubicin 1/04, Gemcitabine Taxotere 3/04-6/04
22	imatinib 5/02-11/02, imatinib 3/03-12/03, Phase I trial BIBF1120 4/04-10/04
23	Capecitabine 7/04 - 8/04, de Gramont 9/04 - 11/04
24	BSO+Omentectomy 6/00 , Radiotherapy Para-aortic Nodes 4/04, Carboplatin 8/00-1/01, Etanercept 7/01–10/01 Paclitaxel 11/01 - 3/02, cyclophosphamide, Methotrexate & celecoxib 8/03-2/04
25	London lung Study 12 cisplatin etoposide+/-Thalidomide 7/04-10/04
26	Radiotherapy 1/05
27	excision melanoma right calf 9/04, right groin dissection 10/04, DTIC 12/04-1/05
28	Right nephrectomy+adrenalectomy 5/03, IFN+IL-2+5FU(RE04) 10/03-12/03 , Sorafenib 8/04-1/05
29	Right Radical Nephrectomy/Adrenalectomy 4/04, Interferon alpha 5/04-9/04, Palliative RT 7/04-8/04, Vertebroplasty 1/05, Gemcitabine 9/04-12/04, Tarceva+Bevacizumab 12/04-3/05
30	Oesophagectomy 6/03, Epirubicin cisplatin capecitabine 7/03-9/03, Capecitabine+Mitomycin C 10/04-2/05
31	Nephrectomy 6/04, Interferon 7/04-10/04, Tarceva+Bevacizumab 1/05-3/05
32	Carboplatin/Paclitaxel & Carboplatin/Topotecan 01/03–06/03 , Removal Pelvic Cyst 8/03, Liposomal Doxorubicin 10/04–2/05
33	Hysterectomy 3/97 , Carboplatin x 6 4/97–9/97 , Carboplatin , Liposomal Doxorubicin, Topotecan 11/04
34	Radioactive Iodine 220mCi 1/05
35	TAH+BSO+Omentectomy 10/03 , Gemcitabine+Taxol+Carboplatin 11/03–4/04
36	Laparotomy+peritoneal biopsy, 9/01, Docetaxel+Carboplatin(SCOTROC2 trial) 11/01-5/02, Interval debulking 01/02, Vaginal repair 3/02, Altretamine 12/03-5/04, Cisplatin+Etoposide 8/04-9/04, Caelyx 3/05-4/05

Table 6.3 Continued	
37	12/00 TAH+BSO+Omentectomy, 2/01-5/01 Carboplatin x 5, 8/03 Radiotherapy 45Gy in 15# to Lt hip+femur, 7/04 Pamidronate monthly, 1/04-6/04 Tamoxifen, 6/04-7/04 Altretamine, 8/04-12/04 Carboplatin + Taxol x6
38	Left nephrectomy 9/04, RE04(IFN+IL2+5FU) 10/04-1/05
39	Temozolomide 2/05, High dose Interferon alpha 20MU 4/05-5/05
40	Doxorubicin+Ifosfamide 2/05 , Gemcitabine+Docetaxel 5/05–6/05
41	Wide local excision Nasal Lesion 3/2002, Neck Dissection 8/04, DTIC x2 5/05
42	BSO+Pelvic Clearance 12/04, Carboplatin+Paclitaxel x3 01/05–2/05, Carboplatin+Doxorubicin x3 3/05
43	Excision Left ankle melanoma 4/01, Lt groin recurrence 9/04 +pelvic disease, DTIC x6 cycles 4/05
44	Excision Melanoma 6/03, Right Axillary Dissection 1/05, DTIC+Sorafenib 8/05–9/05
45	Anterior Resection Rectum 3/03, 5FU+FA 5/03–10/03, Partial Hepatectomy+RFA Liver 2/04, Oxaliplatin+Capecitabine 3/04, Oxaliplatin+Capecitabine+Bevacizumab 7/04–10/04 , Capecitabine+Bevacizumab 10/04–11/04, Bevacizumab 11/04–3/05, Further RFA Liver 4/05, Cetuximab 6/05–7/05, Irinotecan+Cetuximab 7/05 , Cetuximab 9/05
46	Gemcitabine+Carboplatin 4/05–7/05 , Thalidomide/Placebo 7/05–10/05

TAH = Total abdominal hysterectomy
BSO = Bilateral salpingo-oophorectomy

Table 6.4 – Sites of Metastatic Disease & Tumour Measurements			
Trial No.	**Primary**	**Site of Metastases**	**Measurement (mm) after 0,2,4,6 cycles Treatment**
01	Ovary	Peritoneum,ascites	N/E
02	Ovary	Nodes,Liver,local	aortocaval node 24mm to 16mm cycle 4
03	Ovary	Peritoneum,Ascites	N/E
04	Ovary(Primary Peritoneal)	peritoneum,nodes,lung,effusion	N/E
05	Ovary	nodes,local(ovary)	Right adnexa 24,27,30,32, Right comm iliac LN 38,36,22,22
06	Ovary	Peritoneum,Mediastinal LN	N/E
07	Ovary	Pleural effusion,pleural,mediastinal LN,liver, pelvic mass,retroperitoneum	pelvic mass 148,152,149,166, retroperitoneal LN 18,18,18,18, Rt Inguinal LN 24,24,28,27
08	Colorectal(sigmoid)	nodes,liver,lung	Left para-aortic 28,32 liver 173,179 liver 42,55 liver 50,59
09	Ovary	nodes,effusion,ascites,peritoneum	N/E
10	melanoma	nodes,lung,skin,soft tissue	Right SCF 50,49,55 s/c lesion 1 38,32,40 lesion 2 42,52,56, lesion 3 71,70,72. Right lower lobe lung met 20,20,20
11	Cholangiocarcinoma	Liver	liver 85,90
12	Colorectal(sigmoid)	Liver,Lung,nodes,peritoneum	liver met 120,131, para-aortic LN 20,20
13	Ovary	liver	liver 20,17
14	Testicle(Teratoma)	nodes,liver,lung	Right Internal Iliac 35,72
15	Renal	local,nodes(Left SCF),ascites	Left SCF 52,55,41,34 Retroperitoneal node 65,74,75,76 Right renal bed 72,82,81,98 Right external iliac node 54,58,54,58 Right paracolic mass 65,67,67,73
16	Oesophagus	Supraclavicular fossa(SCF) mass,liver	Right SCF 37,42,42 Liver metastasis 90,92,87
17	Ovary	local,pleural effusion,peritoneum,soft tissue,ascites	Abdominal wall nodule 60,67
18	Ovary	local+nodes	vaginal vault mass 27,24,27 Right external iliac 19,19,17 aortocaval node 18,17,13
19	Colorectal(Rectum)	Lung,Liver,para-aortic LN	liver 27, 65
20	NSCLC	Primary	No RECIST assessments
21	Uterus (Leiomyosarcoma)	primary,lung	pelvic mass 145, lung 18
22	GIST	liver,peritoneum,ascites,pleural effusion	liver 104, 55
23	Colorectal(sigmoid)	primary,nodes,lung,liver	liver 55,60,67 liver 30,31,31, small lung mets
24	Ovary	local+nodes	N/E Off Study

25	SCLC	Right upper lobe,Right hilum,liver,lung	Right lung mass 50,25
26	Thyroid(Anaplastic)	Primary,Nodes,Lung	Thyroid tumour 90mm, tiny lung mets
27	melanoma	Left SCF,retrocrural node	Left SCF 45,44 Retrocrural 35,35
28	Renal	Mediastinal node,lung,liver	Precarinal 32,35 subcarinal LN 57,58 adrenal met 25,30
29	Renal	local+regional nodes,lung,liver,bone	N/A
30	Oesophagus	subcarinal node,lung,liver,spleen,primary	subcarinal 42,32, spleen 72,35, liver 72,40, liver 80,58,
31	Renal	Lung,Liver	N/A
32	Ovary	Liver,Nodes	N/A
33	Ovary	Effusion ,Ascites,GI	N/A
34	Thyroid(Papillary)	Lung,Pleural effusion	N/A
35	Ovary	N/A	N/A
36	Ovary	GI,Nodes	pelvic mass 110, 90 peritoneal mass 28,24
37	Ovary	Lung,Bone,Nodes	Right lung met 58,53 Left lung met 69,44 Right pelvic LN 38,36
38	Renal	liver,pleural nodule,hilar,(Brain)	Right pleural nodule 35,37,36 Liver 18,10,10
39	melanoma	Lung,Liver,Skin,Soft Tissue,Nodes	N/A
40	Soft Tissue Sarcoma	Lung	N/A
41	melanoma	Liver,Lung,Nodes	Right paratracheal node 25 ,Left lower lobe nodule 38 ,Right lobe liver 91
42	Ovary(MMMT)	Pelvic mass	Pelvic mass 60,135,135 & 20,48,35
43	Melanoma	paracardiac nodes,pleural,retroperitoneal, common iliac,internal+external iliac	Left external iliac nodal mass 120,
44	melanoma	Right SCF,Liver,Right adrenal	Right SCF 30,8,7,0 liver met 20,17,9,0 Right adrenal 48,40,45,48
45	Colorectal(rectum)	Liver,Nodes	N/A
46	NSCLC(large cell)	Lung primary,hilar nodes	Lung primary 85,80,65,61 left hilar node 45,45,37,40

N/E – Not Evaluable by RECIST criteria N/A – Information not available from database at time of writing

Table 6.5 – Subjects' Response

Trial No.	Arm	Cohort	No. Cycles	Clinical Improvement	RECIST Best Response*	Ca125 Response (>50%)**
01	Carbo	1	6	Yes	N/E(SD)	Yes 585,226,68,85,97,88
02	Taxol	1	6	Yes	PR	Yes 268,156,149,85,82,79
03	Taxol	1	1	No	N/E(PD)	No 297,48
04	Taxol	1	3	No	PD	No 5976,7038
05	Taxol	1	6	Yes	SD	Yes 1879,1395,845,862,680,514
06	Taxol	2	4	No	N/E(PD)	Yes 852,428,483,190
07	Carbo	1	6	Yes	SD	No 576,423,417,367,527,811
08	Carbo	1	2	No	SD	N/A
09	Taxol	2	5	No	N/E(SD)	Yes 1222,380,196,130,149,121
10	Carbo	2	4	Yes	PD	N/A
11	Taxol	2	2	No	SD	N/A
12	Carbo	2	2	No	PD	N/A
13	Carbo	2	2	No	SD	No 289,461,355
14	Carbo	3	2	No	PD	N/A
15	Carbo	3	6	Yes	SD	N/A
16	Taxol	3	4	No	SD	N/A
17	Carbo	3	3	No	SD	No 1581,1409,1268,1085
18	Taxol	3	6	Yes	SD	Yes 1499,488,323,282,323,469,766
19	Taxol	3	1	No	N/E	N/A
20	Taxol	4	4	No	SD	N/A
21	Carbo	4	1	No	N/E(PD)	N/A
22	Taxol	4	1	No	N/E(PD)	N/A
23	Carbo	4	6	Yes	SD	N/A
24	Taxol	5	1	No	N/E	No 129,123
25	Taxol	4	4	Yes	PR	N/A
26	Taxol	4	2	No	PD	N/A
27	Taxol	5	2	Yes	PD	N/A
28	Carbo	4	3	No	SD	N/A
29	Carbo	4	1	No	N/E	N/A
30	Taxol	5	6	Yes	PR	N/A
31	Taxol	5	6	No	SD	N/A
32	Carbo	4	6	Yes	PR	No 294,248,259,404,591,875,1101
33	Taxol	5	4	No	PD	Yes 2759,2247,1280,967,466,367,254
34	Carbo	4	5	Yes	SD	N/A
35	Triplet	1	6	Yes	PR	Yes 1080,1139,1257,325,97, 56, 39
36	Triplet	1	6	Yes	SD	Yes 1008,874,587,449,449,308
37	Triplet	1	6	Yes	PD	No 269,280,456, 501,530,551
38	Triplet	1	5	No	SD	N/A
39	Triplet	2	2	No	PD	N/A
40	Triplet	2	6	No	SD	N/A
41	Triplet	2	6	Yes	SD	N/A
42	Triplet	3	4	No	PD	N/A
43	Triplet	3	2	No	SD	N/A
44	Triplet	2	6	Yes	PR	N/A
45	Triplet	2	2	No	PD	N/A
46	Triplet	2	6	Yes	SD	N/A

* PD–Progressive disease, SD–Stable disease. PR–Partial response. N/A –Not applicable (non ovarian)
** Value prior to each cycle of treatment

Table 6.6 – Response In 18 Ovarian Cancer Patients

Patient ID	Number Of Previous Treatment Regimens (Surgery, Radiation, Chemotherapy)	Platinum Response Status (Sensitive / Resistant)	RECIST Best Response*	GCIG Ca125 Response (>50%)*
01	4	S	-	Yes
02	5	S	PR	Yes
03	4	S	-	No
04	7	R	PD	No
05	5	S	SD	Yes
06	5	S	-	Yes
07	4	R	SD	No
09	4	R	-	Yes
13	13	R	SD	No
17	8	S	SD	No
18	4	S	SD	Yes
24	6	S	-	No
32	2	S	PR	No
33	3	S	PD	Yes
35	2	S	PR	Yes
36	5	S	SD	Yes
37	7	S	PD	No
42	3	R	PD	-

* Patients Not Evaluable signified by "-"

Table 6.7 - RECIST Best Response Summary

Response	Number Pts	% Evaluable Pts	% Clinical Improvement	Site of Response
N/E	9	-	11%(1/9)	
CR	0	0%	-	
PR	6	16%	100%(6/6)	02(Ca ovary) – aortocaval node 25(SCLC) – Right lung 30(Ca oesophagus) – Splenic metastasis, liver metastases 32(ca ovary) 35(ca ovary) 44(melanoma) – Right SCF, liver, adrenal
SD	20	54%	45%(9/20)	
PD	11	30%	27%(3/11)	

Vital Signs

The following **Figures 6.1 – 6.9** illustrate the changes observed in patients' vital signs following infusion of CA4P.

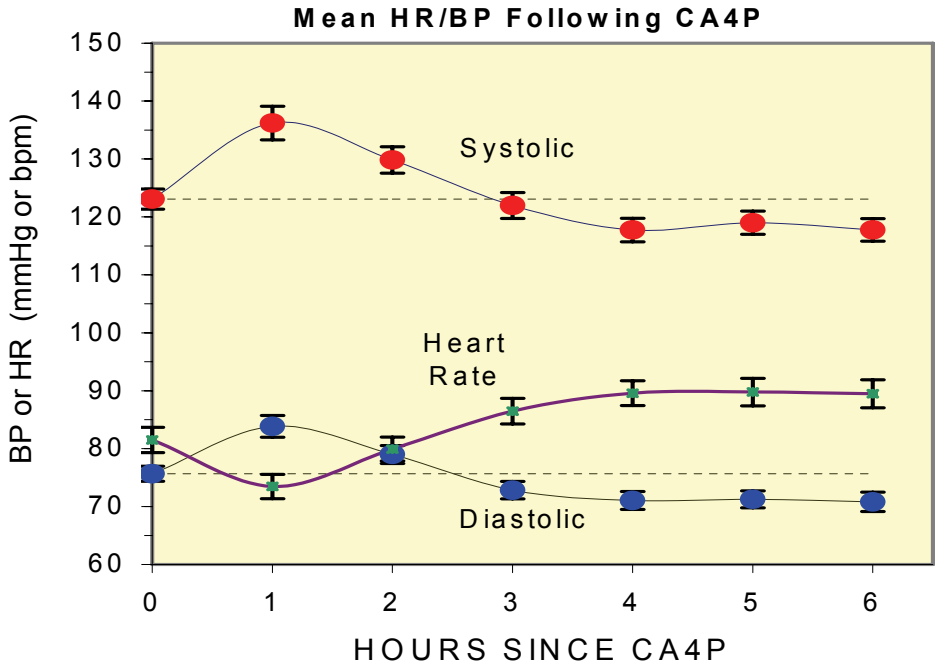

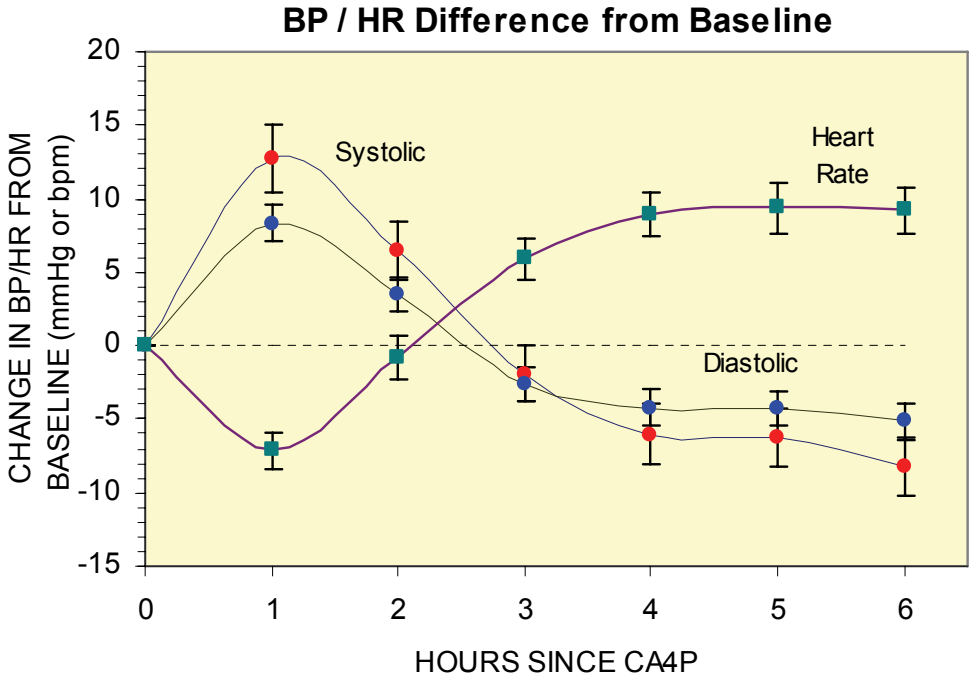

Figures 6.1 & 6.2 - Change In Mean Vital Signs Following CA4P Infusion

Mean±Standard Error. Dotted line – Mean baseline value. Significant rise in BP and fall in HR is seen after an hour due to alterations in peripheral resistance, with a corresponding increase in heart rate at 3 – 4 hrs as BP falls. Change in systolic BP at 1hr from baseline $2p<0.000001$ (2-sided group t-test)

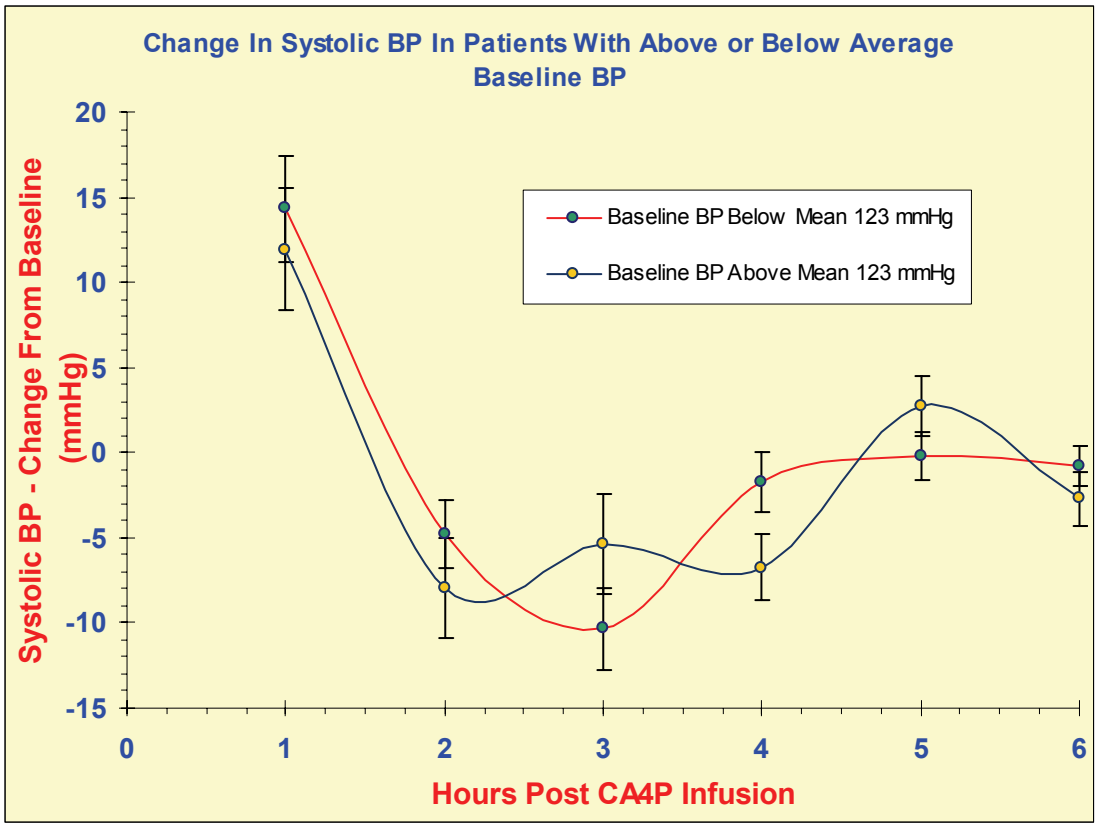

Figure 6.3

BP Change Following CA4P (Patients with Baseline BP Above/Below Mean)

Mean±SE, p=ns. Patients with baseline BP above average are not more prone to alterations in BP following CA4P infusion. Those with below average baseline BP appear to have greater fluctuation in BP following CA4P infusion. Thanks to Gavin Shreeves, data manager, for assistance in producing this data.

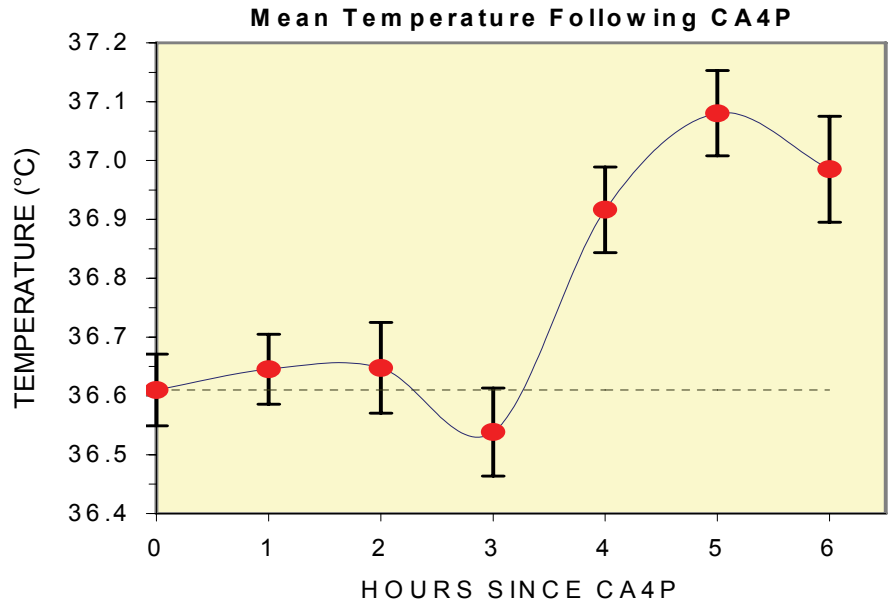

Figure 6.4 - Mean Temperature Following CA4P Infusion

Mean±SE. Dotted line – mean baseline value. At 6hrs from baseline, 2p=0.00005 (2-sided group t-test)

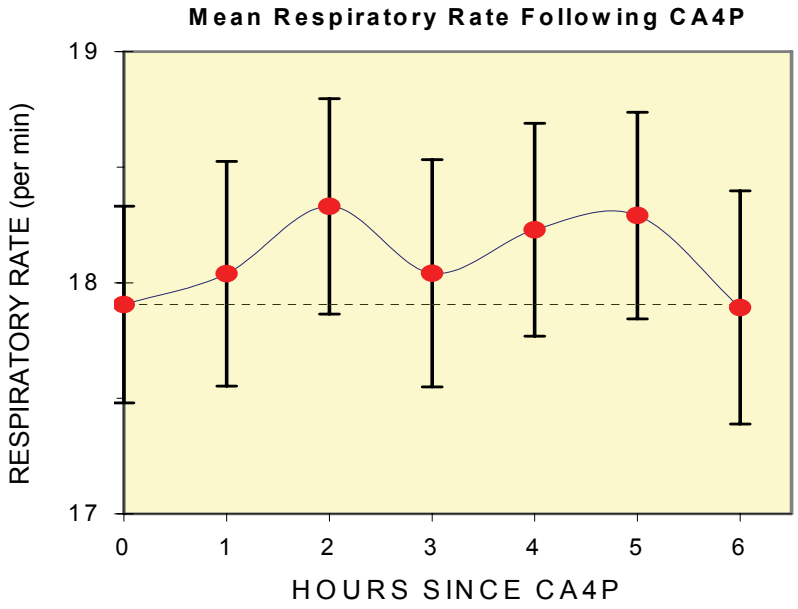

Figure 6.5 - Mean Respiratory Rate Following CA4P Infusion

Mean±SE. No significant changes seen.

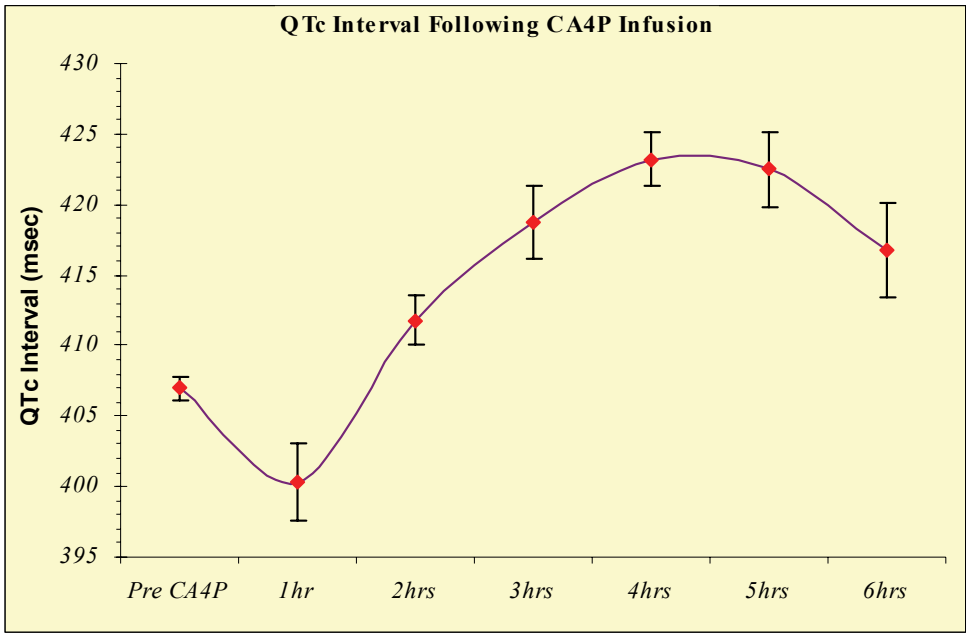

Figure 6.6 - Mean QTc Interval Following CA4P Infusion

Mean±SE. Significant prolongation of QTc Interval seen 4 hrs following CA4P infusion (within the normal range) 2p<0.0000001 (2-sided group t-test)

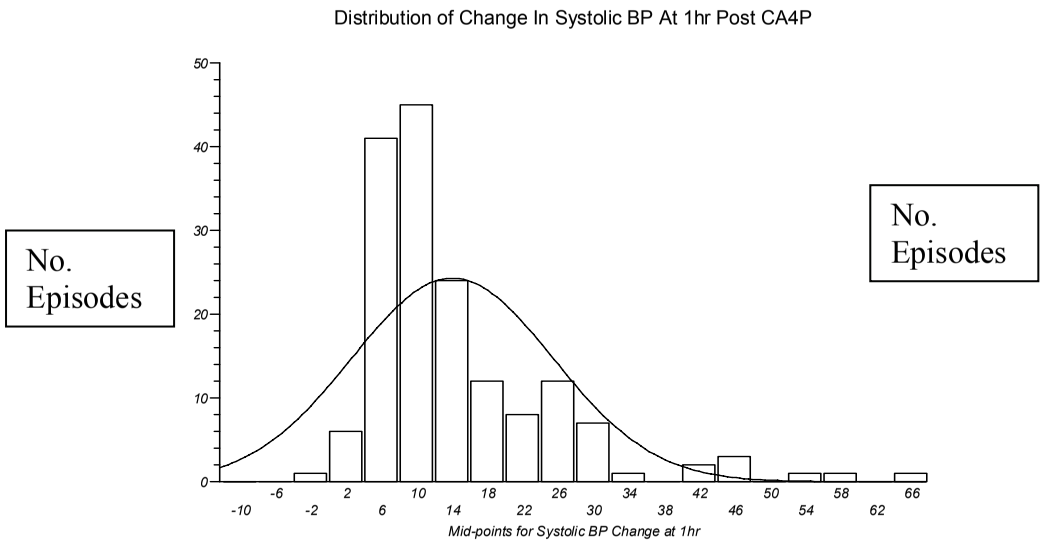

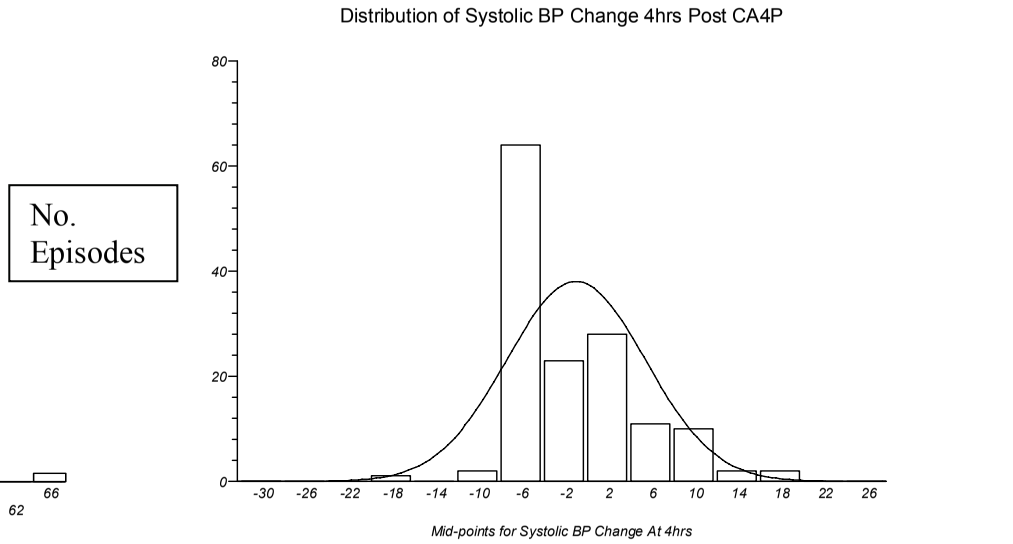

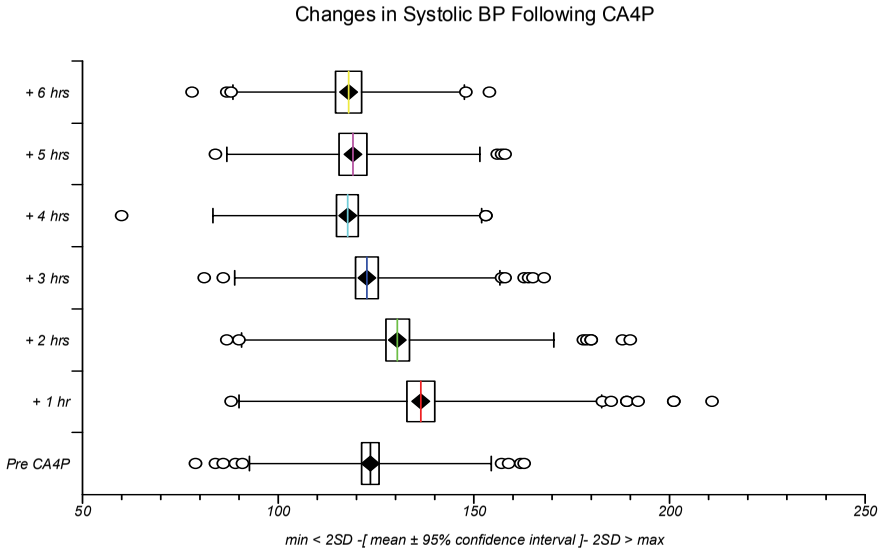

Fig 6.7 a,b,c Histogram plots (a,b) and 'Box & Whisker' plot (c) of the distribution of change (mmHg) in systolic BP following CA4P infusion. Coloured line represents the mean value.

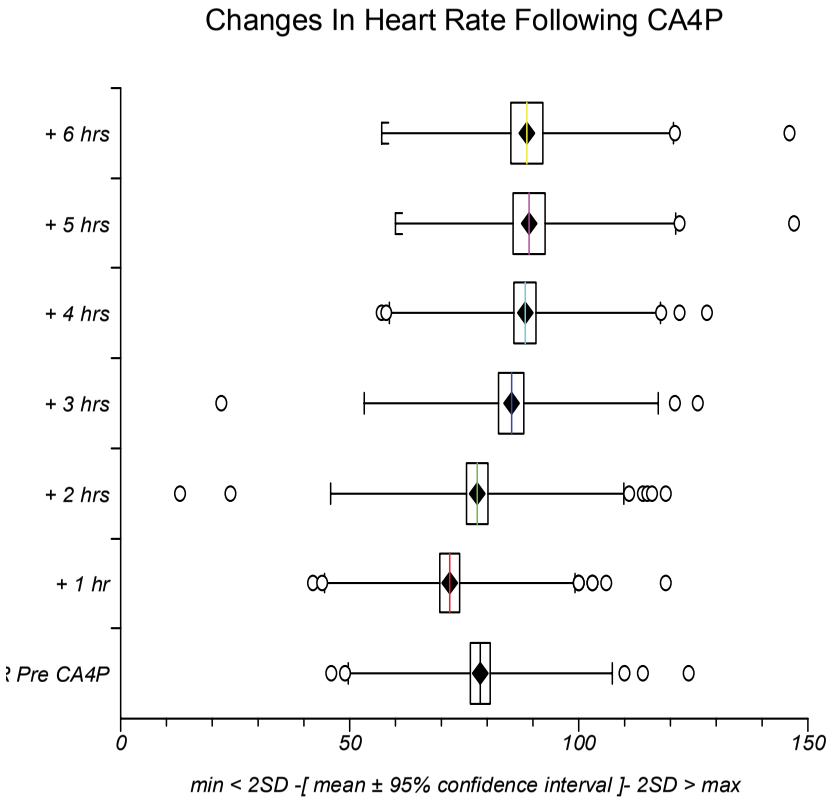

Figure 6.8 Box & whisker plot of the distribution of change in heart rate following CA4P.

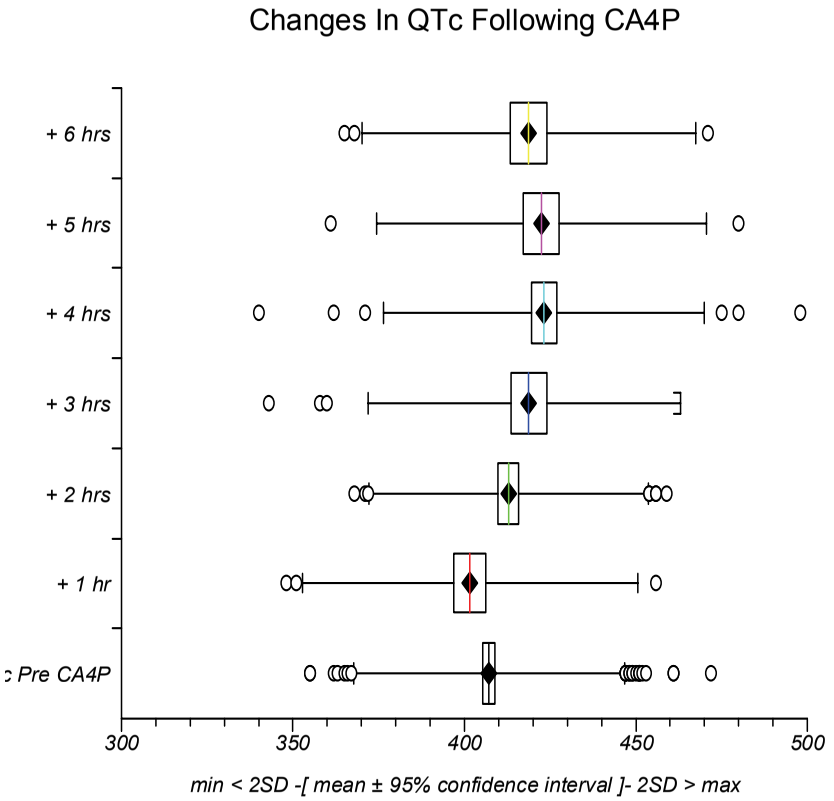

Figure 6.9 Box & whisker plot of the distribution of change in QTc interval following CA4P.

Haematological Toxicity

Figures 6.10 – 6.12 and **Table 6.8** illustrate the haematological toxicity observed in patients during the study.

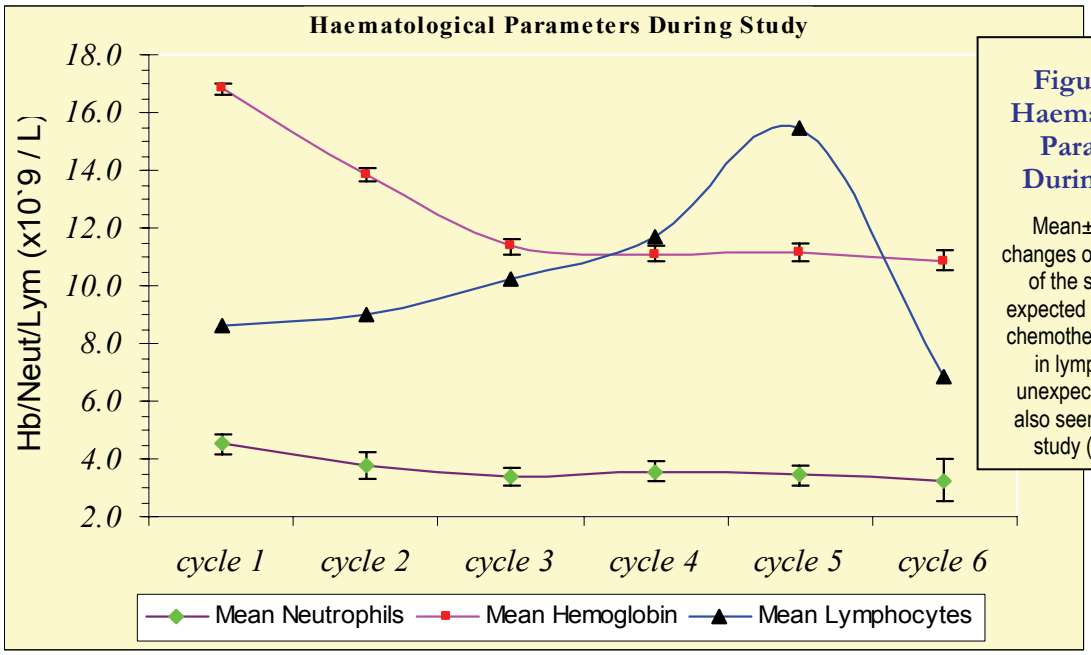

Figure 6.10 - Haematological Parameters During Study.

Mean±SE. These changes over the course of the study are as expected from cytotoxic chemotherapy. The rise in lymphocytes is unexpected, and was also seen in the A5B7 study (Chapter 2)

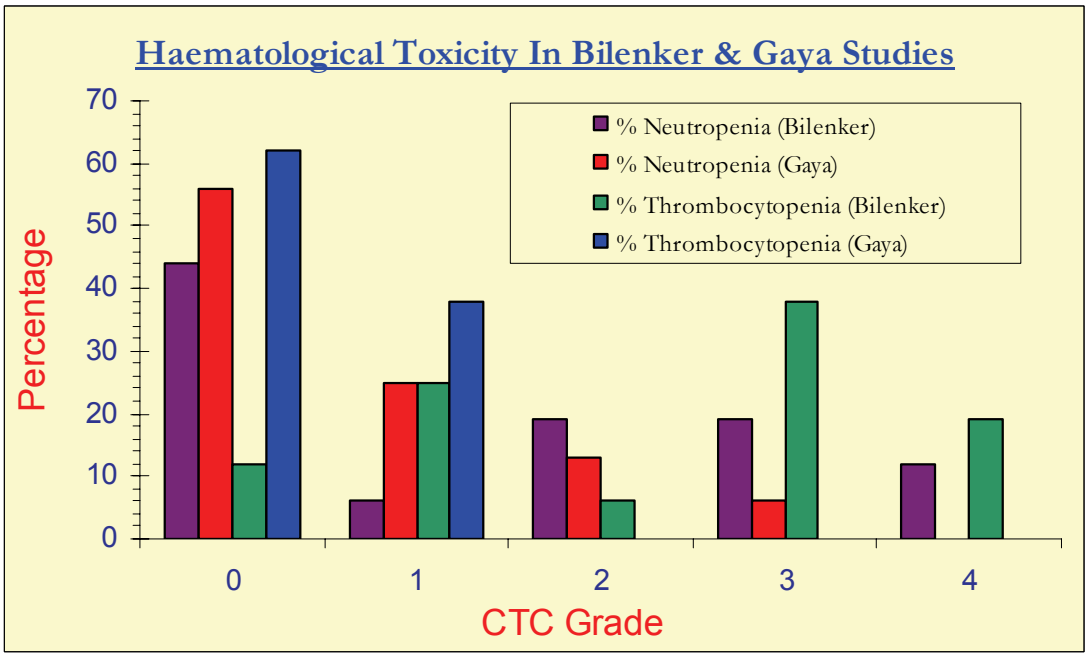

Fig. 6.11: Comparison of Haematological Toxicity With Bilenker Study (Bilenker et al., 2005). Neutropenia & thrombocytopenia greatly reduced in this study with carboplatin administered 20-22hrs post CA4P.

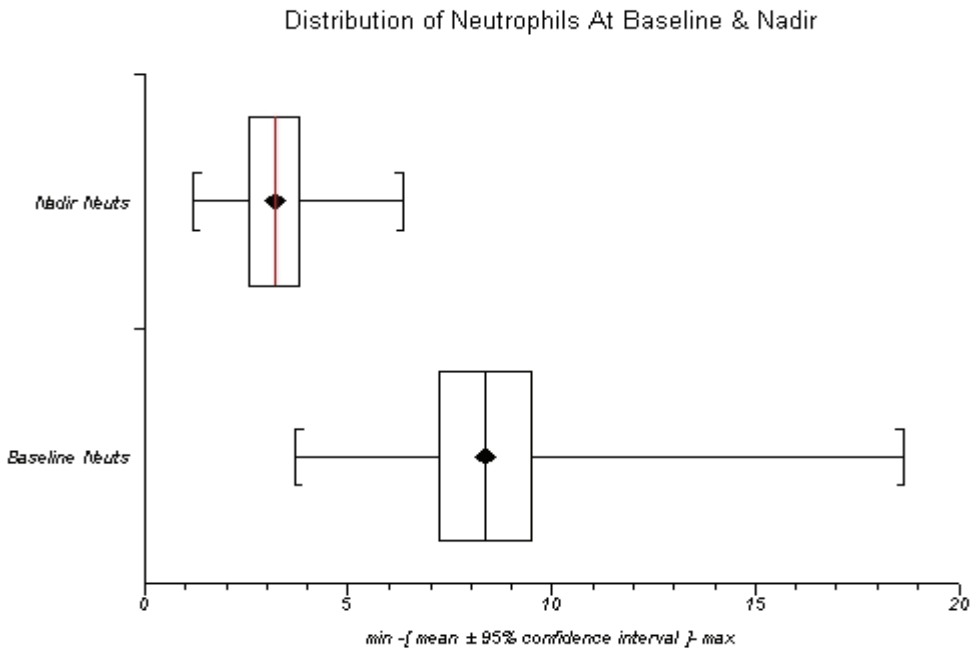

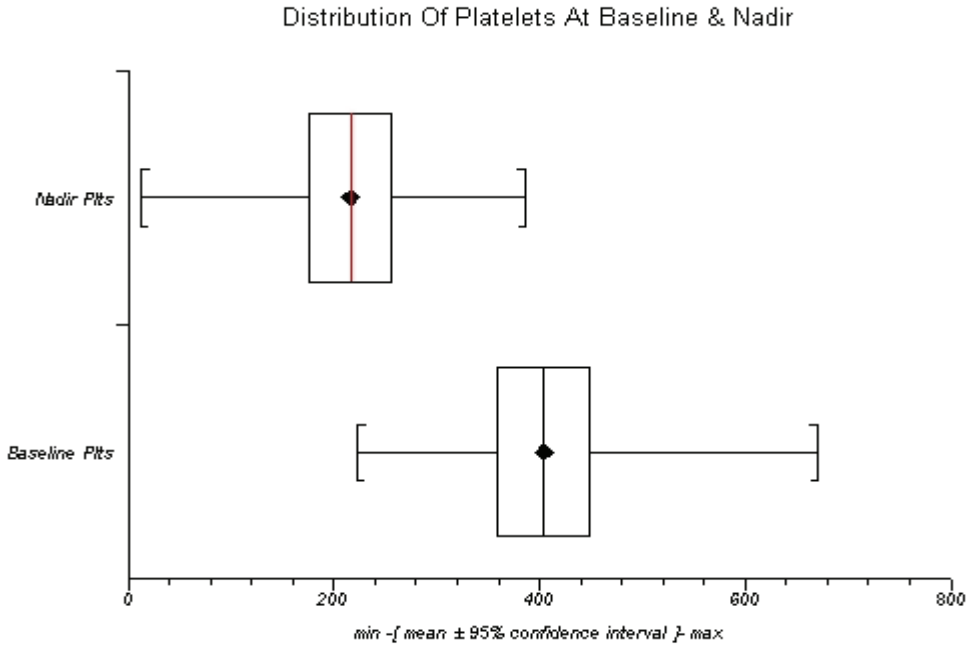

Figure 6.12a,b Box & whisker plots illustrating neutrophil and platelet distributions at baseline (Day 1) and nadir. Blood counts were taken weekly during the study, the lowest counts are illustrated. Myelosuppression is as expected.

Table 6.8 - Overall Haematological Toxicity In The Three Arms. Number of episodes illustrated.

CTC Grade 1	Carboplatin	Paclitaxel	Triplet	Total
Anaemia	7	9	5	21
Lymphopenia	3	2	2	7
Neutropenia	2			2
Thrombocytopenia	4	2	7	13
Leucopenia	2	2	1	5
CTC Grade 2	**Carboplatin**	**Paclitaxel**	**Triplet**	**Total**
Anaemia	6	5	6	17
Lymphopenia				0
Neutropenia	2	6	2	10
Thrombocytopenia	1			1
Leucopenia	2	6	7	15
CTC Grades 3-4	**Carboplatin**	**Paclitaxel**	**Triplet**	**Total**
Anaemia		1	1	2
Lymphopenia	2	3	1	6
Neutropenia			8	8
Thrombocytopenia		1	1	2
Leucopenia			2	2

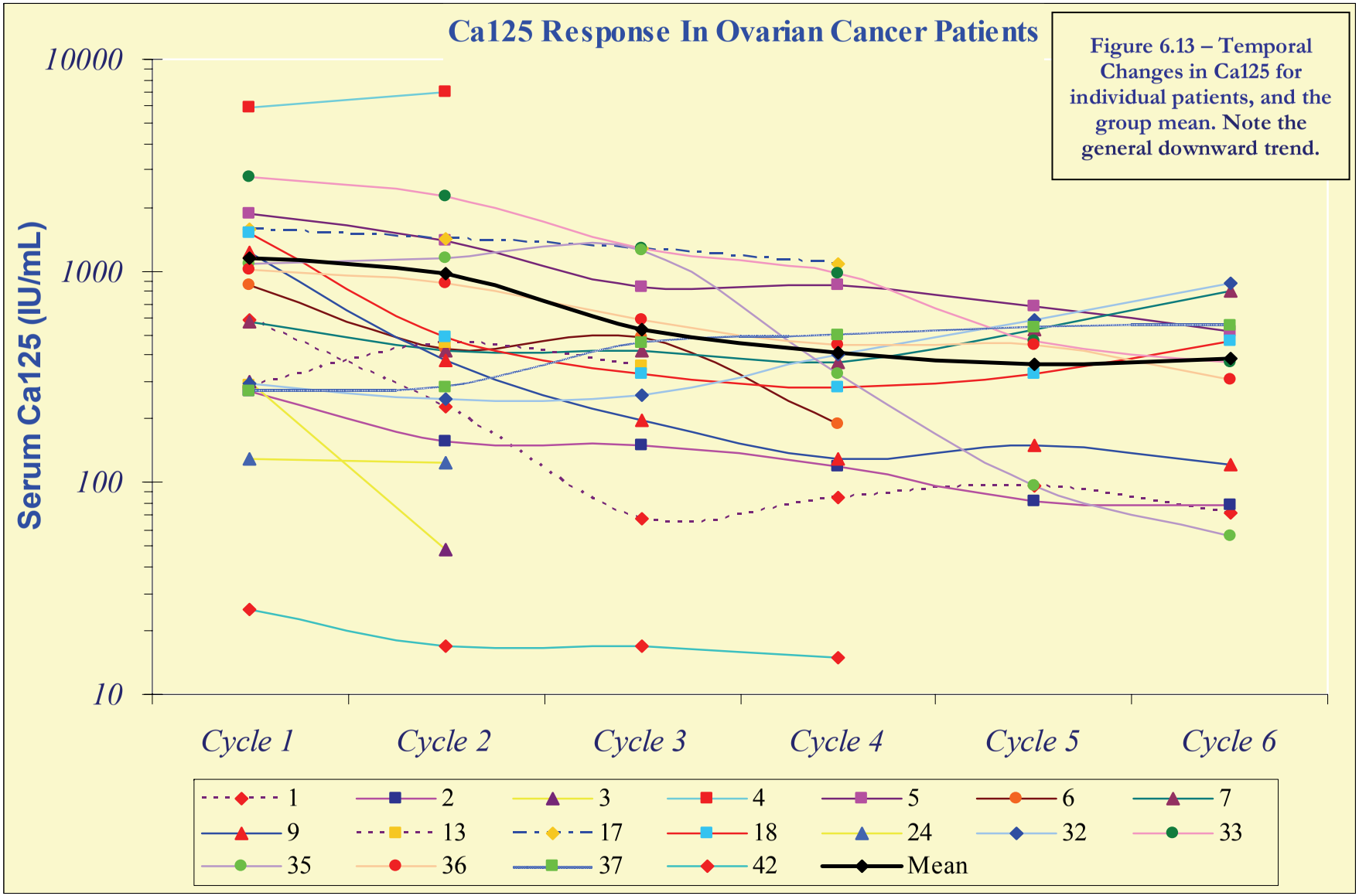

Figure 6.13 – Temporal Changes in Ca125 for individual patients, and the group mean. Note the general downward trend.

Pharmacokinetics

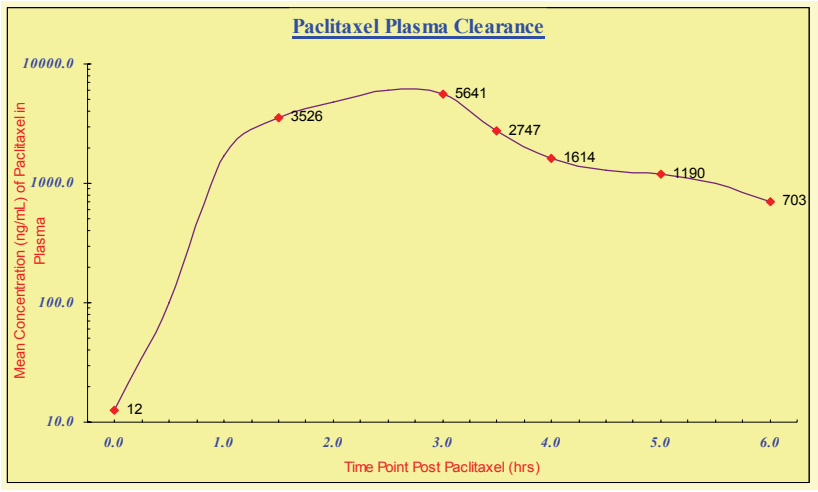

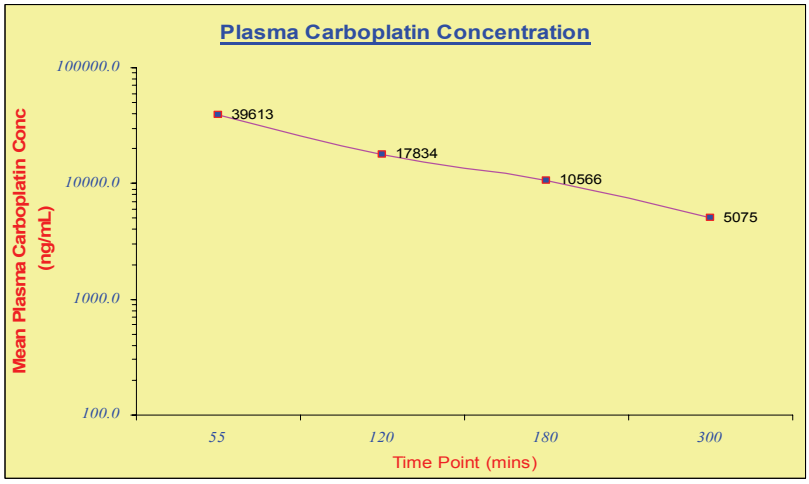

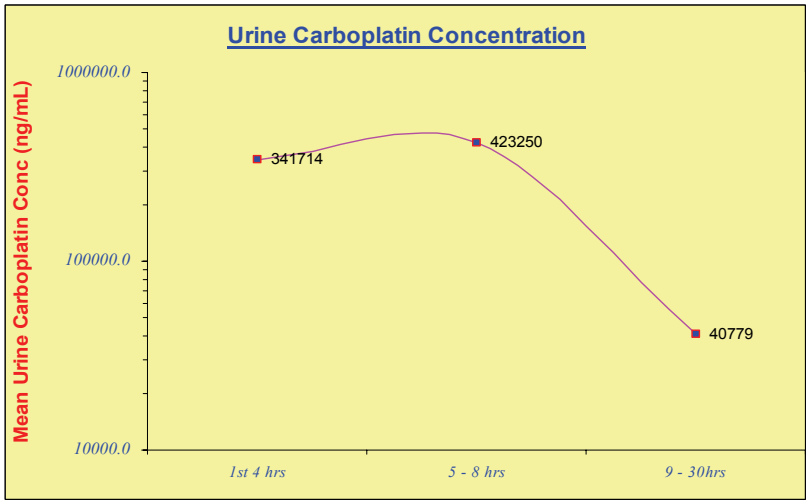

Figs. 6.14a,b,c – Plasma & Urinary Paclitaxel & Carboplatin Clearance Pharmacokinetics

Courtesy of Covance: N=31 Paclitaxel analysis (complete). Carboplatin analysis final data incomplete (n=8) Paclitaxel plasma concentrations decline in a biphasic manner. The initial rapid decline represents distribution to the peripheral compartment and elimination of the drug. The later phase is due, in part, to a relatively slow efflux of paclitaxel from the peripheral compartment. Carboplatin exhibits linear pharmacokinetics. Urinary PK, n=8 Patients with creatinine clearances of approximately 60 mL/min or greater excrete 65% of the dose in the urine within 12 hours and 71% of the dose within 24 hours. Source: www.rxlist.com. There is NO evidence of delayed excretion of cytotoxic drugs following CA4P administration

Table 6.9. Carboplatin pharmacokinetics and blood count nadirs. Eyeballing the results there is no obvious relationship between degree of neutropenia or thrombocytopenia and carboplatin AUC or C_{max}. PK measured by Covance Clinical Research Unit, USA. www.covance.com

Patient ID	Carboplatin AUC given to patient	CA4P mg/m^2	Paclitaxel Dose mg/m^2	Carboplatin AUC mmol.h.l^{-1}	Carboplatin C_{max} mM	Hb nadir x10^9/L	Neuts nadir x10^9/L	Plt nadir x10^9/L
10	4	45	-	67190	24700	12.7	2.31	203
12	4	45	-	67990	24800	8.5	5.40	302
13	4	45	-	144390	105000	12.0	2.26	147
14	5	45	-	96430	41100	11.0	2.72	103
15	5	45	-	92480	31900	8.6	3.32	175
17	5	45	-	87250	41300	10.0	3.31	165
21	5	54	-	111770	31200	10.1	2.85	106
23	5	54	-	89660	33200	10.6	2.51	215
32	5	54	-	76710	21000	10.1	1.78	172
34	5	54	-	54570	11500	12.4	1.60	196
39	5	63	175	66340	15700	9.7	0.63	323
41	5	63	175	64170	21100	10.5	0.68	137

Non-Haematological Toxicity

Table 6.10. Drug-Related Toxicity seen in 5 or more patients (Number of episodes per CTC grade)

Toxicity:	Carboplatin Arm			Paclitaxel Arm			Triplet Arm			Total
	G1	G2	G3	G1	G2	G3	G1	G2	G3	
Fatigue	4	5	3	5	7		3	6		33
Hypertension	6	1	1	9		1	8	1	1	28
Pain, other	4	4	1	3	7	3		5	1	28
Paraesthesia	6		1	8	1	1	6	3		26
Alopecia	2			2	12		1	8		25
Tachycardia	10			8			6			24
Hypotension	4	1		6	3		8	1		23
Nausea	4	5		4	2		3	5		23
Pain, abdominal	5	1	1	2	4	2		1	1	17
Pain, headache	1	5	1	3	1		1	4		16
Fever	5			6	3		1			15
Vomiting	3	2	1	3	3		1	1	1	15
Constipation		4		1	4		1	3		13
Diarrhoea	2	1		3	1	1	1	2	1	12
Flushing	3	1		1			2	1		8
Itching	3			1			4			8
Infection		1			1	2	2	1		7
Anorexia	1	1					4	1		7
Myalgia	1			3			2	1		7
Oedema	2	1		1	1		1			6
Rash		1		1	1		3			6
Stomatitis	1			1	1		2			5
Dyspnoea	2	1			1		1			5
Itching, perianal	3			1			1			5
Muzzy head	2			2			1			5

Table 6.11. Toxicities seen in less than 5 patients but including at least one grade 3 or 4 event.

Toxicity:	Carboplatin Arm				Paclitaxel Arm			Triplet Arm			Total
	G1	G2	G3	G4	G1	G2	G3	G1	G2	G3	
Agitation	2		1		1						4
Allergic reaction				1			1	1			3
Motor Neuropathy		1	1				1				3
Cough		1			1		1				3
Dysphasia	1		1								2
Ataxia									1	1	2
Dehydration							1				1
Incontinence			1								1
Sepsis			1								1

Table 6.12 – Serious Adverse Events, Including Grade 4 Toxicity

Patient ID	SAE	Drug Related
03	Intestinal Obstruction	No
06	Catheter Sepsis Hydronephrosis Death	No
09	Central Line Infection Nausea & Vomiting	No Possibly
13	Clonic Convulsion Nausea & Vomiting Neck Pain	No Possibly No
14	Rectal Haemorrhage	No
16	Upper Abdominal Pain	Possibly
17	Drug Hypersensitivity Reaction Food Poisoning	Carboplatin No
19	Abdominal Pain Abdominal Distension Death	No No No
20	Lower Respiratory Tract Infection	Unlikely
21	Renal Failure Sepsis	Unlikely
24	Abdominal Pain Anorexia Pyrexia Fatigue	No No No No
25	Lower Respiratory Tract Infection	No
29	Asthenia	Possibly
30	Dehydration	No
36	Constipation Dehydration	Unlikely No
39	Dehydration	No
43	Ataxia	CA4P DLT

Discussion

We have shown CA4P combination therapy to be safe and well-tolerated with promising indications of activity especially in ovarian cancer (Gaya et al,2005). We have also demonstrated safe and effective scheduling of CA4P with carboplatin with no delayed renal excretion or increased toxicity.

The alterations in vital signs following CA4P have been documented previously in single agent phase I CA4P studies (Anderson et al., 2003; Dowlati et al., 2002; Rustin et al., 2003), and the A5B7 study (**Chapter 2**), and are thought to be due to alterations in peripheral resistance (Ley et al., 2007; Prise et al., 2002; Tozer et al., 1999). In this study, following CA4P there was a mean 13mmHg rise in systolic BP, and a mean 9mmHg rise in diastolic BP one hour after infusion, with a corresponding mean 7 bpm fall in HR.

Patients with a baseline BP above the mean of 124/75 did not experience greater alterations in vital signs than those with baseline BP below the mean. Longstanding vascular disease may alter the body's ability to adapt to the vascular assault of CA4P, or the endothelium may already be damaged and therefore more prone to CA4P endothelial cell attack. These patients certainly have a higher degree of pre-existing endothelial damage as a result of their hypertension (Ferroni et al., 2006; Taddei et al., 2006), however we have not demonstrated that they are significantly more prone to alterations in peripheral resistance following the CA4P endothelial assault. These patients are also more likely to suffer cardiovascular complications following CA4P (Chaplin et al., 2006).

A rise in core body temperature was demonstrated, most pronounced 4h following CA4P. This is most likely an inflammatory response to the CA4P induced endothelial cell damage, and has been previously demonstrated *in vitro* (Brooks et al., 2003). Rises in neutrophil counts were documented in the A5B7 study 4 hours following CA4P.

The effect of CA4P on cardiac conduction has been well documented (Cooney et al., 2004). Our study showed a mean 15ms lengthening of the QTc interval four hours following CA4P infusion within the normal range, with no significant clinical consequences. Phase I single agent studies showed normalisation of QTc by 24 hours (Anderson et al., 2003; Dowlati et al., 2002; Rustin et al., 2003).

Haematological toxicity was not increased with the addition of CA4P from that expected with the cytotoxic agents alone. It has been previously shown that paclitaxel antagonises the thrombocytopenic effects of carboplatin in the megakaryoblast cell line MEG-01, and this may account for some of the reduced haematological toxicity seen in our study (Guminski et al., 2001), in addition to scheduling, as only two cases of grade 3 thrombocytopenia were observed. Rates of grade 3 neutropenia or anaemia were as expected and not dose limiting.

The importance of the chronological scheduling of CA4P and cytotoxic chemotherapy can be dramatically illustrated by Bilenker's Phase I trial of CA4P in combination with carboplatin in advanced malignancy (Bilenker et al., 2005). The study was terminated early after sixteen patients received 40 cycles of CA4P at doses escalating from just 27 - 36mg/m^2, with carboplatin dosed to an initial AUC5. Carboplatin was given as a 30min infusion on day 1 followed one hour later by CA4P infused over 10min.

Interestingly in this study, platelet trends were analysed in the context of a previously published formula relating carboplatin dosage and changes in platelet count (Egorin et al., 1984):

$$Carboplatin\ Dosage(mg/m^2) = \left(\frac{0.091 \times Creatinine\ Clearance}{Body\ Surface\ Area \times \left[\frac{\mathrm{Pr}etreatment\ Plt - Plt\ Nadir\ Desired}{(\mathrm{Pr}etreatment\ Plt \times 100) - 17} \right]} \right) + 86$$

Out of six patients at the first dose level of CA4P 27mg/m^2 with carboplatin AUC5, there was one case of grade 3 neutropenia lasting six weeks, which was considered a DLT. There were also three cases of grade 3 thrombocytopenia. At the next dose level of CA4P 36mg/m^2 with carboplatin AUC5, two out of six patients experienced dose limiting grade 4 thrombocytopenia, and another two grade 3 thrombocytopenia. There were also two cases of grade 4 neutropenia. The last four patients received CA4P 36mg/m^2 with carboplatin AUC4. Grades 2 and 3 thrombocytopenia, and grade 3 neutropenia occurred at this dose level. Non-haematological toxicity was generally mild, and not dose limiting. Six out of 16 patients showed RECIST stable disease.

Using the formula above, the authors concluded that the predicted mean platelet nadir was 127, whereas the actual mean platelet nadir was 117. The mean ratio of observed AUC to predicted AUC was 1.16. Linear regression analysis indicated a strong correlation between the observed to predicted ratio of carboplatin AUC with CA4 AUC (p=0.008) (**Fig 6.15**), highly suggestive of a pharmacokinetic interaction.

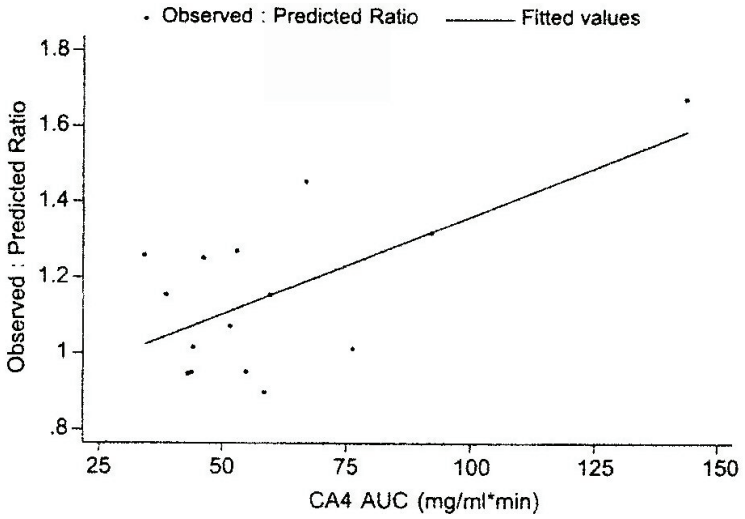

Fig. 6.15 Plot of Observed/Predicted Ratio Of Carboplatin AUC by CA4 AUC (mg x min/mL) with Fitted Regression Line (p=0.008) From Bilenker (Bilenker et al., 2005)

This data suggests that when giving CA4P in combination with carboplatin the reduction in renal perfusion induced by CA4P must recover prior to administering the carboplatin. Giving carboplatin 24 hours after CA4P has been shown in the murine model to be as effective as giving it 1 or 4 hours apart (Siim et al., 2003; Staflin et al., 2006). Twenty four hours after CA4P administration it is suspected that there is rapid proliferation of the viable tumour rim stimulated by circulating endothelial progenitor cells (Shaked et al., 2006). This might therefore be the best time to give carboplatin. In clinical practice carboplatin is frequently given in combination with paclitaxel for lung and ovarian cancers. As this combination showed enhanced activity when given with CA4P in the murine model and better therapies are needed for these cancers, a clinical trial was indicated. In view of the toxicity seen by Bilenker and colleagues we planned our dose escalation study initially combining CA4P with carboplatin or paclitaxel as doublets before combining all three drugs. The difference in haematological toxicity is dramatically illustrated in **Table 6.13** and **Figure 6.11**. **Table 6.9** shows there is no obvious relationship between degree of neutropenia or thrombocytopenia and carboplatin AUC

or C_{max} so the difference is due to the timing of administration of carboplatin following renal recovery from the CA4P effect.

Table 6.13: Comparison of haematological toxicity in two studies following carboplatin + CA4P. N=16 in both studies

CTC Grade	% Neutropenia (Bilenker)	% Neutropenia (Gaya)	% Thrombocytopenia (Bilenker)	% Thrombocytopenia (Gaya)
0	44	56	12	62
1	6	25	25	38
2	19	13	6	0
3	19	6	38	0
4	12	0	19	0

The most efficacious timing of cytotoxic agents in relation to CA4P is unknown. Our regimen of administering the cytotoxics 20h after CA4P has shown activity and little increased toxicity. The pharmacokinetic data confirms no delayed excretion of carboplatin or paclitaxel following CA4P. The increased cell killing would probably result from death of hypoxic cells at the tumour core after CA4P followed by conventional cytotoxic cell death 20h later. This resistant proportion of hypoxic cells, which would conventionally lead to repopulation of the tumour, may be reduced with the increased cell killing of the combination therapy. CA4P has also recently shown increased antitumour activity in combination with radiotherapy in lung cancer & prostate cancer (Mandeville et al., 2007; Ng et al., 2007).

There is no noticeable increase in toxicity from combination therapy with the addition of CA4P. CA4P was well tolerated up to the MTD of 63mg/m^2. The toxicity of paclitaxel and carboplatin was as expected – fatigue, paraesthesia, alopecia, nausea, diarrhoea, anorexia, myelosuppression. Side effects from the CA4P were mild and short lived, consisting mainly of CTC grade 1 toxicities – tumour pain, fatigue, flushing, pruritis, headaches,nausea, and hypertension. The DLT was neurological – cerebellar ataxia, as confirmed in previous studies (Dowlati et al., 2002; Rustin et al., 2003). The majority of serious adverse events were not drug related, or unexpected, until DLT was reached (**Table 6.12**).

There were some dramatic tumour responses with therapy. 27% of patients with RECIST PD and 45% of those with SD experienced a clinical improvement in

symptoms. Overall RECIST assessment showed 16% PR, 54% SD and 30% PD. Patient 02 experienced a reduction in an aorto-caval lymph node from 24mm to 16mm; patient 25 a lung metastasis reduced from 50mm to 25mm; patient 30 a splenic metastasis (72mm to 35mm) and liver metastasis (72mm to 40mm). Patient 40 showed a reduction in right supraclavicular metastasis (30mm to 7mm) and a liver metastasis (20mm to 9mm).

Of 18 heavily pretreated patients with ovarian cancer (including one case of fallopian tube carcinoma), half had a Ca125 fall over 50%. Of 13 RECIST assessible patients there were 3 partial responses and 6 cases of disease stability through the study. Of 5 platinum resistant patients, 3 responded, one had a Ca125 drop >50%, and two had RECIST SD. CA4P induced cell death from vascular shutdown occurs independently of the platinum sensitivity of the tumour cell; it is dependent solely on the endothelial cell damage within any particular tumour cell population. The response of platinum resistant ovarian cancer to the combination therapy will be assessed further in the Phase II component of the study.

Conclusions

The combination of CA4P with Paclitaxel and Carboplatin at doses of 63mg/m^2, 175mg/m^2, and AUC5 respectively, is safe, well tolerated, and shows early indications of activity in heavily pretreated patients. Haematological toxicity is greatly reduced administering cytotoxics 20-22h post CA4P due to normalisation of renal function. The combinations appear particularly active in both platinum sensitive and platinum resistant ovarian cancer. These doses will be used in the Phase II component of the study in patients with platinum resistant ovarian cancer, and are also being used in non small cell lung cancer (NSCLC) in combination with Bevacizumab. Further dose escalation of CA4P with these cytotoxic agents would not be safe on the basis of significant phase I preclinical and clinical combination data. CA4P efficacy data in combination with other cytotoxic agents is awaited.

References

Anderson, H.L., Yap, J.T., Miller, M.P., Robbins, A., Jones, T. & Price, P.M. (2003). Assessment of pharmacodynamic vascular response in a phase I trial of combretastatin A4 phosphate. *J Clin Oncol*, **21,** 2823-30.

Bilenker, J.H., Flaherty, K.T., Rosen, M., Davis, L., Gallagher, M., Stevenson, J.P., Sun, W., Vaughn, D., Giantonio, B., Zimmer, R., Schnall, M. & O'Dwyer, P.J. (2005). Phase I trial of combretastatin a-4 phosphate with carboplatin. *Clin Cancer Res*, **11,** 1527-33.

Bilenker JH , S.J., Rosen MA , Gallagher M , Flaherty KT , Algazy K , Sun W , Schnall M , O'Dwyer PJ. (2003). Phase Ib trial of combretastatin A4 Phosphate (CA4P) in combination with carboplatin in patients with advanced cancer. *Proc Am Soc Clin Oncol*, **22,** Abstract 889.

Brooks, A.C., Kanthou, C., Cook, I.H., Tozer, G.M., Barber, P.R., Vojnovic, B., Nash, G.B. & Parkins, C.S. (2003). The vascular targeting agent combretastatin A-4-phosphate induces neutrophil recruitment to endothelial cells in vitro. *Anticancer Res*, **23,** 3199-206.

Chaplin, D.J. & Dougherty, G.J. (1999). Tumour vasculature as a target for cancer therapy. *Br J Cancer*, **80 Suppl 1,** 57-64.

Chaplin, D.J., Horsman, M.R. & Siemann, D.W. (2006). Current development status of small-molecule vascular disrupting agents. *Curr Opin Investig Drugs*, **7,** 522-8.

Cooney, M.M., Radivoyevitch, T., Dowlati, A., Overmoyer, B., Levitan, N., Robertson, K., Levine, S.L., DeCaro, K., Buchter, C., Taylor, A., Stambler, B.S. & Remick, S.C. (2004). Cardiovascular safety profile of combretastatin a4 phosphate in a single-dose phase I study in patients with advanced cancer. *Clin Cancer Res*, **10,** 96-100.

Dowlati, A., Robertson, K., Cooney, M., Petros, W.P., Stratford, M., Jesberger, J., Rafie, N., Overmoyer, B., Makkar, V., Stambler, B., Taylor, A., Waas, J., Lewin, J.S., McCrae, K.R. & Remick, S.C. (2002). A phase I pharmacokinetic and translational study of the novel vascular targeting agent combretastatin a-4 phosphate on a single-dose intravenous schedule in patients with advanced cancer. *Cancer Res*, **62,** 3408-16.

Egorin, M.J., Van Echo, D.A., Tipping, S.J. & al., e. (1984). Pharmacokinetics and Dosage Reduction of cis-diamine(1,1-cyclobutanedicarboxylato)platinum in Patients With Impaired Renal Function. *Cancer Res*, **44,** 5432 - 5438.

Ferroni, P., Basili, S., Paoletti, V. & Davi, G. (2006). Endothelial dysfunction and oxidative stress in arterial hypertension. *Nutr Metab Cardiovasc Dis*, **16,** 222-33.

Galbraith, S.M., Maxwell, R.J., Lodge, M.A., Tozer, G.M., Wilson, J., Taylor, N.J., Stirling, J.J., Sena, L., Padhani, A.R. & Rustin, G.J. (2003). Combretastatin A4 phosphate has tumor antivascular activity in rat and man as demonstrated by dynamic magnetic resonance imaging. *J Clin Oncol*, **21,** 2831-42.

Grosios, K., Loadman, P.M., Swaine, D.J., Pettit, G.R. & Bibby, M.C. (2000). Combination chemotherapy with combretastatin A-4 phosphate and 5-fluorouracil in an experimental murine colon adenocarcinoma. *Anticancer Res*, **20,** 229-33.

Guminski, A.D., Harnett, P.R. & deFazio, A. (2001). Carboplatin And Paclitaxel Interact Antagonistically In A Megakaryoblast Cell Line - A Potential Mechanism For Paclitaxel-Mediated Sparing Of Carboplatin Induced Thrombocytopenia. *Cancer Chemother Pharmacol*, **48,** 229 - 234.

Ley, C.D., Horsman, M.R. & Kristjansen, P.E. (2007). Early effects of combretastatin-A4 disodium phosphate on tumor perfusion and interstitial fluid pressure. *Neoplasia*, **9,** 108-12.

Mandeville, H.C., Ng, Q., Milner, J., Taylor, N.J., Stirling, J.J., Padhani, A.R., d'Arcy, A.J., Collins, D.J., Saunders, M.I. & Hoskin, P.J. (2007). CA4P and External Beam Radiotherapy in Prostate Cancer with Assessment of Effect by DCE-MRI. *Clin Oncol (R Coll Radiol)*, **19,** S38.

Ng, Q.S., Goh, V., Carnell, D., Meer, K., Padhani, A.R., Saunders, M.I. & Hoskin, P.J. (2007). Tumor antivascular effects of radiotherapy combined with combretastatin a4 phosphate in human non-small-cell lung cancer. *Int J Radiat Oncol Biol Phys*, **67,** 1375-80.

Prise, V.E., Honess, D.J., Stratford, M.R., Wilson, J. & Tozer, G.M. (2002). The vascular response of tumor and normal tissues in the rat to the vascular targeting agent, combretastatin A-4-phosphate, at clinically relevant doses. *Int J Oncol*, **21,** 717-26.

Rustin, G.J. (2003). Use of CA-125 to assess response to new agents in ovarian cancer trials. *J Clin Oncol*, **21,** 187s-193s.

Rustin, G.J., Galbraith, S.M., Anderson, H., Stratford, M., Folkes, L.K., Sena, L., Gumbrell, L. & Price, P.M. (2003). Phase I clinical trial of weekly combretastatin A4 phosphate: clinical and pharmacokinetic results. *J Clin Oncol*, **21,** 2815-22.

Shaked, Y., Ciarrocchi, A., Franco, M., Lee, C.R., Man, S., Cheung, A.M., Hicklin, D.J., Chaplin, D., Foster, F.S., Benezra, R. & Kerbel, R.S. (2006). Therapy-induced acute recruitment of circulating endothelial progenitor cells to tumors. *Science*, **313,** 1785-7.

Siim, B.G., Lee, A.E., Shalal-Zwain, S., Pruijn, F.B., McKeage, M.J. & Wilson, W.R. (2003). Marked potentiation of the antitumour activity of chemotherapeutic drugs by the antivascular agent 5,6-dimethylxanthenone-4-acetic acid (DMXAA). *Cancer Chemother Pharmacol*, **51,** 43-52.

Staflin, K., Jarnum, S., Hua, J., Honeth, G., Kannisto, P. & Lindvall, M. (2006). Combretastatin A-1 phosphate potentiates the antitumor activity of carboplatin and paclitaxel in a severe combined immunodeficiency disease (SCID) mouse model of human ovarian carcinoma. *Int J Gynecol Cancer*, **16,** 1557-64.

Stevenson, J.P., Rosen, M., Sun, W., Gallagher, M., Haller, D.G., Vaughn, D., Giantonio, B., Zimmer, R., Petros, W.P., Stratford, M., Chaplin, D., Young, S.L., Schnall, M. & O'Dwyer, P.J. (2003). Phase I trial of the antivascular agent combretastatin A4 phosphate on a 5-day schedule to patients with cancer: magnetic resonance imaging evidence for altered tumor blood flow. *J Clin Oncol*, **21,** 4428-38.

Taddei, S., Virdis, A., Ghiadoni, L., Versari, D. & Salvetti, A. (2006). Endothelium, aging, and hypertension. *Curr Hypertens Rep*, **8,** 84-9.

Therasse, P., Arbuck, S.G., Eisenhauer, E.A., Wanders, J., Kaplan, R.S., Rubinstein, L., Verweij, J., Van Glabbeke, M., van Oosterom, A.T., Christian, M.C. & Gwyther, S.G. (2000). New guidelines to evaluate the response to treatment in solid tumors. European Organization for Research and Treatment of Cancer, National Cancer Institute of the United States, National Cancer Institute of Canada. *J Natl Cancer Inst*, **92,** 205-16.

Tozer, G.M., Prise, V.E., Wilson, J., Locke, R.J., Vojnovic, B., Stratford, M.R., Dennis, M.F. & Chaplin, D.J. (1999). Combretastatin A-4 phosphate as a tumor vascular-targeting agent: early effects in tumors and normal tissues. *Cancer Res*, **59,** 1626-34.

Wildiers, H., Ahmed, B., Guetens, G., De Boeck, G., de Bruijn, E.A., Landuyt, W. & van Oosterom, A.T. (2004). Combretastatin A-4 phosphate enhances CPT-11 activity independently of the administration sequence. *Eur J Cancer*, **40,** 284-90.

Chapter 7

Relationship Between Human Tumour Angiogenic Profile And Combretastatin-Induced Vascular Shutdown – An Exploratory Study.

Abstract

CA4P acts most effectively against immature tumour vasculature. We investigated whether histological angiogenic profile can explain the differential sensitivity of human tumours to CA4P, by correlating the kinetic changes demonstrated by DCE-MRI in response to CA4P with tumour immunohistochemical angiogenic markers. Tissue was received from 24 patients (mean age 59, range 32–73, 18 females, 6 males). An angiogenic profile was performed using standard immunohistochemical techniques. Dynamic MRI data were obtained for the same patients before and four hours after CA4P. Three patients showed a statistically significant fall in K^{trans} following CA4P, and only 1 patient a statistically significant fall in $IAUGC_{60}$. There were widespread falls in kinetic parameters om other patients which did not achieve statistical significance. No statistically significant correlations were seen between the continuous or categorical variables and the DCE-MRI kinetic parameters other than between ang-2 and K^{trans} ($p=0.044$). In conclusion, we found no strong relationships between changes in DCE-MRI kinetic parameters and the immunohistochemical angiogenic profile.

Introduction

CA4P is a tubulin-binding selective VDA which causes rapid shutdown of blood flow to tumours with minimal effects on normal vasculature. Tumour endothelial cells are often immunohistochemically immature, lacking smooth muscle and pericyte coverage, and more sensitive to the effects of VDAs probably because the intracellular cytoskeleton is less developed (Tozer et al., 2005). Our aim was to determine human tumour vascular maturity using an immunohistochemical angiogenic profile, and to study any relationship with CA4P response assessed by change in DCE-MRI kinetic parameters (Gaya et al., 2008).

We selected antibodies to differentiate immature vascular endothelium - CD105 (endoglin); CD61 (β_3-integrin); the pericyte marker alpha smooth muscle actin (αSMA); a marker of hypoxia (Glut-1); proliferation marker (Ki-67); and markers associated with the angiogenic switch (VEGF, PDGFB, angiopoietin-1, angiopoietin-2).

Materials & Methods

Following ethics approval, patients enrolled in Mount Vernon Phase I CA4P studies (PH1/066 & PH1/092) who underwent DCE-MRI analysis were identified. Records were obtained from 26 identified patients and tissue was available for 24 (**Table 7.1**). A full set of DCE-MRI data was available for 21. Tissue blocks were coded to conceal patient identity. 4μm sections were cut onto slides, and stained with the panel of antibodies at concentrations and with control samples illustrated in **Table 7.2.**

No patient from the PH1/066 study was alive at the time of this project. The ethics committee approved this study without the need to obtain additional consent from the relatives of the deceased; it was felt this would cause considerable distress to the relatives, in some cases years after their loved ones died. In addition, the stored tissues were considered surplus to clinical requirements. Patients from the PH1/092 study gave full informed consent for their stored tissues to be used. This study was performed in compliance with the Human Tissue Act (2005).

Table 7.1 – Characteristics of Patients' Tumours – G1/2/3 = Well/moderately/poorly differentiated

Patient ID	Phase I Trial	Primary Tumour Site	Nature of Specimen	Histology	Date Specimen Taken	CA4P Dose (mg/m^2)
01	PH1/066 Single Agent CA4P	Paratesticular	Primary Tumour Excision	Spindle Cell Sarcoma	08/1999	52
02		Adrenal		Carcinoma	06/1993	68
03		Uterus		Leiomyosarcoma	03/1999	88
04		Renal		Renal Papillary Carcinoma	11/1997	40
05		Breast		Ductal Carcinoma	02/1993	68
06		Uterus		Leiomyosarcoma	11/1982	52
07		Rectum			01/1997	52
08		Ovary		Papillary Adenocarcinoma	05/1994	5
09		Uterus		Leiomyosarcoma	05/1998	88
10		Peritoneum	Biopsy	Primary Peritoneal Carcinoma	09/1999	52
11		Right tibia	Primary Tumour Excision	Leiomyosarcoma	10/1997	68
12		Ovary		Papillary Serous Adenocarcinoma	03/1994	114
13		Lung	Excision Biopsy Cervical lymph node	G3 Adenocarcinoma	04/1998	40
14		Renal	Primary Tumour Excision	Spindle Cell Renal Carcinoma	12/1999	114
15		Renal		Spindle Cell Renal Carcinoma	08/1999	114
16		Ovary		Papillary Adenocarcinoma	11/1991	88
17		Colon		Grade 3 Adenocarcinoma	11/1998	68
18	PH1/092 (A5B7)	Colon			05/2003	45
19		Colon		G2 Adenocarcinoma	02/1999	45
20		Colon		G3 Adenocarcinoma	11/2001	45
21	PH1/066	Uterus		Leiomyosarcoma	07/1998	N/A
22	PH1/092	Colon		Grade 2 Adenocarcinoma	10/2003	45
23		Colon			08/2001	45
24		Colon			11/2002	45

Table 7.2: Panel of antibodies. The optimum concentrations were previously determined from titration experiments performed by Dr F Daley at the Gray Cancer Institute. Immunostaining for PDGF, CD61, ang-1 and ang-2 were performed by Dr U Qureshi at the NTRAC laboratory,Royal Free Hospital

Antibody	Type of Marker	Source	Concentration	Specificity & Non-Specific Staining	Control Sample
CD34	Vascular	Novocastra NCL-END	1:60	Endothelium, Connective Tissue, erythrocytes	Tonsil
αSMA		Sigma A2547	1:20000	Smooth Muscle	Tonsil
CD105 (Endoglin)		Dako M3527	1:1000	Proliferating endothelium, activated macrophages	Human Breast Carcinoma
CD61 (β_3-integrin)		Novocastra NCL-CD61-308	1:100	Endothelium,Platelets, Megakaryocytes, monocytes, macrophages	Tonsil, Human Placenta
VEGF		Neomarkers MS-1467	1:100	121,165,189 Isoforms	Human Breast Carcinoma
Ki-67	Proliferation	Dako M7240	1:200	345, 395 Isoforms. Nuclear Expression	Tonsil
Glut-1	Hypoxia	Dako A3536	1:200	Erythrocytes,tumour	Tonsil
PDGF	Vascular / Tumour / Stromal	Novocastra NCL-PDEGF P-GF.44c	1:60	Tumour,macrophages, stroma,glia,epithelia	Tonsil, Human Placenta
Angiopoietin -1		Santa Cruz Biotech Inc.H-98 (sc-8357)	1:50	Tumour,Myocardium, vascular smooth muscle,lung,liver	Human Placenta
Angiopoietin -2		Santa Cruz Biotech Inc. H-70 (sc-20718)	1:50	Tumour,Ovary, placenta,uterus	Human Placenta

1) Immunohistochemical Procedures

Sections were deparaffinised in xylene for 5 minutes and rehydrated through graded alcohols (100%, 90%, and 70%) to water. Slides were stained using standard immunohistochemical techniques (**Appendix 2**). A summary of these techniques is presented below.

CD34 and αSMA Doublestaining: Dako's Cytomation Envision doublestain system (K5361) was used performed according to the manufacturer's instructions. The system is based on horseradish peroxidase (HRP) and alkaline phosphatase (ALP) labelled polymers which are conjugated with secondary antibodies against mouse and rabbit immunoglobulins. The polymers do not contain avidin or biotin, and so non-specific staining resulting from endogenous avidin-biotin activity in normal tissues is avoided. The least abundant antigen (CD34) was stained first followed by staining of the most abundant antigen (αSMA), to prevent flooding. Specimens were counterstained using Gills haematoxylin (Surgipath Europe Ltd 01500E) for seven seconds and washed. The samples were not dehydrated

through graded alcohols to xylene, as fast red forms an end product which is soluble in organic compounds; specimens were therefore mounted and coverslipped using an aqueous based mounting medium (Dako Faramount Aqueous Mounting Medium S3025).

CD105: We used Dako's Catalysed Signal Amplification staining system (K1497) and followed the manufacturer's instructions exactly. The system incorporates a signal amplification method, based on the peroxidase-catalyzed deposition of a fluorescein-labelled phenolic compound, followed by a secondary reaction with a peroxidase-conjugated anti-fluorescein (Bobrow MN, 1989; Von Wasielewski R, 1997). Antigen retrieval was not required on the rehydrated slides, using this high sensitivity detection system.

Specimens were first incubated with 3% hydrogen peroxide to quench endogenous peroxidase activity, then incubated with protein block solution to suppress non-specific binding of subsequent reagents, followed by incubation with the mouse primary antibody (CD105). This was followed by sequential incubations with anti-mouse immunoglobulin-HRP, fluorescyl-tyramide hydrogen peroxide (amplification reagent) and anti-fluorescein-HRP. Staining was completed by incubation with diaminobenzidine/hydrogen peroxide, which resulted in a brown precipitate at the CD105 antigen site. Slides were then counterstained for 7 - 8 seconds in Gills Haematoxylin (Surgipath Europe Ltd 01500E), washed, dehydrated through graded alcohols to xylene, mounted using DPX (Surgipath 08600E), and coverslipped.

VEGF, Ki-67, Glut-1: Dako's Universal autostainer machine was used. Antigen retrieval was performed in 0.01M citric acid pH6. Glut-1 & Ki-67 were microwaved for 3 x 4 min and VEGF for 4 x 4 min. Optimum antigen retrieval times were determined from titration experiments. Slides were transferred to the Dako Autostainer containing peroxidase block, the detection reagents (CheMate HRP,Dako K5001), and anti-human antibody (**Table 7.2**) in antibody diluent (Dako S2023). The autostainer programme included 5 minutes in peroxidase block, 1 hour incubation with primary antibody, 30 minute incubation with CheMate secondary and tertiary reagents and 5 minutes in diaminobenzidine substrate. When the programme was complete slides were removed from the machine and counterstained in Gills Haematoxylin for seven seconds, washed in tap water, dehydrated through graded alcohols (70, 90, 100%), cleared in xylene and mounted in DPX.

Ang-1, Ang-2, PDGF, CD61: Benchside manual staining procedures were used (appendix 2). Endogenous peroxidase activity was quenched with 1.5% hydrogen peroxide in methanol

for ten minutes. Antigen retrieval was performed by microwaving in 0.01M citric acid pH6 for ten minutes (ang-1) and twenty minutes (ang-2). After washing in Tris-Buffered Saline Tween (TBST) primary antibody was applied as shown in **Table 7.2,** and incubated overnight at 4°C. After rinsing in TBST, Dako Envision anti-rabbit secondary antibody (K5007) with peroxidase was applied for thirty minutes. Antigen was developed with diaminobenzidine, slides counterstained with haematoxylin, dehydrated, cleared and mounted. For CD61 & PDGF Vectastain's mouse IgG normal horse serum (Vector Labs, California) diluted in TBS was applied for thirty minutes. A horse anti-mouse biotinylated secondary was then applied, followed by incubation with streptavidin-peroxidase reagent.

The integrin most commonly associated with proliferating endothelium is $\alpha_v\beta_3$ (CD51/CD61 Vitronectin receptor complex). The CD51 α_v component is destroyed by the paraffin wax histological fixation method; consequently only the CD61 β_3 component of the integrin was assessable on our sections. The antibody had been tested previously on human tumours (Merono et al., 2002).

2) Immunohistochemical Profile Analysis

Each slide was assessed using a Zeiss Axioskop microscope, with Visilog 5.0 (Noesis) image capture software (**fig. 7.1**). The random field techniques described by Eberhard (Eberhard et al., 2000) were used. Every fifth field was captured digitally at x400 magnification (**figures 7.2 – 7.13**). At least twenty fields were captured per slide. In small samples the entire specimen was captured. Any immunoreactive endothelial cells that were separate from adjacent microvessels were considered countable vessels, and recorded as the number of vessels per high power field (HPF). αSMA staining was analysed concurrently - any $CD34^+$ vessel also αSMA^+ was recorded. Mean microvessel density (MVD/mm^2) and pericyte coverage index (PCI) were calculated after analysing at least 20 random fields per slide (**Table 7.3**). To determine the Ki-67 proliferation index(%) or Glut-1 hypoxia index(%) each slide was scanned at low & high magnification. A semi-quantitative visual assessment was made across the slide of the proportion of tumour cells staining positively (**Table 7.3**).

The following antigens were analysed using a categorical scale, with the proportion of immunoreactive cells graded as weak, moderate or strong by direct visual assessment at low (x50) and high (x400) magnification (**Table 7.3**). The most appropriate cut off values were selected from previous studies. *VEGF:* Absent (<5%), weak (5 – 25%), moderate (25 –

50%), strong (>50%) (Erdem et al., 2007). *Ang-1/2:* Cytoplasmic expression predominantly and grading system as for VEGF (J. Lind et al., 2005). *PDGF:* Highly expressed in stroma; absent (<1% tumour staining), weak (1 – 10%), moderate (10 – 25%) and strong (>25%) (Barnhill et al., 1996).

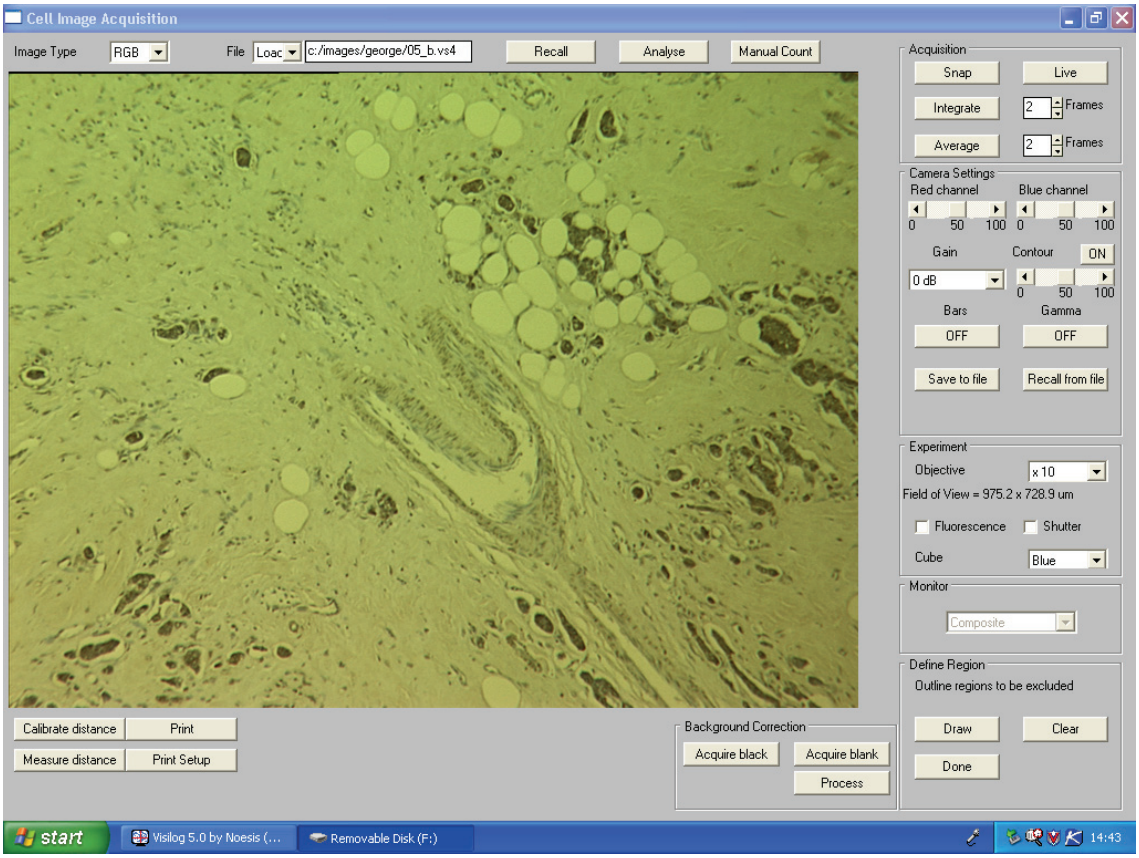

Figure 7.1 Visilog 5.0 Software, used for microscope image capture and analysis.

Random results were checked by an experienced immunohistochemist (FD), who had not seen the initial data. In case of disagreement as to the correct result, that slide was analysed by a Consultant Histopathologist. The author was trained to use the software and to analyse the samples by Dr Frances Daley in the Gray Cancer Institute, Northwood, UK.

3) DCE-MRI Data

DCE-MRI involves the rapid acquisition of sets of T1-weighted images through tumour as an intravenous bolus of contrast agent is injected. The change in signal intensity over time can be analysed with mathematical models (Tofts, 1997). Quantitative kinetic parameters are derived which provide information about tumour microcirculation as they are indirectly related to perfusion, vascular permeability and vessel surface area (d'Arcy, 2006).

Studies were performed on a 1.5 Tesla scanner as previously described (see Chapter 3 and (Galbraith et al., 2003)). Images were analysed using specialist software (Magnetic Resonance Imaging Workbench (MRIW), Institute of Cancer Research, London) (d'Arcy, 2006). A dynamic analysis was performed using MRIW for each pixel within the ROI on each slice. MRIW converts signal intensities of the T1-weighted DCE-MRI dataset into T1 relaxation rates and then into Gd-DTPA concentrations for individual voxels, using the methods described by Parker (Parker et al., 1997). Standardised terms were employed as defined in Tofts (Tofts et al., 1999). The percentage change from mean baseline kinetic parameters following CA4P was calculated (**Table 7.4**).

4) Statistical Analysis

Measurement error (Bland & Altman, 1996) was used to define repeatability confidence intervals for the MRI parameters. Linear regression & correlation analysis were used to test for relationships between the continuous variables and MRI parameters. Analysis of Variance (ANOVA) was used to test for relationships between categorical variables and MRI parameters.

Results

Tissue was received from 24 patients (mean age 59, range 32 – 73, 18 females, 6 males). 18 patients were taken from the PH1/066 single agent UK CA4P trial (Rustin et al., 2003), and 6 from the PH1/092 CA4P + A5B7 anti-CEA antibody study (currently unpublished). The most common histological subtypes (**Table 7.1**) were colorectal adenocarcinoma(7), uterine leiomyosarcoma(4) and ovarian adenocarcinoma(3). The age of the tumour blocks varied between 6 months and 21 years. All but one block contained primary tumour from surgical specimens, not metastatic tissue as patients were not rebiopsied before entrance to the phase I trials. We only studied patients who received doses of CA4P 40-114 mg/m^2 that have been associated with changes in DCE-MRI kinetic parameters. There was excellent agreement in scoring between samples analysed by the author and random samples analysed by Dr Daley. No samples had to be referred to a 3rd opinion.

There was wide intrapatient variability in kinetic parameter change following CA4P (**Table 7.4**). Percentage change in K^{trans} from mean baseline following CA4P varied between +111%

and -75%, and $IAUGC_{60}$ between +186% and -90%. In reality, only falls in these parameters (consistent with tumour vascular shutdown) are clinically significant. The 95% confidence interval for K^{trans} change (determined from repeatability analysis in the individual studies and repeated with the combined data) was -62.5% to +166.5%, $IAUGC_{60}$±80%. There was no obvious visual relationship seen between CA4P dose and fall in kinetic parameters (**Table 7.4**). Three patients (3, 10, 12) showed a statistically significant fall in K^{trans} following CA4P, and only 1 patient (12) a statistically significant fall in $IAUGC_{60}$.

There was wide variation in CD34 MVD & PCI (**Fig. 7.14**). Lowest values for PCI (01, 14, 15, 21) were sarcomas. The two tumours with highest MVD (03, 24) were a leiomyosarcoma and adenocarcinoma respectively. High PCI should indicate a more mature vascular network within the tumour – 04, the highest PCI, is a renal papillary carcinoma, and renal tumours are known for their vascularity.

Tumours with the highest proportion of $CD105^{+}$ vessels were 03 (leiomyosarcoma), 11 (leiomyosarcoma), 14 (spindle cell renal carcinoma) and 24 (colorectal adenocarcinoma).

Glut-1 expression was at a low level in most specimens studied. Several tumours showed marked hypoxia – 21 (leiomyosarcoma), 10 (primary peritoneal carcinoma), 12 (papillary serous ovarian adenocarcinoma), 15 (spindle cell renal carcinoma), and 22 (colorectal adenocarcinoma). The tumours with the highest ki-67 proliferation index were 18 (colorectal adenocarcinoma), 10 (primary peritoneal carcinoma), 12 (papillary serous ovarian adenocarcinoma), 22 & 23 (colorectal adenocarcinoma). The most hypoxic tumour (21) also had the lowest proliferation index.

Highest ang-1 expression levels were in 02 (adrenal carcinoma), 06 (uterine leiomyosarcoma), and 24 (colorectal adenocarcinoma) **fig. 7.15**. Most tumours expressed PDGF only in stromal tissue. The five specimens expressing tumour PDGF were 04 (renal papillary carcinoma), 10 (primary peritoneal carcinoma), 16 (papillary ovarian adenocarcinoma), 21 (uterine leiomyosarcoma), and 24 (colorectal adenocarcinoma). Ang-2 was expressed in all the tumour specimens analysed, and in many at a high level.

No statistically significant correlations were seen between the continuous or categorical variables and the DCE-MRI kinetic parameters (**Tables 7.5 & 7.6**) other than between ang-2 and K^{trans}($p=0.044$). Upon visual inspection of **Tables 7.3 & 7.4**, there are no obvious relationships between the angiogenic profile and the DCE-MRI data.

Patient ID	Mean CD34 MVD/mm^2	Mean SMA PCI(%)	Mean CD105 MVD/mm^2	VEGF	Ki-67	Glut-1	Ang-1	Ang-2	PDGF	Mean CD61 MVD/mm^2
01	153.67	31.70	6.88	0	ND	0.5%	ND	ND	ND	ND
02	96.33	66.85	20.64	1	0.5%	1.0%	3	1	0	47.02
03	182.34	54.58	64.22	0	20.0%	0.5%	1	2	0	18.35
04	97.48	85.73	53.90	2	15.0%	15.0%	2	3	2	19.50
05	127.29	73.69	57.34	2	30.0%	10.0%	1	2	0	26.38
06	26.38	47.50	13.76	0	1.0%	1.0%	3	3	0	11.47
07	157.11	50.99	11.47	1	10.0%	1.0%	1	1	0	19.50
08	92.89	24.67	5.73	1	15.0%	20.0%	1	1	0	9.17
09	137.61	59.03	10.32	0	10.0%	1.0%	2	1	0	17.20
10	96.33	41.54	38.99	2	50.0%	30.0%	0	2	1	43.58
11	151.38	72.51	59.63	0	2.0%	0.5%	1	2	0	10.32
12	60.78	55.58	19.50	2	40.0%	30.0%	0	1	0	6.88
13	83.72	57.14	10.32	2	5.0%	0.5%	1	1	0	1.15
14	160.55	20.53	76.83	2	10.0%	5.0%	1	2	0	29.82
15	150.23	30.60	30.96	1	15.0%	25.0%	1	3	0	19.50
16	110.09	77.43	27.52	0	15.0%	1.0%	2	1	2	11.47
17	123.85	57.90	29.82	2	20.0%	5.0%	2	3	0	5.73
18	65.37	66.37	24.08	3	60.0%	20.0%	1	3	0	16.06
19	128.44	44.58	16.06	2	30.0%	10.0%	1	2	0	24.08
20	90.60	80.15	26.38	2	30.0%	5.0%	2	2	0	6.88
21	79.13	32.63	36.70	3	1.0%	60.0%	1	3	1	27.52
22	82.57	79.83	11.47	2	40.0%	25.0%	2	2	0	9.17
23	142.09	60.85	3.40	3	40.0%	2.0%	1	1	0	8.52
24	178.90	53.00	73.39	2	25.0%	15.0%	3	3	1	12.61

Table 7.3 – Tabulated Results of Antibody Immunostaining. For CD34, SMA, CD105, CD61, result is the mean of twenty or more fields of view analysed. ND = not done, due to lack of tissue availability. MVD = microvessel density (Number vessels/0.0436 – HPF area at x400) PCI = pericyte coverage index ($SMA^+/CD34^+$ x 100). 0 – Absent, 1 – weak, 2 – moderate, 3 – strong Eyeballing tables 7.3 & 7.4 there is no obvious relationship between CA4P dose and angiogenic profile, or MRI kinetic parameter change and angiogenic profile.

Table 7.4 Percentage Change in DCE-MRI kinetic parameters 4h following CA4P. 95% Confidence Interval For K^{trans} change is -62.5% to +166.5%, v_e ±29%, k_{ep} -41.8% to +71.8%, $IAUGC_{60}$±80% . Values outside the 95% confidence intervals are in bold. There is no obvious relationship in this series between CA4P dose and fall in kinetic parameters, or correlation with vascular markers. There are 3 missing patients: 08 CA4P dose too low, 21 no data. 22 motion artefact.

Patient ID	CA4P Dose mg/m²	% Change K^{trans} post CA4P	% Change v_e post CA4P	% Change k_{ep} post CA4P	% Change $IAUGC_{60}$ post CA4P
04	40	63.27	24.03	-20.49	15.66
13		15.02	**-65.84**	30.19	**186.00**
18	45	-22.91	3.36	**-48.46**	-8.38
19		26.53	-1.92	**-85.80**	17.99
20		39.71	8.94	**-57.64**	31.94
23		-30.32	-0.96	-31.34	-30.03
24		36.51	-1.66	-18.95	29.43
01	52	-29.56	7.27	-30.12	-12.26
06		65.75	18.76	34.98	**146.30**
07		7.38	-5.74	14.72	-23.81
10		**-67.14**	**-30.34**	**-51.33**	-58.92
02	68	-30.61	-20.91	-5.76	-19.23
05		1.59	-3.88	-10.51	-7.32
11		-0.35	-11.52	-10.98	-17.02
17		111.84	-26.64	216.06	-15.44
03	88	**-75.20**	**-44.06**	**-64.82**	-57.65
09		-58.02	-13.26	**-52.53**	-58.26
16		33.01	-13.83	50.55	-1.88
12	114	**-65.49**	-27.99	67.59	**-90.21**
14		-20.00	-3.71	-16.43	-13.87
15		93.46	76.58	86.10	**82.38**

Results - Example Images

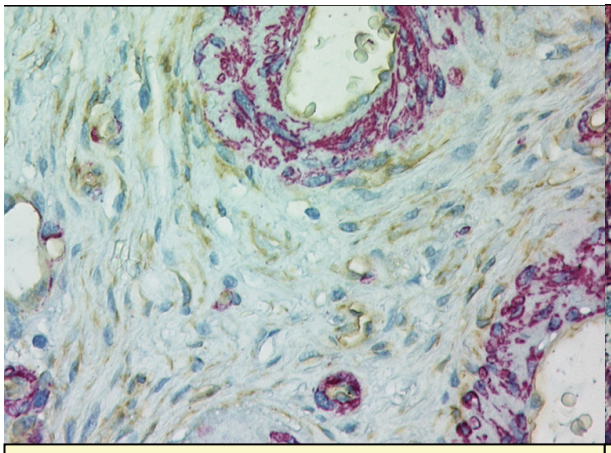

Fig 7.2 – CD34 (brown) staining endothelium, with non specific connective tissue uptake, & SMA (red) staining pericytes and perivascular connective tissue x400, Patient 09

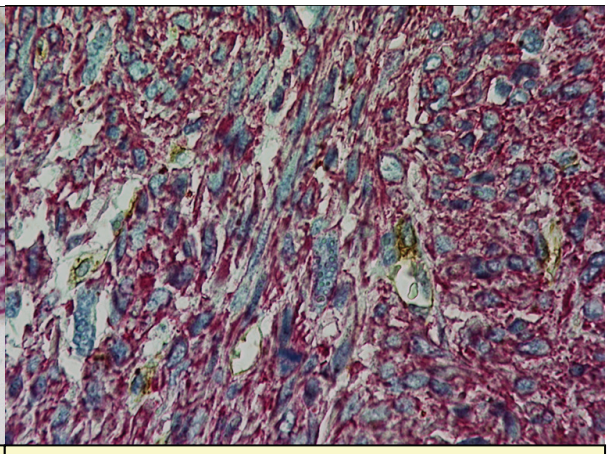

Fig 7.3 Illustrates the difficulty of analysing vessels in sarcomas, where there is widespread uptake of SMA in the connective tissue tumour, 'flooding' visualisation of vessels (brown). CD34 was counted as single stain

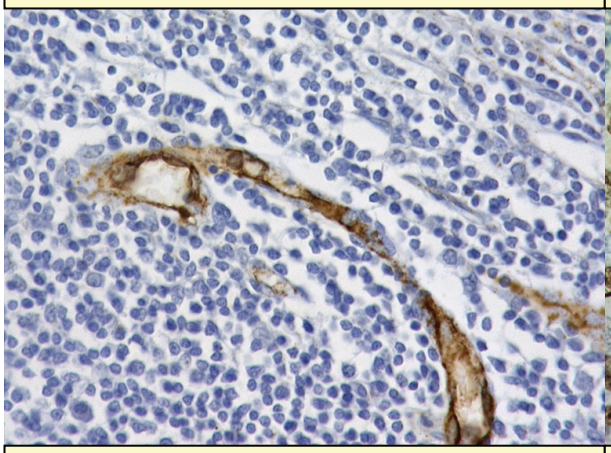

Fig 7.4 – CD105+ immature vessel (brown) within a poorly differentiated colorectal cancer (x400) Pt 24

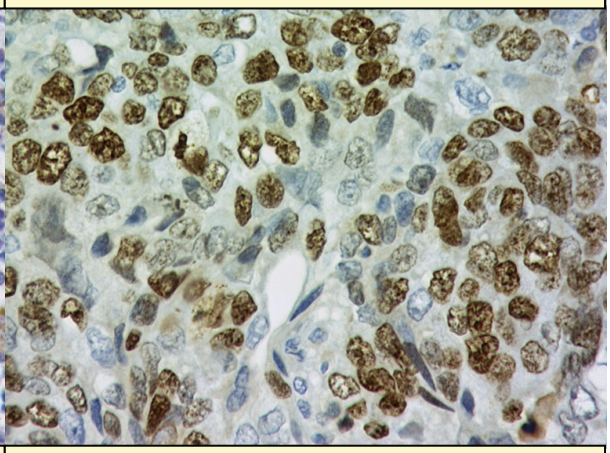

Fig 7.5 – patient 10, Ki67 tumour nuclear proliferation (x400) Ki-67+ nuclei brown. High proliferative index

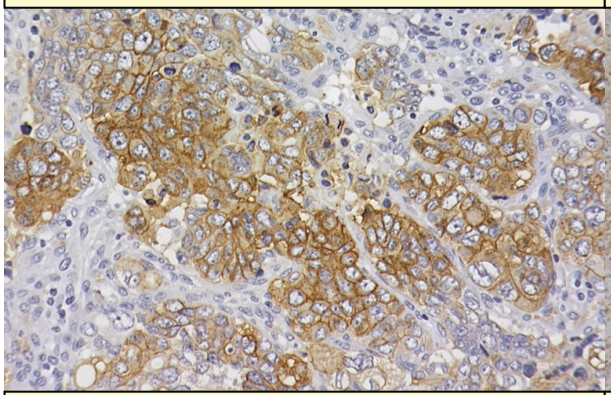

Fig 7.6 – patient 10 Glut-1 stain for hypoxic tumour cells (brown) x200. Note both membrane and cytoplasmic staining

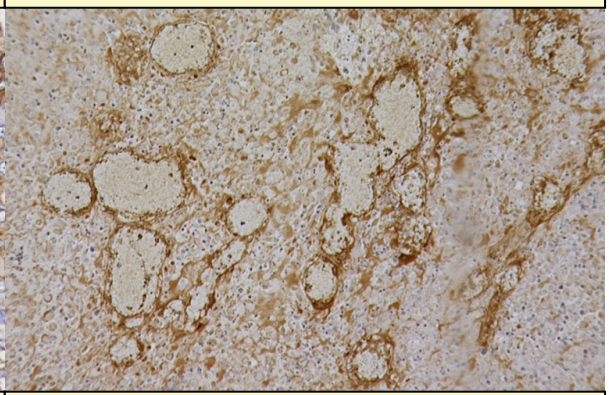

Fig 7.7 – VEGF Strongly Positive (brown) , **patient 23 x100. Staining endothelial cells, stromal cells and cytoplasmic positivity**.

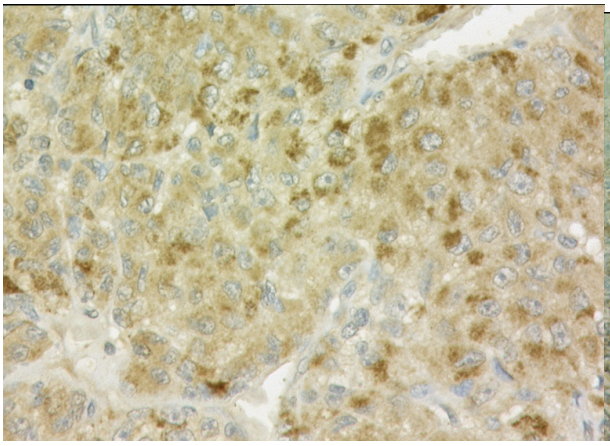

Fig 7.8 – Patient 02, Angiopoietin-1 (x400) – Predominantly cytoplasmic uptake in tumour, with non specific clumping of antibody in places (?precipitation)

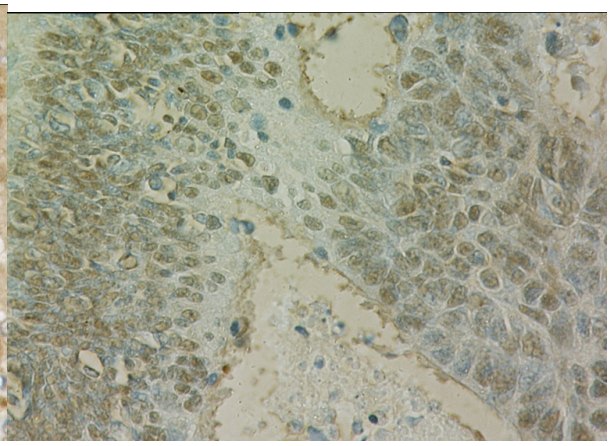

Fig 7.9 – Angiopoietin 2, Patient 19 Colorectal adenocarcinoma (x400) Note platelet staining within blood vessels, nuclear and cytoplasmic staining, vessels well visualised.

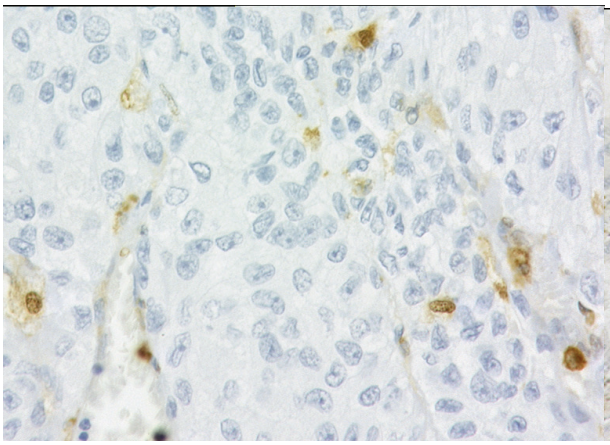

Fig 7.10 – Patient 02, PDGF (brown nuclei) x400. Many slides showed stromal uptake only. Here, scattered tumour nuclei stain positive, and macrophages

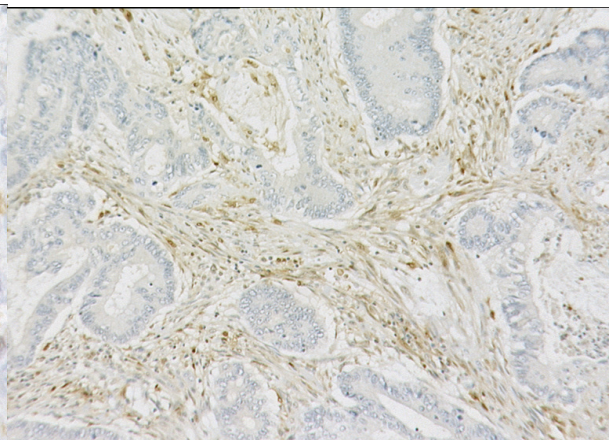

Fig 7.11 – Example, Patient 22 PDGF x100 to illustrate strong stromal uptake, no uptake at all within tumour

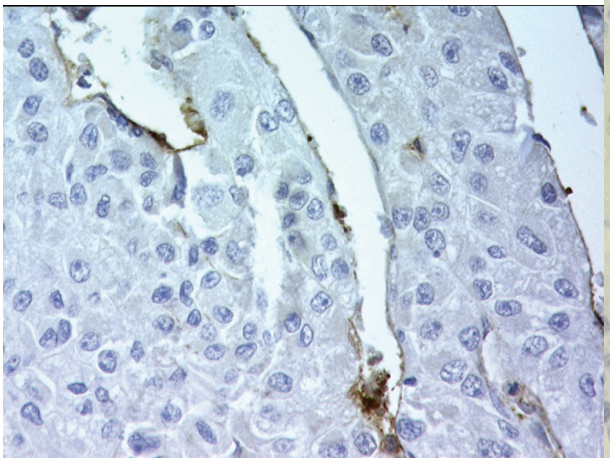

Fig 7.12 – Patient 02 CD61 (x400) – Illustrates immature vessels and endothelial cells within tumour

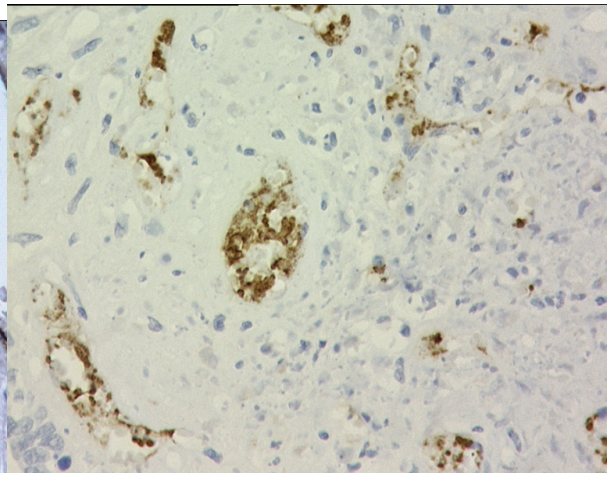

Fig 7.13 – 08 CD61 (x400) – non specific staining of the antibody in cases, which was not included in the analysis

Table 7.5 and 7.6 – Correlation Coefficients and regression analysis between continuous, categorical variables, and MRI parameters. a) Correlation Coefficients (r^2) and statistical significance between continuous variables, and MRI parameters (n=21). The majority of calculations yield a negative regression line i.e. fall in MRI parameter following CA4P is greater if higher MVD. b) ANOVA test for relationships between categorical variables and MRI parameters (F value, degrees of freedom and p value shown). Regression graphs in **appendix 3**.

MRI Parameter	Continuous Immunohistochemical Variable					
	CD34 MVD	αSMA PCI	CD105 MVD	CD61 MVD	Ki-67 (%)	Glut-1 (%)
K^{trans} min^{-1}	r^2<-0.001 p=0.98	r^2=-0.079 p=0.23	r^2<-0.001 p=0.957	r^2=-0.011 p=0.539	r^2=-0.077 p=0.233	r^2=0.018 p=0.488
v_e %	r^2=0.002 p=0.867	r^2=-0.124 p=0.128	r^2=-0.052 p=0.335	r^2<-0.001 p=0.983	r^2<-0.001 p=0.868	r^2=0.020 p=0.556
k_{ep} min^{-1}	r^2=-0.0035 p=0.805	r^2=-0.020 p=0.556	r^2=0.007 p=0.731	r^2=-0.046 p=0.285	r^2=-0.112 p=0.170	r^2=0.037 p=0.416
$IAUGC_{60}$ mM $Gd.s^{-1}$	r^2<-0.001 p=0.899	r^2=-0.095 p=0.185	r^2=-0.002 p=0.852	r^2<-0.001 p=0.925	r^2=-0.011 p=0.478	r^2=0.036 p=0.422

MRI Parameter	Categorical Variable			
	Ang-1	Ang-2	PDGF	VEGF
K^{trans} min^{-1}	F = 0.965 df (3,15) p=0.435	F = 3.812 df (2,16) p=0.044	F = 0.197 df (2,16) p=0.823	F = 1.654 df (3,16) p=0.217
v_e %	F = 1.801 df (3,15) p=0.190	F = 1.472 df (2,16) p=0.259	F = 0.484 df (2,16) p=0.625	F = 1.764 df (3,16) p=0.194
k_{ep} min^{-1}	F = 0.720 df (3,15) p=0.556	F = 3.698 df (2,16) p=0.048	F = 0.565 df (2,16) p=0.579	F = 0.963 df (3,16) p=0.434
$IAUGC_{60}$ mM $Gd.s^{-1}$	F = 1.284 df (3,15) p=0.316	F = 1.728 df (2,16) p=0.209	F = 0.468 df (2,16) p=0.635	F = 2.064 df (3,16) p=0.145

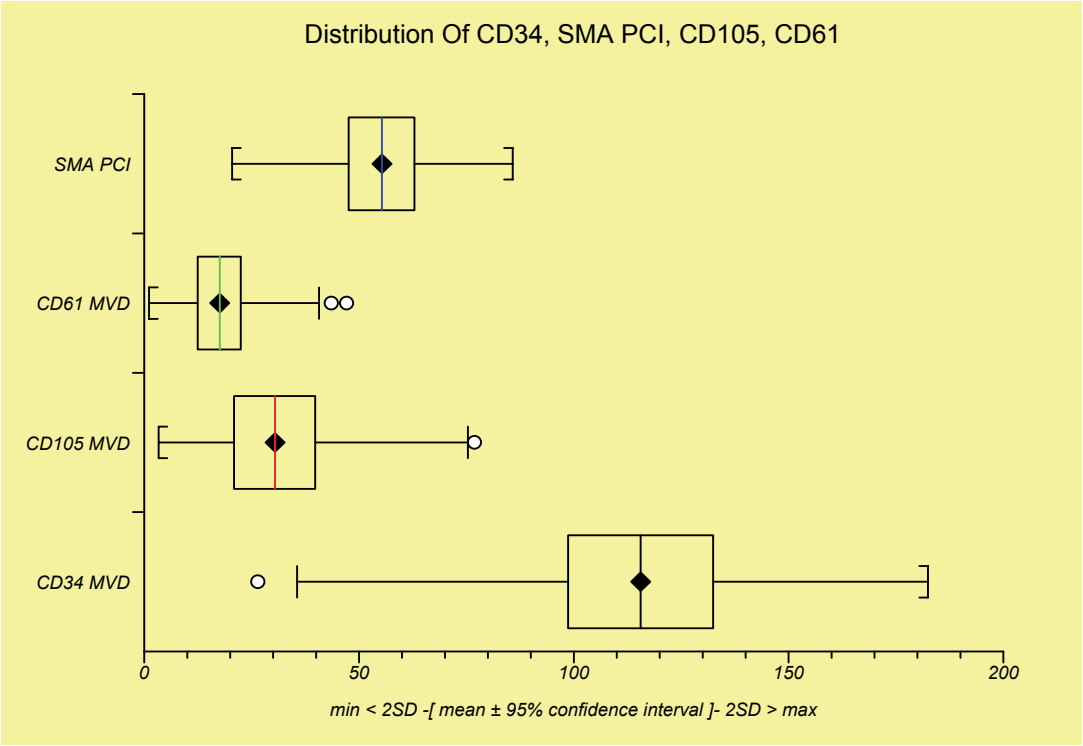

Fig. 7.14 Distribution of CD34, SMA PCI, CD105, CD61 - confidence intervals around the mean show that the majority of tumours fall close around the mean values, however there are outliers which may skew the results. The box represents the mean ± 95% confidence interval. The whiskers represent minimum and maximum values. The X-axis represents MVD (/mm²)

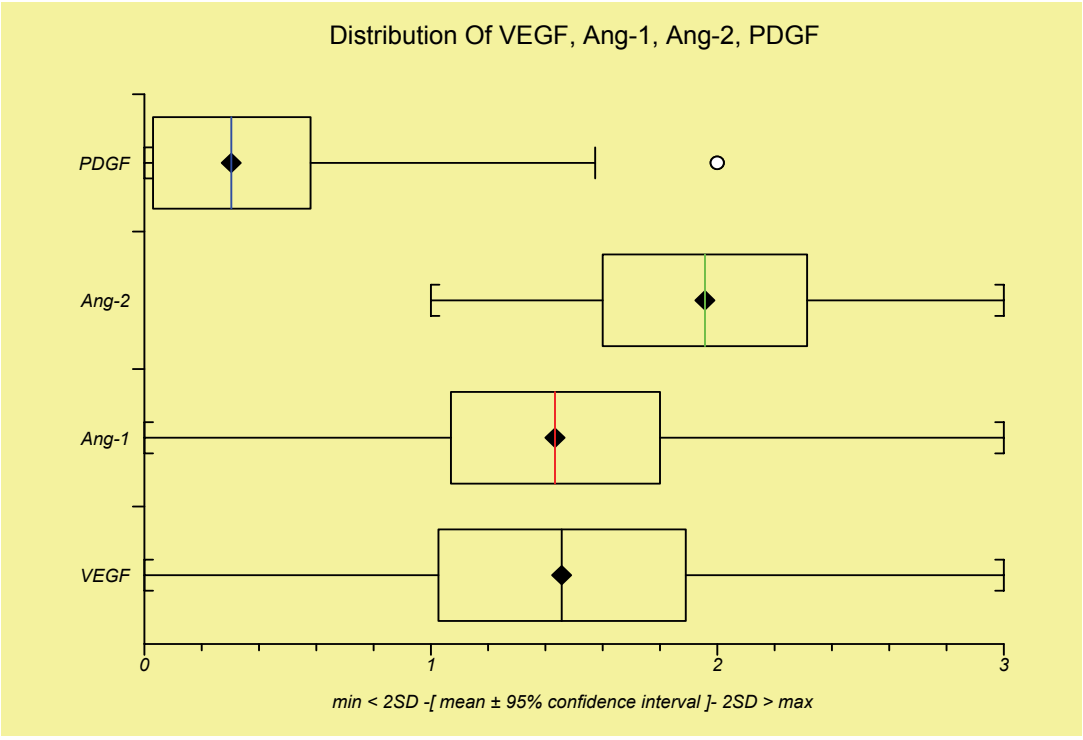

Figure 7.15 - Box & Whisker plot. Wide distributions for these categorical variables

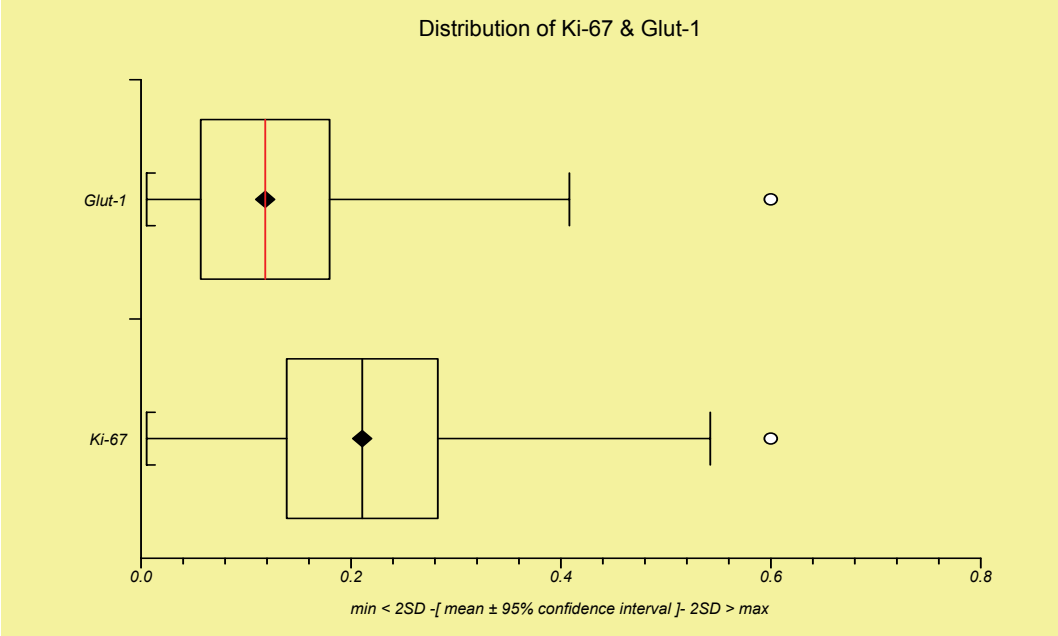

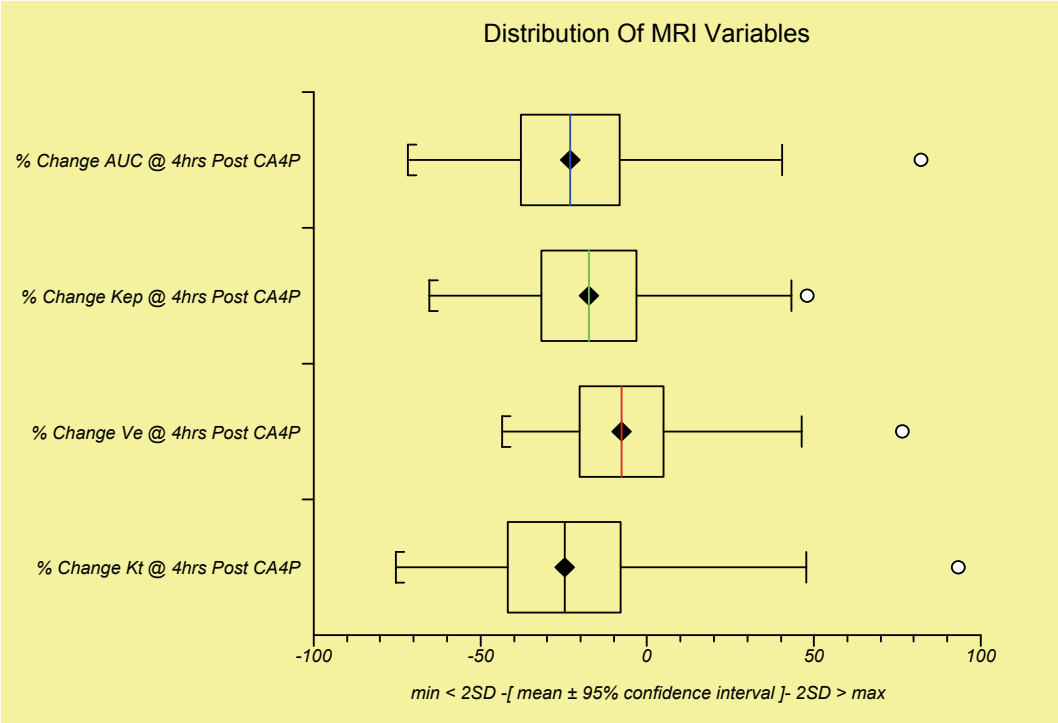

Figures 7.16, 7.17 – Box & Whisker plots. Wide distributions for the categorical variables, however MRI parameters are more tightly distributed about the mean. The X-axis represents categories in and percentage in 7.16

Discussion

We found no strong visual or statistical relationships between changes in DCE-MRI kinetic parameters and the immunohistochemical angiogenic profile (see also **Appendix 3** and Gaya AM et al 2008). This suggests that immunohistochemical analysis of patients' tumours is unlikely to be useful in predicting response to VDA therapy. There is enormous variability seen both in the DCE-MRI kinetic parameters and the immunohistochemistry. It is difficult to know whether the variability is related to the MRI and immunohistochemical techniques or is due to specific tumour characteristics that are of interest to us e.g. vascular maturity.

Antibody selection was chosen to give a broad selection of vascular markers. Antibodies against vascular endothelium, immature vascular endothelium, pericytes, proliferation marker and antibodies against molecules or receptors intimately involved in the angiogenic process were all chosen. All antibodies were purchased from commercial suppliers and had been previously tested on human samples. In addition, all antibodies were validated in the laboratory before use by Dr Frances Daley and Dr Uzma Qureshi. Titration experiments were also performed to determine the optimum concentrations.

The variability of CD34 and CD105 MVD is consistent with previous studies. MVD has been correlated with risk of metastasis, prediction of efficacy of anti-cancer therapy, and prognosis in a variety of tumour types (Barresi et al., 2007; Calvin et al., 2007; Des Guetz et al., 2006; Gadducci et al., 2006; Gulubova & Vlaykova, 2007; Kavantzas et al., 2007; Trivella et al., 2007; Zhao et al., 2006). The PCI results agree with Eberhard's data (Eberhard et al., 2000). We have found no evidence that mature vasculature with higher PCI responds poorly to CA4P, or that immature $CD105^+$ vasculature responds better. Tumours with higher CD34 MVD may also have higher $CD105^+$ MVD, however it does not necessarily follow that active angiogenesis takes place.

Generally, CD31 has been accepted as the pan-endothelial marker of choice for paraffin sections (Hasan et al., 2002). In a review by Fox (Fox et al., 2001), when studies on breast cancer with multivariate analysis that used antibodies to CD31 or CD34 were examined, most revealed a positive association with relapse free survival (13/14) and all for overall survival (OS) (12/12). With studies using Factor VIII, only 8/13 were positive for RFS and 7/10 for OS. When I attempted CD31/αSMA double staining, the antibody was far less reliable as a pan endothelial marker. Despite using double stain block solution, it appeared that the addition of the 2^{nd} antibody was affecting the distribution of the first. We felt that

the weak stromal cross reactivity with CD34 would not interfere with the identification of vessels, so CD34 was used as the pan endothelial marker for this study.

The two validated methods of microscopic vessel counting are the random point scoring system 'Chalkley Counting' (Chalkley, 1943; Fox et al., 1995; Smith et al., 1988) and the 'random field' methods (Eberhard et al., 2000), although few studies have directly compared these two methods of microvessel quantification (Fox et al., 1995). It was felt that a random field method of counting was preferable as some of the tumour samples, especially diagnostic biopsies, were too small for Chalkley counting.

There are a number of aspects of this study which undermine the power of our conclusions. We obtained only small numbers of samples with a heterogeneous mix of different tumour types. However, our sample was limited to patients who had received CA4P and undergone DCE-MRI. Within the ANOVA categorical analysis especially, this greatly reduced the statistical power. Our paraffin blocks, up to 21 years old, were taken from the primary surgical procedure whilst patients received CA4P during Phase I trials many years later after metastatic relapse. There is a loss of staining intensity for several markers in stored tissue slides over time (Bertheau et al., 1998; Van den Broek & Van de Vijver, 2000), and the degradation in antigenicity may begin after as little as 3-6 months. It is however controversial and less well documented whether antigenicity decreases in tissue blocks as well (Fergenbaum et al., 2004). Our slides were cut from the tissue blocks within a few months of staining. In addition, most antibodies used at the Gray Cancer Institute are tested for this phenomenon (Frances Daley, Personal Communication 2006). There are also suggestions that the angiogenic phenotype might continuously evolve from primary tumour through to metastasis (Sullivan & Graham, 2007).

PDGF stromal expression may be clinically significant in inducing tumour angiogenesis. The recruitment of stromal fibroblast cells can be critical for tumour angiogenesis (Dong et al., 2004). Tumour-stroma interactions play a significant role in tumour development and progression. Alterations in the stromal microenvironment, including enhanced angiogenesis, modified extracellular matrix composition, inflammatory cells, and protease activity are essential regulatory factors of tumour growth and invasion (Mueller & Fusenig, 2002). PDGF probably has a major role in signalling for tumour pericyte recruitment. PDGF receptors within the stroma also have a function as regulators of tumour interstitial fluid pressure, tumour transvascular transport and tumour drug uptake (Ostman, 2004).

There were widespread falls in MRI kinetic parameters following CA4P however for most patients these did not achieve statistical significance. For some this was because the CA4P dose received was below the threshold level of 50 mg/m^2 (Galbraith et al., 2003) - for others the CA4P simply did not have the expected tumour blood flow effect. 95% CI for K^{trans} change was -62.5% to +166.5%, $IAUGC_{60}$±80%. Conversely, taking the two separate trials individually, in PH1/066 the lower 95% confidence limit for K^{trans} was -44% and in PH1/092 it was -76.5%. This wide DCE-MRI parameter variability is in line with previously published data (Padhani et al., 2002; Taylor et al., 2004; Taylor et al., 2006). Combining DCE-MRI data from separate studies can adversely affect statistical confidence intervals due to the differences in scan sequences and calibration methods used (Taylor et al., 2006). There was wide intrapatient variability, patient motion, and an estimated arterial input function. Modified Fritz-Hansen arterial input co-efficients, which are currently used, demonstrate better reproducibility (Fritz-Hansen et al., 1996; Taylor et al., 2007). Averaging the kinetic parameters over a whole lesion also dilutes the effect of CA4P central vascular shutdown because of relative sparing at the tumour periphery.

MVD does not reflect the functional properties of vessels, including permeability, which contribute to DCE-MRI parameters. Studies reporting correlations between MRI parameters and MVD have therefore found only moderate associations (Su et al., 2003; Tuncbilek et al., 2004). Several studies (Buckley et al., 1997; Stomper et al., 1997; Su et al., 2003) show conflicting data relating immunohistochemical expression with DCE-MRI parameters. The different analysis methods used may have affected the results. Hawighorst (Hawighorst et al., 1998) showed that MRI parameters were better indicators of patient survival than MVD or VEGF.

The significant correlation between ang-2 and K^{trans} is probably a false positive statistical quirk due to the sheer number of variables tested. However it might be explained thus: Angiopoietins are involved in the angiogenic switch (Ahmad et al., 2001; Tanaka et al., 2003). Ang-1 stabilises vessels by maintaining pericyte coverage; ang-2 promotes pericyte removal, which in the presence of VEGF facilitates the angiogenic response and in the absence of VEGF induces vessel regression (Bach et al., 2007; Moon et al., 2006; Shim et al., 2007; Winter et al., 2007). Depending on the tumour model, stabilization of blood vessels by ang-1 may either promote tumour angiogenesis or reduce tumour growth (Metheny-Barlow & Li, 2003). Wang (Wang et al., 2007) has shown ang-2 correlates with active angiogenesis in human colorectal carcinomas, and that ang-2 also correlates with VEGF. Thus, unstable

immature ang-2 expressing vasculature undergoing neoangiogenesis is probably more susceptible to the effects of VDAs and thus detectable by DCE-MRI.

Conclusions

There was wide intrapatient variability in angiogenic profile expression, and DCE-MRI analysis also revealed widespread falls in kinetic parameters following CA4P. There is no obvious correlation between falls in MRI kinetic parameters and vascular markers, however sample numbers were small. Immunohistochemical analysis of patients' tumours is unlikely to be useful in predicting response to VDA therapy.

This was an exploratory study which we hoped would suggest some leads for further analysis. This study could be expanded to look at larger population numbers and use fresh tumour samples of a single cancer type; this could be performed for example as a biological sub study within a phase 1, 2 or 3 drug trial, especially as functional imaging is now becoming more widely available (Gaya et al., 2008). To date however this has not been carried out.

References

Ahmad, S.A., Liu, W., Jung, Y.D., Fan, F., Reinmuth, N., Bucana, C.D. & Ellis, L.M. (2001). Differential expression of angiopoietin-1 and angiopoietin-2 in colon carcinoma. A possible mechanism for the initiation of angiogenesis. *Cancer*, **92,** 1138-43.

Bach, F., Uddin, F.J. & Burke, D. (2007). Angiopoietins in malignancy. *Eur J Surg Oncol*, **33,** 7-15.

Barnhill, R.L., Xiao, M., Graves, D. & Antoniades, H.N. (1996). Expression of platelet-derived growth factor (PDGF)-A, PDGF-B and the PDGF-alpha receptor, but not the PDGF-beta receptor, in human malignant melanoma in vivo. *Br J Dermatol*, **135,** 898-904.

Barresi, V., Cerasoli, S., Vitarelli, E. & Tuccari, G. (2007). Density of microvessels positive for CD105 (endoglin) is related to prognosis in meningiomas. *Acta Neuropathol (Berl)*, **114,** 147-56.

Bertheau, P., Cazals-Hatem, D., Meignin, V. & al., e. (1998). Variability Of Immunohistochemical Reactivity On Stored Paraffin Slides. *J Clin Pathol*, **51,** 370 - 374.

Bland, J. & Altman, D. (1996). Measurement Error Proportional To The Mean. *BMJ*, **313,** 744.

Bobrow MN, H.T., Shaughnessy KJ, Litt GJ. (1989). Catalysed Reporter Deposition, A Novel Method Of Signal Amplification. Application To Immunoassays. *J Immunol Methods*, **125,** 279.

Buckley, D.L., Drew, P.J., Mussurakis, S., Monson, J.R. & Horsman, A. (1997). Microvessel density of invasive breast cancer assessed by dynamic Gd-DTPA enhanced MRI. *J Magn Reson Imaging*, **7,** 461-4.

Calvin, D.P., Hammond, M.E., Pajak, T.F., Trotti, A.M., Meredith, R.F., Rotman, M., Jones, C.U., Byhardt, R.W., Demas, W.F., Ang, K.K. & Fu, K.K. (2007). Microvessel density >or=60 does not predict for outcome after radiation treatment for locally advanced head and neck squamous cell carcinoma: results of a correlative study from the Radiation Therapy Oncology Group (RTOG) 90-03 Trial. *Am J Clin Oncol*, **30,** 406-19.

Chalkley, H. (1943). Method For The Quantitative Morphologic Analysis Of Tissues. *J Natl Cancer Inst*, **4,** 47 - 53.

d'Arcy, J.A., Collins, D.J. , Padhani A.R. , Walker-Samuel S. , Suckling J. , Leach M.O. (2006). Informatics in Radiology. Magnetic Resonance Imaging Workbench: Analysis and Visualisation of Dynamic Contrast Enhanced MR Imaging Data. *Radiographics*, **26,** 621 - 632.

Des Guetz, G., Uzzan, B., Nicolas, P., Cucherat, M., Morere, J.F., Benamouzig, R., Breau, J.L. & Perret, G.Y. (2006). Microvessel density and VEGF expression are prognostic factors in colorectal cancer. Meta-analysis of the literature. *Br J Cancer*, **94,** 1823-32.

Dong, J., Grunstein, J., Tejada, M., Ferrara, N. & al., e. (2004). VEGF Null Cells Require PDGF Alpha Signalling Mediated Stromal Fibroblast Recruitment For Tumorigenesis. *Embo J*, **23,** 2800 - 2810.

Eberhard, A., Kahlert, S., Goede, V., Hemmerlein, B., Plate, K.H. & Augustin, H.G. (2000). Heterogeneity of angiogenesis and blood vessel maturation in human tumors: implications for antiangiogenic tumor therapies. *Cancer Res*, **60,** 1388-93.

Erdem, O., Erdem, M., Erdem, A., Memis, L. & Akyol, G. (2007). Expression of vascular endothelial growth factor and assessment of microvascular density with CD 34 and endoglin in proliferative endometrium, endometrial hyperplasia, and endometrial carcinoma. *Int J Gynecol Cancer*.

Fergenbaum, J., Garcia-Closas, M., Hewitt, S., Lissowska, J., Sakoda, L. & Sherman, M. (2004). Loss of Antigenicity In Stored Sections of Breast Cancer Tissue Microarrays. *Cancer Epidemiol Biomarkers Prev*, **13,** 667 - 672.

Fox, S., Leek, R., Weekes, M., Whitehouse, R., Gatter, K. & Harris, A. (1995). Quantitation And Prognostic Value Of Breast Cancer Angiogenesis: Comparison Of Microvessel Density, Chalkley Count, And Computer Image Analysis. *J Pathol*, **177,** 275 - 283.

Fox, S.B., Gasparini, G. & Harris, A.L. (2001). Angiogenesis: pathological, prognostic, and growth-factor pathways and their link to trial design and anticancer drugs. *Lancet Oncol*, **2,** 278-89.

Fritz-Hansen, T., Rostrup, E., Larsson, H.B., Sondergaard, L., Ring, P. & Henriksen, O. (1996). Measurement of the arterial concentration of Gd-DTPA using MRI: a step toward quantitative perfusion imaging. *Magn Reson Med*, **36,** 225-31.

Gadducci, A., Ferrero, A., Cosio, S., Zola, P., Viacava, P., Dompe, D., Fanelli, G., Ravarino, N., Motta, M., Cristofani, R. & Genazzani, A.R. (2006). Intratumoral microvessel density in advanced epithelial ovarian cancer and its use as a prognostic variable. *Anticancer Res*, **26,** 3925-32.

Galbraith, S.M., Maxwell, R.J., Lodge, M.A., Tozer, G.M., Wilson, J., Taylor, N.J., Stirling, J.J., Sena, L., Padhani, A.R. & Rustin, G.J. (2003). Combretastatin A4 phosphate has tumor antivascular activity in rat and man as demonstrated by dynamic magnetic resonance imaging. *J Clin Oncol*, **21,** 2831-42.

Gaya, A.M., Daley, F., Taylor, N.J., Tozer, G., Qureshi, U., Padhani, A.R., Pedley, R.B., Begent, R., Wellsted, D., Stirling, J.J. & Rustin, G.J. (2008). Relationship Between Human Tumour Angiogenic Profile And Combretastatin-Induced Vascular Shutdown – An Exploratory Study. *Br J Cancer*, **99,** 321 - 326.

Gulubova, M. & Vlaykova, T. (2007). Prognostic significance of mast cell number and microvascular density for the survival of patients with primary colorectal cancer. *J Gastroenterol Hepatol*.

Hasan, J., Byers, R. & Jayson, G.C. (2002). Intra-tumoural microvessel density in human solid tumours. *Br J Cancer*, **86,** 1566-77.

Hawighorst, H., Weikel, W., Knapstein, P.G., Knopp, M.V., Zuna, I., Schonberg, S.O., Vaupel, P. & van Kaick, G. (1998). Angiogenic activity of cervical carcinoma: assessment by functional magnetic resonance imaging-based parameters and a histomorphological approach in correlation with disease outcome. *Clin Cancer Res*, **4,** 2305-12.

J. Lind, A., Wikstrom, P., Granfors, T., Egevad, L., Stattin, P. & Bergh, A. (2005). Angiopoietin 2 expression is related to histological grade, vascular density, metastases, and outcome in prostate cancer. *Prostate*, **62,** 394-9.

Kavantzas, N., Paraskevakou, H., Tseleni-Balafouta, S., Aroni, K., Athanassiades, P., Agrogiannis, G. & Patsouris, E. (2007). Association between microvessel density and histologic grade in renal cell carcinomas. *Pathol Oncol Res*, **13,** 145-8.

Merono, A., Lucena, C., Lopez, A., Garrido, J.J., Perez de, L.L. & Llanes, D. (2002). Immunohistochemical analysis of beta3 integrin (CD61): expression in pig tissues and human tumors. *Histol Histopathol*, **17,** 347-52.

Metheny-Barlow, L.J. & Li, L.Y. (2003). The enigmatic role of angiopoietin-1 in tumor angiogenesis. *Cell Res*, **13,** 309-17.

Moon, W.S., Park, H.S., Yu, K.H., Jang, K.Y., Kang, M.J., Park, H. & Tarnawski, A.S. (2006). Expression of angiopoietin 1, 2 and their common receptor Tie2 in human gastric carcinoma: implication for angiogenesis. *J Korean Med Sci*, **21,** 272-8.

Mueller, M.M. & Fusenig, N.E. (2002). Tumor-stroma interactions directing phenotype and progression of epithelial skin tumor cells. *Differentiation*, **70,** 486-97.

Ostman, A. (2004). PDGF receptors-mediators of autocrine tumor growth and regulators of tumor vasculature and stroma. *Cytokine Growth Factor Rev*, **15,** 275-86.

Padhani, A.R., Hayes, C., Landau, S. & Leach, M.O. (2002). Reproducibility of Quantitative Dynamic MRI Of Normal Human Tissues. *NMR Biomed*, **15,** 143 - 154.

Parker, G., Suckling, J., Tanner, S., Padhani, A., Revell, P., Husband, J. & Leach, M. (1997). Probing tumor microvascularity by measurement, analysis and display of contrast agent uptake kinetics. *J Magn Reson Imaging*, **7,** 564 - 574.

Rustin, G.J., Galbraith, S.M., Anderson, H., Stratford, M., Folkes, L.K., Sena, L., Gumbrell, L. & Price, P.M. (2003). Phase I clinical trial of weekly combretastatin A4 phosphate: clinical and pharmacokinetic results. *J Clin Oncol*, **21,** 2815-22.

Shim, W.S., Ho, I.A. & Wong, P.E. (2007). Angiopoietin: a TIE(d) balance in tumor angiogenesis. *Mol Cancer Res*, **5,** 655-65.

Smith, K., Hill, S., Begg, A. & Denekamp, J. (1988). Validation of the Fluorescent Dye Hoescht 33342 As A Vascular Space Marker In Tumours. *Br J Cancer*, **57,** 247 - 253.

Stomper, P.C., Winston, J.S., Herman, S., Klippenstein, D.L., Arredondo, M.A. & Blumenson, L.E. (1997). Angiogenesis and dynamic MR imaging gadolinium enhancement of malignant and benign breast lesions. *Breast Cancer Res Treat*, **45,** 39-46.

Su, M.Y., Cheung, Y.C., Fruehauf, J.P., Yu, H., Nalcioglu, O., Mechetner, E., Kyshtoobayeva, A., Chen, S.C., Hsueh, S., McLaren, C.E. & Wan, Y.L. (2003). Correlation of dynamic contrast enhancement MRI parameters with microvessel density and VEGF for assessment of angiogenesis in breast cancer. *J Magn Reson Imaging*, **18,** 467-77.

Sullivan, R. & Graham, C.H. (2007). Hypoxia-driven selection of the metastatic phenotype. *Cancer Metastasis Rev*, **26,** 319-31.

Tanaka, S., Sugimachi, K., Yamashita, Y., Shirabe, K., Shimada, M. & Wands, J.R. (2003). Angiogenic switch as a molecular target of malignant tumors. *J Gastroenterol*, **38 Suppl 15,** 93-7.

Taylor, N., Lankester, K., Ah-See, M.-L., Stirling, J., Rustin, G., Makris, A., D'Arcy, J., Walker-Samuel, S., Leach, M. & Padhani, A. (2004). Reproducibility of T1 and T2* weighted dynamic contrast-enhanced MRI: a multiparametric comparison of breast and abdominal tumours. *Proc ISMRM***,** Abstract 1975.

Taylor, N.J., d'Arcy, J.A., Walker-Samuel, S., Lankester, K.J., Collins, D.J., Knowles, B., White, D.L., Miaux, Y., Suhy, J., Guermazi, A., Stirling, J.J., Wallace, T., Koh, D.-M., Tang, A., Lee, C., Rustin, G.J.S., Leach, M.O. & Padhani, A.R. (2006). Single and multi-centre DCE-MRI reproducibility in Phase I clinical trials. In *Proc. I.S.M.R.M* pp. Abstract 766: 14th Annual Meeting.

Taylor, N.J., Tunariu, N., Ah-See, M.-L., Stirling, J.J., Beresford, M.J., Makris, A., d'Arcy, J.A., Collins, D.J. & Padhani, A.R. (2007). Effects of arterial input functions on dynamic MRI kinetic parameter estimates:
an analysis of parameter variability and model fitting in breast cancer patients. In *Proc ISMRM* pp. Abstract 1975: 15th Annual Meeting.

Tofts, P.S. (1997). Modeling tracer kinetics in dynamic Gd-DTPA MR imaging. *J Magn Reson Imaging*, **7,** 91 - 101.

Tofts, P.S., Brix, G., Buckley, D.L., Evelhoch, J.L., Henderson, E., Knopp, M.V., Larsson, H.B., Lee, T.Y., Mayr, N.A., Parker, G.J., Port, R.E., Taylor, J. & Weisskoff, R.M. (1999). Estimating kinetic parameters from dynamic contrast-enhanced T(1)-weighted MRI of a diffusable tracer: standardized quantities and symbols. *J Magn Reson Imaging*, **10,** 223-32.

Tozer, G.M., Kanthou, C. & Baguley, B.C. (2005). Disrupting tumour blood vessels. *Nat Rev Cancer*, **5,** 423-35.

Trivella, M., Pezzella, F., Pastorino, U., Harris, A.L. & Altman, D.G. (2007). Microvessel density as a prognostic factor in non-small-cell lung carcinoma: a meta-analysis of individual patient data. *Lancet Oncol*, **8,** 488-99.

Tuncbilek, N., Karakas, H.M. & Altaner, S. (2004). Dynamic MRI in indirect estimation of microvessel density, histologic grade, and prognosis in colorectal adenocarcinomas. *Abdom Imaging*, **29,** 166-72.

Van den Broek, L. & Van de Vijver, M. (2000). Assessment Of Problems In Diagnostic And Research Immunohistochemistry Associated With Epitope Instability In Stored Paraffin Sections. *Appl Immunohistochem Mol Morphol*, **8,** 316 - 321.

Von Wasielewski R, M.M., Gignac S, Wilkens L, Werner M, Georgii A. (1997). Tyramine Amplification Technique In Routine Immunochemistry. *J Histochem Cytochem*, **45,** 1455.

Wang, H.L., Deng, C.S., Lin, J., Pan, D.Y., Zou, Z.Y. & Zhou, X.Y. (2007). Expression of angiopoietin-2 is correlated with vascularization and tumor size in human colorectal adenocarcinoma. *Tohoku J Exp Med*, **213,** 33-40.

Winter, S.F., Acevedo, V.D., Gangula, R.D., Freeman, K.W., Spencer, D.M. & Greenberg, N.M. (2007). Conditional activation of FGFR1 in the prostate epithelium induces angiogenesis with concomitant differential regulation of Ang-1 and Ang-2. *Oncogene*, **26,** 4897-907.

Zhao, H.C., Qin, R., Chen, X.X., Sheng, X., Wu, J.F., Wang, D.B. & Chen, G.H. (2006). Microvessel density is a prognostic marker of human gastric cancer. *World J Gastroenterol*, **12,** 7598-603.

Final Summary

The work for this thesis began in 2003, and completed in 2005. There was a delay in waiting for additional clinical trial data before the write-up could commence. Consequently much has progressed in the field of vascular targeting in the intervening five years. Antiangiogenic agents are now routinely used in clinical practice, new generations of molecules are being developed, and VDAs are now into phase 3 study.

The A5B7 study has completed and publication is pending (Meyer et al., 2009). Lessons have been learnt which will be applied in future Radioimmunotherapy combination trials. CA4P has moved into a phase 2 study in platinum resistant ovarian cancer (with paclitaxel and carboplatin) following the success of UKCTC-207, and in anaplastic thyroid cancer (in combination with doxorubicin). There is a phase 2 study in NSCLC of paclitaxel and carboplatin with CA4P and Bevacizumab following a promising phase I, and a prostate cancer phase 2 study of docetaxel in combination with CA4P. DMXAA is now being tested in a phase 3 trial with paclitaxel and carboplatin in non small cell lung cancer and AVE8062 is also now in phase 3 trials.

The latest MRI scanners can image so much faster that direct estimation of the arterial input function is now possible, which will greatly improve reproducibility, and reduce scanning time. The higher resolution available on new 3T magnets and developments in MRI coil technology will also provide interesting new data. Publication of our DCE-MRI and cardiac output data is pending but has been published so far in abstract form (Andrew M Gaya et al., 2008; Gaya et al., 2008). DCE-MRI is now a well accepted surrogate endpoint in trials of antiangiogenic agents and VDAs. There are no plans to look further at perfusion CT to assess late vascular changes with CA4P, but late effects of other long acting anti-vascular compounds can be seen (Koukourakis et al., 2007; Ma et al., 2008; Sabir et al., 2008).

The immunohistochemistry project had many pitfalls, not least the age of the tissue and the heterogeneity of tumour types. New studies are now being designed where biopsy of tumour tissue throughout treatment leads to direct assessment of the effects of antivascular drugs (Dickler et al., 2008) and changes in vascular chemistry. I believe that prediction of patients' response to VDAs and/or antiangiogenic agents on the basis of immunohistochemical marker expression and genetic analysis is not too far away. Despite the many problems encountered during this research the future does look bright in this field.

References

Andrew M Gaya, N Jane Taylor, Tarun Mittal, J James Stirling, David J Collins, James d'Arcy, Gordon J Rustin, Tim Meyer, David Wellsted & Padhani, A.R. (2008). Cardiac output changes and variability of DCE-MRI response between patients and between lesions following infusion of the vascular disruptive agent Combretastatin-A4 Phosphate (CA4P). In *NCRI Annual Conference*: Birmingham, UK.

Dickler, M.N., Rugo, H.S., Eberle, C.A., Brogi, E., Caravelli, J.F., Panageas, K.S., Boyd, J., Yeh, B., Lake, D.E., Dang, C.T., Gilewski, T.A., Bromberg, J.F., Seidman, A.D., D'Andrea, G.M., Moasser, M.M., Melisko, M., Park, J.W., Dancey, J., Norton, L. & Hudis, C.A. (2008). A phase II trial of erlotinib in combination with bevacizumab in patients with metastatic breast cancer. *Clin Cancer Res*, **14,** 7878-83.

Gaya, A., Taylor, N.J., Stirling, J.J., Rustin, G.J., Padhani, A. & Goh, V. (2008). Early & Late Tumour Vasculature Changes Following the Vascular Disruptive Agent (VDA) Combretastatin-A4-Phosphate (CA4P) Using Dynamic Contrast Enhanced MRI (DCE-MRI) and Perfusion CT. In *ESGAR* pp. Abstract 31227: Istanbul, Turkey.

Koukourakis, M.I., Mavanis, I., Kouklakis, G., Pitiakoudis, M., Minopoulos, G., Manolas, C. & Simopoulos, C. (2007). Early antivascular effects of bevacizumab anti-VEGF monoclonal antibody on colorectal carcinomas assessed with functional CT imaging. *Am J Clin Oncol*, **30,** 315-8.

Ma, S.H., Le, H.B., Jia, B.H., Wang, Z.X., Xiao, Z.W., Cheng, X.L., Mei, W., Wu, M., Hu, Z.G. & Li, Y.G. (2008). Peripheral pulmonary nodules: relationship between multi-slice spiral CT perfusion imaging and tumor angiogenesis and VEGF expression. *BMC Cancer*, **8,** 186.

Meyer, T., Gaya, A.M., Dancey, G., Rustin, G.J. & Begent, R. (2009). A Phase I/II Trial of Radioimmunotherapy (RIT) with 131Iodine-Labelled A5B7 Anti-CEA Antibody (131I-A5B7) in Combination with Combretastatin-A4-Phosphate (CA4P) In Advanced Gastrointestinal Carcinomas. *Clin Cancer Res*, **(Submitted for publication)**.

Sabir, A., Schor-Bardach, R., Wilcox, C.J., Rahmanuddin, S., Atkins, M.B., Kruskal, J.B., Signoretti, S., Raptopoulos, V.D. & Goldberg, S.N. (2008). Perfusion MDCT enables early detection of therapeutic response to antiangiogenic therapy. *AJR Am J Roentgenol*, **191,** 133-9.

Appendices

Appendix 1 - Overview of MRI Physics

Atomic nuclei containing odd numbers of protons or neutrons possess nuclear spin visible by MRI. These nuclei possess positive charge, and thus induce magnetic fields (they are moving charged particles). Each nucleus is effectively a tiny magnet spinning on its long axis. MRI is derived from the interaction of this nuclear 'spin' with an externally applied magnetic field. ^{1}Hydrogen, which possesses a single proton, is commonly used as it is abundant in tissue and produces the strongest signal. Other isotopes such as ^{13}carbon, ^{19}fluorine, ^{23}sodium or ^{31}phosphorus have also been used. A magnetic dipole moment vector with a defined magnitude and axis of rotation can represent each of the nuclear spins present in a defined volume of tissue. These vectors are orientated randomly in all directions, so when summed, the net magnetisation vector is zero.

If the tissue is placed in an external magnetic field, $\underline{B}_0$ (units = tesla, T) there is an interaction between the nuclear spins and $\underline{B}_0$ such that individual spins rotate, or 'precess', gyroscopically around the axis of $\underline{B}_0$ and the magnetic dipole moment vector of each spin lines up either parallel or anti-parallel to $\underline{B}_0$. The spins precess at a frequency proportional to the magnetic field strength of $\underline{B}_0$, known as the Larmor frequency:

$$\underline{\omega}_0 = \gamma \underline{B}_0 \qquad (1)$$

where $\underline{\omega}_0$ is the Larmor frequency(radian.s^{-1}), γ is the gyromagnetic ratio(s^{-1}.T^{-1}) of the nuclear spin and $\underline{B}_0$ is the external magnetic field(T). γ is a constant which is an intrinsic property of a particular nuclear spin. For a 1.5T magnet the Larmor frequency is approximately 63MHz but can vary depending upon the scanner.

Hydrogen nuclei can exist at two energy levels. Nuclei at the lower energy level have magnetic vectors aligned parallel with $\underline{B}_0$(spin-up), as this requires less energy than anti-parallel(spin-down) alignment. A tiny excess number of hydrogen nuclei (7/10 million) have magnetic vectors in anti-parallel alignment, creating a net magnetisation vector, $\underline{M}_0$, in the same direction as $\underline{B}_0$

The application of a radio-frequency (RF) pulse, $\underline{B}_1$, at the Larmor (resonance) frequency, in the transverse (XY) plane (i.e. perpendicular to $\underline{B}_0$), causes the nuclear spins to precess around $\underline{B}_1$ instead so the net magnetisation vector rotates out of alignment with $\underline{B}_0$. The flip angle, α, is the angle of rotation produced by $\underline{B}_1$. For example, a flip angle of 90^0 indicates an RF pulse of sufficient energy to rotate $\underline{M}_0$ into the transverse (XY) plane, where it is now termed $\underline{M}_1$.

At equilibrium the spins will populate the lower of the energy states in slight preference to the higher. If the spins are at a temperature T then it can be shown that this difference in the populations is

$$\frac{\text{no. of spin}\uparrow}{\text{no. of spin}\downarrow} = e^{\frac{-\Delta E}{kT}} \qquad \textbf{(2)}$$

and for a group of nuclei precessing randomly around the main field there will be a resultant macroscopic magnetisation $\mathbf{M}_o$ pointing along the Z axis. This is responsible for the bulk magnetic susceptibility χ_o since

$$M_o = \chi_o B_o \qquad \textbf{(3)}$$

If a resonant radiofrequency field is applied, the net absorption of energy will decrease the z component M_z and create an in-phase component in the xy plane M_{xy}.

There is now a moving magnetic field in the transverse plane that induces voltage in a receiver coil. This electric voltage is the magnetic resonance signal. Once the RF pulse is switched off, the net magnetisation vector will realign with $\underline{B}_0$ along the longitudinal (Z) axis (as the nuclear spins will rotate back to precess around $\underline{B}_0$). As only magnetisation in the transverse plane (XY) can induce voltage in the receiver coil, the MR signal will decay as $\underline{M}_1$ rotates back to $\underline{M}_0$ – known as 'free induction decay'. An MR image can be constructed from this signal, though it is usually too fast to allow spatial encoding and so other RF pulses are generally used, in sequence with magnetic field gradients, to form encoded echoes. These can then be Fourier transformed into final images.

The RF pulse provides the energy required to excite nuclear spins from the lower energy level to the higher energy level – but only if its frequency is at the 'resonant' Larmor frequency. The moment the RF pulse ceases, the excited spins will revert to the lower energy level in a process called 'relaxation', which is a re-establishment of thermal equilibrium. There are two relaxation processes: the recovery of longitudinal magnetisation (M_Z) and the decay of transverse magnetisation (M_{XY}) – governed by relaxation time constants, T_1 and T_2 respectively.

T_1 ('spin-lattice' relaxation) depends on how quickly nuclear spins give up energy to the surrounding tissue or 'lattice' and is defined as the time taken for M_Z to return to 63% of its original value (M_0), i.e. to increase M_Z by a factor of e (**Figure 8.1a)**.

T_2('spin-spin' relaxation) depends on the interaction with adjacent spins. At the end of the RF pulse, all spins are precessing in the transverse (XY) plane (assuming a 90^0 flip angle has been applied) at the same frequency and are 'in phase' with each other. Once the RF pulse is switched off, the precessional frequency of a particular spin is altered by interactions with adjacent nuclear spins, resulting in a gradual loss of phase coherence and hence transverse magnetisation. T_2 is defined as the time taken for M_{XY} to decay to 37% of its maximum value, i.e. to decrease M_{XY} by a factor of e (**Figure 8.1b)**.

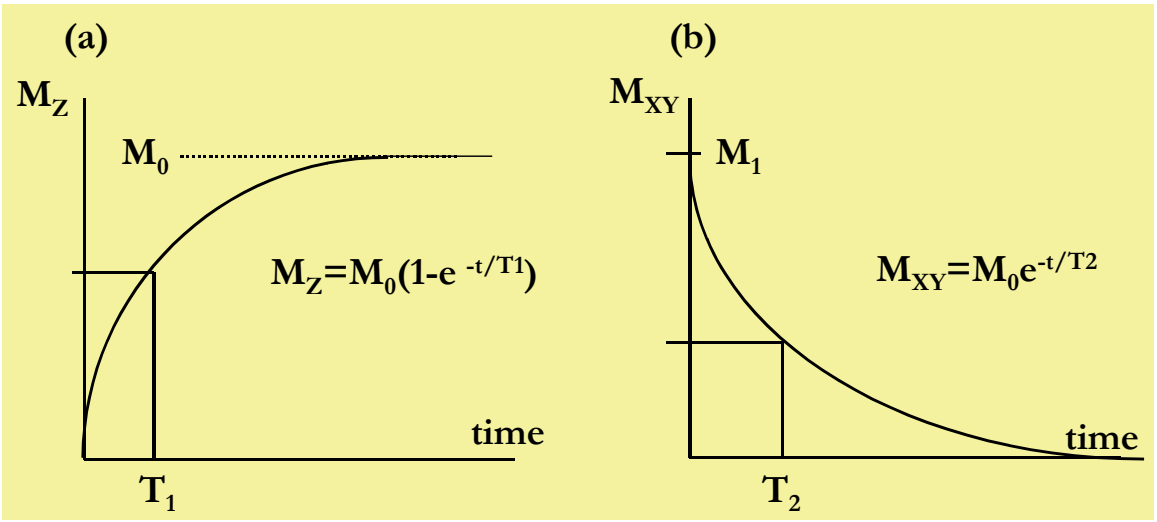

Figure 8.1a: T_1 relaxation time-curve, Fig 8.1b: T_2 relaxation time-curve

B_0 is not uniform, as there are local field distortions due to magnetic susceptibility differences between different tissues and the imperfect winding of the magnet coil. 'Magnetic susceptibility' is a measure of the degree to which a material becomes magnetised when placed in a magnetic field. Air, bone and other tissues all have different magnetic susceptibilities, resulting in distortions in $\underline{B}_0$ at interfaces between different structures. Local inhomogeneities in $\underline{B}_0$ will influence the rate of decay of transverse magnetisation. The effective transverse relaxation under these circumstances is faster than T_2 and the term T_2* is used to describe it and:

$$\frac{1}{T_2 *} = \frac{1}{T_2} + \frac{1}{T_2{}^+} \tag{4}$$

where T_2^+ is the extra relaxation component due to $\underline{B}_0$ inhomogeneities. The T2 relaxivity (R2) is equal to 1/T2 and similarly $R2^*=1/T2^*$. These are important in BOLD imaging.

FLASH MRI (Fast Low Angle Shot MRI) is a basic measuring principle for rapid MRI. FLASH sequences allow for a drastic shortening of the measuring times without a substantial loss in image quality. The measuring principle led to a broad range of completely new imaging sequences. For example, cross-sectional images with acquisition times of a few seconds enable MRI studies of the thorax and abdomen within a single breathhold, dynamic acquisitions synchronized to the electrocardiogram generate movies of the beating heart, and sequential acquisitions monitor the differential uptake of contrast media into body tissues.

The FLASH technique is a gradient echo sequence which combines a low-flip angle radio-frequency excitation of the NMR signal with a rapid repetition of the basic sequence. The repetition time (see below) is usually much shorter than the typical T1 relaxation time of the protons in biological tissue.

Image Contrast

Tissues have characteristic T_1 and T_2 values. T_1 values in the body vary between about 0.2 and 4 seconds and are longer than T_2 values. To create an image, a particular sequence of RF pulses and magnetic field gradients is applied – called a pulse sequence. The size, direction,

timing and frequency of these pulses and gradients can be manipulated such that tissues with different relaxation times will have different signal intensities and there is contrast between them in the resultant image. The repetition time (TR) is the time between acquisition of one phase encoded line and the next. The echo time (TE) is the time between centre of the initial pulse and the time when the MR signal is measured. On a 'T_1-weighted image' (short TR, short TE), tissues with a short T_1 appear bright and those with a long T_1 appear dark. The opposite occurs with a T_2 weighted image (long TR, long TE): tissues with a long T_2 appear bright whereas those with a short T_2 appear dark.

k-space is a formalism widely used in MRI, introduced by Ljunggren and Twieg. *k*-space is the temporary image space in which data from digitized MR signals are stored during data acquisition. When *k*-space is full (at the end of the scan), the data are mathematically processed using Fourier transformation to produce a final image. Thus *k*-space holds raw data before reconstruction. During the scan, *k*-space is filled with raw data one line per TR.

MRI visible protons are those within soft tissues and liquids. Solid tissues such as bone have a fixed lattice and appear black on all image types. Image contrast may also be produced by using pulse sequences sensitive to the relative number of mobile protons available within a tissue. This is termed 'proton density' (PD) image contrast. For example, cerebrospinal fluid has a high proton density whereas brain tissue has a lower proton density. The proton density is responsible for the maximum magnitude of signal generated by a given tissue (signal amplitude). Proton density contrast is regarded as 'basic' MR contrast as it is not dependent on tissue relaxation times. Measured PD images do have some T_1 and T_2 contrast by the nature of the sequence timings used in their measurement.

Image contrast may be enhanced by the use of intravenous contrast agents such as the low molecular weight agent gadolinium diethylene triamine pentaacetic acid (Gd-DTPA, or gadopentetate dimeglumine (Magnevist®)). Gd-DTPA is paramagnetic[1], as the gadolinium

[1] A paramagnetic material will develop a weak attractive force if placed in an magnetic field.

ion contains seven unpaired electrons and so has a large magnetic dipole moment. The presence of Gd-DTPA in a tissue shortens the T_1 and T_2 relaxation times, increasing the 'relaxation rates', $1/T_1$ and $1/T_2$, such that

$$\frac{1}{T_{1obs}} = \frac{1}{T_1(0)} + r_1 C \qquad (5)$$

where $1/T_{1obs}$ is the observed value in the presence of Gd-DTPA, $1/T_1(0)$ is the innate value, C is the concentration of Gd-DTPA(mM) and r_1 is the 'relaxivity' of Gd-DTPA in $mM^{-1}.s^{-1}$ (specific relaxation rate of Gd-DTPA). (The equation may be written in a similar fashion substituting T_2 for T_1). The effect of Gd-DTPA is to increase signal intensity on a T_1-weighted image (as tissues with a short T_1 are bright) and to decrease signal intensity on a T_2 (or T_2*) weighted image (as tissues with a short T_2 are dark). Gd-DTPA is used primarily as a T_1-agent as its effect on T_1 is greater than on T_2 for the same dose of contrast agent (as $T_1 > T_2$).

Gd-DTPA is an extracellular contrast agent and has an excellent safety record. In a study of over 5000 patients, an adverse reaction rate of 2.2% was reported. The commonest event was flushing, and the rate of anaphylaxis currently estimated is 1/200,000. This compound contains unpaired electrons, which produce a dipole-dipole interaction with proton nuclear spins, enhancing their relaxation. It is excreted renally, with a plasma half-life of 90 minutes. Recently, a disease known as Nephrogenic Systemic Fibrosis or Nephrogenic Fibrosing Dermopathy (NSF/NFD) that occurs in patients with kidney failure has been described. Our patients were required to have a GFR>50 mls/min.

Gd-DTPA has a low molecular weight (0.57 kD) and so diffuses out of blood vessels into the extracellular space (except in cerebral imaging when the blood-brain barrier is intact). Tumour vessels are more permeable than normal vessels, so Gd-DTPA diffuses more rapidly into tumour EES than into normal tissue EES, providing contrast by increasing tumour signal intensity on T_1-weighted images.

Conversion of Signal Intensity into Gd-DTPA concentration

Signal intensity on spoiled gradient echo images (the T_1-weighted sequence used) is given by:

$$S = S_{\max} \sin\alpha \frac{1-\exp(-TR/T_1)}{1-\cos\alpha \times \exp(-TR/T_1)} \times \exp(-TE/T_2*) \quad (6)$$

where S_{max}. is the maximal signal intensity (for TR>>T_1 and TE<< T_2) and α is the flip angle.

If TE << T_2*, the term exp (-TE/T_2*) can be ignored and equation(6) simplified to:

$$S = S_{\max} \times [1-\exp(-K \times TR/T_1)] \quad (7)$$

where K is a flip angle correction factor (Hittmair et al.,1994) and is equal to 1.40 for our acquisition conditions (obtained by simulation). The ratio of signal intensity at time t, S_t to baseline (pre-contrast) signal intensity, S_0, is then:

$$S_t / S_0 = \frac{1-\exp[-K \times TR/T_1(t)]}{1-\exp[-K \times TR/T_1(0)]} \quad (8)$$

where T_1(t) is the post-contrast signal intensity at time t, and T_1(0) is the pre-contrast relaxation time respectively.

T_1(0) is calculated from an inversion recovery sequence (see below) and T_1(t) calculated by rearranging equation(8):

$$1/T_1(t) = -\frac{1}{K \times TR} \times \ln\left[1 - \frac{S_t}{S_0}(1-\exp[-K \times TR/T_1(0)]\right] \quad (9)$$

The concentration of Gd-DTPA present at time t, C_t, can then be calculated from equation(9) (Donahue et al., 1994):

$$C_t = \frac{\left(1/T_1(t) - 1/T_1(0)\right)}{r_1} \quad (10)$$

where r_1 is the longitudinal relaxivity of protons in vivo due to Gd-DTPA ($mM^{-1}.s^{-1}$). r_1 is estimated to be $4.5 mM^{-1}s^{-1}$ for a 1.5T system (Donahue et al., 1994).

Calculation of $T_1(0)$

In an inversion recovery sequence, a 180° pulse is applied which flips the net magnetisation vector down to the –Z axis. When the pulse is removed, longitudinal magnetisation (M_Z) will begin to relax back to alignment with B_0 (along the +Z axis). This is described by equation (11):

$$M_Z = M_0[1 - 2\exp(-t/T_1)] \tag{11}$$

where M_0 is the equilibrium magnetisation.

If a 90° pulse is applied after a time known as 'inversion time', TI (time from the original inverting 180° pulse) then M_Z will be converted into M_{XY} (magnetisation in the transverse (XY) plane) and it will induce a signal. The resultant signal intensity is a measure of M_Z. If a series of 180° and 90° pulses are applied with varying inversion times, then a graph of signal intensity versus inversion time can be plotted and fitted to the equation below:

$$S(TI) = M_Z(TI) = M_0[1 - 2\exp(-TI/T_1)] \tag{12}$$

where S(TI) is the signal intensity at inversion time, TI. As TI$\rightarrow\infty$, full relaxation will have occurred so signal intensity will$\rightarrow M_0$. Values for the two unknown parameters T_1 and M_0 may be obtained from curve-fitting. The proton density-weighted image can be used to get a ratio which is used with a lookup table to get T1 rather than the inversion recovery method. The lookup is made by imaging a eurospin phantom with multiple gels of differing and known T1 values as per Parker (1997), and it is important for accuracy:

Appendix 2 – Standard Immunostaining Protocols

Preparation of Solutions and Reagents

TRIS Buffer Saline(TBS)

8.1g Sodium Chloride added to 100ml Tris Buffer, made up to 1000ml with deionised water, pH adjusted to 7.6. Intensity of staining is affected by the pH and buffer ion concentration.

TRIS Buffered Saline Tween(TBST)

For automated staining 0.04% TBST. Add 40µl of Tween-20 to 100ml TBS. Manual staining 0.05% TBST. Add 50µl of Tween-20 to 100ml TBS.

Dilution of Antibodies

Primary Antibodies are diluted in '*Dako antibody diluent*' to an optimal concentration. Optimum antibody titre is defined as the highest dilution of an antibody that results in maximum specific staining with the least amount of background staining under specific conditions. Secondary antibodies are diluted in TBS. Dilutions of these reagents can vary from batch to batch.

Diaminobenzadine(DAB) for HRP

Automated staining using Dako ChemMate HRP/ChemMate Envision HRP reagents: Mix 20µl Diaminobenzidine solution with 980µl of substrate buffer containing hydrogen peroxide and preservative. Manual staining using Vector labs DAB substrate kit: To 5ml of distilled H_2O add 2 drops of buffer stock solution and mix, 4 drops DAB and mix, 2 drops Hydrogen Peroxide and mix. If a grey-black stain is desired add 2 drops of Nickel solution and mix.

Fast Red for AP (Dako double stain kit)

Transfer 3ml of Buffered Substrate to test tube and add a Fast Red tablet. Dissolve and mix thoroughly.

Removal of paraffin wax prior to staining

Label slides with name of antigen to be demonstrated and place in a staining rack making sure that control slides are included. Place in a bath of Xylene for 5min followed by consecutive

baths of 100, 90 and 70% Industrial Methylated Spirit each for 2min. Transfer to running tap water, and then proceed with staining protocol.

Antigen Retrieval -Pre-treatment of samples prior to staining.

Demonstration of antigens in formalin fixed paraffin material may in some instances rely on prior treatment with either proteolytic enzymes or by heat induced epitope retrieval (HEIR).

Heat Induced Epitope Retrieval (HIER)

- Place 250ml of 10mM citric acid, or 1mM EDTA into a plastic trough and alter to appropriate pH using 2M sodium hydroxide (Dependent on antigen and can be pH2-10)
- Put slides into a rack, place in trough and cover in microwave
- Set high power for 4min
- After 4min replace lost fluid with distilled water
- Repeat last 2 steps as necessary (dependent on antibody)
- When microwaving is complete remove trough, top up with water and leave to stand for 20min. Place rack in sink and leave slides to wash for 5min
- Continue staining protocol

Autostainer Procedure

Automatic staining with Dako Autostainer – Used for VEGF, Ki-67, Glut-1

- Enter slide information
- Enter number of slides to be stained
- Click on *Auto* until *Program* appears. Click on desired staining method e.g. ChemMate, Envision, ABC
- Click on *Program* until Auto appears
- Click on the blank box for each slide in the Primary Antibody column.
- Once all the slides have an antibody assigned to them left click on *Next* (Run time message appears, indicating protocol length, number of probe washes, amount of buffer and deionised water needed)
- Check volume of all reagents Click on *OK*.
- Place reagent vials in the white rack on the Autostainer as indicated on the screen.
- Place slides for current run in the Autostainer racks as indicated on the screen.
- Click on *Start Run*.
- When the run is complete the machine beeps. Click on *Yes* to save run log.
- The slides can now be removed and placed in running tap water prior to counterstaining. The machine should be wiped dry.
- Counterstaining: Place slides in a bath of Gills Haematoxylin for 7-15sec, remove and wash in running tap water for 5min.
- Place slides in bath of 70% IMS for 2min, followed by consecutive baths of 90% and 100% IMS each for 2min.
- Transfer slides to 2 consecutive baths of Xylene, 2min in each.
- Remove a slide from the staining rack & place a small amount of mounting media onto an appropriately sized cover slip and place on top of the section. Remove any air bubbles formed, wipe off any excess mounting media and allow drying.
- Slides are ready for analysis.

DakoCytomation Envision® Doublestain System – Used for CD34 + SMA

Reagents used :

- Peroxidase block – 0.03% hydrogen peroxide containing sodium azide
- Labelled polymer HRP – Horseradish peroxidase labelled polymer conjugated to affinity purified goat anti-rabbit and goat anti-mouse immunoglobulins in Tris-HCl buffer containing stabilising protein and an anti-microbial agent
- Diaminobenzidine(DAB) substrate buffer – Imidazole–HCl buffer, pH7.5, containing hydrogen peroxide and an anti-microbial agent.
- DAB Chromogen – 3,3'–diaminobenzidine in chromogen solution
- Doublestain block reagent
- Labelled polymer AP – Alkaline phosphatase labelled polymer conjugated to affinity purified goat anti-rabbit and goat anti-mouse immunoglobulins in phosphate buffered saline buffer containing stabilising protein and 0.015mmol/L sodium azide.
- Substrate buffer for Fast Red – Substrate buffered naphthol solution in Tris buffer.
- Fast Red tablets – 3mg Fast Red per tablet.

Staining Protocol

1) Tap off excess buffer and wipe slides
2) Apply peroxidase block to specimen
3) Incubate 5min.
4) Rinse gently with buffer solution
5) Place in fresh buffer bath
6) Tap off excess buffer and wipe slides
7) Apply primary antibody to specimen
8) Incubate for 60min
9) Repeat 4&5
10) Repeat 1
11) Apply labelled polymer HRP to specimen

12) Incubate 30min
13) Repeat 4&5
14) Repeat 1
15) Apply DAB solution to specimen
16) Incubate for 10min
17) Rinse with distilled water
18) Repeat 1
19) Apply doublestain block to specimen
20) Incubate 3min
21) Repeat 4&5
22) Repeat 1
23) Apply second antibody to specimen
24) Incubate 60min
25) Repeat 4&5
26) Repeat 1
27) Apply labelled polymer AP to specimen
28) Incubate 30min
29) Repeat 4&5
30) Repeat 1
31) Apply fast red substrate chromogen solution to specimen
32) Incubate for 5–10min
33) Rinse with distilled water
34) Immerse slides in bath of aqueous haematoxylin solution(7sec)
35) Rinse in tap water
36) Mount (aqueous mounting medium)

DakoCytomation CSA II Staining System – Used for CD105(Endoglin) Staining Procedure

1) Remove excess liquid from slide
2) Apply hydrogen peroxide block to specimen
3) Incubate 5min

4) Rinse gently with wash buffer solution (3 times in 5min to reduce non-specific background staining)

5) Repeat 1

6) Apply protein block

7) Incubate 5min at room temperature

8) Don't rinse off protein block!

9) Repeat 1

10) Apply primary antibody (Mouse anti-human CD105)

11) Incubate 60min

12) Repeat 4&1

13) Apply anti-mouse immunoglobulin – HRP to specimen

14) Incubate 15min

15) Repeat 4&1

16) Apply amplification reagent to specimen

17) Incubate 15min at room temperature (protect from light)

18) Repeat 4&1

19) Apply anti-fluorescein-HRP to specimen

20) Incubate 15min at room temperature

21) Repeat 4&1

22) Apply DAB substrate chromogen to specimen

23) Incubate for 7min

24) Rinse with distilled water

25) Counterstain with haematoxylin(7sec)

26) Dehydrate specimens down to xylene

27) Mount

Manual Staining Procedures For Other Antibodies

Angiopoietin 1

Antibody : Santa Cruz Biotech H-98 Cat No. sc-8357 Rabbit Polyclonal

Control – Human placenta, formalin fixed, paraffin embedded

1) Deparaffinise sections in histoclear for 10min
2) Rehydrate in alcohol
3) Block endogenous peroxidase in 1.5% hydrogen peroxide in methanol for 10min
4) Wash in tap water
5) Microwave in 0.01M citrate buffer pH6 for 10min
6) Repeat 4
7) Wash in TBST
8) Apply Ang-1 antibody diluted 1/50 and leave overnight at 4°c
9) Repeat 7
10) Apply Dako Envision Anti Rabbit Secondary Antibody, Cat No. K5007 with peroxidase, for 30min
11) Repeat 7
12) Apply DAB
13) Counterstain in haematoxylin, dehydrate, clear and mount.

Angiopoietin 2

Antibody : Santa Cruz Biotech H-70 Cat No. sc-20718 Rabbit polyclonal

Control – Human placenta, formalin fixed, paraffin embedded

Method as for Ang-1 except microwave in citrate buffer for 20min

CD61 (beta-3 integrin)

Antibody : Novacastra NCL-CD61-308

Control – Human tonsil and placenta, frozen or paraffin

1) Deparaffinise sections in histoclear for 10min
2) Dehydrate in IMS and wash in tap water
3) Block endogenous peroxidase in 1.5% hydrogen peroxide in methanol for 10min
4) Wash in tap water
5) Microwave in Dako's 'Target Retrieval Solution' S1700 or 0.01M citrate buffer pH6 for 20–30min

6) Repeat 4

7) Apply Vectastain's mouse IgG normal horse serum diluted in Tris buffered saline(TBS) for 30min

8) Apply CD61 antibody diluted in TBS 1/100, for either 1 hour or overnight at 4°c.

9) Wash in TBS

10) Apply horse anti-mouse biotinylated secondary, diluted in TBS, for 1h

11) Repeat 9

12) Apply ABC diluted in TBS for 30min

13) Repeat 9

14) Apply DAB diluted in distilled water for up to 10min

15) Wash in tap water

16) Counterstain, dehydrate and mount

PDGF

Novacastra NCL-PDEGF

Control – human tonsil and placenta, paraffin embedded

Method as for CD61, except primary antibody dilution is 1/60 in TBS.

Appendix 3 - Vascular Immunohistochemistry Additional Data

a) Correlations between Continuous Variables & K^{trans}

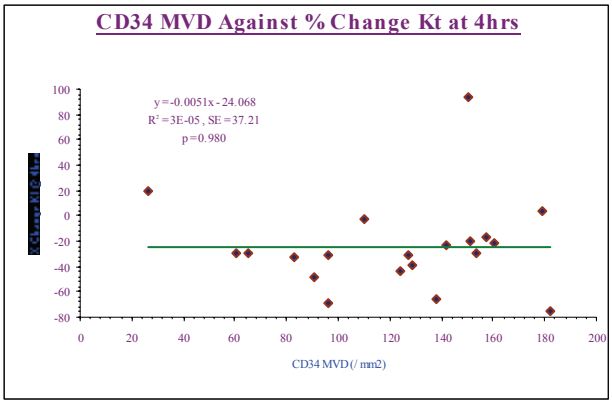

a

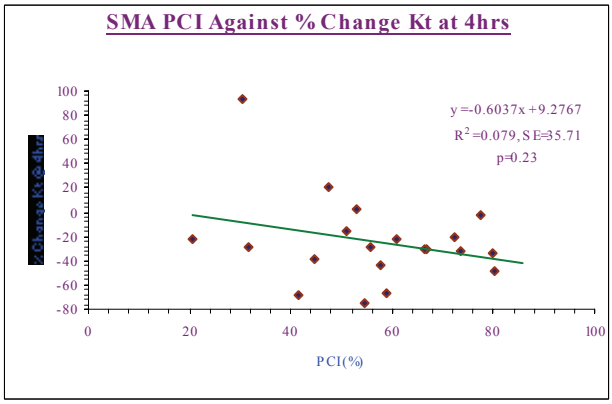

b

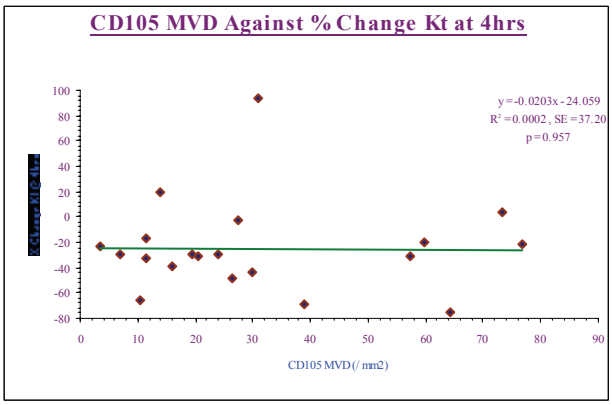

c

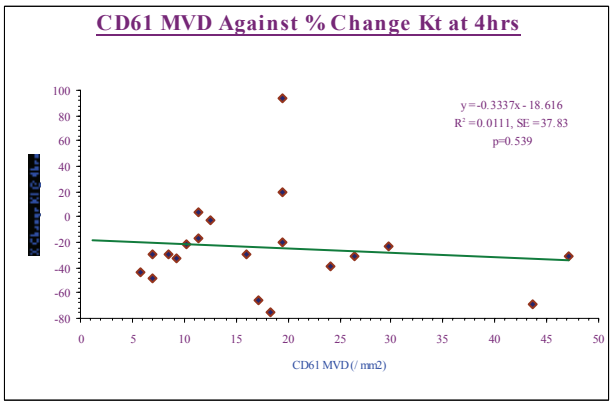

d

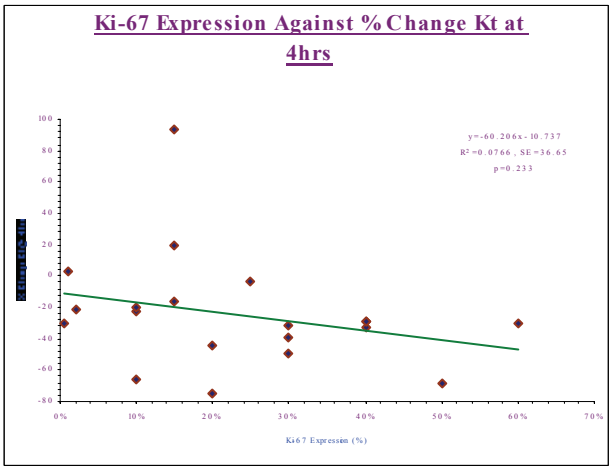

e

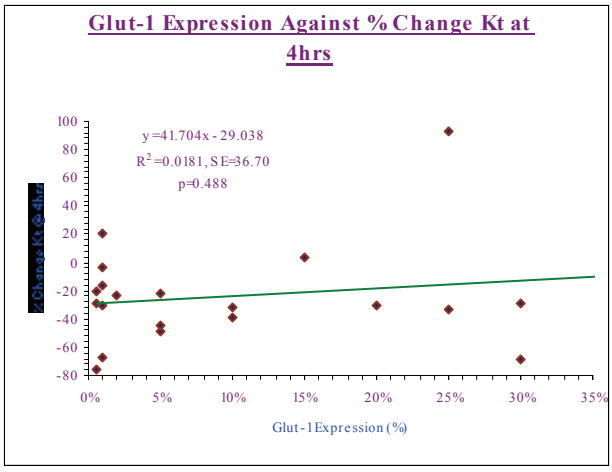

f

Fig 8.2(a – f). Correlation between the continuous variables CD34,SMA,CD105,CD61,Ki-67,Glut-1 against percentage change in K^{trans} 4hrs post CA4P. There are no correlations of any clinical significance. Lines of best fit are predominantly horizontal, indicating no correlation. The slopes of the best fit line are expressed in the format y=mx+c. Regression statistics calculated using Microsoft Excel. Correlation co-efficients are shown with standard error. p-values were calculated using t-test. SMA & Ki-67 report p values(t-test) of 0.23. For SMA(b) this result is the opposite expected. Tumours with higher SMA PCI (more mature vessels) should be less likely to respond to CA4P, however the vascular effect assessed on DCE-MRI appears to be greater! For Ki-67(e), there is a general trend towards more rapidly proliferating tumours having a greater change in blood flow after CA4P.

b) Correlations between Continuous Variables & v_e

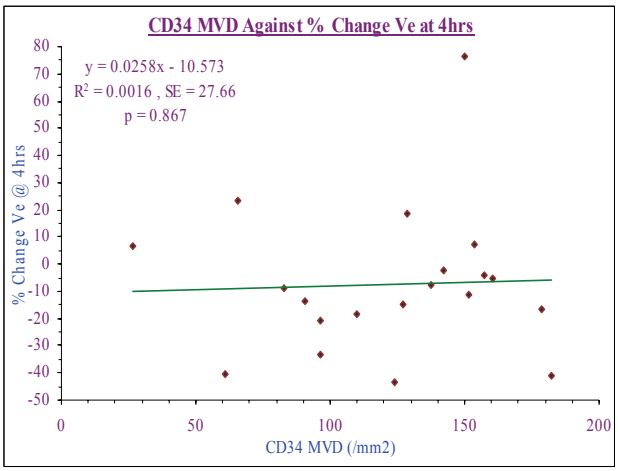

a

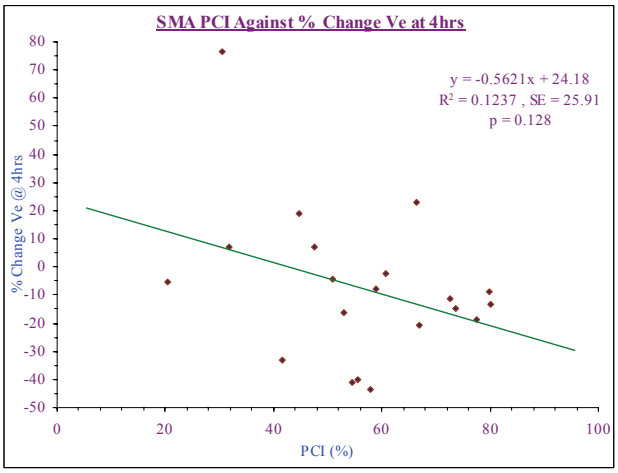

b

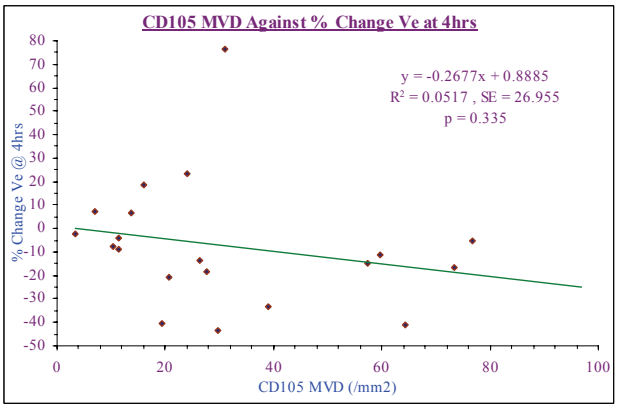

c

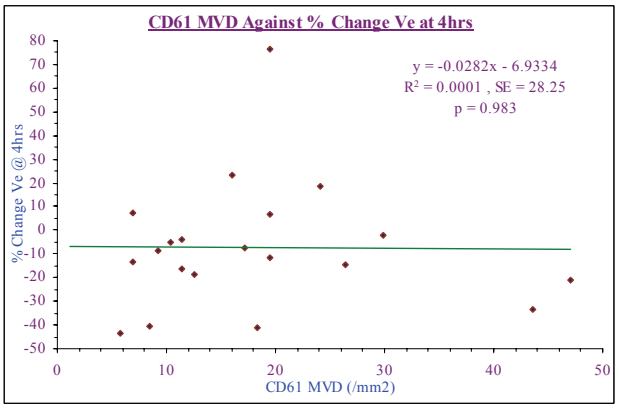

d

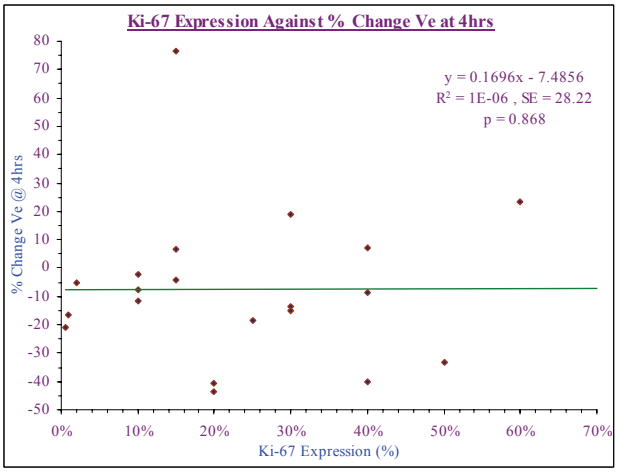

e

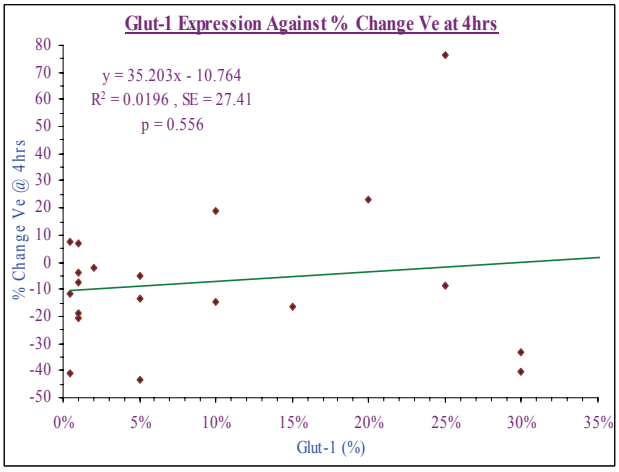

f

Fig 8.3(a – f). Correlation between the continuous variables CD34,SMA,CD105,CD61,Ki-67,Glut-1 against percentage change in v_e 4h post-CA4P. There are no correlations of any significance. Lines of best fit are predominantly horizontal, indicating no correlation. The slopes of the best fit line are expressed in the format y=mx+c. Regression statistics calculated using Microsoft Excel. Correlation co-efficients are shown with standard error. P-values were calculated using t-test. Again, SMA & ve initially looks promising R=0.12, p=0.128. However, again the tumours with the highest PCI(mature) appear to have the sharpest drop in ve 4h post-CA4P, the opposite predicted. There is a trend in favour of CD105/ve (p=0.335) suggesting tumours with more immature vasculature may respond on MRI.

c) Correlations between Continuous Variables & k_{ep}

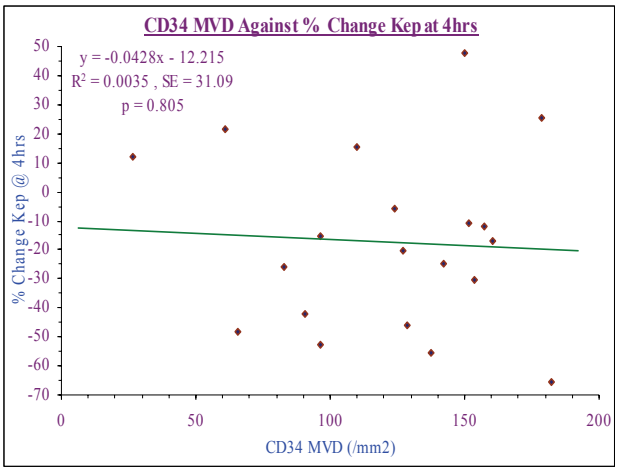

a

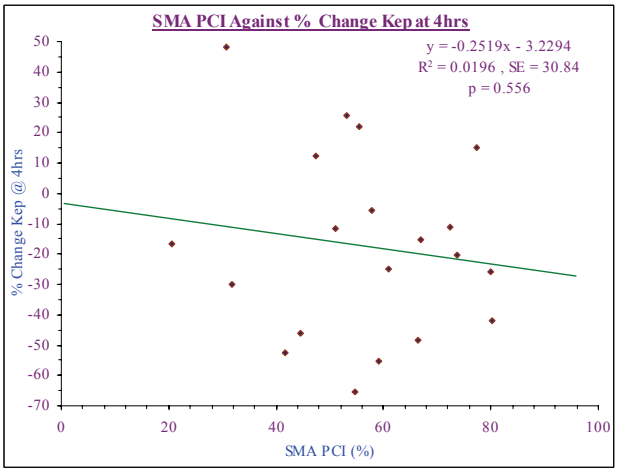

b

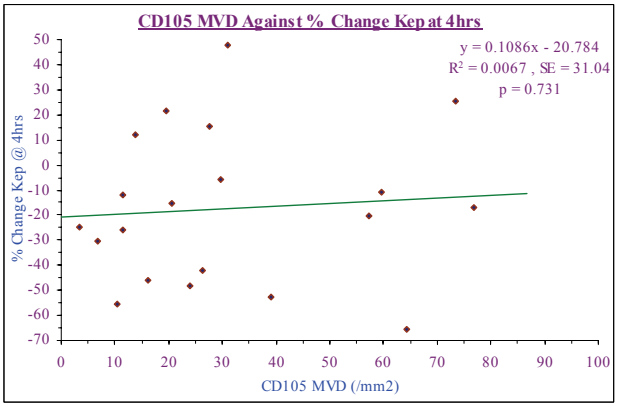

c

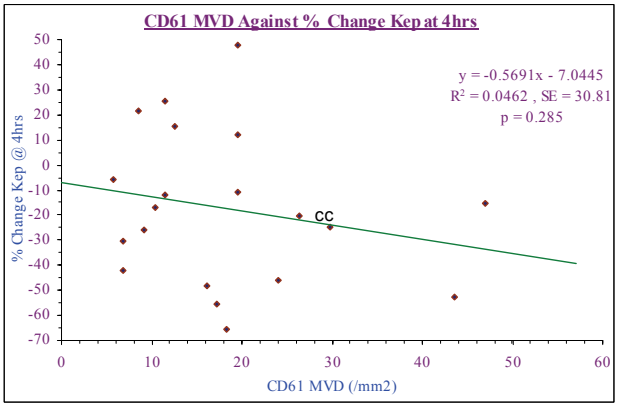

d

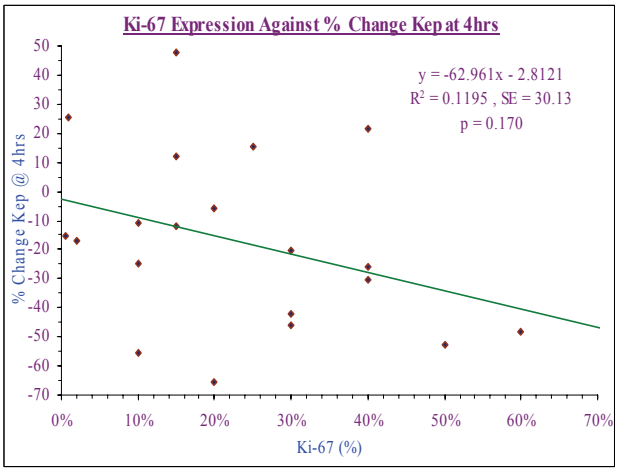

e

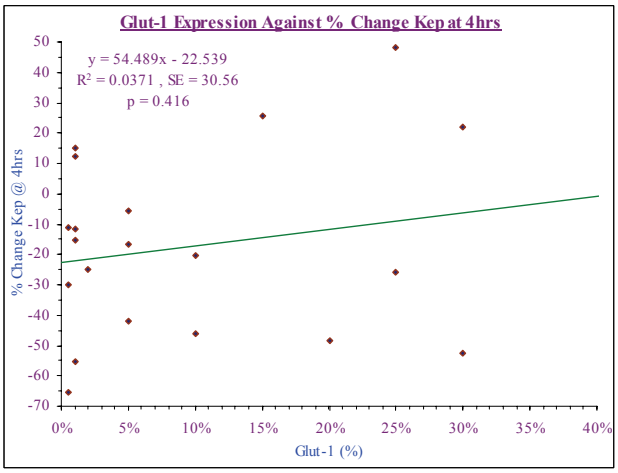

f

Fig 8.4(a – f). Correlation between the continuous variables CD34,SMA,CD105,CD61,Ki-67,Glut-1 against percentage change in k_{ep} 4h post-CA4P. There are no correlations of any clinical significance. The lines of best fit are predominantly horizontal. The only correlation showing any general trend is graph e) Ki-67/kep, p=0.17, suggesting a trend towards greater response to CA4P on DCE-MRI for more actively proliferating tumours. Graph f) Glut-1/kep may be skewed as most of the data points are at the lower end of the scale, making a correlation line of best fit difficult.

d) Correlations between Continuous Variables & $IAUGC_{60}$

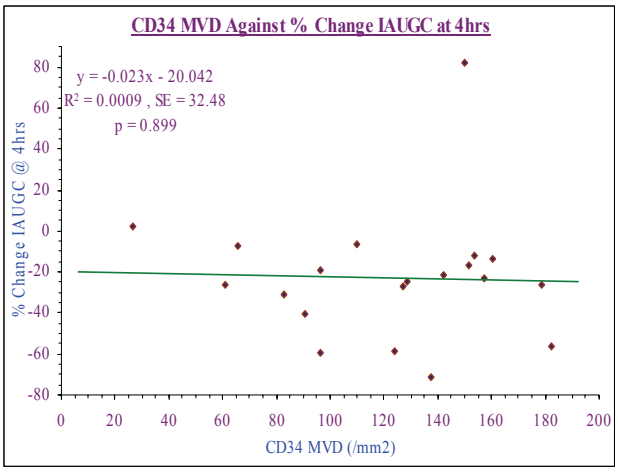

a

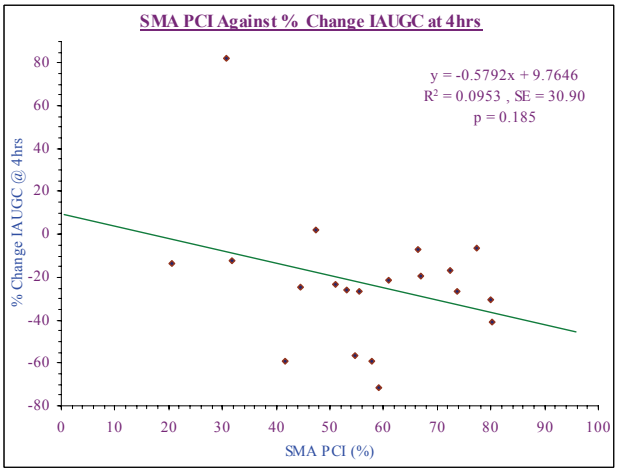

b

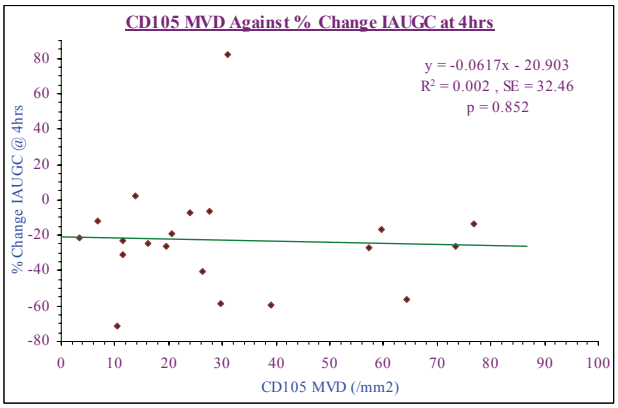

c

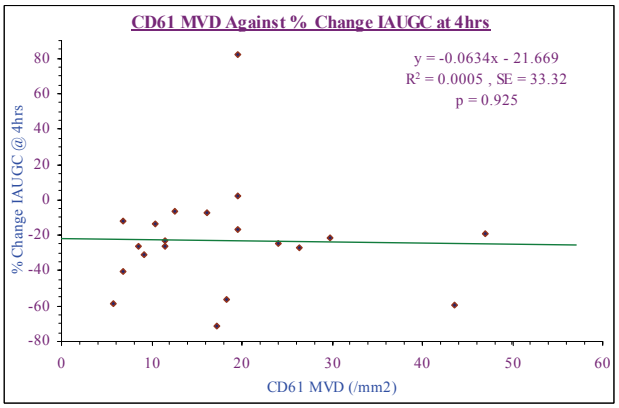

d

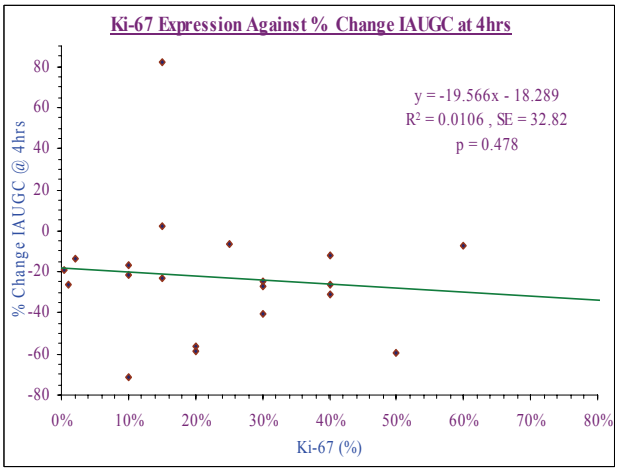

e

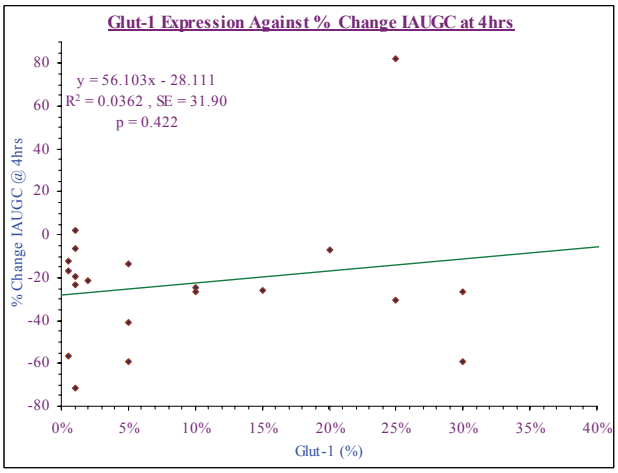

f

Fig 8.5(a – f). Correlation between the continuous variables CD34,SMA,CD105,CD61,Ki-67,Glut-1 against percentage change in $IAUGC_{60}$ 4h post-CA4P. There are no correlations of any clinical significance. The only graph showing a general trend, p=0.185, is b)SMA/IAUGC, however, again the trend is the opposite expected, with the more mature vascular tumours seeming to undergo a greater drop in MRI parameter following CA4P

e) Angiopoietin-1 & MRI Parameters

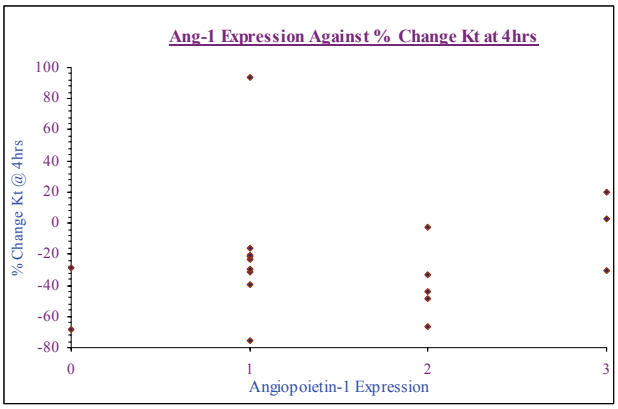

a

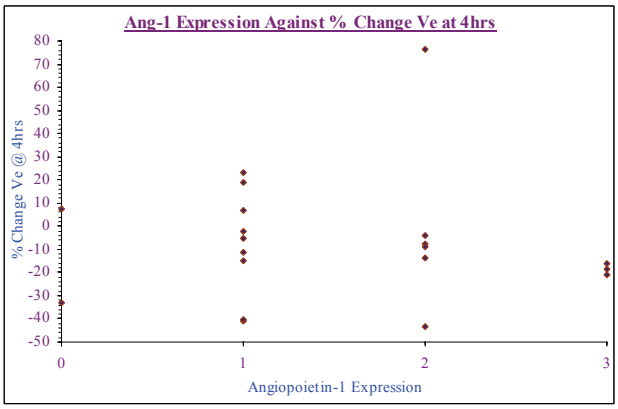

b

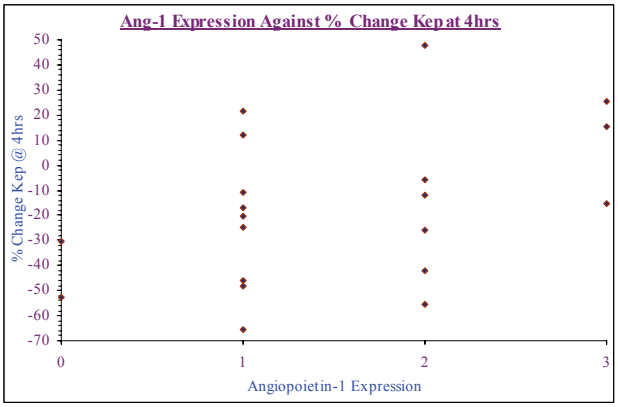

c

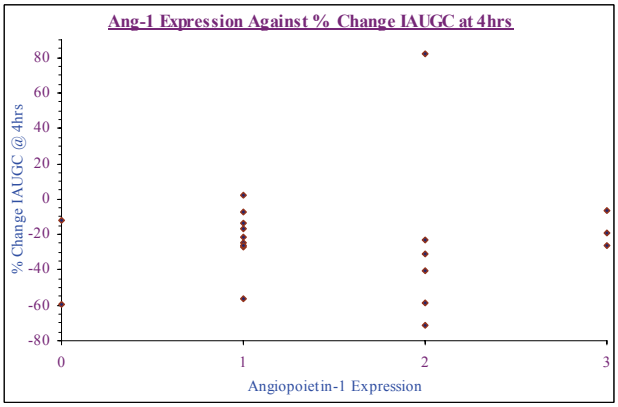

d

Fig 8.6(a–d). Relationship between Ang-1 against percentage change in K^{trans},v_e,k_{ep},$IAUGC_{60}$ 4h post-CA4P. Graphs produced using Microsoft Excel. Regression analysis and Correlation is not valid for use on categorical or interval variables. Instead we must use ANOVA (Analysis Of Variance). Statistics calculated using SPSS v11.0. The ANOVA analysis table for these graphs with explanations, is shown below. Note the graph of ang-1 against ve, which appears to show a trend in favour of increasing change in the MRI parameter with higher expression.

Angiopoietin-1 ANOVA Test

Table 8.1 – Angiopoietin-1 ANOVA Descriptives

Descriptives

			N	Mean	Std. Deviation	Std. Error	95% Confidence Interval for Mean		Minimum	Maximum	Between-Component Variance
							Lower Bound	Upper Bound			
% Ch Kt @ 4hrs	0		2	-48.5289	27.79451	19.65369	-298.2526	201.1949	-68.18	-28.88	
	1		9	-18.2226	45.47287	15.15762	-53.1761	16.7310	-75.22	93.54	
	2		5	-39.1215	23.56999	10.54082	-68.3875	-9.8555	-66.56	-2.90	
	3		3	-2.5218	25.76178	14.87357	-66.5176	61.4740	-30.61	20.00	
	Total		19	-24.4334	37.18700	8.53128	-42.3569	-6.5098	-75.22	93.54	
	Model	Fixed Effects			37.29549	8.55617	-42.6704	-6.1963			
		Random Effects				8.55617[a]	-51.6629[a]	2.7962[a]			-11.41986
% Ch Ve @ 4hrs	0		2	-36.7173	5.00807	3.54124	-81.7131	8.2784	-40.26	-33.18	
	1		9	4.4167	32.87741	10.95914	-20.8551	29.6885	-40.87	76.58	
	2		5	-18.4138	14.63148	6.54340	-36.5812	-.2464	-43.43	-7.73	
	3		3	-10.1479	14.88497	8.59384	-47.1243	26.8284	-20.91	6.84	
	Total		19	-8.2209	27.45098	6.29769	-21.4519	5.0100	-43.43	76.58	
	Model	Fixed Effects			25.78361	5.91517	-20.8288	4.3870			
		Random Effects				8.73723	-36.0267	19.5849			125.44009
% Ch Kep @ 4hrs	0		2	-15.3441	52.44794	37.08629	-486.5702	455.8819	-52.43	21.74	
	1		9	-21.8196	32.25845	10.75282	-46.6156	2.9765	-65.28	48.03	
	2		5	-22.6807	28.15582	12.59167	-57.6408	12.2794	-55.23	15.29	
	3		3	7.5061	20.85498	12.04063	-44.3005	59.3128	-15.30	25.61	
	Total		19	-16.7342	30.99525	7.11080	-31.6734	-1.7949	-65.28	48.03	
	Model	Fixed Effects			31.74535	7.28288	-32.2573	-1.2111			
		Random Effects				7.28288[a]	-39.9116[a]	6.4432[a]			-66.50850
% Ch AUC @ 4hrs	0		2	-42.6596	23.17479	16.38705	-250.8769	165.5576	-59.05	-26.27	
	1		9	-11.8945	37.92647	12.64216	-41.0473	17.2584	-56.26	82.38	
	2		5	-41.7371	25.26166	11.29736	-73.1035	-10.3706	-71.65	-6.57	
	3		3	-14.3837	14.64011	8.45247	-50.7518	21.9844	-25.98	2.07	
	Total		19	-23.3792	32.39003	7.43078	-38.9907	-7.7678	-71.65	82.38	
	Model	Fixed Effects			31.64983	7.26097	-38.8556	-7.9029			
		Random Effects				8.64894	-50.9040	4.1455			66.98975

a. Warning: Between-component variance is negative. It was replaced by 0.0 in computing this random effects measure.

Table 8.2 – Angiopoietin 1 - ANOVA Test

ANOVA

		Sum of Squares	df	Mean Square	F	Sig.
% Ch Kt @ 4hrs	Between Groups	4027.409	3	1342.470	.965	.435
	Within Groups	20864.308	15	1390.954		
	Total	24891.716	18			
% Ch Ve @ 4hrs	Between Groups	3592.095	3	1197.365	1.801	.190
	Within Groups	9971.921	15	664.795		
	Total	13564.016	18			
% Ch Kep @ 4hrs	Between Groups	2176.193	3	725.398	.720	.556
	Within Groups	15116.507	15	1007.767		
	Total	17292.700	18			
% Ch AUC @ 4hrs	Between Groups	3858.374	3	1286.125	1.284	.316
	Within Groups	15025.679	15	1001.712		
	Total	18884.053	18			

a) For each of the MRI variables K^{trans},v_e,k_{ep},$IAUGC_{60}$, they are subdivided into component parts fitting into category 0,1,2, & 3, with a total of 19 samples analysed. Means, SD and confidence intervals for each category are shown, and finally a 'between component' variance is calculated. Note that for 2 variables this variance is negative, which is statistically meaningless, and probably due to the small sample size in that category.

b) ANOVA test – There is no statistically significant relationship, however the ang-1/v_e relationship is interesting and worth mentioning, p=0.19 . There appears to be a trend in favour of increasing MR response in tumours with higher expression. However it can also be seen that the number of samples in the higher expression categories is very limited.

f) Angiopoietin-2 & MRI Parameters

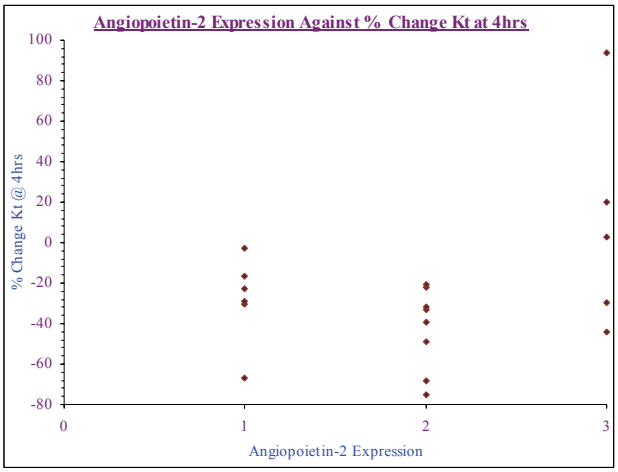

a

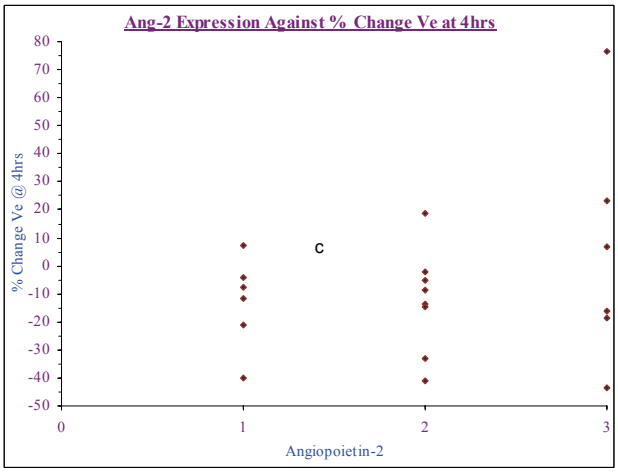

b

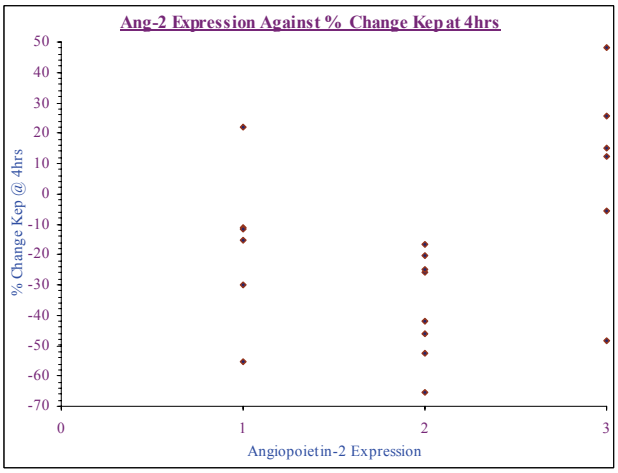

c

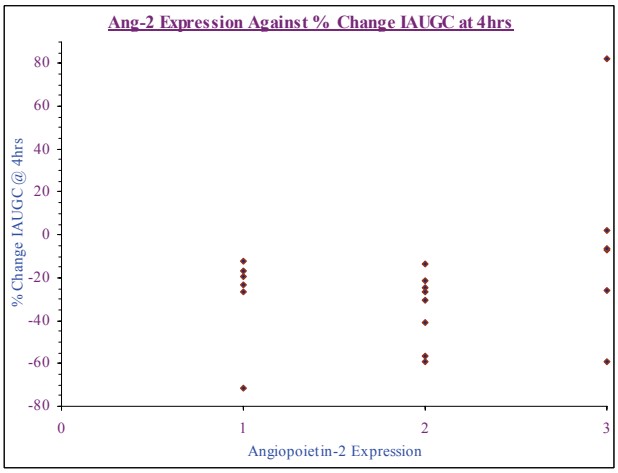

d

Fig 8.7(a–d). Relationship between the Categorical Variable Ang-2 against percentage change in K^{trans},v_e,k_{ep},$IAUGC_{60}$ 4h post-CA4P. Note the graphs of ang-2 against Ktrans & kep. There may be a U-shaped distribution, although sample size is small.

Angiopoietin-2 ANOVA Test

Table 8.3 – Angiopoietin-2 ANOVA Descriptives

Descriptives

			N	Mean	Std. Deviation	Std. Error	95% Confidence Interval for Mean		Minimum	Maximum	Between-Component Variance
							Lower Bound	Upper Bound			
% Ch Kt @ 4hrs	1		6	-28.0169	21.39489	8.73443	-50.4694	-5.5643	-66.56	-2.90	
	2		8	-42.2934	20.34432	7.19280	-59.3017	-25.2851	-75.22	-20.55	
	3		5	8.4429	54.01994	24.15845	-58.6317	75.5176	-44.39	93.54	
	Total		19	-24.4334	37.18700	8.53128	-42.3569	-6.5098	-75.22	93.54	
	Model	Fixed Effects			32.46013	7.44686	-40.2200	-8.6467			
		Random Effects				14.85428	-88.3462	39.4795			477.08005
% Ch Ve @ 4hrs	1		6	-15.6200	14.28499	5.83182	-30.6112	-.6289	-40.26	-2.13	
	2		8	-13.6528	18.01440	6.36905	-28.7132	1.4076	-40.87	18.75	
	3		5	9.3491	45.17751	20.20400	-46.7462	65.4444	-43.43	76.58	
	Total		19	-8.2209	27.45098	6.29769	-21.4519	5.0100	-43.43	76.58	
	Model	Fixed Effects			26.75813	6.13874	-21.2344	4.7926			
		Random Effects				7.51867	-40.5711	24.1293			54.42826
% Ch Kep @ 4hrs	1		6	-11.6720	28.01552	11.43729	-41.0725	17.7285	-55.23	21.74	
	2		8	-34.9448	19.30477	6.82527	-51.0840	-18.8056	-65.28	-10.98	
	3		5	6.3282	36.37822	16.26883	-38.8413	51.4977	-48.46	48.03	
	Total		19	-16.7342	30.99525	7.11080	-31.6734	-1.7949	-65.28	48.03	
	Model	Fixed Effects			27.18751	6.23724	-29.9565	-3.5118			
		Random Effects				12.25035	-69.4432	35.9748			321.05267
% Ch AUC @ 4hrs	1		6	-28.0614	22.40622	9.14730	-51.5753	-4.5475	-71.65	-6.57	
	2		8	-33.5488	17.04713	6.02707	-47.8005	-19.2970	-59.05	-13.40	
	3		5	-1.4894	52.40445	23.43598	-66.5581	63.5793	-59.02	82.38	
	Total		19	-23.3792	32.39003	7.43078	-38.9907	-7.7678	-71.65	82.38	
	Model	Fixed Effects			31.15418	7.14726	-38.5308	-8.2277			
		Random Effects				9.51256	-64.3085	17.5500			113.80310

Table 8.4 – Ang-2 ANOVA Test

ANOVA

		Sum of Squares	df	Mean Square	F	Sig.
% Ch Kt @ 4hrs	Between Groups	8033.156	2	4016.578	3.812	.044
	Within Groups	16858.560	16	1053.660		
	Total	24891.716	18			
% Ch Ve @ 4hrs	Between Groups	2108.052	2	1054.026	1.472	.259
	Within Groups	11455.964	16	715.998		
	Total	13564.016	18			
% Ch Kep @ 4hrs	Between Groups	5466.133	2	2733.066	3.698	.048
	Within Groups	11826.567	16	739.160		
	Total	17292.700	18			
% Ch AUC @ 4hrs	Between Groups	3354.721	2	1677.360	1.728	.209
	Within Groups	15529.332	16	970.583		
	Total	18884.053	18			

a) For each of the MRI variables K^{trans},v_e,k_{ep},$IAUGC_{60}$, they are subdivided into component parts fitting into category 0,1,2, & 3, with a total of 19 samples analysed. Means, SD and confidence intervals for each category are shown, and finally a 'between component' variance is calculated.

b) ANOVA test – Two relationships are statistically significant, that between ang-2 & K^{trans}($p=0.044$) and ang-2 and k_{ep}($p=0.048$). There appears to be a U-shaped relationship, with the largest MRI changes visible with moderate expression, however smaller changes visible at lower and higher concentrations of angiopoietin-2. However it can also be seen that the number of samples in the higher expression categories is very limited.

g) PDGF & MRI Parameters

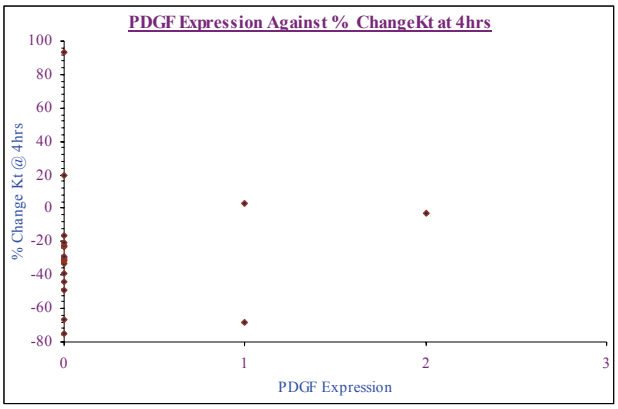

a

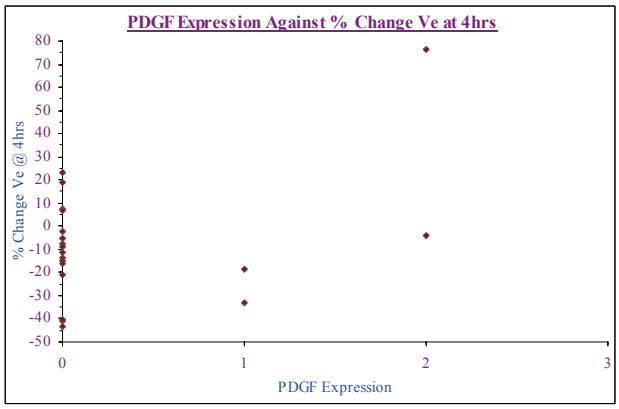

b

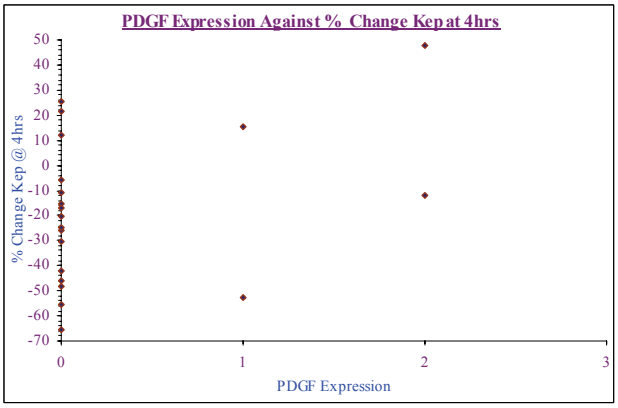

c

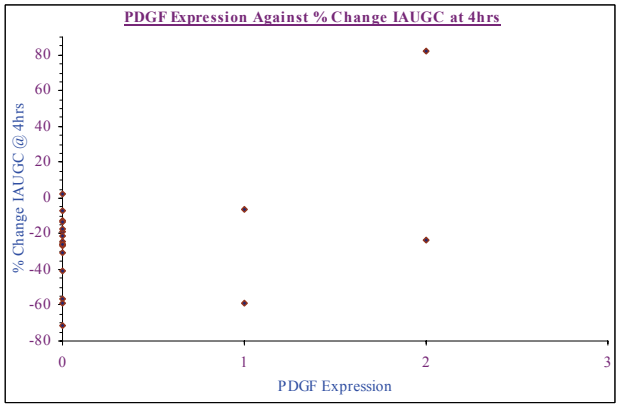

d

Fig 8.8(a–d). Relationship between the Categorical Variable PDGF against percentage change in K^{trans},v_e,k_{ep},$IAUGC_{60}$ 4h post-CA4P. Very few tumour samples stained positively for PDGF, it was predominantly a stromal stain. Thus, the sample size is very small.

PDGF ANOVA Test

Table 8.5 – PDGF ANOVA Descriptives

Descriptives

			N	Mean	Std. Deviation	Std. Error	95% Confidence Interval for Mean		Minimum	Maximum	Between-Component Variance
							Lower Bound	Upper Bound			
% Ch Kt @ 4hrs	0		16	-24.7624	38.08509	9.52127	-45.0565	-4.4683	-75.22	93.54	
	1		2	-32.5666	50.36860	35.61598	-485.1105	419.9774	-68.18	3.05	
	2		1	-2.9026	.	.	.	.	-2.90	-2.90	
	Total		19	-24.4334	37.18700	8.53128	-42.3569	-6.5098	-75.22	93.54	
	Model	Fixed Effects			38.96642	8.93951	-43.3843	-5.4824			
		Random Effects				8.93951[a]	-62.8970[a]	14.0303[a]			-463.44017
% Ch Ve @ 4hrs	0		16	-5.5040	29.03941	7.25985	-20.9780	9.9700	-43.43	76.58	
	1		2	-24.7771	11.87800	8.39901	-131.4966	81.9425	-33.18	-16.38	
	2		1	-18.5793	.	.	.	.	-18.58	-18.58	
	Total		19	-8.2209	27.45098	6.29769	-21.4519	5.0100	-43.43	76.58	
	Model	Fixed Effects			28.27366	6.48642	-21.9715	5.5297			
		Random Effects				6.48642[a]	-36.1297[a]	19.6879[a]			-156.78483
% Ch Kep @ 4hrs	0		16	-19.1511	29.55944	7.38986	-34.9023	-3.4000	-65.28	48.03	
	1		2	-13.4086	55.18519	39.02182	-509.2278	482.4106	-52.43	25.61	
	2		1	15.2861	.	.	.	.	15.29	15.29	
	Total		19	-16.7342	30.99525	7.11080	-31.6734	-1.7949	-65.28	48.03	
	Model	Fixed Effects			31.77245	7.28910	-32.1864	-1.2820			
		Random Effects				7.28910[a]	-48.0966[a]	14.6283[a]			-166.83733
% Ch AUC @ 4hrs	0		16	-22.0377	33.95469	8.48867	-40.1309	-3.9445	-71.65	82.38	
	1		2	-42.5155	23.37865	16.53120	-252.5643	167.5333	-59.05	-25.98	
	2		1	-6.5718	.	.	.	.	-6.57	-6.57	
	Total		19	-23.3792	32.39003	7.43078	-38.9907	-7.7678	-71.65	82.38	
	Model	Fixed Effects			33.39197	7.66064	-39.6191	-7.1394			
		Random Effects				7.66064[a]	-56.3403[a]	9.5818[a]			-225.40999

a. Warning: Between-component variance is negative. It was replaced by 0.0 in computing this random effects measure.

Table 8.6 – PDGF ANOVA Test

ANOVA

		Sum of Squares	df	Mean Square	F	Sig.
% Ch Kt @ 4hrs	Between Groups	597.605	2	298.803	.197	.823
	Within Groups	24294.111	16	1518.382		
	Total	24891.716	18			
% Ch Ve @ 4hrs	Between Groups	773.617	2	386.808	.484	.625
	Within Groups	12790.399	16	799.400		
	Total	13564.016	18			
% Ch Kep @ 4hrs	Between Groups	1140.886	2	570.443	.565	.579
	Within Groups	16151.815	16	1009.488		
	Total	17292.700	18			
% Ch AUC @ 4hrs	Between Groups	1043.678	2	521.839	.468	.635
	Within Groups	17840.374	16	1115.023		
	Total	18884.053	18			

a) For each of the MRI variables K^{trans},v_e,k_{ep},$IAUGC_{60}$, they are subdivided into component parts fitting into category 0,1,2, & 3, with a total of 19 samples analysed. Means, SD and confidence intervals for each category are shown, and finally a 'between component' variance is calculated.

b) ANOVA test – None of the relationships are statistically significant. The sample sizes are too small. There are only two values for weak staining, and 1 value for moderate staining, no values for strong staining within the tumour.

h) VEGF & MRI Parameters

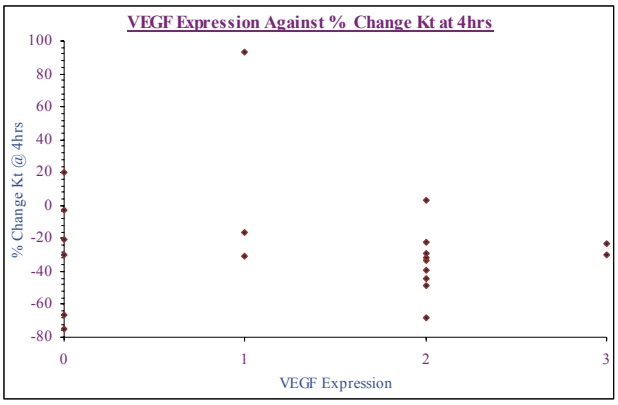

a

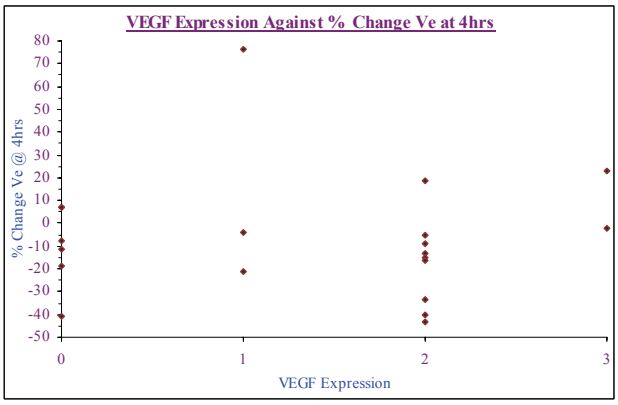

b

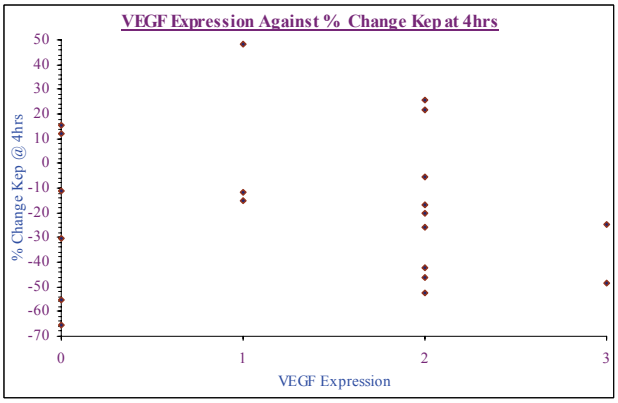

c

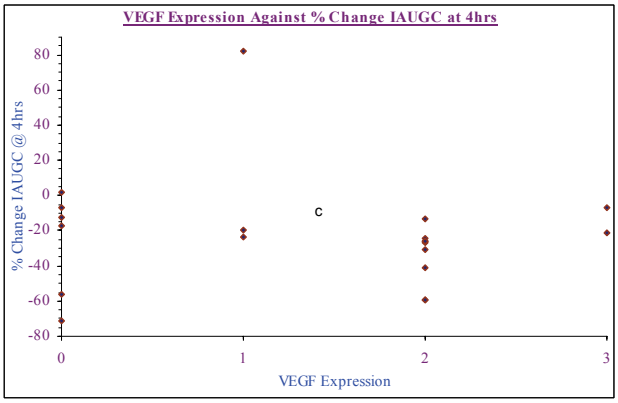

d

Fig 8.9(a–d). Relationship between the Categorical or Interval Variable VEGF against percentage change in K^{trans},v_e,k_{ep},$IAUGC_{60}$ 4h post-CA4P. There are no obvious graphical relationships.

VEGF ANOVA Test

Table 8.7 – VEGF ANOVA Descriptives

Descriptives

			N	Mean	Std. Deviation	Std. Error	95% Confidence Interval for Mean		Minimum	Maximum	Between-Component Variance
							Lower Bound	Upper Bound			
% Ch Kt @ 4hrs	0		6	-29.1343	36.60799	14.94515	-67.5520	9.2835	-75.22	20.00	
	1		3	15.5634	67.91366	39.20997	-153.1435	184.2703	-30.61	93.54	
	2		9	-34.7536	19.58697	6.52899	-49.8095	-19.6977	-68.18	3.05	
	3		2	-26.4500	5.00763	3.54093	-71.4418	18.5417	-29.99	-22.91	
	Total		20	-24.6899	36.21335	8.09755	-41.6383	-7.7415	-75.22	93.54	
	Model	Fixed Effects			34.47783	7.70948	-41.0332	-8.3465			
		Random Effects				10.74958	-58.8999	9.5201			172.66910
% Ch Ve @ 4hrs	0		6	-10.7636	17.95720	7.33100	-29.6085	8.0813	-40.87	7.27	
	1		3	17.1833	52.11643	30.08944	-112.2811	146.6477	-20.91	76.58	
	2		9	-17.4340	19.36480	6.45493	-32.3191	-2.5489	-43.43	18.75	
	3		2	10.5066	17.86755	12.63427	-150.0270	171.0402	-2.13	23.14	
	Total		20	-7.4462	26.94249	6.02452	-20.0557	5.1632	-43.43	76.58	
	Model	Fixed Effects			25.45064	5.69094	-19.5105	4.6180			
		Random Effects				8.25463	-33.7161	18.8237			110.00644
% Ch Kep @ 4hrs	0		6	-22.3538	33.83524	13.81318	-57.8618	13.1541	-65.28	15.29	
	1		3	6.9789	35.59800	20.55251	-81.4514	95.4092	-15.30	48.03	
	2		9	-17.9652	27.95669	9.31890	-39.4546	3.5242	-52.43	25.61	
	3		2	-36.5963	16.77959	11.86496	-187.3549	114.1624	-48.46	-24.73	
	Total		20	-17.4033	30.31660	6.77900	-31.5919	-3.2147	-65.28	48.03	
	Model	Fixed Effects			30.40633	6.79906	-31.8166	-2.9899			
		Random Effects				6.79906[a]	-39.0409[a]	4.2344[a]			-7.66869
% Ch AUC @ 4hrs	0		6	-26.9490	29.76091	12.14984	-58.1812	4.2832	-71.65	2.07	
	1		3	13.3088	59.84852	34.55356	-135.3631	161.9808	-23.22	82.38	
	2		9	-34.0422	15.81924	5.27308	-46.2020	-21.8825	-59.05	-13.40	
	3		2	-14.1572	10.27898	7.26833	-106.5101	78.1958	-21.43	-6.89	
	Total		20	-22.8231	31.62410	7.07136	-37.6236	-8.0226	-71.65	82.38	
	Model	Fixed Effects			29.26164	6.54310	-36.6938	-8.9523			
		Random Effects				10.42141	-55.9887	10.3425			202.44208

a. Warning: Between-component variance is negative. It was replaced by 0.0 in computing this random effects measure.

Table 8.8 – VEGF ANOVA Test

ANOVA

		Sum of Squares	df	Mean Square	F	Sig.
% Ch Kt @ 4hrs	Between Groups	5897.195	3	1965.732	1.654	.217
	Within Groups	19019.529	16	1188.721		
	Total	24916.724	19			
% Ch Ve @ 4hrs	Between Groups	3428.293	3	1142.764	1.764	.194
	Within Groups	10363.764	16	647.735		
	Total	13792.057	19			
% Ch Kep @ 4hrs	Between Groups	2670.107	3	890.036	.963	.434
	Within Groups	14792.717	16	924.545		
	Total	17462.824	19			
% Ch AUC @ 4hrs	Between Groups	5301.698	3	1767.233	2.064	.145
	Within Groups	13699.894	16	856.243		
	Total	19001.592	19			

a) For each of the MRI variables K^{trans},v_e,k_{ep},$IAUGC_{60}$, they are subdivided into component parts fitting into category 0,1,2, & 3, with a total of 19 samples analysed. Means, SD and confidence intervals for each category are shown, and finally a 'between component' variance is calculated.

b) ANOVA – None of the relationships are statistically significant. Only 2 samples are present in the 'strong staining' category.

Appendix 4 – Perfusion CT Mathematical Modelling

Mathematical modelling techniques employed during Perfusion CT include both uni-and bi-compartmental analysis methods. Uni-compartment techniques based on the Fick principle are most commonly used to estimate perfusion (blood flow per unit volume of tissue). This effectively considers the intravascular and EES as a single compartment. By evaluating data for time points prior to the moment when contrast medium appears in the draining veins of the tissue of interest, perfusion may be calculated either from the maximal slope of the tissue concentration–time curve known as the slope method (Miles et al.,2000) or from its peak height normalized to the AIF (known as the peak or Mullani-Gould method (Miles et al.,2000; Miles & Griffiths,2003).

a. Slope method

Perfusion (Flow/Volume) can be calculated as the maximum slope of tissue enhancement curve divided by the maximum arterial enhancement. c(t) is peak tissue enhancement, and a*(t) is the gamma fit to the arterial curve to correct for recirculation.

$$\frac{F}{V} = \frac{\frac{\mathrm{d}}{\mathrm{d}t}[c(t)]|_{\max}}{a(t)|_{\max}} \qquad (3)$$

The principle advantage of the slope method is that it allows calculation of perfusion sooner, as the tissue time enhancement curve reaches its peak gradient well before its peak enhancement value. This reduces the chance of the no venous out flow assumption being broken. The peak arterial enhancement and maximum slope in most tissues occur prior to any recirculation thus avoiding the requirement of curve modelling. The earlier time of perfusion assessment also reduces the likelihood of patient movement and may enable perfusion studies in a single breath hold. However, the slope technique is innately sensitive to noise as the data set is differentiated.

b. Peak method

Perfusion is calculated as the concentration of contrast material in the tissue divided by the difference between total amount of contrast material that has flowed into the tissue and the amount of contrast material that has flowed out of the tissue (equation 4). Typically perfusion is calculated at time t'. By restricting the time of measurement to prior to the time the contrast starts to flow out of the tissue, the venous term in the denominator becomes zero, thus:

$$\frac{F}{V} = \frac{c(t')|_{\max}}{\int_0^{t'} a^*(t)\mathrm{d}t} \qquad (4)$$

The method is prone to underestimation of higher values of perfusion as the assumption of "no venous washout" is violated at high flow. Failure to correct the arterial time enhancement curve for recirculation can lead to an over estimation of the area under the curve causing a decrease of perfusion values.

c. Patlak analysis

A two compartment model based on Patlak analysis is used for measurements of capillary permeability and blood volume; this simplified model assumes the back flux of contrast medium from EES to intravascular space is negligible, which holds for the first 1 to 2 minutes following contrast injection (Miles et al.,2000). Consider the one-way transfer of contrast medium from the blood to the ECF with a blood clearance value of contrast, α. The amount of contrast medium that has left the blood will be α times the amount of blood that has flowed through the tissue. The concentration of contrast medium or the enhancement of the ECF will be α /V × AUC of the blood curve, where V is the volume of the tissue. The enhancement of the tissue due to blood in the tissue is determined by the relative blood volume to tissue volume (rBV) multiplied by the concentration of contrast medium in the blood. Thus the total concentration of contrast medium, i.e. enhancement of the tissue at time t' is given by the sum of the concentrations of the contrast medium in the blood and ECF (equation 5).

$$c(t') = \mathrm{rBV}\ b(t') + \frac{\alpha}{V}\int_0^{t'} b(t)\mathrm{d}t \qquad (5)$$

Rearranging this equation gives:

$$\frac{c(t')}{b(t')} = \mathrm{rBV} + \frac{\alpha}{V}\frac{\int_0^{t'} b(t)\mathrm{d}t}{b(t')} \qquad (6)$$

in the form y=mx+c. A plot of the ratio of the tissue to blood concentration, c(t')/b(t'), against the ratio of the AUC of the blood curve to the blood concentration, for various time values, t', has an intercept of the tissue's relative blood volume and a slope equal to the blood clearance per unit volume or permeability.

References

Donahue, K., Burstein, D., Gray, M. (1994). Studies Of Gd-DTPA Relaxivity And Proton Exchange Rates In Tissue. *Magnetic Resonance In Medicine*, **32,** 66 - 76.

Hittmair, K., Gomiscek, K., Kramer, J. (1994). Method For The Quantitative Assessment Of Contrast Agent Uptake In DCE-MRI. *Magnetic Resonance In Medicine*, **31,** 567 - 571.

Miles, K.A., Charnsangavej, C., Lee, T.Y. (2000). Application of CT in the investigation of angiogenesis in oncology. *Acad Radiol*, **7,** 840-50.

Miles, K.A. & Griffiths, M.R. (2003). Perfusion CT: a worthwhile enhancement? *Br J Radiol*, **76,** 220-31.

Acknowledgements

Funding for this project was courtesy of a Cancer Research UK clinical fellowship grant, and kindly supplemented by the Cancer Treatment & Research Trust (CTRT).

This entire project would not have been possible without the kind help and assistance of the following people:

Royal Free Hospital : Richard Begent, Tim Meyer, Shokri Othman, Uzma Qureshi, Barbara Pedley, Cath Sully, John Violet, Astrid Mayer, Surinder Sharma, Natalie Griffin, Moore Ward nursing staff, Geoff Boxer, John Buscombe, Radiopharmacy staff – Georgie, Pei San, PET department staff

Mount Vernon Hospital : Gordon Rustin my principal supervisor, Paul Nathan, Linda Swift, Breda & Liz, Jane Boxall, Linda Poupard, Lisa Saunders, Gavin Shreeves, Jo Evans, Maggie, Clare Ackers, Dan Patterson, Raj Sinha, Paul Adjzenstejn, Kate Lankester, Dick Ashford, Rob Glynne-Jones, chemotherapy unit staff, Michael Powell, all in R&D & Ethics for your help and advice.

Paul Strickland Scanner Centre : Anwar Padhani, Vicky Goh, Jane Taylor, James Stirling, Linda Culver, MRI and CT radiographers, Martin Leach and James D'Arcy at the Royal Marsden who continue the evolution of MRIW

Gray Cancer Institute : Frances Daley, Sonia Noble, Gill Tozer, Sally Hill, Mike Stratford, Roz Locke

University of Hertfordshire Health R&D Support Unit : Dr David Wellsted, Dr David Stott, Dr Sue Cliffe

OXiGENE : Scott Young, Dan McCarthy, Fred Driscoll, Annette Le Blanc, Dai Chaplin, Ann Marseilles, Theresa L'Homme, Ronny Oren

CR-UK : Claire Cruickshank, Carolyn Hayward, Elizabeth Howard, Sheena Damodharan, Karen Owen and all in the Drug Development Office

Mum & Dad, Futgens, Max Leven de Vere, Zuzu Sultan, Andy Easton, Healix International, Marion.

Special thanks to my wife Juliet for her constant support, encouragement and advice during the whole project. I simply could not have completed this without you. Thanks also to my colleagues at St Bartholomew's, and Guy's & St Thomas' Hospitals for their understanding, unselfishly continuing to encourage, support & nurture the write up of this thesis despite a heavy clinical workload!

To my newborn son Joel Adam, you have given meaning to everything. Now it all makes sense.

Lastly, and most importantly, to all the patients who contributed to this project, gave up so much of their time, and made it possible.